

การหาแรงพลศาสตร์ในเพลลาของยานพาหนะหลายคันเคลื่อนที่บนสะพานต่อเนื่อง
จากผลตอบสนองโมเมนต์ดัด



นาย พัทธพงษ์ อาสนจินดา

สถาบันวิทยบริการ

จุฬาลงกรณ์มหาวิทยาลัย

วิทยานิพนธ์นี้เป็นส่วนหนึ่งของการศึกษาตามหลักสูตรปริญญาวิศวกรรมศาสตรดุษฎีบัณฑิต

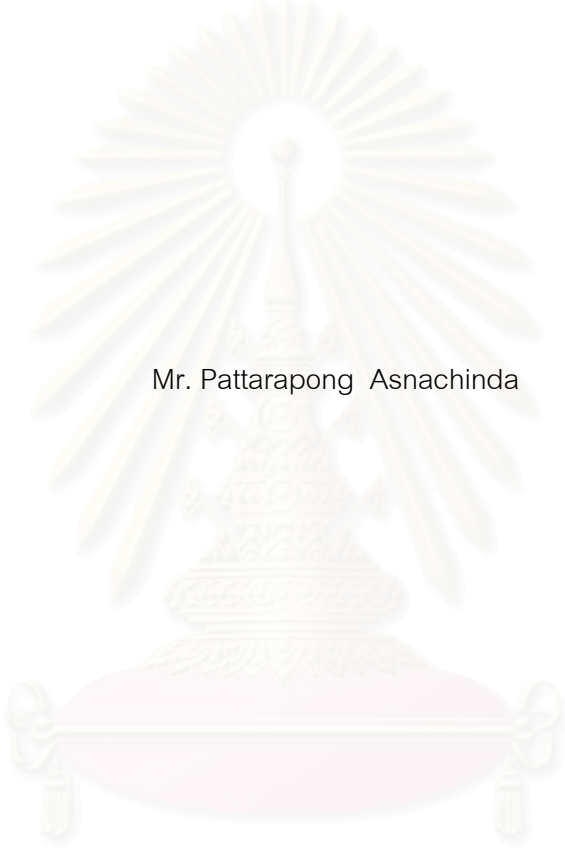
สาขาวิชาวิศวกรรมโยธา ภาควิชาวิศวกรรมโยธา

คณะวิศวกรรมศาสตร์ จุฬาลงกรณ์มหาวิทยาลัย

ปีการศึกษา 2550

ลิขสิทธิ์ของจุฬาลงกรณ์มหาวิทยาลัย

DYNAMIC AXLE LOADS IDENTIFICATION OF MULTIPLE VEHICLES MOVING ON
CONTINUOUS BRIDGE FROM BENDING MOMENT RESPONSES



Mr. Pattarapong Asnachinda

สถาบันวิทยบริการ
จุฬาลงกรณ์มหาวิทยาลัย

A Dissertation Submitted in Partial Fulfillment of the Requirements
for the Degree of Doctor of Philosophy Program in Civil Engineering

Department of Civil Engineering

Faculty of Engineering

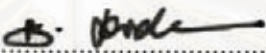
Chulalongkorn University

Academic Year 2007


Copyright of Chulalongkorn University

Thesis Title DYNAMIC AXLE LOADS IDENTIFICATION OF MULTIPLE
VEHICLES MOVING ON CONTINUOUS BRIDGE FROM BENDING
MOMENT RESPONSES
By Mr. Pattarapong Asnachinda
Field of Study Civil Engineering
Thesis Advisor Associate Professor Tospol Pinkaew, D.Eng.

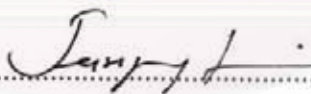
Accepted by the Faculty of Engineering, Chulalongkorn University in Partial Fulfillment
of the Requirements for the Doctoral Degree


..... Dean of the Faculty of Engineering
(Associate Professor Boonsom Lerdhirunwong, Ph.D.)

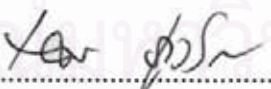
THESIS COMMITTEE


..... Chairman
(Professor Panitan Lukkunaprasit, Ph.D.)


..... Thesis Advisor
(Associate Professor Tospol Pinkaew, D.Eng.)


..... Member
(Associate Professor Teerapong Senjuntichai, Ph.D.)


..... Member
(Associate Professor Thitima Jintanawan, Ph.D.)


..... Member
(Associate Professor Nakhorn Poovarodom, Ph.D.)

พิทพงษ์ อาสนจินดา : การหาแรงพลศาสตร์ในเพลารองยานพาหนะหลายคันเคลื่อนที่บนสะพาน
ต่อเนื่องจากผลตอบสนองของโมเมนต์ดัด. (DYNAMIC AXLE LOADS IDENTIFICATION OF
MULTIPLE VEHICLES MOVING ON CONTINUOUS BRIDGE FROM BENDING MOMENT
RESPONSES) อ. ที่ปรึกษา : รศ.ดร. ทศพล ปิ่นแก้ว, 171 หน้า.

งานวิจัยนี้ได้ทำการนำเสนอวิธีการหาแรงทางพลศาสตร์ในเพลารองยานพาหนะหลายคันซึ่งเคลื่อนที่บนสะพาน
ต่อเนื่องแบบหลายช่วง โดยมีวัตถุประสงค์จะพัฒนาเทคนิคที่เหมาะสมในการนำไปใช้งานเพื่อหาแรงทางพลศาสตร์ในเพลารอง
ยานพาหนะจากผลตอบสนองของสะพานที่ตรวจวัด โดยอาศัยหลักการวิเคราะห์ปัญหาแบบย้อนกลับด้วยการแปลง
ผลตอบสนองของสะพานให้ย้อนกลับเป็นแรงกระทำแบบจุดที่เปลี่ยนแปลงค่าตามเวลา ปัญหาดังกล่าวสามารถทำการหา
คำตอบได้โดยการใช้วิธีการขอพดิโมเรชั่นยกกำลังสองน้อยที่สุดร่วมกับวิธีเชิงอนุกรมฟูริเยร์ ได้ถูกนำมาใช้และเพื่อจะ
ปรับปรุงความถูกต้องและกำจัดความยุ่งยากในการเลือกใช้ค่าตัวแปรเรกูลารีไรเซชันที่เหมาะสมที่สุด ในงานวิจัยนี้ได้นำ
เทคนิคการปรับปรุงองค์ประกอบทางสถิติ (USC) มาประยุกต์ใช้งานด้วย

เพื่อที่จะตรวจสอบประสิทธิภาพของวิธีการหาแรงที่นำเสนอ ได้ทำการศึกษาดูการสร้างแบบจำลองคอมพิวเตอร์
และการทำการทดสอบ แบบจำลองย่อยส่วนสะพานต่อเนื่องแบบสามช่วงและแบบจำลองย่อยส่วนยานพาหนะแบบสองเพลารอง
จำนวนสองคันจึงได้ถูกออกแบบ และประกอบในห้องปฏิบัติการ การศึกษาได้ทำการพิจารณาถึงผลกระทบที่มีต่อความ
ถูกต้องของการหาแรงจากปัจจัยต่าง ๆ ที่เกี่ยวข้องได้แก่ สัญญาณรบกวนเนื่องจากการตรวจวัด, การจำลองระบบการหาแรง,
มวล, ความเร็วในการเคลื่อนที่, ระยะห่างเพลารอง, จำนวนเพลารองยานพาหนะ, ความขรุขระของพื้นผิวสะพาน รวมไปถึง
รูปแบบการเคลื่อนที่ที่หลากหลายอันเนื่องมาจากการสั่นของยานพาหนะหลายคัน โดยได้ทำการตรวจวัดค่าแรงทาง
พลศาสตร์ที่เกิดขึ้นจริงในเพลารองแบบจำลองยานพาหนะขณะเคลื่อนที่และนำไปใช้ในการประเมินความถูกต้องแม่นยำของ
วิธีการหาแรง

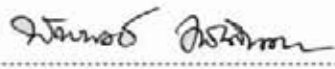
จากผลการทดสอบ พบว่าเทคนิคการปรับปรุงองค์ประกอบทางสถิตินั้นเพิ่มความถูกต้องแม่นยำและมีความคงทน
ในการแก้ปัญหาได้อย่างมีประสิทธิภาพ โดยเฉพาะอย่างยิ่งในการปรับปรุงข้อบกพร่องจากการสูญหายของแรงในเพลารองในช่วง
บริเวณจุดรองรับภายในของสะพาน และยังพบว่ามวลของยานพาหนะ, ความเร็วในการเคลื่อนที่, ระยะห่างเพลารอง และความ
ขรุขระของพื้นผิวสะพานมีผลกระทบต่อความถูกต้องของการหาแรงอย่างมีนัยสำคัญ ยานพาหนะที่มีมวลหนัก ระยะห่างเพลารอง
ที่ยาวและเคลื่อนที่ด้วยความเร็วต่ำบนพื้นผิวสะพานที่ราบเรียบ จะสามารถหาแรงทางพลศาสตร์ในเพลารองได้ถูกต้องและ
แม่นยำมากกว่ายานพาหนะที่มีน้ำหนักเบา ระยะห่างเพลารองที่สั้นและเคลื่อนที่ด้วยความเร็วสูงบนสะพานที่มีพื้นผิวที่ขรุขระ

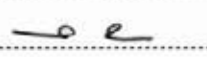
นอกจากนั้นยังพบว่าวิธีการหาแรงมีความคงทนและสามารถหาแรงทางพลศาสตร์ในเพลารองยานพาหนะหลาย
คันที่เคลื่อนที่หลากหลายรูปแบบได้อย่างถูกต้องแม่นยำโดยปราศจากปัญหาการขัดแย้งระหว่างแรงในเพลารองจากการเคลื่อนที่
ทับซ้อนกันของยานพาหนะและการเคลื่อนที่ผ่านจุดรองรับของสะพาน เนื่องจากแรงในเพลารองแต่ละแรงนั้นถูกคำนวณอย่าง
อิสระและถูกควบคุมด้วยเส้นอิทธิพลทางสถิติจากระเบียบวิธีของเทคนิคการปรับปรุงองค์ประกอบทางสถิติ ผลการ
เปรียบเทียบความเทียบเคียงระหว่างสัญญาณโมเมนต์ดัดที่ตรวจวัดและที่ถูกรสร้างขึ้นแสดงว่าวิธีการหาแรงที่นำเสนอนั้นมี
ความถูกต้อง โดยความแม่นยำของแรงทางพลศาสตร์ที่หาได้ในทุกกรณีที่ทำการศึกษา มีความคลาดเคลื่อนไม่เกิน 13%
นอกจากนี้ยังได้แสดงผลการหาแรงในเพลารองกรณีที่สัญญาณตรวจวัดไม่สมบูรณ์พร้อมให้ข้อเสนอแนะในการนำไป
ประยุกต์ใช้จริงด้วย

ภาควิชา.....วิศวกรรมโยธา.....

สาขาวิชา.....วิศวกรรมโยธา.....

ปีการศึกษา.....2550.....

ลายมือชื่อนิสิต..... .....

ลายมือชื่ออาจารย์ที่ปรึกษา..... .....

4771875221 : MAJOR CIVIL ENGINEERING

KEY WORD: VEHICLE AXLE LOAD/ LOAD IDENTIFICATION/ MOVING FORCE/ REGULARIZATION

PATTARAPONG ASNACHINDA: DYNAMIC AXLE LOADS IDENTIFICATION OF MULTIPLE VEHICLES MOVING ON CONTINUOUS BRIDGE FROM BENDING MOMENT RESPONSES.

THESIS ADVISOR: ASSOC. PROF. TOSPOL PINKAEW, D.Eng., 171 pp.

The identification of multiple vehicle dynamic axle loads on multi-span continuous bridge is proposed. The objective is to develop a practical technique to determine dynamic axle loads of multiple vehicles based on measured bridge responses. Following the concept of inverse problem of returning bridge responses into time-varying point loads, the solution can be determined using least squares regularization optimization via singular value decomposition (SVD) method. The updated static component (USC) technique is adopted to improve the accuracy and eliminate the difficulty of an optimal regularization selection.

The computer simulation and experimental studies are conducted to investigate the effectiveness of the proposed method. A small scaled model of a three-span, continuous bridge and two scaled 2-axle vehicles are designed and fabricated. Study of identification accuracy affected by related parameters including measurement noise, system modeling, vehicle mass, moving speed, axle spacing, number of vehicle axle, bridge surface roughness as well as various moving schemes of multiple vehicle travel are considered. The actual dynamic axle loads of the vehicle models during their travel are directly measured and used in accuracy evaluation.

From the obtained results, it is observed that the employed technique effectively improves the accuracy and robustness of the identified loads, particularly around the internal bridge supports in which the problem of zero identified loads are eliminated. Vehicle mass, moving speed, axle spacing and bridge surface roughness significantly affect to identification accuracy. A heavy, widely spaced axle vehicle traveling with slow speed on smooth surface bridge yields better accuracy of identified axle loads than a light, closely spaced axle vehicle moving with fast speed on rough surface bridge.

In addition, it is found that the method is robust and accurately identifies dynamic axle loads for all moving schemes of vehicles. No conflict of the identified axle loads during axle overlapping or passing the bridge support is observed because the axle loads are independently identified and controlled by static influence lines from the USC algorithm. The comparison between the measured and reconstructed bending moments indicates that the approach is correct. The accuracy of identified dynamic axle loads for all cases of study is within relative percentage error of 13%. Moreover, axle load identification with incomplete measurement information is investigated and recommendations toward the real application of the proposed identification system are also given.

Department:.....CIVIL ENGINEERING.....

Student's signature: *Pattarapong Asnachinda*

Field of Study:.....CIVIL ENGINEERING.....

Advisor's signature: *Tospol Pinkaew*

Academic year:.....2007.....

ACKNOWLEDGEMENTS

This dissertation cannot be completely achieved without helps and supports from many persons. First, I would like to express thankfulness to my research supervisor, Associate Professor Tospol Pinkaew for very helpful suggestions, his time, financial support, kindness and continuous support throughout this research and study. I would also like to thank Associate Professor Jeffrey A. Laman from the Pennsylvania State University for his insight, guidance and very useful information in research work and research journal preparation while staying in United States. Sincere appreciation to dissertation committee members, Professor Panitan Lukkunaprasit, Associate Professor Teerapong Senjuntichai, Associate Professor Thitima Jintanawan and Associate Professor Nakhorn Poovarodom, who gave valuable suggestions for research completeness.

Thanks go to Commission on higher education, Ministry of education for their financial support, providing the Ph.D. program scholarship for all study expenses in Thailand and United States at the Pennsylvania State University. Thanks to Ratchadapiseksompot foundation who offered financial support with 90th year Chulalongkorn University grant in research experiment. Also thanks to graduate school of Chulalongkorn University for partially support for expense in participating research presentation in an international conference at Porto, Portugal.

Great appreciation goes to Dr. Chaloeiphon Lorattanasane for his kind support in instruments for experiment. Thanks to my colleagues and friends for their help in research work and our friendship.

Finally, special thanks go to my family, parents and sisters for their endless support, dedication and love throughout this endeavor.

CONTENTS

	page
Abstract (Thai).....	iv
Abstract (English).....	v
Acknowledgements.....	vi
Contents.....	vii
List of Tables.....	xi
List of Figures.....	xiv
Chapter I Introduction.....	1
1.1 Background and Motivation.....	1
1.2 Problem Statement.....	2
1.3 Research Objectives.....	4
1.4 Methodology.....	4
1.5 Scope of Research.....	4
1.5.1 Scope of Analytical Study.....	5
1.5.2 Scope of Experimental Study.....	6
1.6 Dissertation Organization.....	6
Chapter II Literature Review.....	7
2.1 General.....	7
2.2 Weigh-In-Motion.....	7
2.2.1 Traditional Weigh-In-Motion.....	8
2.2.2 Bridge Weigh-In-Motion.....	9
2.2.3 Accuracy Classification of WIM.....	10
2.3 Vehicle-Bridge Interaction.....	12
2.4 Moving Loads Identification.....	17
2.4.1 Single-Span Simply Supported Bridge.....	17
2.4.2 Multi-Span Continuous Bridge.....	24
2.5 Summary.....	26
Chapter III Theory of Vehicle-Bridge Interaction and Moving Loads Identification System.....	27
3.1 General.....	27
3.2 Dynamics of Vehicle-Bridge Interaction System.....	27
3.2.1 Finite Element Method of Structural Formulation.....	28

3.2.2 Assumption of Dynamics System.....	28
3.2.3 Vehicle Model.....	28
3.2.4 Bridge Model.....	33
3.2.5 Bridge Surface Roughness.....	39
3.2.6 Vehicle-Bridge Interaction.....	39
3.3 Relationship of Axle Loads and Bridge Bending Moments.....	44
3.4 Moving Loads Identification.....	45
3.4.1 Problem Statement.....	48
3.4.2 Optimization with Tikhonov Regularization.....	50
3.4.3 Loads Identification using Singular Value Decomposition.....	52
3.4.4 Accuracy Improvement with Updated Static Component Technique.....	53
Chapter IV Numerical Study of Axle Loads Identification Using Computer Simulation.....	56
4.1 General.....	56
4.2 Accuracy of Moving Loads Identification.....	56
4.2.1 Conventional Moving Loads Identification.....	58
4.2.2 Moving Loads Identification with Optimal Regularization.....	59
4.2.3 Moving loads identification with USC regularization.....	60
4.3 The Study of Related Parameters Effecting to Axle Loads Identification.....	64
4.3.1 Regularization Parameter.....	65
4.3.2 Number and Location of Measurement Stations.....	68
4.3.3 Structural Discretization and Sampling Rate.....	70
4.3.4 Vehicle Mass and Moving Speed.....	71
4.3.5 Bridge Surface Roughness.....	73
4.3.6 Front Axle to Gross Weight Ratio (FGR) and Axle Spacing to Span Ratio (ASSR).....	74
4.3.7 Number of Moving Loads and Level of Measurement Noise.....	76
4.3.8 Headway and Vehicle Speed Ratio.....	77
4.3.8.1 Short headway movement.....	78
4.3.8.2 Overtaking movement.....	79
4.3.8.3 Side-by-side movement.....	80
4.3.9 Vehicle Type and Axle Loads Configuration.....	81

4.4 Summary.....	84
Chapter V Experimental Study of Axle Loads Identification Using Scaled Model	85
5.1 General.....	85
5.2 Experimental Design.....	85
5.2.1 Design of Bridge Model.....	85
5.2.2 Design of Vehicle Model.....	87
5.3 Experimental Set-Up.....	88
5.4 Single Vehicle Axle Load Identification.....	91
5.4.1 Two-Axle Vehicle.....	91
5.4.1.1 Effect of vehicle mass and moving speed.....	91
5.4.1.2 Effect of transverse direction of vehicle travel.....	93
5.4.1.3 Effect of road surface roughness.....	95
5.4.2 Four-axle vehicle.....	100
5.5 Multiple Vehicle Axle Load Identification.....	107
5.5.1 Short headway movement.....	111
5.5.2 Overtaking movement.....	114
5.5.3 Side-by-side movement.....	114
5.6 Summary.....	118
Chapter VI Axle Loads Identification with Incomplete Measurement	
Information.....	121
6.1 General.....	121
6.2 Axle Loads Identification with Incomplete Velocity Information.....	121
6.3 Axle Loads Identification with Incomplete Bending Moment	
Information.....	125
6.4 Axle Loads Identification with Bridge Response of Target Span.....	129
6.5 Summary.....	133
Chapter VII Conclusions and Recommendations for Application.....	135
7.1 Conclusions.....	135
7.1.1 Axle Loads Identification from Bridge Bending Moment.....	135
7.1.2 Axle Loads Identification with Incomplete Measurement	
Information.....	136
7.2 Recommendations.....	137
7.2.1 Recommendations toward Real Application.....	138
7.2.2 Recommendations for Further Study.....	138

References.....	140
Appendices.....	146
Appendix A Model Calibration.....	147
I. Calibration of Model Vehicle.....	147
II. Calibration of Bridge Model.....	149
Appendix B Data Acquisition and Noise Filtering.....	154
Appendix C Axle Load Identification with Incomplete Measurement Information.....	157
I. Axle Loads Identification with Incomplete Velocity Information.....	157
II. Axle Loads Identification with Incomplete Bending Moment Information.....	162
III. Axle Loads Identification with Bridge Response of Target Span.....	167
Vita.....	171



สถาบันวิทยบริการ
จุฬาลงกรณ์มหาวิทยาลัย

LIST OF TABLES

	page
Table 2.1 Width of the accuracy classes (COST 323).....	10
Table 2.2 Classification and criteria of WIM sites (COST 323).....	11
Table 2.3 ASTM WIM system classification.....	12
Table 2.4 Functional Performance Requirements for WIM Systems.....	12
Table 4.1 Parameters of the bridge used in numerical study.....	57
Table 4.2 Comparison of RPE (%) of two functional moving loads identification from various identification methods.....	60
Table 4.3 Comparison of RPE (%) of four functional moving loads identification from various identification methods.....	61
Table 4.4 Comparison of RPE (%) of single vehicle axle loads identification from various identification methods.....	62
Table 4.5 Comparison of RPE (%) of two-vehicle axle loads identification from various identification methods.....	62
Table 4.6 Parameter of vehicle model used in vehicle-bridge interaction.....	64
Table 4.7 Identification error from different influence parameters at various regularization parameters.....	67
Table 4.8 Sensor arrangements of single-span simply supported bridge.....	68
Table 4.9 Sensor arrangements of three spans continuous bridge.....	68
Table 4.10 Comparison of RPE (%) of vehicle axle load identification on single- span simply supported bridge from various sensor number and location.....	69
Table 4.11 Comparison of RPE (%) of vehicle axle load identification on 3-span continuous bridge from various sensor number and location.....	69
Table 4.12 Identification error of single vehicle axle load identification from single span simply supported bridge for different discretization and sampling rate.....	70
Table 4.13 Identification error of single vehicle axle load identification on 3- span continuous bridge from different vehicle mass and moving speed.....	72

Table 4.14 Comparison of RPE (%) of single vehicle axle load identification from different magnitude of bridge surface roughness and moving speed.....	73
Table 4.15 Identification error of single vehicle axle load identification from 3-span continuous bridge for different front axle to gross weight ratio and axle spacing to span ratio.....	75
Table 4.16 Identification error of moving load identification on 3-span continuous bridge from different number of loads and measurement noise level.....	77
Table 4.17 Movement scenarios of two-vehicle axle load identification.....	78
Table 4.18 Identification error of two-vehicle axle loads identification from various bridge approach time interval and velocity ratio.....	79
Table 4.19 Identification error of vehicle axle load from different vehicle category.....	82
Table 5.1 Parameters of real and scaled bridge models.....	87
Table 5.2 Arrangement of obstructive objects used as surface roughness study..	96
Table 5.3 RPE (%) of identified axle loads of a two-axle vehicle traveling on the bridge with various roughness patterns.....	99
Table 5.4 Experimental scenarios and results of four-axle vehicle load identification.....	103
Table 5.5 Experimental scenarios and results of four-axle vehicle load identification (identified with optimal λ).....	105
Table 5.6 Experimental scenarios of two-vehicle axle load identification.....	109
Table 5.7 Correlation coefficients of identified vehicle axle loads from different two-vehicle axle load identification scenarios.....	111
Table 5.8 Correlation coefficients of reconstructed bending moments from different two-vehicle axle load identification scenarios.....	118
Table 6.1 Sensor patterns of vehicle axle load identification with removed measurement stations providing identification error within 6%.....	127
Table 6.2 RPE of identified axle load and correlation coefficients of bending moments in the case of over-determined problem from experiment identified with target span.....	130

Table 6.3	RPE of identified axle load and correlation coefficients of bending moments in the case of under-determined problem from experiment identified with target span.....	131
Table A.1	Calibrated coefficients and variables of the experimental bridge model.....	152
Table C.1	RPE (%) of 2-axle vehicle re-identified its axle load with simplified vehicle position by assuming moving speed of vehicle travel to be constant.....	157
Table C.2	RPE (%) of multiple vehicles identification re-identified its axle load with simplified vehicle position by assuming moving speed of vehicle travel to be constant.....	158
Table C.3	Sensor pattern of vehicle axle load identification with removed measurement stations.....	163
Table C.4	RPE (%) and correlation coefficients of identified axle loads from identification with sensor removal.....	165

LIST OF FIGURES

		page
Figure 1.1	Diagram of research methodology.....	5
Figure 2.1	Bridge WIM system.....	10
Figure 2.2	Schematic block diagram of dynamic bridge-vehicle interaction (Green and Cebon, 1997).....	14
Figure 3.1	Vehicle-bridge system of n -span continuous bridge.....	29
Figure 3.2	Free body diagram of vehicle-bridge system.....	30
Figure 3.3	A finite beam element with 4 degrees of freedom.....	33
Figure 3.4	Nodal loads from external load.....	37
Figure 3.5	Multiple vehicles-bridge system of n -span continuous bridge.....	44
Figure 3.6	Measuring point in beam element.....	44
Figure 3.7	Multiple moving loads-bridge system used in axle load identification.....	46
Figure 3.8	Computational procedures of load identification through regularization with update static component (USC) technique.....	55
Figure 4.1	Typical identified axle loads of two vehicles' axle load identification from conventional method: (a) front axle load of 1 st vehicle, (b) rear axle load of 1 st vehicle, (c) front axle load of 2 nd vehicle and (d) rear axle load of 2 nd vehicle.....	58
Figure 4.2	Typical identified axle loads of two vehicles' axle load identification from optimal regularization method: (a) front axle load of 1 st vehicle, (b) rear axle load of 1 st vehicle, (c) front axle load of 2 nd vehicle and (d) rear axle load of 2 nd vehicle.....	59
Figure 4.3	Typical identified axle loads of two vehicles' axle load identification from regularization method with USC technique: (a) front axle load of 1 st vehicle, (b) rear axle load of 1 st vehicle, (c) front axle load of 2 nd vehicle and (d) rear axle load of 2 nd vehicle.....	61
Figure 4.4	RPE of identified loads of four concentrated loads identification with various order of regularization parameter at measurement noise level of 5%: (a) single-span simply supported bridge and (b) three spans continuous bridge.....	63

Figure 4.5	Plots of identification error of vehicle axle loads from various order of regularization parameter: (a) vehicle mass, (b) vehicle speed, (c) FGR, (d) ASSR, (e) bridge surface roughness and (e) two-vehicle axle load identification.....	66
Figure 4.6	Identification error of single vehicle axle load identification from 3-span continuous bridge with various sampling rates and number of beam elements per bridge span: (a) front axle load and (b) rear axle load.....	71
Figure 4.7	Identification error of single vehicle axle load identification from 3-span continuous bridge with various sampling rates and number of beam elements per bridge span: (a) front axle load and (b) rear axle load.....	72
Figure 4.8	Identification error of single vehicle axle load identification from 3-span continuous bridge with various levels of vehicle speeds and bridge surface roughness: (a) front axle load and (b) rear axle load...	74
Figure 4.9	Identification error of single vehicle axle load identification from 3-span continuous bridge for different front axle to gross weight ratio and axle spacing to span ratio: (a) front axle load and (b) rear axle load.....	75
Figure 4.10	Identification error of two-vehicle axle load identification from 3-span continuous bridge with various vehicle speed ratio and bridge approach time interval: (a) front axle load of 1 st vehicle, (b) rear axle load of 1 st vehicle, (c) front axle load of 2 nd vehicle and (d) rear axle load of 2 nd vehicle.....	80
Figure 4.11	Plots of identification error of different vehicle category from various order of regularization parameter: (a) H-20, (b) PA-EX9, (c) PA-EX2, (d) SHV-3S2 and (e) PA-EX6.....	83
Figure 5.1	Plot of relationship between natural frequencies against span length observed from 898 highway bridges in Europe.....	86
Figure 5.2	Comparison of typical bending moment signals from full scale RC deck slab bridge model and scaled steel bridge model.....	87
Figure 5.3	Experimental set up.....	89

Figure 5.4	Photographs of instruments used in experiment: (a) 48-channel data logger, (b) completion bridge box, (c) optical sensor, (d) photoelectric sensor, (e) DC motor and (f) tension-compression load cell.....	90
Figure 5.5	Typical measured signal of the optical sensor reading used for vehicle's position measurement.....	91
Figure 5.6	RPE of identified dynamic axle load of single vehicle load identification: (a) front axle load and (b) rear axle load.....	92
Figure 5.7	Time histories of identified axle load of a two-axle vehicle with 30 kg GVM traveling with slow speed: (a) front axle load and (b) rear axle load.....	93
Figure 5.8	Time histories of identified axle load of a two-axle vehicle with 10 kg GVM traveling with fast speed: (a) front axle load and (b) rear axle load.....	94
Figure 5.9	Travel paths of vehicles controlled by aluminum guide rails.....	94
Figure 5.10	RPE of identified dynamic axle loads of single model vehicle traveling on different transverse positions of the bridge.....	95
Figure 5.11	Acrylic plate used as an obstructive object of vehicle travel for the study on effect of bridge surface roughness.....	96
Figure 5.12	Time histories of actual axle loads of a two-axle vehicle, 25 kg GVM traveling on different roughness pattern: (a) roughness pattern I (b) roughness pattern II and (c) roughness pattern III.....	97
Figure 5.13	Time histories of bending moment responses of a two-axle vehicle, 25 kg GVM traveling on different roughness pattern: (a) roughness pattern I (b) roughness pattern II and (c) roughness pattern III.....	98
Figure 5.14	Time histories of identified axle load of a two-axle vehicle, 20 kg GVM traveling on smooth surface: (a) front axle (b) rear axle.....	100
Figure 5.15	Time histories of identified axle load of a two-axle vehicle, 20 kg GVM traveling on roughness pattern I: (a) front axle (b) rear axle....	101
Figure 5.16	Time histories of identified axle load of a two-axle vehicle, 20 kg GVM traveling on roughness pattern II: (a) front axle (b) rear axle...	102
Figure 5.17	Axle spacings and trailer connection of four-axle vehicle model.....	102

Figure 5.18	RPE of identified axle load of four-axle vehicle with different GVM ratio and moving speed: (a) 1 st Axle load, (b) 2 nd Axle load, (c) 3 rd Axle load, and (d) 4 th Axle load.....	104
Figure 5.19	RPE of identified axle load of four-axle vehicle with different GVM ratio and moving speed (identified with optimal λ): (a) 1 st Axle load, (b) 2 nd Axle load, (c) 3 rd Axle load and (d) 4 th Axle load..	106
Figure 5.20	RPE of identified axle load of four-axle vehicle with different GVM ratio and moving speed (identified with λ of 0.001): (a) 1 st Axle load, (b) 2 nd Axle load, (c) 3 rd Axle load and (d) 4 th Axle load..	107
Figure 5.21	Typical measured bending moments and the corresponding measured axle loads of two-vehicle axle load identification: (a) measured time histories of bridge bending moments, (b) measured time histories of front and rear axle loads of 1 st model vehicle and (c) measured time histories of front and rear axle loads of 2 nd model vehicle	108
Figure 5.22	RPE of identified dynamic axle load of two-vehicle axle load identification: (a) front axle load of 1 st vehicle, (b) rear axle load of 1 st vehicle, (c) front axle load of 2 nd vehicle and (d) rear axle load of 2 nd vehicle	110
Figure 5.23	Identified axle loads of two vehicles with short headway (FLC-3)....	112
Figure 5.24	Zoom of typical identified axle loads of two vehicles (FLC-3).....	113
Figure 5.25	Identified axle loads of two vehicles with overtaking movement (OVT-4).....	115
Figure 5.26	Identified axle loads of two vehicles with side-by-side travel (SBS) ..	116
Figure 5.27	Percentage error of static vehicle gross weight from two vehicle axle load identification: (a) 1st vehicle gross weight and (b) 2nd vehicle gross weight	117
Figure 6.1	Actual and constant speed assumption time histories of vehicle axle position of a 2-axle vehicle, 25 kg GVM traveling at velocity of 1.0 m/s	122
Figure 6.2	Actual and constant speed assumption time histories of bending moment of a 2-axle vehicle, 25 kg GVM traveling at velocity of 1.0 m/s	122

Figure 6.3	Time histories of identified axle loads of a two-axle vehicle moving on three-span continuous bridge with 3.08% position error (GVM = 20 kg, $v = 1.8$ m/s); (a) front axle load (b) rear axle load.....	124
Figure 6.4	Time histories of identified axle loads of a two-axle vehicle moving on three-span continuous bridge with 8.48% position error (GVM = 20 kg, $v = 1.0$ m/s); (a) front axle load (b) rear axle load	125
Figure 6.5	RPE (%) of identified axle loads of two vehicles traveling with overtaking movement (OVT-7) re-identified with incomplete measured bending moment station; (a) 1 st front axle load (b) 1 st rear axle load (c) 2 nd front axle load and (d) 2 nd rear axle load.....	126
Figure 6.6	Time histories of identified axle loads calculated with various number of measurement stations.....	128
Figure 6.7	Time histories of shortening measured bending moments of middle span used in axle load identification: (a) OVT-4 scenario (b) OVT-6 scenario and (c) FLI-1 scenario.....	132
Figure A.1	Calibration chart of a tension/compression load cell used for actual load detection of front axle of 1 st vehicle.....	148
Figure A.2	Calibration chart of a tension/compression load cell used for actual load detection of rear axle of 1 st vehicle.....	148
Figure A.3	Calibration chart of a tension/compression load cell used for actual load detection of front axle of 2 nd vehicle.....	149
Figure A.4	Calibration chart of a tension/compression load cell used for actual load detection of rear axle of 2 nd vehicle.....	149
Figure A.5	Analytical bridge model of continuity modification used in experimental bridge calibration and identification.....	150
Figure A.6	Typical signals of the measured and analytical bending moments of the calibrated bridge model.....	152
Figure A.7	Free vibration strain response at mid-span of the intermediate span of bridge model	153
Figure A.8	Frequency domain of Fast Fourier Transform (FFT) magnitude from free vibration test of bridge model.....	153
Figure B.1	Typical time histories of actual vehicle axle loads observed by tension/compression load cells.....	154

Figure B.2	Frequency domain of Fast Fourier Transform (FFT) magnitude of measured vehicle axle load.....	155
Figure B.3	Typical pre-processed and post-processed bending moments and corresponding measured axle loads: (a) bending moment at section L1/2, (b) bending moment at section L2/2, (c) bending moment at section L3/2, and (d) front and rear axle loads.....	156
Figure C.1	Time histories of identified axle loads of multiple vehicles with short headway scenario (FLC-3) re-identified with constant speed position.....	159
Figure C.2	Time histories of identified axle loads of multiple vehicles with overtaking scenario (OVT-4) re-identified with constant speed position.....	160
Figure C.3	Time histories of identified axle loads of multiple vehicles with side-by-side scenario (SBS) re-identified with constant speed position.....	161
Figure C.4	Time histories of identified axle loads of 30 kg GVM, 2-axle vehicle moving with velocity of 0.2 m/s identified its axle load with response from the target bridge span.....	167
Figure C.5	Time histories of identified axle loads of 30 kg GVM, 2-axle vehicle moving with velocity of 1.8 m/s identified its axle load with response from the target bridge span.....	168
Figure C.6	Time histories of identified axle loads of OVT-4 scenario identified its axle load with response from the target bridge span.....	169
Figure C.7	Time histories of identified axle loads of FLI-1 scenario identified its axle load with response from the target bridge span.....	170

CHAPTER I

INTRODUCTION

1.1 Background and Motivation

The dynamic axle load and gross weight of vehicles are important factors for consideration in the design of new bridges and pavements, the rating and fatigue life assessments of existing bridges and pavements as well as the design code calibration and overweight vehicle control of highway regulations. Road and bridge design live loads are mainly dominated by heavy vehicles such as buses, trucks and trailers as they cause large impact loading, resulting in damage to pavement and highway structures. Although vehicle weight and axle load are specified in weight limit regulations, the weigh station can only measure the static axle load and the gross vehicle weight (GVW). Moreover, the weighing requires the vehicle to stop, requiring a long time for each vehicle to go through the process. Vehicle queuing at the entrance of the weigh station also induces traffic congestion, which means the weighing cannot be observed and carried out thoroughly. Besides, the dynamic axle loads of vehicles are very difficult to measure directly and their configurations differ according to each vehicle category. Therefore, to obtain this significant loading information without traffic disturbance, the Weigh-In-Motion (WIM) system was adopted and developed to indirectly measure the time-histories of vehicle axle loads.

In the past twenty years, many countries have utilized WIM technology to reduce delays and increase enforcement of overweight vehicles. The WIM system is defined by the American Society for Testing and Materials (ASTM) as the process of estimating a moving vehicle's gross weight and the portion of that weight carried by each wheel, axle, or axle group, or combination thereof, by measurement and analysis of dynamic vehicle tire forces. Through WIM technology, the vehicles can be weighed in time domain without disturbing their traveling speeds.

Although WIM has improved weighing station operations, there are various types of WIM scales with various levels of accuracy. As weighing accuracy decreases, the number of vehicles that must proceed to the static scale increases in order to ensure that all potential overweight vehicles are weighed on the static scale. Additionally, if the WIM system underestimates a vehicle's weight, violating trucks could then go through the system without being stopped.

The existing technologies for WIM scales use bending plates and piezoelectric stripes as load cell sensors. However, these technologies are based on weighing detectors embedded in the pavement and thereby disturb the traffic during their installation and maintenance. Therefore, a new alternative system employing a bridge called Bridge Weigh-In-Motion (B-WIM) has been developed since the 1990s. The B-WIM systems deal with an existing instrumented bridge or culvert from the road network and estimate the acting load by converting the measured bridge response. The advantages of this system are that it can be installed and maintained without disturbing the traffic flow and that the drivers passing over the bridge cannot notice the vehicle loads being detected. Additionally, the cost of installation and maintenance of the B-WIM system are lower than the existing WIM. Hence, the identification of dynamic axle loads from bridge responses becomes more attractive since it is much cheaper and easier to install and maintain. However, the accuracy in the axle load identification of B-WIM systems is dependent on the efficiency of hardware and software.

Over the last decade, there have been studies carried out on moving load identification using bridge responses. Based on vehicle-bridge interaction models, the dynamic axle loads of a vehicle moving on a bridge can be identified from the bridge's strains, displacements, accelerations or bending moments by the load-deformation relationship. Many theoretical and experimental studies have been proposed to identify the moving loads. Although early studies found that the identification methods are reliable, the identified dynamic axle loads are noise sensitive and also numerically ill-conditioned, particularly when using acceleration response. However, one drawback of these studies is that they are limited to single-vehicle load identification. The reality is that quite often multiple vehicles are present on the bridge at the same time especially on long-span bridges or continuous bridges. This research study therefore investigates the axle load identification of multiple vehicles moving on bridges.

1.2 Problem Statement

As stated, in this research, the identification of multiple vehicles moving on bridges is studied. The multiple presence of heavy vehicles moving on the bridge at the same time is considered. Using only a single-span bridge for signal measurement as commonly proposed would not be sufficient to observe the variation of axle loads

because the measured time-histories are too short if the vehicles move at high speed. Therefore, the identification of moving loads using a continuous bridge is also considered.

This research presents the analytical and experimental study of the axle load identification of multi-axle and multiple vehicles moving on single-span simply supported bridges and multi-span continuous bridges.

Theoretically, the interaction forces or the axle loads acting upon the bridge can be transformed to the bridge responses using the load-deformation relationship employing vehicle-bridge interaction or moving loads-bridge interaction together with the data concerning the vehicle and bridge properties. Using the bridge responses, axle spacings and vehicle speeds as the input data, the predicted or unknown axle loads can be identified from the optimization process between the measured responses and the analytically reconstructed responses.

Regarding the axle load identification process, the identified loads are the values inducing the least optimization residual error from the objective function. Early research in this area found that the identified loads with simple least square optimization exhibit a large fluctuation and risk causing ill-conditioning when the vehicle passes the bridge supports. Hence, a regularization technique is necessarily adopted in the optimization to decrease the chance of an unrealistic oscillatory solution.

However, mathematically, the solution identified by the above process tends to provide a large identification error in cases when a higher number of unknown loadings are predicted, such as multi-axle vehicles traveling on the bridge at independent velocities. Therefore, this research aims to develop the accuracy and effectiveness of axle load identification depending on how the vehicles are traveling including short headway following, overtaking and side-by-side movements. Additionally, based on the results from previous studies employing regularization techniques, it has been observed that difficulty in assigning an appropriate or optimal regularization parameter is followed. Moreover, ill-conditioning and poor accuracy of determined axle loads at the internal bridge supports found in multi-span continuous bridges identified by existing identification methods need to be corrected. Thus, accuracy improvement in identifying the axle loads of multiple vehicles traveling on a multi-span bridge will be carried out.

1.3 Research Objectives

According to the problems outlined in the above section, the objectives of this study are:

1. To propose the identification method for the dynamic axle loads of multiple vehicles moving on single-span simply supported and multi-span continuous bridges.
2. To study the influences of various parameters on load identification such as axle-spacing-to-span ratio, bridge surface roughness, vehicle configurations, moving formation of vehicles and regularization parameter.
3. To evaluate the effectiveness of identification accuracy and robustness of the identification method using an analytical study by computer simulation.
4. To verify the obtained analytical results using an experimental study with scaled models and to experimentally investigate the feasibility of the proposed method toward real application.

1.4 Methodology

The methodology of this research is schematically described as shown in Figure 1.1. The research consists of analytical and experimental studies. A numerical study based on computer simulation is conducted to investigate the influence of related system parameters and also as a preliminary study for experimental design. The experimental study is carried out in order to verify and evaluate the effectiveness of the identification method previously investigated in the numerical study. Thus, a comparison of the identified results from both numerical and experimental studies are presented and discussed to summarize the effectiveness of the proposed identification method.

1.5 Scope of Research

The scope of the research study mainly consists of two parts, including the scope of the analytical study conducted via numerical simulation on the computer and the scope of the experimental study conducted via scaled model testing carried out in the laboratory.

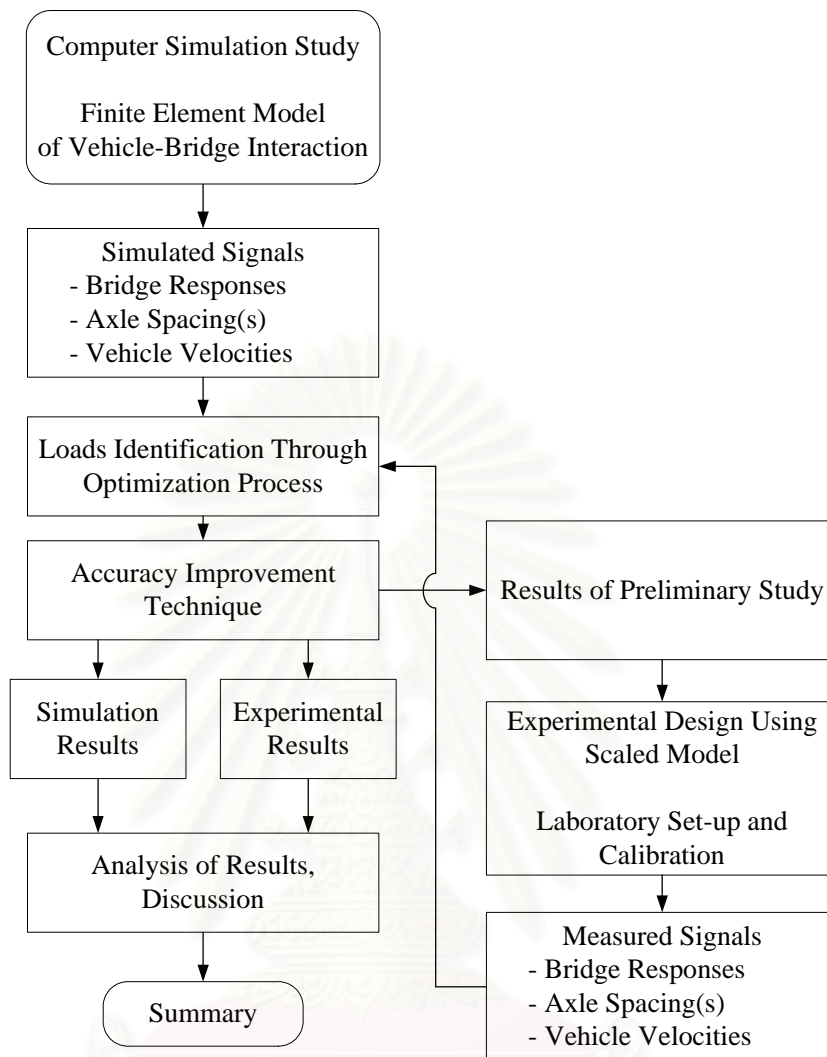


Figure 1.1 Diagram of research methodology

1.5.1 Scope of Analytical Study

1. Vehicle axle load identification for moving vehicles not exceeding two vehicles is considered.
2. The considered vehicle models used in the theoretical and computer simulation studies are four degrees-of-freedom models.
3. A single-span simply supported bridge and a three-span continuous bridge are considered.
4. The measurement signal used in load identification is the sectional bending moment of the bridges.
5. The numerical approach adopted in load identification is an optimization with the least square objective function with Tikhonov regularization.

1.5.2 Scope of Experimental Study

1. The vehicle-bridge system is tested using a small-scale model.
2. The scaled model bridge is a three-span continuous bridge made of steel plate with uniform cross section.
3. The two model vehicles used in the experiment have two axles, non-articulated frames with rubber tires and spring suspensions.
4. The sectional bending moment used in identification is converted from the strain signal directly measured from bridge responses induced by the travel of model vehicles.

1.6 Dissertation Organization

This dissertation consists of seven chapters. Chapter II reviews previous research related to vehicle-bridge interaction, weigh-in-motion system, moving load identification methods and numerical techniques adopted in this field. Chapter III describes the theoretical background used in the formulation of vehicle-bridge interaction, the relationship between moving loads and bridge responses, the optimization statement for moving load identification and the accuracy improvement technique used in this research. Chapter IV presents a numerical study in moving load identification using computer simulation with a parametric study and an effectiveness comparison of existing and proposed identification methods. Chapter V presents the experimental investigation of the proposed identification method by testing with the scaled model. Chapter VI presents the evaluation on tolerance and accuracy robustness of the identification method by conducting identification with incomplete measurement information. Finally, Chapter VII summarizes the obtained results, discusses the limitations of the proposed identification method and provides recommendations for further study and application to the real situation.

CHAPTER II

LITERATURE REVIEW

2.1 General

In this chapter, relevant previous studies including those on vehicle-bridge interaction, weigh-in-motion system and moving load identification are reviewed. Research works relating to theoretical and experimental studies of moving load identification, and numerical techniques used in mathematical models are covered. Based on the useful information in this chapter, the appropriate theoretical and experimental approaches will be applied to the research methodology to achieve the research objectives.

2.2 Weigh-In-Motion

The Weigh-in-Motion (WIM) system has been in use for over 40 years, having first been used for the weight data collection of trucks and their axles for statistical purposes required for pavement design and maintenance. Pavement and bridge structural designs are based on the weight of heavy vehicles traveling on highways. In the 1970s, the first semi-automatic weighing stations consisting of pre-selection WIM scales and downstream axle weighbridges for enforcement in rest or parking areas were designed and built to protect the road infrastructure from damage and to reduce wear and tear. They have continued to be in operation until today. For many years the purpose of weigh stations has been to ensure that trucks do not exceed the legal weights of the localities that are being traveled through. Unfortunately, as the amount of trucks on highways increases, the queue lengths at the weigh stations also increase. When weigh station queues spill back on to the mainline travel lanes, the weigh stations are generally closed and violators can potentially go through the network. As a way of speeding up the process of weighing these heavy vehicles, WIM systems have been installed in many places to screen overweight vehicles. The WIM system provides highway planners and designers with traffic volume and classification data. In addition, WIM equipment also provides planners and designers with equivalent single axle loadings (ESAL) that heavy vehicles place on pavements. Road vehicle enforcement officers use heavy truck axle load data to plan enforcement activities. In summary, the uses of traffic and truck weight data include enforcement, pavement and

bridge design, and legislative and regulatory issues. The use of WIM data should determine the approach chosen in developing the WIM data collection site and the resources required to maintain the site over the expected site design life. The WIM system can be further divided into two systems, which are (1) traditional WIM based on load transformation of the vehicle weight using load cells or other measurements embedded into the roadway pavement, and (2) bridge WIM measuring bridge response for the vehicle load transformation.

2.2.1 Traditional Weigh-In-Motion

Traditional WIM is a weight estimation system employing an instrumented pavement of the roadway surface. Some of the existing measurement technologies for WIM sensors started with load cells, steel plates with strain gauges and were supplemented with low cost sensors using piezo materials, crystal or optical fiber technology (Jacob, 1999) embedded into the roadway surface. Recently, research has also been conducted in determining vehicle weight by pavement strain; however, this technology has not been widely utilized. In each of the systems, a site processor is used to sort and analyze the information obtained from the WIM sensors. Thus, a communication device such as a modem is used to transfer the information to outside locations for further calculation and to ensure that the system is operating properly. Operating software must also be used to interpret the signals from the WIM sensors and be able to generate files that can be used and analyzed by monitoring agencies (McCall et al., 1997).

Due to the high infrastructure and operation costs of these semi-automatic weighing stations, investigations into fully automatic overload enforcement systems have been initiated in recent years: WIM sites with multiple integrated sensor technologies were built and special algorithms were applied to the measurement data with the expectation to achieve higher weight accuracies than with single sensor technology (Sainte-Marie et al., 1998; Stergioulis et al., 1998; Cebon, 1999; Dolcemascolo et al., 2002; Labry et al., 2004). Test sites with Multiple Sensor (MS) WIM arrays were built with different sensor technologies in France (Dolcemascolo, 1999), Germany (Balz/Opitz, 2002), UK, the Netherlands and many other countries.

One benefit of operating the traditional WIM system is that of the aspect of computational time since the vehicle weight can be calculated directly from the load-measurement conversion. However, this system allows large vehicle weight errors to

occur when a vehicle travels quickly. This is because the duration of the vehicle passage on the weighing pad is very short. Moreover, the maintenance cost of this approach is very expensive as the instruments are embedded into the pavement, requiring the instrumented route to be closed for the repairs and replacement of the sensors.

2.2.2 Bridge Weigh-In-Motion

In order to overcome the problem of large weight estimation errors and the expensive maintenance costs found in the traditional WIM system, an alternative approach based on an indirect weight estimation by returning the bridge responses into the acting load known as bridge Weigh-In-Motion (B-WIM) has been developed. Moses et al. (1979) developed the concept of using bridges as scales to weigh trucks in motion. In Australia, a similar system appeared a few years later but was replaced by another that used culverts (Peters, 1986). In the nineties, new bridge WIM (B-WIM) systems were developed independently in Slovenia (Znidaric et al., 1991) and in Ireland (Dempsey et al., 1995). In 1999, a European specification concerning the WIM of roads and vehicles called COST 323 was presented as the recommendations and references for site selection, installation, operation, calibration and assessment by testing of the WIM system. Then further research on the COST 323 project by the European Commission (WAVE, 2001) was continued for the system development of many actions such as weighing capacity, weighing accuracy and standard calibration.

The B-WIM systems deal with an existing instrumented bridge or culvert from the road network as illustrated in Figure 2.1. The instruments are installed in the bridge or culvert structure and the strains measured to provide information about its behavior under moving vehicles. In addition, the axle or vehicle detectors are installed on the pavement to provide data about vehicle type, velocity and axle spacing. Strains are recorded during the time the whole vehicle passes over the structure and such redundant data yields useful information when the influence of dynamic effects due to vehicle-bridge interaction is taken into account.

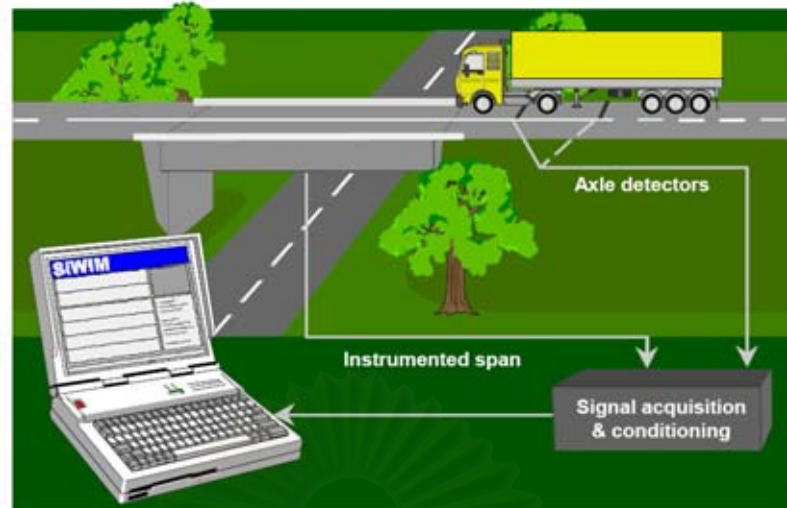


Figure 2.1 B-WIM system

2.2.3 Accuracy Classification of WIM

Several accuracy classes for individual measurements have been defined. Four main criteria are considered. These classes are defined by the confidence intervals of the relative errors with respect to the static loads or weights as shown in Table 2.1.

To date, no multiple-sensor WIM system has been reported to have achieved Class A(5) accuracy but has reached class B+(7) – in accordance with the COST 323 specification. The accuracy of a multiple-sensor WIM array is related to the accuracy of the individual sensors. Moreover, the choice of WIM site also has a great influence on the accuracy, the reliability and the durability of any WIM system. The sites are classified according to the road geometry and the pavement characteristics. Table 2.2 represents the classification and criteria of WIM sites provided by COST 323.

Table 2.1 Width of the accuracy classes (COST 323).

Criteria (type of measurement)	Domain of use	Accuracy Classes: Confidence interval width (%)						
		A(5)	B+(7)	B(10)	C(15)	D+(20)	D(25)	E
1. Gross weight	Gross weight > 3.5 t	5	7	10	15	20	25	>25
Axle load:	Axle load > 1 t							
2. group of axles		7	10	13	18	23	28	>28
3. single axle		8	11	15	20	25	30	>30
4. axle of a group		10	14	20	25	30	35	>35
Speed	V > 30 km/h ⁽¹⁾	2	3	4	6	10	10	>10
Axle spacing		2	3	4	6	10	10	>10
Total flow		1	1	1	3	5	5	>5

(1) For sensors which do not work statically or at very low speed

Table 2.2 Classification and criteria of WIM sites (COST 323)

			WIM site classes		
			I Excellent	II Good	III Acceptable
Rutting (3 m – beam)		Rut depth max. (mm)	≤ 4	≤ 7	≤ 10
Deflection (quasi-static)	Semi-rigid Pavements	Mean deflection (10-2 mm) Left/Right difference (10-2 mm)	≤ 15 ± 3	≤ 20 ± 5	≤ 30 ± 10
	All bitumen Pavements	Mean deflection (10-2 mm) Left/Right difference (10-2 mm)	≤ 20 ± 4	≤ 35 ± 8	≤ 50 ± 12
(13 t – axle)	Flexible Pavements	Mean deflection (10-2 mm) Left/Right difference (10-2 mm)	≤ 30 ± 7	≤ 50 ± 10	≤ 75 ± 15
	Semi-rigid Pavements	Mean deflection (10-2 mm) Left/Right difference (10-2 mm)	≤ 10 ± 2	≤ 15 ± 4	≤ 20 ± 7
Deflection (dynamic)	All bitumen Pavements	Mean deflection (10-2 mm) Left/Right difference (10-2 mm)	≤ 15 ± 3	≤ 25 ± 6	≤ 35 ± 9
	Flexible Pavements	Mean deflection (10-2 mm) Left/Right difference (10-2 mm)	≤ 20 ± 5	≤ 35 ± 7	≤ 55 ± 10

The rutting and deflection values are given for the temperature below or equal 20°C and suitable drainage conditions.

The American Society for Testing and Materials' (ASTM) "Standard Specification for Highway Weigh-in-Motion (WIM) Systems with User Requirements and Test Methods" (ASTM Designation: E 1318-02) classifies four types of WIM systems by different speed range, type of application, and data gathering capabilities. Table 2.3 shows the information for the four types of systems. Table 2.4 shows the functional performance requirements for WIM systems (McCall et al., 1997 and ASTM E 1318-02).

From the classification and specifications listed in the tables above, it is noticed that the accuracy of the system is at its smallest only 5% of the static gross weight of the vehicle.

Although the WIM or the B-WIM systems can estimate the static gross weight of the vehicle accurately, the parameter directly affecting the structural health of the bridge is the dynamic loading from moving vehicles which induces dynamic impact to the pavement. To monitor this action, the WIM systems with static gross weight or static axle loads of the vehicle are inadequate. Therefore, the time-history of moving axle loads is necessary. Additionally, the accuracy in axle load identification of B-WIM systems is dependent on the efficiency of hardware and software, and the cost of installation and maintenance for WIM and B-WIM is very expensive. Hence, the identification of dynamic axle loads from bridge responses becomes a more attractive alternative since it is much cheaper and easier to install and maintain.

Table 2.3 ASTM WIM system classification

	Classification			
	Type I	Type II	Type III	Type IV
Speed Range	10-70 mph (16-113 km/h)	10-70 mph (16-113 km/h)	15-50 mph (24-80 km/h)	0-10 mph (0-16 km/h)
Application	Traffic data collection	Traffic data collection	Weight enforcement station	Weight enforcement station
Number of Lanes	Up to four	Up to four	Up to two	Up to two
Wheel Load	X		X	X
Axle Load	X	X	X	X
Axle-Group Load	X	X	X	X
Gross Vehicle Weight	X	X	X	X
Speed	X	X	X	X
Center-to-Center Axle Spacing	X	X	X	X
Vehicle Class	X	X		
Site Identification Code	X	X	X	X
Lane and Direction of Travel	X	X	X	
Data and Time of Passage	X	X	X	X
Sequential Vehicle Record Number	X	X	X	X
Wheelbase	X	X		
Equivalent Single-Axle Load	X	X		
Violation Code	X	X	X	X

Table 2.4 Functional performance requirements for WIM systems

Function	Tolerance for 95% Probability of Conformity				
	Type I	Type II	Type III	Type IV	
				Value \geq Ib (kg)	\pm Ib (kg)
Wheel Load	$\pm 25\%$		$\pm 20\%$	5000 (2300)	250 (100)
Axle Load	$\pm 20\%$	$\pm 30\%$	$\pm 15\%$	12,000 (5400)	500 (200)
Axle-Group Load	$\pm 15\%$	$\pm 20\%$	$\pm 10\%$	25,000 (11,300)	1200 (500)
Gross-Vehicle Weight	$\pm 10\%$	$\pm 15\%$	$\pm 6\%$	60,000 (27,200)	2500 (1100)
Speed	± 1 mph (2km/h)				
Axle-Spacing	± 0.5 ft (150 mm)				

2.3 Vehicle-Bridge Interaction

The major objective of the WIM system is to identify the axle loads of vehicles. Therefore, the behavior of the dynamic interaction between vehicle and bridge is an important part of a moving load identification system. A method to estimate the fundamental frequency of the vibration behavior of the bridge has been developed. Many approaches such as an empirical method based on span length have a simple function as $f = 100/L$.

However, Cantieni (1983) concluded that this equation yields fundamental frequencies that are definitely too low, while Billing and Green (1984) cited $f = 110/L$ as a useful preliminary design estimate only.

From the single beam analogy, the natural frequencies of a simply supported beam were given by Clough and Penzien (1975) as

$$f_n = \frac{\pi n^2}{2L^2} \sqrt{\frac{EI}{\rho A}}. \quad (2.1)$$

Over the past 30 years, several researchers have investigated the correlation between the observed natural frequencies of bridges and theoretical estimates based on the beam analogy. A method that has been used extensively to estimate the fundamental frequency of mechanical systems is the Rayleigh energy method (Rayleigh, 1877). With an iterative procedure, the initial step often yields a sufficiently accurate result. The initial assumption required for the method is the mode shape, and further interactions converge on a more accurate mode shape.

According to the above mentioned frequency estimation methods, Memory et al. (1994) comparatively studied the free vibration analysis of bridges. The results showed that a bridge with single beam idealization is accurate for a straight, non-skewed bridge and for some continuous superstructures. Many other bridges require an eigenvalue analysis through the finite element method to obtain the correct solution.

The simulation of bridge dynamic response under moving load has been studied and used to investigate the effectiveness of identification methods. Fryba (1973) investigated the vibration of a simply supported beam subjected to various moving loadings. Lin et al. (1990) proposed the finite element method of discrete system for dynamic response analysis, and the accurate model has been studied against the degree of discretization of the structure for a moving load analysis (Rieker JR et al, 1996). It was found that beams with various support boundary conditions subject to a moving load system with general movement profile can be successfully analyzed.

Hwang and Nowak (1991) developed a procedure for calculation of the dynamic load for bridges. Trucks, road surface roughness and bridges were analyzed using the developed model to obtain their dynamic interaction. The two-axle truck and tractor-trailer models were simulated with rigid body in mass, and the suspensions and tires were assumed as vertical springs. The equation motion of the system can be formulated from the vertical and rotational equilibriums. Road profiles were simulated using a stochastic process (power spectral density function). A bridge

was treated as a prismatic beam. The analysis was performed for a single truck and for two trucks side by side. The results revealed that the dynamic loads for heavier trucks are lower and that this is also true for two trucks. The simulation deflection indicated that the dynamic component does not correlate with the static component. Therefore, the dynamic loads are usually lower for heavier trucks as well as the dynamic load for the two trucks is lower than a single truck.

Green and Cebon (1997) studied the bridge-vehicle interaction with a vehicle model with lumped masses supported by springs and dampers using an iterative method. The dynamic interaction between dynamic responses of bridges to dynamic wheel loads is presented. Figure 2.2 is a schematic diagram of bridge-vehicle interaction. The roughness input to the vehicle is the sum of the initial surface profile of the bridge and the dynamic deflection of the bridge. This input excites the vehicle and results in dynamic tire forces. These forces are in turn applied to the bridge and cause larger dynamic displacements of the bridge. This feedback mechanism of interaction forces couples the dynamic responses of the bridge with that of the vehicle. From the diagram, the vehicle-bridge interaction is obtained from the comparison of the bridge responses in an iterative manner.

Yang et al. (1995, 1999 and 2001) developed some vehicle-bridge interaction elements to solve the dynamic coupling problem. The equations of motion were written for the vehicle and bridge. The vehicle equations were first reduced to equivalent stiffness equations using Newmark's discretization scheme. Then the vehicle degrees of freedom were condensed to those of beam elements in contact. The effects of some parameters, such as bridge length, speed were discussed by using mass-spring-dashpot and beam elements (Yang et al., 1995).

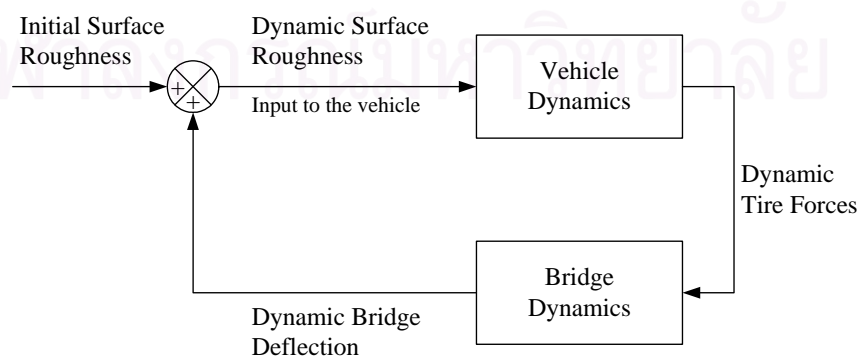


Figure 2.2 Schematic block diagram of dynamic bridge-vehicle interaction (Green and Cebon, 1997)

Henchi et al. (1997) presented an exact dynamic stiffness element under the framework of finite element approximation to study the dynamic response of a multi-span structure under a convoy of moving loads. The multi-span bridge was modeled as a multi-span continuous beam. Using a weak formulation of the virtual work of the Bernoulli-Euler beam model, the dynamic stiffness matrix was obtained. A dynamic model coupled with a discrete FFT algorithm was developed. With the proposed method, using only one element per span, exact frequencies and vibration modes could be obtained.

Henchi et al. (1998) proposed an efficient method to analyze the dynamic interaction problem between a bridge, discretized by a three-dimensional finite element model, and a dynamic system of vehicles running at a prescribed speed. The resolution is performed using a step-by-step solution technique employing a central difference scheme to solve the coupled equation system. In general, there are two approaches to simulate the dynamic vehicle-bridge interaction. The first is based on the uncoupled iteration method, in which each system (vehicles and bridge) is solved separately and an iterative process in each time step is performed to find the equilibrium between bridge and vehicle tires. The other approach to simulate the dynamic interaction between vehicles and bridge consists of solving the super system fully coupled, and the solution is given at each time step without iteration. This non-iteration approach has some advantages that reduce the computational time and compact numerical implementation easily. However, the disadvantages are as follows: modal projection in subspace is indispensable, and if the high frequencies of the bridge participate in the response this will create a problem in the dynamic response; this method is well adapted only for a few number of vehicles present on the bridge at the same time (this remark also applies to the uncoupled modal iterative method).

Marchesiello et al. (1999) presented an analytical approach to the dynamics of multi-span continuous straight bridges subject to multi-degree-of-freedom moving vehicle excitation. The continuous bridge was modeled as a multi-span isotropic plate with its response to external loads being defined by applying the mode superposition principle and taking into account both flexural and torsional mode shapes. The plate was considered proportionally damped and its modes were computed by means of the Rayleigh-Ritz method. The determination of the bridge dynamic response involves an integral equation and therefore requires the iterative procedure. The three-dimensional analysis of bridge-vehicle interaction was implemented including both flexural and

torsional modes of structure, and roughness of the road. The numerical examples were found to be in good agreement with the finite element model thus giving confidence to the analytical results.

Chan et al. (2003) presented the formulation of a bridge-vehicle system with validation using field data. The three-dimensional vehicle model including pitching and twisting motion was considered. For the tire-suspension system, the effect of interleaf friction is represented by a bilinear diagram of the hysteretic type (Veletsos and Huang, 1970). The bridge was modeled using shell elements. The interaction responses were solved using the Newmark method. The obtained responses were validated from the test data and showed that the prediction was valid and feasible. By converting the bridge responses using FFT, the fundamental frequency of the test bridge can be obtained. The parametric study was also presented in terms of dimensionless parameters i.e. mass ratio, speed parameter, frequency ratio and axle spacing parameter. The results showed that the impact factor increases as the frequency ratio increases and decreases as the span length increases. For the mass ratio, the impact factor generally decreases as the mass ratio increases. However, for a low frequency ratio, the impact factor stays almost constant with the mass ratio. In the case of the axle spacing parameter (ASP), the impact factor as well as the ASP increases. The impact factor varies with the vehicle speed but there is no obvious trend. For the same axle spacing parameter, the impact factor increases with the vehicle speed.

Law and Zhu (2005) studied the dynamic behavior of bridge responses under moving vehicles by considering the effect of road surface roughness and the braking of a vehicle. The vehicle was modeled as a tractor-trailer with 7 degrees of freedom. Each vehicle axle had stiffness and damping from the suspensions and tires. The bridge was modeled as a multi-span continuous Bernoulli-Euler beam with a non-uniform cross-section on linear spring supports with large stiffness to simulate bridge piers which are practically not perfectly rigid. The tires were assumed to remain in contact with the bridge surface at all times. The interaction between vehicle and bridge was solved by modal analysis through road surface roughness with an iterative method by checking the tolerance of the calculated responses. The different classes of road roughness as specified in the ISO-8606 from classes A to E were studied. The amplitude of braking force in relative percentage of the gross weight of vehicle, braking rise time, and braking position of the vehicle on the bridge was varied. The

results from numerical examples showed that a vehicle traveling at low speed over a high amplitude of roughness or poor road roughness may experience excitations at frequencies close to its own natural frequencies, generating a large excitation force on the bridge and leading to a large impact factor. Moreover, the suspension system of the vehicle has a significant effect on the dynamic responses, particularly to the braking of the vehicle, of which the pitching action creates large oscillations in the responses at the pitching frequency of the vehicle. It was also observed that the impact factor in the first span of a multi-span bridge is smaller than those in other spans because of the smaller initial conditions of the vehicle at entry on the bridge. Finally, the vehicle braking generates an equivalent impulsive force covering a wide range of frequencies. A large number of vibration modes is therefore required in the computation for higher accuracy of the dynamic responses.

2.4 Moving Load Identification

As previously introduced in section 2.2, the conventional WIM system cannot provide thorough data on the dynamic behavior of vehicle loadings. However, the time-history of axle loads is vital information to the health monitoring of bridges. In the last decade, a series of moving load identification methods has been presented. Most of these methods are based on an inverse problem of vehicle-bridge interaction by using bridge responses as input. Much research conducted on theoretical, experimental or field studies on vehicle weight or axle load determination and some accuracy improvement methods are outlined as follows.

2.4.1 Single-Span Simply Supported Bridge

Thater et al. (1998) proposed the equivalent dynamic filter technique for identification of gross vehicle weight on a bridge. This method separated the dynamic and pseudo-static response by Fast Fourier Transform. The example applications of the proposed method are shown by using computer simulation. It was found that this method is fast and improves the predicted gross truck weight up to 5% of actual weight. However, this method cannot predict the axle load of a truck. Moreover, in the case of a high-speed vehicle or short-span bridge, the vibration frequency of the bridge from the moving vehicle is close to the natural frequency of the bridge. Therefore, the filter technique cannot be used accurately.

Law et al. (1997) proposed the time-domain identification method for axle loads on the bridge by using a set of second order differential equations and identified the axle load histories by convolution in time domain. The identified moving loads were assumed to be a group of point loads with constant spacing. The solution can be obtained by performing a direct inverse of the relationship between measured responses and unknown acting loads. The study concluded that it is possible to use measured responses to identify moving forces in the time domain with good agreement between measured and calculated responses. However, the identified solution incurs large error at the times when axles approach and leave the bridge.

The frequency-time domain method was proposed by Law et al. (1999). This method identifies axle loads from only the vibration responses induced by the point loads as the input without knowledge of the vehicle characteristics. This method performs the Fourier transformation of the load-response relationship and identifies the axle load histories by using a least-square method. It was found that the maximum error of this method is up to 20 % when both measured bending moment and acceleration are used.

Chan et al. (1999) proposed a closed-form solution method to identify moving dynamic loads on bridges using the bridge responses caused by such loads. The closed-form solution can be obtained to identify the time-varying moving loads. The set of equations that led to the solution was based on Euler's beam equation, and a two-axle vehicle model was developed to generate the theoretical responses and the corresponding interactive forces. The identification error was calculated from the percentage error between the generated interactive forces and the identified force. The study found that the bridge responses used can be the bending moment as obtained from strain gauges or displacement as obtained from linear transducers. The identification from the bending moment gives better results compared with using displacement. Besides, although the problem is contaminated with noise, the acceptable solution can be obtained by performing noise filtering.

Chan et al. (2000a and 2001) theoretically and experimentally conducted comparative studies on moving force identification. A laboratory study using bridge strain responses as input in the identification was presented. A comparative study of interpretive, time-domain and frequency-time domain methods was discussed. The parametric study on related measurements and input parameters i.e. sampling frequency, number of used modes, vehicle speed level and number of sensors were

conducted to obtain the most appropriate method corresponding to the accuracy and computational time. The study concluded that the best method was the time-domain method which is the most robust method to identify the problem with higher accuracy and also capable of identifying the axle loads of high speed vehicles. Moreover, the computational time for the time-domain method is shorter than other methods.

Chan et al. (2000b) studied the moving force identification by using a prestressed concrete bridge test. A two-axle heavy vehicle was hired for the calibration test of the field measurement. The dynamic bending moments caused by both hired and in-service vehicles were acquired. Dynamic axle forces were identified by means of the time-domain method. Gross weights were obtained by summing up the equivalent static axle load of each axle calculated by performing pseudo-static load test, and were compared with those measured at the static weigh station. Results show that the axle forces can be identified with the error in results less than 10 % for both hired and in-service vehicles.

Law and Zhu (2000) conducted a comparative study on different beam models in moving force identification. The Tikhonov regularization technique was employed in the least-square formulation to provide bounds to the ill-conditioned results in the identification problem. The calculation of the optimal regularization parameter can be obtained by plotting an L-Curve as proposed by Hansen (1992). Although the problem is noise sensitivity, the obtained results from experimental testing in laboratory identified by improved algorithm were less sensitive to noise and provided satisfactory accuracy. The results also indicated that the Timoshenko beam model was found to be better than the Euler-Bernoulli beam model.

Zhu and Law (2000) presented a method to identify moving loads on a bridge deck modeled as an orthotropic rectangular plate. The dynamic behavior of the bridge deck under moving loads was analyzed using the orthotropic plate theory and modal superposition principle, and the Tikhonov regularization procedure was applied to provide bounds to the identified forces in the time domain. The identified results using a beam model and a plate model of the bridge deck were compared, and the conditions under which the bridge deck could be simplified as an equivalent beam model were discussed. Computer simulations and laboratory tests showed the effectiveness and the validity of the proposed method in identifying forces traveling along the central line or at an eccentric path on the bridge deck. However, an

appropriate regularization parameter needs to be used for the accuracy of identification.

Law, Chan and Zeng (2001) studied the identification procedure using the regularization technique. The accuracy of moving load identification was influenced by the regularization parameter. Therefore, an appropriate regularization parameter was required to accurately identify the loads. However, there were problems with this parameter because it depended on vehicle properties such as the vehicle mass, moving speed, vehicle configuration and it also involved significant effort and a long computing time to determine the optimal regularization parameter.

Law and Fang (2001) presented a new method of moving force identification by using the dynamic programming technique with a regularization parameter. The forces in the state-space formulation of the dynamic system are identified in the time domain using a recursive formula based on several distributed measurements of the responses of the structure. The results from the simulation study and laboratory work show great improvements over the previous methods in both accuracy and time consumption of identification. Similar to the previous research, it was found that the accuracy of identification depended on the appropriate regularization parameter.

European Commission DG VII – Transport: WAVE (2001) developed another identification technique for moving loads on bridge using the least-square method with optimization technique. Since the axle loads are assumed to be constants on the bridge, the parameters in the optimization become velocity, number of axles, axle spacing and total weight. A two-dimensional bridge model was used to study the effect of the eccentricity of the bridge. A field test was carried out to verify the accuracy of identification. The results show that the static load of a vehicle has error in the range of $\pm 10\%$.

Zhu and Law (2002) presented a time domain method to identify moving loads on a continuous beam from the measured structural vibration response. The regularization technique was used to provide bounds on the solution. Numerical examples demonstrated that a larger number of modes should be included in the identification when accelerations are used instead of strains. An appropriate regularization can reduce the effect of noise. This method can be used with moving load identification by time domain method and frequency-time domain method by using singular value decomposition (SVD). It was found that the regularization parameter is found to have a very important function in reducing the noise effect and

it may also be used to reduce the errors in the time domain method and frequency-time domain method.

Yu and Chan (2002) measured the bending moment responses of a bridge by using a scaled model in a laboratory. The time domain method (TDM) and frequency-time domain method (FTDM) were used for identifying the two moving wheel loads of a vehicle moving across a bridge. The pseudo-inverse matrix (PI) technique and singular value decomposition technique (SVD) were adopted for solving the over-determined system equation in the TDM and FTDM. The effects of bridge and vehicle parameters on the TDM and FTDM were also investigated. The results showed that the SVD technique can effectively improve accuracy of identification when using TDM and FTDM. However, the variation of the regularization parameter has more influence on the identification accuracy.

Zhu and Law (2002) conducted a parametric study on moving force identification as the practical aspects. The limitations and merits of two identification methods were presented. One was based on the exact solution method (ESM) and the other was based on the finite element method (FEM) with orthogonal function expression. Through simulation and laboratory, the effect of different influencing factors was studied. It was found that identification using FEM can more effectively reduce identification error than ESM due to measurement noise. In the case of the modal truncation, the FEM requires a smaller number of vibration modes than ESM at the same noise level. Both ESM and FEM provide the same order of identification error when six sensors or more are used but the error from ESM is much larger than FEM with respect to increasing noise levels. As well as other mentioned parameters, at the same sampling rate, FEM also provides lower identification error than ESM at the same noise level.

Zhu and Law (2003) applied the proposed identification method to identify moving loads on a bridge deck. The dynamic behavior of the bridge deck was analyzed using the orthotropic plate theory and mode superposition technique. The regularization technique was again employed to stabilize the computations. It was found that the method can identify moving loads with a small eccentricity and fail to identify loads with a large eccentricity. The torsional modes were found to be very important in the identification even when the group of loads was moving along the centerline of the bridge deck.

Law et al. (2004) proposed a moving load identification method based on finite element method and condensation technique. Numerical simulations and experimental results demonstrated the efficiency and accuracy of the method to identify a system of general moving loads or interaction forces between the vehicle and the bridge deck. The number of master degrees-of-freedom of the system selected should be smaller than or equal to the number of measured points, and the identified results are relatively not sensitive to the sampling frequency, velocity of vehicle, measurement noise level and road surface roughness when a minimum of eight beam elements are used to model the bridge with measured information from three measuring points.

Yu and Chan (2004) applied the time-domain and frequency-time domain methods to identify the multi-axle vehicle loads from bridge bending moment responses. Two direct solutions including the pseudo inverse and singular value decomposition methods used for over-determined set of equations were adopted. A three-axle vehicle model was designed and constructed in the laboratory for validation tests. The results showed that the identified multi-axle vehicle loads were reasonable and acceptable for both the articulated and nonarticulated vehicles. The moving force identification system could correctly identify the multi-axle vehicle loads even if the middle axle of the nonarticulated vehicles was hanging in the air. Three different types of suspension systems, i.e. rigid connection, sprung connection, and pre-compressed sprung connection between vehicle frame and axle respectively, were incorporated in the vehicle models. Results showed that the suspension systems made an obvious impact on the dynamic characteristics of vehicles and identification accuracy.

From all the mentioned methods it can be concluded that the effective moving load identification methods need an optimal regularization parameter. To obtain the appropriate parameter, significant computation effort and time are required. Moreover, it has been found that the optimal regularization parameter depends greatly on vehicle properties such as vehicle mass, velocity, vehicle configuration, etc. Therefore, in actual application, only the sub-optimal regularization parameter can be determined. To overcome this problem, a regularization method with an iterative technique called the updated static component (USC) technique was proposed (Akarawittayapoom, 2003; Pinkaew, 2006). This method decomposes the axle loads into static and dynamic components and keeps updating the static component through

the regularization of the associated dynamic component until the convergent solution is achieved.

Akarawittayapoom (2003) studied the moving load identification method using the dynamic programming method and improved the accuracy by adopting the USC technique. Computer simulation and a scaled model test in laboratory were employed to investigate the accuracy of this method and the effect of the variables to the identification method. It was found that the velocity and the roughness of the surface have more influence than other variables. The obtained results show that the accuracy of static weight identification is within the range of $\pm 5\%$.

Asnachinda (2004) and Pinkaew and Asnachinda (2007) studied the dynamic programming method to identify the truck weight using a scaled model test in the laboratory. The test investigated the effects of various factors including mass and velocity of truck, roughness of bridge surface, transverse position of truck, type of bridge support e.g. simple support and continuous bridges, and number of truck axles. Moreover, the dynamic axle loads of the truck model were measured in order to study their characteristics. It was found that using the strain obtained from averaging strains in the same section can significantly reduce the torsional effect of the bridge due to the transverse position of the truck. The identification error increases as the roughness level increases. The effect of support conditions was considered. The one-span bridge with simple supports yields better weight identification results than those from the continuous bridge. It was also found that a weight error of about $\pm 5\%$ is achieved when a two-axle truck moves on a one-span simple support bridge with a smooth surface. However, this error becomes as high as $\pm 20\%$ for the fixed end bridge with a high surface roughness.

Foongsook (2005) studied moving truck weight identification by actual field testing using the dynamic programming method with USC technique. The study considered the effects of mass, velocity, the moving path of the truck and the surface roughness of the bridge. A prestressed concrete bridge spanning 9.43 meters in length and 14 meters in width was chosen. A 10-wheel truck weighing between 20-26 tons was used. The 36 strain gauges were installed to record the strain signals during the passages of the truck for use in moving load identification. After 51 truck passages, it was found that by averaging the section strain with the weighing procedure to identify the truck weight provided sufficient identification accuracy. In general, the

identification results exhibited identification errors within $\pm 50\%$, $\pm 10\%$, $\pm 6\%$ for front axle weight, rear axle weight and total weight, respectively.

2.4.2 Multi-Span Continuous Bridge

Zhu and Law (1999) studied a continuous bridge modeled as a multi-span continuous Timoshenko beam with non-uniform cross-section. The vibration behavior of the beam under moving loads was analyzed according to Hamilton's principle with the intermediate point constraints represented by a very stiff linear spring. An identification method based on the modal superposition and least-square technique with non-negative damping coefficient was developed to identify the moving forces in time domain. The obtained computer simulation results showed that the identification error is acceptable when the number of measuring points is not less than the number of vibration modes. Moreover, the damped least-square method is better than the least squares method in suppressing the unbounded ill-conditioned forces.

Zhu and Law (2001) presented analytical vibration mode shapes with the orthogonal function to obtain the derivatives of the bridge modal responses used in moving loads identification on a multi-span bridge. This method was proposed since using assumed mode shapes often leads to unnecessary errors due to their inherent inaccuracy. The unknown moving loads were predicted from the least-square regularization method where the optimal regularization parameter was determined from the GCV method. The simulation found that the method was effective for identifying the moving loads in time domain. Acceptable solutions were obtained with some errors particularly concerning the interior supports of the multi-span bridge where the identified loads were close to zero. It was therefore suggested that more mode shapes should be used to identify the moving forces at locations close to the supports.

Zhu and Law (2003) presented a study on the effect of the moving speed of the vehicle in interaction forces identification. The time-history of a vehicle's position on the bridge is part of the required information for input in the identification system. However, in a real situation, the vehicle may not cross the bridge at a constant speed. The effect of incomplete velocity information was therefore considered. A multi-span bridge was adopted to investigate the problem. Based on the mode superposition method in response analysis and the least-square regularization method, the identified loads were determined from bridge strain and acceleration responses. The results

showed that the method can identify individual axle loads traveling at non-uniform speed with small error on both single and multi-span bridges. The accurate weight of the vehicle was also obtained for the vehicle braking on top of the bridge. In addition, it was observed that the identified results from multi-span continuous bridges are more sensitive to the noise level than those from single span bridges. There are large errors in the identified loads near the supports because of the ill-conditioning of the problem with zero force at the support. A smaller regularization parameter was suggested for use for the time duration near the support.

Zhu and Law (2005) developed a moving load identification method for a multi-span continuous bridge with elastic supports. A method based on modal superposition and regularization technique was adopted. The vertical translation and rotational springs were included in the model to simulate the elastic bearings and to support the fixity conditions of the bridge. The results from numerical examples indicated that the proposed method could identify the moving loads accurately on the multi-span bridge with elastic restraints from strain or acceleration measurements. The identification from acceleration responses is less sensitive to the measurement noise than those from strains. Vertical support stiffness has a large influence on identification error, particularly when the flexural stiffness of the beam is small. Similar to past studies, the identified forces around internal bridge supports were subject to large error with high fluctuation.

Chan and Ashebo (2006) theoretically and experimentally studied the identification of moving force on a continuous bridge. The bridge was analyzed using modal superposition satisfying all boundary conditions. The forces were identified from the least-square method without regularization through the singular value decomposition method to avoid difficulty in determination of the optimal regularization parameter and to provide robust solutions. The number and location of sensors used in the identification system were studied. The results indicated that it is possible to identify the moving load on a continuous bridge with bending moment responses. However, the identified forces around bridge supports provide large identification errors. Identification using a target span was then considered and it was found that the accuracy was improved but the time-history of the force for all systems was not completed.

2.5 Summary

From the previous research, it is found that many approaches of moving load identification have been studied and developed. The vehicle-bridge system can be solved either through modal analysis using mode superposition through the exact solution method or the finite element method. It was found that moving load identification based on system formulation employing the finite element method is more robust to noise level and appropriate for practice than the exact solution method. The simple least-square objective function has been widely used in the optimization procedure. The regularization technique has been adopted to overcome this noise sensitivity problem. The difficulty in assigning an optimal regularization can be solved through use of an updated static component (USC) technique.

Drawing on the above information summarized from early studies, this research study proposes the axle load identification of multiple vehicles traveling on a multi-span continuous bridge. The structural modeling of the vehicles and the continuous bridges employs the finite element method. The least-square function with regularization term is used as an objective function in the optimization of axle load identification. The singular value decomposition (SVD) method is adopted in order to improve solution robustness. The updated static component (USC) technique is adopted as an accuracy improvement procedure. Moreover, another contribution of this study is the consideration of multiple vehicle identification. Discussion on identification accuracy affected by different vehicle categories and various travel scenarios between two vehicles are presented through numerical study. In addition, an effectiveness investigation of the proposed method is presented through the experimental results from scaled model testing.

CHAPTER III

THEORY OF VEHICLE-BRIDGE INTERACTION AND MOVING LOADS IDENTIFICATION SYSTEM

3.1 General

This chapter explains the theoretical formulation adopted in this research. The related theoretical background of this problem mainly consists of the following three parts: (1) the vehicle-bridge interaction, (2) the identification part using the optimization method and (3) the additional modification part for accuracy improvement using a numerical technique. Initially, from the physical characteristic information of vehicles and bridge, the mathematical model for describing their dynamic interaction is simulated. Then the relationship between the moving loads and bridge responses is formulated to obtain the theoretical bridge responses induced by the passage of heavy vehicles used in the optimization against the measured responses. Later, assigning vehicles axle spacing, moving speed and measured responses as the input, the optimization process is used to identify the most feasible moving loads producing least residual error in the objective function. Finally, an accuracy improvement technique is adopted in order to overcome the mathematical weakness of the solution.

3.2 Dynamics of Vehicle-Bridge Interaction System

To construct the mathematical model of the vehicle-bridge system, it is essential to understand the behavior of the interaction between the vehicles and the bridge to depict its principal characteristics. Generally, there are two approaches to simulating the dynamic interaction response between bridge and vehicle. The first is solved by the uncoupled iteration method. The bridge and vehicle system is solved separately and uses an iterative process in each time step to find the equilibrium between the bridge and vehicle interaction. The other approach to simulate the vehicle-bridge interaction is to solve the fully coupled system of bridge and vehicle. In this research, the latter approach is employed to simulate the dynamic interaction response because it can assemble the bridge and vehicle into one coupled system which can be simultaneously solved at each time step without any iteration.

3.2.1 Finite Element Method of Structural Formulation

The vehicle-bridge system can be simulated in the modal decomposition analysis method but is subject to modal truncation error in the dynamic response. Besides, it is difficult to apply a method based on the continuous system and modal superposition technique to complicated structures. Therefore, the dynamic response analysis for discrete system is preferred in this research since the bridge structure is complicated, especially when the multi-span continuous bridges are considered. The finite element method is then adopted in the vehicle-bridge interaction model of the simulation system and also in the bridge model of the identification system.

Modeling accuracy has been studied against the degree discretization of the structure for a moving load analysis (Reiker et al., 1996). It was noted that beams with various boundary conditions, including intermediate supports, and subjected to a moving load system with a general movement profile and external excitation can be successfully analyzed with accurate responses compared to those obtained from modal superposition analysis (Lin and Trethewy, 1990). In addition, the simulated responses are relatively not sensitive to the sampling frequency and number of data (Zhu and Law, 2004).

3.2.2 Assumptions concerning the Dynamics System

The following assumptions are made concerning the dynamics system of the vehicle-bridge model.

1. The bridge behavior under acting loads is assumed as linear elastic.
2. The changes in the system characteristics such as stiffness, damping and mass matrices of the vehicle and the bridge during the passage of vehicles are negligible.
3. Structural damping is included in the analysis.
4. The bridge structure may not be at rest before the application of loads.
5. There is no restriction on the type of force history to be identified.
6. The Euler-Bernoulli beam model is used with the shear effect neglected.

3.2.3 Vehicle Model

Figure 3.1 shows a vehicle-bridge model in which a vehicle moves over a bridge at a speed $v(t)$. The four degree-of-freedom vehicle models consisting of vertical displacement, rotation of vehicle mass, vertical displacement of front and rear

axle suspension mass presented by Mulcahy (1983) are studied. The equation of the motion of the vehicle can be derived using the equilibrium of the vehicle system in each degree-of-freedom as shown in Figure 3.2.

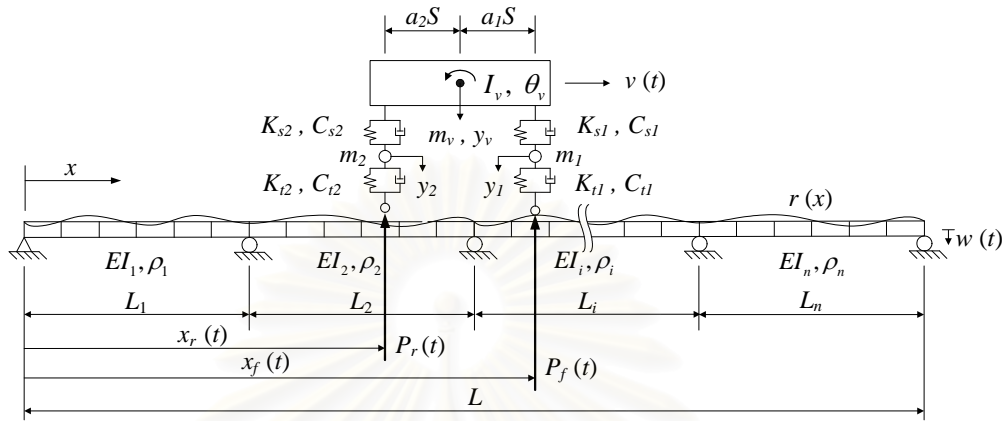


Figure 3.1 Vehicle-bridge system of n -span continuous bridge

Let

m_v	=	mass of the vehicle
I_v	=	mass rotational moment of inertia of the vehicle
m_1	=	mass of front axle suspension
m_2	=	mass of rear axle suspension
K_{s1}, K_{s2}	=	suspension stiffness of front and rear axle
C_{s1}, C_{s2}	=	suspension damping of front and rear axle
K_{t1}, K_{t2}	=	tire stiffness of front and rear axle
C_{t1}, C_{t2}	=	tire damping of front and rear axle
S	=	axle spacing
L	=	span length of bridge
$x_f(t), x_r(t)$	=	positions of the front and rear axle respectively at time t
$P_f(t), P_r(t)$	=	front and rear axle force respectively at time t
v	=	velocity of vehicle
θ_v	=	rotation of vehicle mass
y_v	=	vertical displacement of vehicle
y_1, y_2	=	vertical displacement of front and rear suspension mass

- $w(t)$ = vertical dynamic deflection of bridge
 $r(x)$ = road surface roughness at the location x
 a_1, a_2 = center of gravity ratio of vehicle from front and rear axle.

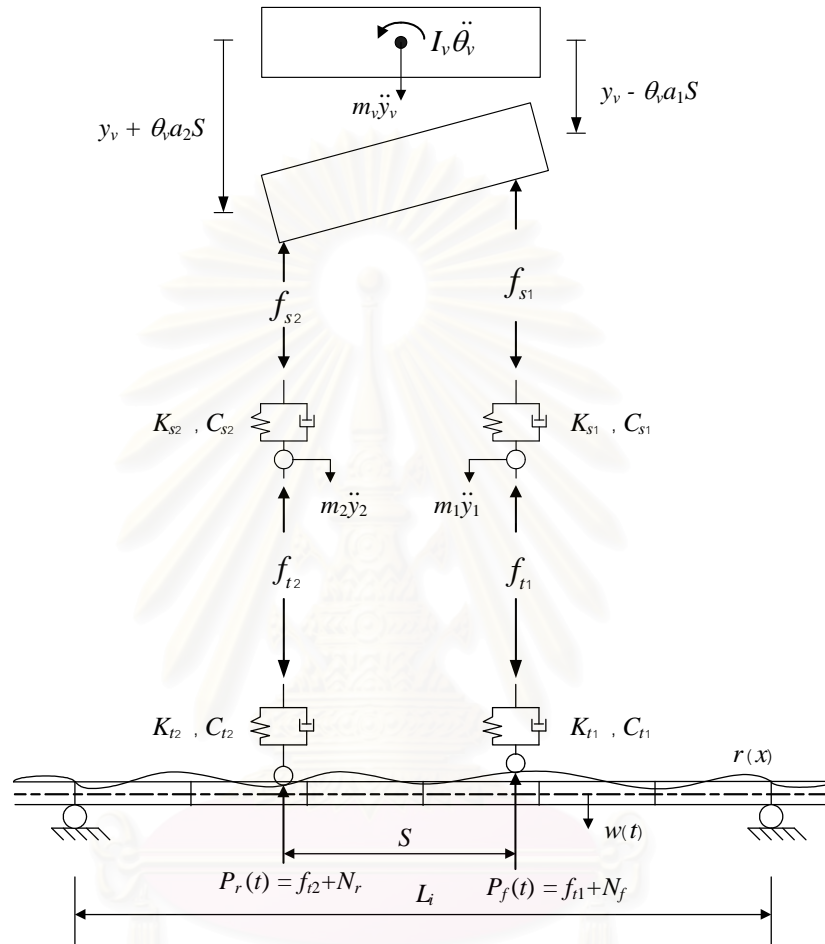


Figure 3.2 Free body diagram of vehicle-bridge system

Consider the vertical force equilibrium of vehicle mass:

$$\sum F = m_v \ddot{y}_v \quad ; \quad -f_{s1} - f_{s2} = m_v \ddot{y}_v \quad (3.1)$$

where

$$\begin{aligned}
 f_{s1} &= K_{s1}(y_v - \theta_v a_1 S - y_1) + C_{s1}(\dot{y}_v - \dot{\theta}_v a_1 S - \dot{y}_1) \\
 f_{s2} &= K_{s2}(y_v + \theta_v a_2 S - y_2) + C_{s2}(\dot{y}_v + \dot{\theta}_v a_2 S - \dot{y}_2).
 \end{aligned}$$

Substituting f_{s1}, f_{s2} in Eq. (3.1), the equilibrium of vertical motion of vehicle mass becomes:

$$\begin{aligned}
& m_v \ddot{y}_v + (C_{s1} + C_{s2}) \dot{y}_v + (K_{s1} + K_{s2}) y_v \\
& + (-C_{s1} a_1 S + C_{s2} a_2 S) \dot{\theta}_v + (-K_{s1} a_1 S + K_{s2} a_2 S) \theta_v \\
& + (-C_{s1}) \dot{y}_1 + (-K_{s1}) y_1 + (-C_{s2}) \dot{y}_2 + (-K_{s2}) y_2 = 0
\end{aligned} \tag{3.2}$$

Consider rotation of vehicle mass at center of gravity:

$$\sum M_c = I_v \ddot{\theta}_v \quad ; \quad f_{s1} a_1 S - f_{s2} a_2 S = I_v \ddot{\theta}_v \tag{3.3}$$

Substituting f_{s1}, f_{s2} in Eq. (3.3), the equilibrium of rotation of vehicle mass becomes:

$$\begin{aligned}
& I_v \ddot{\theta}_v + (-C_{s1} a_1 S + C_{s2} a_2 S) \dot{y}_v + (-K_{s1} a_1 S + K_{s2} a_2 S) y_v \\
& + (C_{s1} a_1^2 S^2 + C_{s2} a_2^2 S^2) \dot{\theta}_v + (K_{s1} a_1^2 S^2 + K_{s2} a_2^2 S^2) \theta_v \\
& + (C_{s1} a_1 S) \dot{y}_1 + (K_{s1} a_1 S) y_1 + (-C_{s2} a_2 S) \dot{y}_2 + (-K_{s2} a_2 S) y_2 = 0
\end{aligned} \tag{3.4}$$

Consider the vertical equilibrium of suspension mass m_1 :

$$\sum F = m_1 \ddot{y}_1 \quad ; \quad f_{s1} - f_{t1} = m_1 \ddot{y}_1 \tag{3.5}$$

where

$$\begin{aligned}
f_{t1} &= K_{t1} (y_1 - \Delta_1) + C_{t1} (\dot{y}_1 - \dot{\Delta}_1) \\
\Delta_1 &= (w_1(x_f(t), t) + r(x_f(t))) \\
\dot{\Delta}_1 &= (\dot{w}_1(x_f(t), t) + \dot{r}(x_f(t)))
\end{aligned} \tag{3.6}$$

Substituting f_{s1}, f_{t1} in Eq. (3.5), the equilibrium of vertical motion of suspension mass m_1 becomes:

$$\begin{aligned}
& m_1 \ddot{y}_1 + (-C_{s1}) \dot{y}_v + (-K_{s1}) y_v + (C_{s1} a_1 S) \dot{\theta}_v + (K_{s1} a_1 S) \theta_v \\
& + (C_{s1}) \dot{y}_1 + (K_{s1}) y_1 = -f_{t1}
\end{aligned} \tag{3.7}$$

Consider the vertical equilibrium of suspension mass m_2 :

$$\sum F = m_2 \ddot{y}_2 \quad ; \quad f_{s2} - f_{t2} = m_2 \ddot{y}_2 \tag{3.8}$$

where

$$f_{t2} = K_{t2}(y_2 - \Delta_2) + C_{t2}(\dot{y}_2 - \dot{\Delta}_2)$$

$$\Delta_2 = (w_2(x_r(t), t) + r(x_r(t))) \quad (3.9)$$

$$\dot{\Delta}_2 = (\dot{w}_1(x_r(t), t) + \dot{r}(x_r(t)))$$

Substituting f_{s2}, f_{t2} in Eq. (3.8), the equilibrium of vertical motion of suspension mass m_2 becomes:

$$\begin{aligned} m_2 \ddot{y}_2 + (-C_{s2}) \dot{y}_v + (-K_{s2}) \dot{y}_v + (-C_{s2} a_2 S) \dot{\theta}_v + (-K_{s2} a_2 S) \theta_v \\ + (C_{s2}) \dot{y}_2 + (K_{s2}) y_2 = -f_{t2} \end{aligned} \quad (3.10)$$

Thus, the equations of motion for the vehicle can be written in matrix form based on Eq. (3.2), (3.4), (3.7) and (3.10) as follows:

$$\mathbf{M}_v \ddot{\mathbf{Y}}(t) + \mathbf{C}_v \dot{\mathbf{Y}}(t) + \mathbf{K}_v \mathbf{Y}(t) = \mathbf{P}_v(t) \quad (3.11)$$

where

$$\mathbf{M}_v = \begin{bmatrix} m_v & 0 & 0 & 0 \\ 0 & I_v & 0 & 0 \\ 0 & 0 & m_1 & 0 \\ 0 & 0 & 0 & m_2 \end{bmatrix}$$

$$\mathbf{C}_v = \begin{bmatrix} C_{s1} + C_{s2} & (-C_{s1} a_1 + C_{s2} a_2) S & -C_{s1} & -C_{s2} \\ (-C_{s1} a_1 + C_{s2} a_2) S & (C_{s1} a_1^2 + C_{s2} a_2^2) S & C_{s1} a_1 S & -C_{s2} a_2 S \\ -C_{s1} & C_{s1} a_1 S & C_{s1} & 0 \\ -C_{s2} & -C_{s2} a_2 S & 0 & C_{s2} \end{bmatrix}$$

$$\mathbf{K}_v = \begin{bmatrix} K_{s1} + K_{s2} & (-K_{s1} a_1 + K_{s2} a_2) S & -K_{s1} & -K_{s2} \\ (-K_{s1} a_1 + K_{s2} a_2) S & (K_{s1} a_1^2 + K_{s2} a_2^2) S & K_{s1} a_1 S & -K_{s2} a_2 S \\ -K_{s1} & K_{s1} a_1 S & K_{s1} & 0 \\ -K_{s2} & -K_{s2} a_2 S & 0 & K_{s2} \end{bmatrix}$$

$$\mathbf{Y}(t) = \{y_v(t) \quad \theta_v(t) \quad y_1(t) \quad y_2(t)\}^T$$

\mathbf{P}_v is the force terms containing the interaction force vector and static force vector as follows:

$$\mathbf{P}_v(t) = -\begin{Bmatrix} \mathbf{0} \\ \mathbf{P}_{int}(t) \end{Bmatrix} + \begin{Bmatrix} \mathbf{0} \\ \mathbf{M}_s \end{Bmatrix} = -\begin{Bmatrix} 0 \\ 0 \\ P_f(t) \\ P_r(t) \end{Bmatrix} + \begin{Bmatrix} 0 \\ 0 \\ N_f \\ N_r \end{Bmatrix}$$

$$P_f(t) = (f_{t1}(t) + N_f) = K_{t1}(y_1(t) - \Delta_1(t)) + C_{t1}(\dot{y}_1(t) - \dot{\Delta}_1(t)) + N_f$$

$$P_r(t) = (f_{t2}(t) + N_r) = K_{t2}(y_2(t) - \Delta_2(t)) + C_{t2}(\dot{y}_2(t) - \dot{\Delta}_2(t)) + N_r$$

$$N_f = (m_1 + a_2 m_v)g$$

$$N_r = (m_2 + a_1 m_v)g$$

3.2.4 Bridge Model

The bridge structure is considered as an n -spans continuous bridge and is discretized by the finite element method using beam elements as shown in Figure 3.2. The finite beam element has 2 nodes with respect to 4 degree-of-freedom in vertical displacement and rotational displacement at both ends as shown in Figure 3.3.

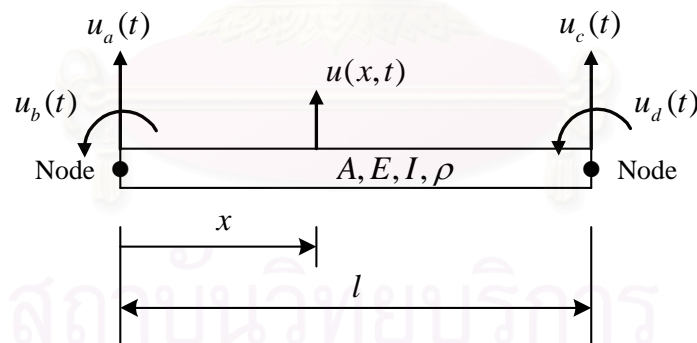


Figure 3.3 A finite beam element with 4 degree-of-freedom

Where

- A = cross-section area of beam element
- E = modulus of elasticity of beam element
- I = moment of inertia of beam element
- ρ = mass per unit length of beam element
- l = length of beam element

Let $u(x,t)$ is the deflection of the bridge at distance x at time t . Thus, the governing equation of beam at position x and at time t can be expressed by:

$$\frac{\partial^2}{\partial x^2} \left[EI \frac{\partial^2 u(x,t)}{\partial x^2} \right] = 0. \quad (3.12)$$

For the bridge having constant EI , Eq. (3.12) can be rewritten as:

$$\frac{\partial^4 u(x,t)}{\partial x^4} = 0 \quad (3.13)$$

The solution of Eq. (3.13) can be expressed in polynomial form as:

$$u(x,t) = c_1(t)x^3 + c_2(t)x^2 + c_3(t)x + c_4(t) \quad (3.14)$$

where $c_i(t)$ is the coefficient of the polynomial form with constant value.

The boundary conditions of beam element are:

$$\begin{aligned} u(0,t) &= u_1(t) & u(l,t) &= u_3(t) \\ \frac{\partial u(0,t)}{\partial x} &= u_2(t) & \frac{\partial u(l,t)}{\partial x} &= u_4(t) \end{aligned} \quad (3.15)$$

Substituting (3.15) in Eq. (3.14), the constant values become:

$$\begin{aligned} c_4(t) &= u_1(t) \\ c_3(t) &= u_2(t) \\ c_2(t) &= \frac{1}{l^2} [3(u_3 - u_1) - l(2u_2 + u_4)] \\ c_1(t) &= \frac{1}{l^3} [2(u_1 - u_3) - l(u_2 + u_4)]. \end{aligned} \quad (3.16)$$

Substituting (3.16) in Eq. (3.14), the displacement equation of beam element at position x and at time t can be expressed as follows:

$$\begin{aligned} u(x,t) &= \left[1 - \frac{3x^2}{l^2} + \frac{2x^3}{l^3} \right] u_1(t) + l \left[\frac{x}{l} - \frac{2x^2}{l^2} + \frac{x^3}{l^3} \right] u_2(t) \\ &+ \left[\frac{3x^2}{l^2} - \frac{2x^3}{l^3} \right] u_3(t) + l \left[-\frac{x^2}{l^2} + \frac{x^3}{l^3} \right] u_4(t) \end{aligned} \quad (3.17)$$

It is noted that the coefficient terms in front of $u_i(t)$ are the shape functions of the displacements of the beam element.

The mass matrix of the beam element can be formulated by introducing Eq. (3.17) into the kinetic energy equation as:

$$T(t) = \frac{1}{2} \int_0^l \rho A \left[\frac{\partial u(x,t)}{\partial t} \right]^2 dx \quad (3.18)$$

Thus, Eq. (3.18) can be rewritten in the form:

$$T(t) = \frac{1}{2} \dot{\mathbf{u}}^T \mathbf{M} \dot{\mathbf{u}} \quad (3.19)$$

The matrix \mathbf{M} is the elemental mass matrix and $\dot{\mathbf{u}}$ is the time derivative of the elemental displacement vector $\mathbf{u}(t)$ defined as:

$$\mathbf{u}(t) = \begin{bmatrix} u_1(t) \\ u_2(t) \\ u_3(t) \\ u_4(t) \end{bmatrix} \quad (3.20)$$

Equating Eq. (3.18) to Eq. (3.19) with help of Eq. (3.20), the elemental mass matrix of beam element is:

$$\mathbf{M} = \frac{\rho A l}{420} \begin{bmatrix} 156 & 22l & 54 & -13l \\ 22l & 4l^2 & 13l & -3l^2 \\ 54 & 13l & 156 & -22l \\ -13l & -3l^2 & -22l & 4l^2 \end{bmatrix} \quad (3.21)$$

The stiffness matrix can be determined by replacing Eq. (3.17) into strain energy equation:

$$V(t) = \frac{1}{2} \int_0^l EI \left[\frac{\partial^2 u(x,t)}{\partial x^2} \right]^2 dx \quad (3.22)$$

The Eq. (3.22) can be rewritten as:

$$V(t) = \frac{1}{2} \mathbf{u}^T \mathbf{K} \mathbf{u}. \quad (3.23)$$

$\mathbf{u}(t)$ is defined in (3.20), The stiffness matrix of the beam element becomes:

$$\mathbf{K} = \frac{EI}{l^3} \begin{bmatrix} 12 & 6l & -12 & 6l \\ 6l & 4l^2 & -6l & 2l^2 \\ -12 & -6l & 12 & -6l \\ 6l & 2l^2 & -6l & 4l^2 \end{bmatrix} \quad (3.24)$$

The elemental damping matrix of the bridge system is derived by the free vibration system as follows:

$$\mathbf{M}\ddot{\mathbf{u}} + \mathbf{C}\dot{\mathbf{u}} + \mathbf{K}\mathbf{u} = 0 \quad (3.25)$$

Multiplying both sides by the inverse of mass matrix, \mathbf{M}^{-1} , the Eq.(3,25) yields:

$$\ddot{\mathbf{u}} + \bar{\mathbf{C}}\dot{\mathbf{u}} + \bar{\mathbf{K}}\mathbf{u} = 0 \quad (3.26)$$

where

$$\begin{aligned} \bar{\mathbf{C}} &= \mathbf{M}^{-1}\mathbf{C} \\ \bar{\mathbf{K}} &= \mathbf{M}^{-1}\mathbf{K}. \end{aligned}$$

Transforming \mathbf{u} to modal coordinate vector, \mathbf{q} , as :

$$\mathbf{u} = \mathbf{V}\mathbf{q} \quad (3.27)$$

In which, the vector \mathbf{V} is the eigenvector of matrix $\bar{\mathbf{K}}$.

Substituting Eq. (3.27) into Eq. (3.26) and multiplying by \mathbf{V}^{-1} , it is found that:

$$\mathbf{I}\ddot{\mathbf{q}} + \mathbf{V}^{-1}\bar{\mathbf{C}}\mathbf{V}\dot{\mathbf{q}} + \mathbf{V}^{-1}\bar{\mathbf{K}}\mathbf{V}\mathbf{q} = 0 \quad (3.28)$$

$$\mathbf{I}\ddot{\mathbf{q}} + \mathbf{C}^*\dot{\mathbf{q}} + \mathbf{K}^*\mathbf{q} = 0 \quad (3.29)$$

where

$$\begin{aligned} \mathbf{K}^* &= \mathbf{V}^{-1}\bar{\mathbf{K}}\mathbf{V} \\ &= \begin{bmatrix} \omega_1^2 & 0 & \cdots & 0 \\ 0 & \omega_2^2 & \ddots & \vdots \\ \vdots & \ddots & \ddots & 0 \\ 0 & \cdots & 0 & \omega_n^2 \end{bmatrix} \end{aligned} \quad (3.30)$$

Assuming \mathbf{C}^* has an orthogonality property like matrix \mathbf{K}^* , yields:

$$\begin{aligned} \mathbf{C}^* &= \mathbf{V}^{-1}\bar{\mathbf{C}}\mathbf{V} \\ &= \begin{bmatrix} 2\xi_1\omega_1 & 0 & \cdots & 0 \\ 0 & 2\xi_2\omega_2 & \ddots & \vdots \\ \vdots & \ddots & \ddots & 0 \\ 0 & \cdots & 0 & 2\xi_n\omega_n \end{bmatrix} \end{aligned} \quad (3.31)$$

where

ξ_i = damping ratio of the corresponding i^{th} mode shape

ω_i = natural frequency of the corresponding i^{th} mode shape.

Thus, the matrices $\bar{\mathbf{C}}$ and \mathbf{C}^* can be obtained as follows:

$$\bar{\mathbf{C}} = \mathbf{V}\mathbf{C}^*\mathbf{V}^{-1} \quad (3.32)$$

$$\mathbf{C} = \mathbf{M}\bar{\mathbf{C}} \quad (3.33)$$

Therefore, the equation of motion for the bridge can be written as:

$$\mathbf{M}_b \ddot{\mathbf{R}}(t) + \mathbf{C}_b \dot{\mathbf{R}}(t) + \mathbf{K}_b \mathbf{R}(t) = \mathbf{P}_b(t) \quad (3.34)$$

where \mathbf{M}_b = assembled mass matrix of the bridge
 \mathbf{C}_b = assembled damping matrix of the bridge
 \mathbf{K}_b = assembled stiffness matrix of the bridge
 $\mathbf{R}(t)$ = global response vector of the bridge
and $\mathbf{P}_b(t)$ = external acting load vector of the bridge

The external acting load vector of the bridge is the interaction force transformed to be the nodal loads of the bridge's degree-of-freedom.

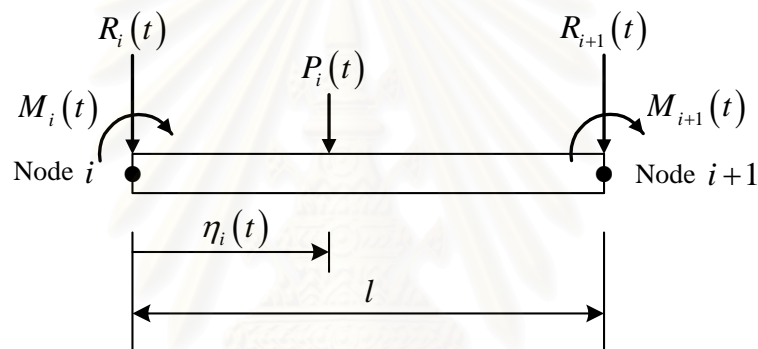


Figure 3.4 Nodal loads from external load

Figure 3.4 shows the beam element with an acting load and its equivalent nodal loads

where $\eta_i(t)$ = the distance of the external acting load $P_i(t)$ from the left node of the beam element.

The nodal loads from external load as shown in Figure 3.4 can be expressed as:

$$R_i(t) = \left(1 - \frac{3\eta_i(t)^2}{l^2} + \frac{2\eta_i(t)^3}{l^3} \right) P_i(t)$$

$$M_i(t) = \left(\eta_i(t) - \frac{2\eta_i(t)^2}{l} + \frac{\eta_i(t)^3}{l^2} \right) P_i(t)$$

$$R_{i+1}(t) = \left(\frac{3\eta_i(t)^2}{l^2} - \frac{2\eta_i(t)^3}{l^3} \right) P_i(t)$$

$$M_{i+1}(t) = \left(\frac{\eta_i(t)^3}{l^2} - \frac{\eta_i(t)^2}{l} \right) P_i(t) \quad (3.35)$$

where

$R_i(t), R_{i+1}(t)$ = vertical load of node i^{th} and $i+1^{th}$ of the element respectively

M_i, M_{i+1} = bending moment of node i^{th} and $i+1^{th}$ of the element

respectively.

From the above equations, the shape function of the j^{th} element used to transform the external acting load to the nodal load vector can be written as:

$$\mathbf{H}_j = \left\{ 1 - 3\left(\frac{\eta}{l}\right)^2 + 2\left(\frac{\eta}{l}\right)^3 \quad \eta\left(\frac{\eta}{l} - 1\right)^2 \quad 3\left(\frac{\eta}{l}\right)^2 - 2\left(\frac{\eta}{l}\right)^3 \quad \eta\left(\frac{\eta}{l}\right)^2 - \frac{\eta^2}{l} \right\}^T. \quad (3.36)$$

In case of the global external load shape function, the Eq. (3.36) can be expanded in the following form

$$\mathbf{H}_c = \left\{ \begin{array}{cccccccc} 0 & \cdots & 0 & \cdots & 0 & \cdots & \mathbf{H}_1 & \cdots & 0 \\ 0 & \cdots & 0 & \cdots & \mathbf{H}_i & \cdots & 0 & \cdots & 0 \\ 0 & \cdots & \mathbf{H}_{N_p} & \cdots & 0 & \cdots & 0 & \cdots & 0 \end{array} \right\}^T \quad (3.37)$$

where

\mathbf{H}_c = an $NN \times N_p$ matrix with zero entries except at the degree-of-freedoms corresponding to the nodal displacements of the beam elements on which the load is acting,

NN = the number of degree-of-freedoms of the bridge after considering the boundary condition

and N_p = the number of external acting loads.

From the Eq. (3.37), the interaction force between the vehicle and the bridge can be transformed to be the nodal loads by using the relationship between the nodal load and the global load as follows:

$$\mathbf{P}_b(t) = \mathbf{H}_c(x(t)) \cdot \mathbf{P}_{int}(t) \quad (3.38)$$

$$\mathbf{P}_{int}(t) = \{P_1(t), P_2(t), \dots, P_{N_p}(t)\}^T \quad (3.39)$$

where

$\mathbf{P}_b(t)$ = nodal load vector of bridge

$\mathbf{H}_c(x(t))$ = transformation vector from external loads to nodal loads
 $\mathbf{P}_{int}(t)$ = vehicle-bridge interaction force vector with respect to number of axles.

Therefore, the equation of motion of the bridge can be rewritten as:

$$\mathbf{M}_b \ddot{\mathbf{R}}(t) + \mathbf{C}_b \dot{\mathbf{R}}(t) + \mathbf{K}_b \mathbf{R}(t) = \mathbf{H}_c(x(t)) \mathbf{P}_{int}(t) \quad (3.40)$$

3.2.5 Bridge Surface Roughness

In this research, the road surface roughness as given in the ISO-8606 specification is adopted. It is often related to the vehicle speed which is described by the velocity power spectrum density (PSD) and the displacement PSD. The general form of the displacement PSD of the road roughness surface is given as:

$$S_d(f) = S_d(f_0) \left(\frac{f}{f_0} \right)^{-\alpha} \quad (3.41)$$

where f_0 is the reference spatial frequency (= 0.1 cycles/m); α is an exponent of the PSD, and f is the spatial frequency (cycles/m). Eq. (3.41) gives an estimate on the degree of the roughness of the road by the $S_d(f_0)$ value. This classification is made by assuming a constant vehicle velocity PSD and taking $\alpha = 2$. The ISO specification also gives the PSDs for different classes of roads.

Based on this ISO specification, the road surface roughness in the time domain can be simulated by applying the inverse fast Fourier transformation on $S_d(f_0)$ as follows:

$$r(x) = \sum_{i=1}^N \sqrt{4S(f_i)\Delta f} \cos(2\pi f_i x + \theta_i) \quad (3.42)$$

where $f_i = i\Delta f$ is the spatial frequency, $\Delta f = 1/(N\Delta)$, Δ is the distance interval between successive ordinates of the surface profile, N is the number of data points, and θ_i is a set of independent random phase angles uniformly distributed between 0 and 2π .

3.2.6 Vehicle-Bridge Interaction

To formulate the vehicle-bridge interaction as the equation of motion of the vehicle-bridge system, all degree-of-freedom, both for vehicle and bridge, must be

solved simultaneously. Therefore, the equation of motion of the vehicle-bridge system is the combination of mass, damping, stiffness and interaction force terms corresponding to all degree-of-freedom.

From the equation of motion of the vehicle and the bridge, in the case of the number of axles, $N_p = 2$, recalling the interaction force vector as:

$$\begin{aligned} \mathbf{P}_{int}(t) &= \begin{Bmatrix} P_f(t) \\ P_r(t) \end{Bmatrix} \\ &= \begin{Bmatrix} K_{t1}(y_1(t) - w_1(x_f(t), t) - r(x_f(t))) + C_{t1}(\dot{y}_1(t) - \dot{w}_1(x_f(t), t) - \dot{r}(x_f(t))) \\ K_{t2}(y_2(t) - w_2(x_r(t), t) - r(x_r(t))) + C_{t2}(\dot{y}_2(t) - \dot{w}_2(x_r(t), t) - \dot{r}(x_r(t))) \end{Bmatrix} \\ &\quad + \begin{Bmatrix} (m_1 + a_2 m_v)g \\ (m_2 + a_1 m_v)g \end{Bmatrix} \end{aligned} \quad (3.43)$$

It is noticed that the above interaction force term consists of degree-of-freedom for both vehicle and bridge. Thus the equation of motion of the vehicle and bridge must be rearranged as follows:

Once the response of the bridge, $\mathbf{R}(t)$ is obtained, the deflection of the bridge at position x and at time t can be calculated from:

$$w(x, t) = \mathbf{H}_c^T(x(t)) \cdot \mathbf{R}(t) \quad (3.44)$$

The time derivative of the bridge's deflection is

$$\dot{w}(x, t) = \frac{\partial \mathbf{H}_c^T(x(t))}{\partial x} \cdot \mathbf{R}(t) \cdot \dot{x}(t) + \mathbf{H}_c^T(x(t)) \cdot \dot{\mathbf{R}}(t). \quad (3.45)$$

Substituting Eq. (3.44) and (3.45) in Eq. (3.43) yields

$$\begin{aligned} P_f(t) &= K_{t1}(y_1(t) - \mathbf{H}_c^T(x_f(t)) \cdot \mathbf{R}(t) - r(x_f(t))) \\ &\quad + C_{t1} \left(\dot{y}_1(t) - \frac{\partial \mathbf{H}_c^T(x_f(t))}{\partial x} \cdot \mathbf{R}(t) \cdot v(t) - \mathbf{H}_c^T(x_f(t)) \cdot \dot{\mathbf{R}}(t) \right) + (m_1 + a_2 m_v)g \\ P_r(t) &= K_{t2}(y_2(t) - \mathbf{H}_c^T(x_r(t)) \cdot \mathbf{R}(t) - r(x_r(t))) \\ &\quad + C_{t2} \left(\dot{y}_2(t) - \frac{\partial \mathbf{H}_c^T(x_r(t))}{\partial x} \cdot \mathbf{R}(t) \cdot v(t) - \mathbf{H}_c^T(x_r(t)) \cdot \dot{\mathbf{R}}(t) \right) + (m_2 + a_1 m_v)g \end{aligned} \quad (3.46)$$

The Eq. (3.46) can be rewritten in matrix form as:

$$\begin{aligned}
\begin{Bmatrix} P_f(t) \\ P_r(t) \end{Bmatrix} &= \begin{bmatrix} K_{t1} & 0 \\ 0 & K_{t2} \end{bmatrix} \cdot \begin{Bmatrix} y_1(t) \\ y_2(t) \end{Bmatrix} + \begin{bmatrix} C_{t1} & 0 \\ 0 & C_{t2} \end{bmatrix} \cdot \begin{Bmatrix} \dot{y}_1(t) \\ \dot{y}_2(t) \end{Bmatrix} \\
&- \begin{bmatrix} K_{t1} \cdot \mathbf{H}_c^T(x_f(t)) + C_{t1} \cdot v(t) \cdot \frac{\partial \mathbf{H}_c^T(x_f(t))}{\partial x} \\ K_{t2} \cdot \mathbf{H}_c^T(x_r(t)) + C_{t2} \cdot v(t) \cdot \frac{\partial \mathbf{H}_c^T(x_r(t))}{\partial x} \end{bmatrix} \cdot \{\mathbf{R}(t)\} \\
&- \begin{bmatrix} C_{t1} \cdot \mathbf{H}_c^T(x_f(t)) \\ C_{t2} \cdot \mathbf{H}_c^T(x_r(t)) \end{bmatrix} \cdot \{\dot{\mathbf{R}}(t)\} - \begin{Bmatrix} K_{t1} \cdot r(x_f(t)) \\ K_{t2} \cdot r(x_r(t)) \end{Bmatrix} + \begin{Bmatrix} (m_1 + a_2 m_v) \cdot g \\ (m_2 + a_1 m_v) \cdot g \end{Bmatrix}
\end{aligned} \tag{3.47}$$

Introducing Eq. (3.47) into the vehicle's equation of motion (3.11), the equilibrium for the vehicle's degree-of-freedom becomes

$$\begin{aligned}
&\begin{bmatrix} \mathbf{0} & \mathbf{0} & \mathbf{0} \\ \mathbf{0} & \mathbf{M}_{v1} & \mathbf{0} \\ \mathbf{0} & \mathbf{0} & \mathbf{M}_{v2} \end{bmatrix} \begin{Bmatrix} \ddot{\mathbf{R}} \\ \ddot{\mathbf{Y}} \end{Bmatrix} + \begin{bmatrix} \mathbf{0} & \mathbf{0} & \mathbf{0} \\ \mathbf{0} & \mathbf{C}_{v11} & \mathbf{C}_{v12} \\ -\mathbf{C}_t \cdot \mathbf{H}^T(x) & \mathbf{C}_{v21} & \mathbf{C}_{v22} + \mathbf{C}_t \end{bmatrix} \begin{Bmatrix} \dot{\mathbf{R}} \\ \dot{\mathbf{Y}} \end{Bmatrix} \\
&+ \begin{bmatrix} \mathbf{0} & \mathbf{0} \\ \mathbf{0} & \mathbf{K}_{v11} & \mathbf{K}_{v12} \\ -\mathbf{K}_t \cdot \mathbf{H}^T - \mathbf{C}_t \cdot v \cdot \partial \mathbf{H}^T(x) / \partial x & \mathbf{K}_{v21} & \mathbf{K}_{v22} + \mathbf{K}_t \end{bmatrix} \begin{Bmatrix} \mathbf{R} \\ \mathbf{Y} \end{Bmatrix} = \begin{Bmatrix} \mathbf{0} \\ \mathbf{0} \\ -\mathbf{K}_t \cdot \mathbf{r}(x) \end{Bmatrix}
\end{aligned} \tag{3.48}$$

where

$$\begin{aligned}
\mathbf{M}_{v1} &= \begin{bmatrix} m_v & 0 \\ 0 & I_v \end{bmatrix}; \mathbf{M}_{v2} = \begin{bmatrix} m_1 & 0 \\ 0 & I_2 \end{bmatrix} \\
\mathbf{C}_{v11} &= \begin{bmatrix} C_{s1} + C_{s2} & (-C_{s1}a_1 + C_{s2}a_2)S \\ (-C_{s1}a_1 + C_{s2}a_2)S & (C_{s1}a_1^2 + C_{s2}a_2^2)S^2 \end{bmatrix}; \\
\mathbf{C}_{v12} &= \begin{bmatrix} -C_{s1} & -C_{s2} \\ C_{s1}a_1S & -C_{s2}a_2S \end{bmatrix}; \mathbf{C}_{v21} = \begin{bmatrix} -C_{s1} & C_{s1}a_1S \\ -C_{s2} & -C_{s2}a_2S \end{bmatrix}; \\
\mathbf{C}_{v22} &= \begin{bmatrix} C_{s1} & 0 \\ 0 & C_{s2} \end{bmatrix}; \mathbf{K}_{v11} = \begin{bmatrix} K_{s1} + K_{s2} & (-K_{s1}a_1 + K_{s2}a_2)S \\ (-K_{s1}a_1 + K_{s2}a_2)S & (K_{s1}a_1^2 + K_{s2}a_2^2)S^2 \end{bmatrix}; \\
\mathbf{K}_{v12} &= \begin{bmatrix} -K_{s1} & -K_{s2} \\ K_{s1}a_1S & -K_{s2}a_2S \end{bmatrix}; \mathbf{K}_{v21} = \begin{bmatrix} -K_{s1} & K_{s1}a_1S \\ -K_{s2} & -K_{s2}a_2S \end{bmatrix}; \\
\mathbf{K}_{v22} &= \begin{bmatrix} K_{s1} & 0 \\ 0 & K_{s2} \end{bmatrix}; \mathbf{C}_t = \begin{bmatrix} C_{t1} & 0 \\ 0 & C_{t2} \end{bmatrix}; \mathbf{K}_t = \begin{bmatrix} K_{t1} & 0 \\ 0 & K_{t2} \end{bmatrix}; \\
\mathbf{r} &= \begin{Bmatrix} r(x_f(t)) \\ r(x_r(t)) \end{Bmatrix}; \mathbf{Y} = \{y_v \quad \theta_v \quad y_1 \quad y_2\}^T.
\end{aligned}$$

Similar to Eq. (3.48), introducing Eq. (3.47) into the bridge's equation of motion Eq. (3.40), the equilibrium for the bridge's degree-of-freedom becomes

$$\begin{aligned}
 & \begin{bmatrix} \mathbf{M}_b & \mathbf{0} & \mathbf{0} \\ \mathbf{0} & \mathbf{0} & \mathbf{0} \\ \mathbf{0} & \mathbf{0} & \mathbf{0} \end{bmatrix} \begin{Bmatrix} \ddot{\mathbf{R}} \\ \ddot{\mathbf{Y}} \end{Bmatrix} + \begin{bmatrix} \mathbf{C}_b + \mathbf{H}(x) \cdot \mathbf{C}_t \cdot \mathbf{H}^T(x) & \mathbf{0} & -\mathbf{H}(x) \cdot \mathbf{C}_t \\ \mathbf{0} & \mathbf{0} & \mathbf{0} \\ \mathbf{0} & \mathbf{0} & \mathbf{0} \end{bmatrix} \begin{Bmatrix} \dot{\mathbf{R}} \\ \dot{\mathbf{Y}} \end{Bmatrix} \\
 & + \begin{bmatrix} \mathbf{K}_b + \mathbf{H}(x) \cdot \mathbf{K}_t \cdot \mathbf{H}^T(x) & \mathbf{0} & -\mathbf{H}(x) \cdot \mathbf{K}_t \cdot v \cdot \partial \mathbf{H}(x) / \partial x \cdot \mathbf{C}_t \\ \mathbf{0} & \mathbf{0} & \mathbf{0} \\ \mathbf{0} & \mathbf{0} & \mathbf{0} \end{bmatrix} \begin{Bmatrix} \mathbf{R} \\ \mathbf{Y} \end{Bmatrix} \\
 & = \begin{Bmatrix} -\mathbf{H}(x) \cdot \mathbf{K}_t \cdot \mathbf{r}(x) + \mathbf{H}(x) \cdot \mathbf{M}_s \\ \mathbf{0} \\ \mathbf{0} \end{Bmatrix}
 \end{aligned} \tag{3.49}$$

where

$$\mathbf{M}_s = \begin{Bmatrix} (m_1 + a_2 m_v) g \\ (m_2 + a_1 m_v) g \end{Bmatrix}.$$

From the combination of Eq. (3.48) and Eq. (3.49), the global equation of motion of vehicle-bridge interaction system is expressed as follows:

$$\begin{aligned}
 & \begin{bmatrix} \mathbf{M}_b & \mathbf{0} & \mathbf{0} \\ \mathbf{0} & \mathbf{M}_{v1} & \mathbf{0} \\ \mathbf{0} & \mathbf{0} & \mathbf{M}_{v2} \end{bmatrix} \begin{Bmatrix} \ddot{\mathbf{R}} \\ \ddot{\mathbf{Y}} \end{Bmatrix} + \begin{bmatrix} \mathbf{C}_b + \mathbf{H}(x) \cdot \mathbf{C}_t \cdot \mathbf{H}^T(x) & \mathbf{0} & -\mathbf{H}(x) \cdot \mathbf{C}_t \\ \mathbf{0} & \mathbf{C}_{v11} & \mathbf{C}_{v12} \\ -\mathbf{C}_t \cdot \mathbf{H}^T(x) & \mathbf{C}_{v21} & \mathbf{C}_{v22} + \mathbf{C}_t \end{bmatrix} \begin{Bmatrix} \dot{\mathbf{R}} \\ \dot{\mathbf{Y}} \end{Bmatrix} \\
 & + \begin{bmatrix} \mathbf{K}_b + \mathbf{H}(x) \cdot \mathbf{K}_t \cdot \mathbf{H}^T(x) & \mathbf{0} & -\mathbf{H}(x) \cdot \mathbf{K}_t \cdot v \cdot \partial \mathbf{H}(x) / \partial x \cdot \mathbf{C}_t \\ \mathbf{0} & \mathbf{K}_{v11} & \mathbf{K}_{v12} \\ -\mathbf{K}_t \cdot \mathbf{H}^T(x) & \mathbf{K}_{v21} & \mathbf{K}_{v22} + \mathbf{K}_t \end{bmatrix} \begin{Bmatrix} \mathbf{R} \\ \mathbf{Y} \end{Bmatrix} \\
 & = \begin{Bmatrix} -\mathbf{H}(x) \cdot \mathbf{K}_t \cdot \mathbf{r}(x) + \mathbf{H}(x) \cdot \mathbf{M}_s \\ \mathbf{0} \\ -\mathbf{K}_t \cdot \mathbf{r}(x) \end{Bmatrix}
 \end{aligned} \tag{3.50}$$

Eq. (3.50) is the vehicle-bridge interaction equation, and Eq. (3.47) is the front and rear axle load equations which are composed of the static load of the vehicle and the dynamic interaction force between the vehicle and the bridge. The vehicle-bridge interaction equation can be solved step-by-step using either a direct integration method such as Newmark's β method or a discretization method by state-space formulation.

For the multiple vehicles system, in the case of two 2-axle vehicles as shown in Figure 3.5, the equation of motion of two vehicles / bridge system is expressed as:

$$\begin{aligned}
 & \begin{bmatrix} \mathbf{M}_b & \mathbf{0} & \mathbf{0} \\ \mathbf{0} & \mathbf{M}_{v1} & \mathbf{0} \\ \mathbf{0} & \mathbf{0} & \mathbf{M}_{v2} \end{bmatrix} \begin{Bmatrix} \ddot{\mathbf{R}} \\ \ddot{\mathbf{Y}}_1 \\ \ddot{\mathbf{Y}}_2 \end{Bmatrix} + \begin{bmatrix} \mathbf{C}_b + \mathbf{H} \cdot \mathbf{C}_{t1} \cdot \mathbf{H}^T & -\mathbf{H} \cdot \mathbf{C}_{t1} & -\mathbf{H} \cdot \mathbf{C}_{t2} \\ -\mathbf{C}_{t1} \cdot \mathbf{H}^T & \mathbf{C}_{v1} + \mathbf{C}_{t1} & \mathbf{0} \\ -\mathbf{C}_{t2} \cdot \mathbf{H}^T & \mathbf{0} & \mathbf{C}_{v2} + \mathbf{C}_{t2} \end{bmatrix} \begin{Bmatrix} \dot{\mathbf{R}} \\ \dot{\mathbf{Y}}_1 \\ \dot{\mathbf{Y}}_2 \end{Bmatrix} \\
 & + \begin{bmatrix} \mathbf{K}_b + \mathbf{H} \cdot \mathbf{K}_{t1} \cdot \mathbf{H}^T & -\mathbf{H} \cdot \mathbf{K}_{t1} \cdot v_1(t) \cdot \partial \mathbf{H} / \partial x \cdot \mathbf{C}_{t1} & -\mathbf{H} \cdot \mathbf{K}_{t2} \cdot v_2(t) \cdot \partial \mathbf{H} / \partial x \cdot \mathbf{C}_{t2} \\ -\mathbf{K}_{t1} \cdot \mathbf{H}^T & \mathbf{K}_{v1} + \mathbf{K}_{t1} & \mathbf{0} \\ -\mathbf{K}_{t2} \cdot \mathbf{H}^T & \mathbf{0} & \mathbf{K}_{v2} + \mathbf{K}_{t2} \end{bmatrix} \begin{Bmatrix} \mathbf{R} \\ \mathbf{Y}_1 \\ \mathbf{Y}_2 \end{Bmatrix} \\
 & = \begin{Bmatrix} -\mathbf{H} \cdot \mathbf{K}_{tt} \cdot \mathbf{r} + \mathbf{H} \cdot \mathbf{M}_s \\ -\mathbf{K}_{t1} \cdot \mathbf{r} \\ -\mathbf{K}_{t2} \cdot \mathbf{r} \end{Bmatrix}
 \end{aligned} \tag{3.51}$$

where the mass, damping and stiffness matrices of i^{th} vehicle are represented as follows:

$$\begin{aligned}
 \mathbf{M}_{vi} &= \begin{bmatrix} m_{vi} & 0 & 0 & 0 \\ 0 & I_{vi} & 0 & 0 \\ 0 & 0 & m_{1i} & 0 \\ 0 & 0 & 0 & m_{2i} \end{bmatrix}; \mathbf{M}_s = \begin{Bmatrix} (m_{11} + a_{21}m_{v1})g \\ (m_{21} + a_{11}m_{v1})g \\ (m_{12} + a_{22}m_{v2})g \\ (m_{22} + a_{12}m_{v2})g \end{Bmatrix}; \\
 \mathbf{C}_{vi} &= \begin{bmatrix} C_{s1i} + C_{s2i} & (-C_{s1i}a_{1i} + C_{s2i}a_{2i})S_i & -C_{s1i} & -C_{s2i} \\ (-C_{s1i}a_{1i} + C_{s2i}a_{2i})S_i & (C_{s1i}a_{1i}^2 + C_{s2i}a_{2i}^2)S_i & C_{s1i}a_{1i}S_i & -C_{s2i}a_{2i}S_i \\ -C_{s1i} & C_{s1i}a_{1i}S_i & C_{s1i} & 0 \\ -C_{s2i} & -C_{s2i}a_{2i}S_i & 0 & C_{s2i} \end{bmatrix}; \\
 \mathbf{K}_{vi} &= \begin{bmatrix} K_{s1i} + K_{s2i} & (-K_{s1i}a_{1i} + K_{s2i}a_{2i})S_i & -K_{s1i} & -K_{s2i} \\ (-K_{s1i}a_{1i} + K_{s2i}a_{2i})S_i & (K_{s1i}a_{1i}^2 + K_{s2i}a_{2i}^2)S_i & K_{s1i}a_{1i}S_i & -K_{s2i}a_{2i}S_i \\ -K_{s1i} & K_{s1i}a_{1i}S_i & K_{s1i} & 0 \\ -K_{s2i} & -K_{s2i}a_{2i}S_i & 0 & K_{s2i} \end{bmatrix}; \\
 \mathbf{C}_{ti} &= \begin{bmatrix} 0 & 0 & 0 & 0 \\ 0 & 0 & 0 & 0 \\ 0 & 0 & C_{t1i} & 0 \\ 0 & 0 & 0 & C_{t2i} \end{bmatrix}; \mathbf{K}_{ti} = \begin{bmatrix} 0 & 0 & 0 & 0 \\ 0 & 0 & 0 & 0 \\ 0 & 0 & K_{t1i} & 0 \\ 0 & 0 & 0 & K_{t2i} \end{bmatrix}; \\
 \mathbf{C}_{tt} &= \begin{bmatrix} \mathbf{C}_{t1} & \mathbf{0} \\ \mathbf{0} & \mathbf{C}_{t2} \end{bmatrix}; \mathbf{K}_{tt} = \begin{bmatrix} \mathbf{K}_{t1} & \mathbf{0} \\ \mathbf{0} & \mathbf{K}_{t2} \end{bmatrix}; \mathbf{r} = \begin{Bmatrix} r(x_{f1}(t)) \\ r(x_{r1}(t)) \\ r(x_{f2}(t)) \\ r(x_{r2}(t)) \end{Bmatrix}.
 \end{aligned}$$

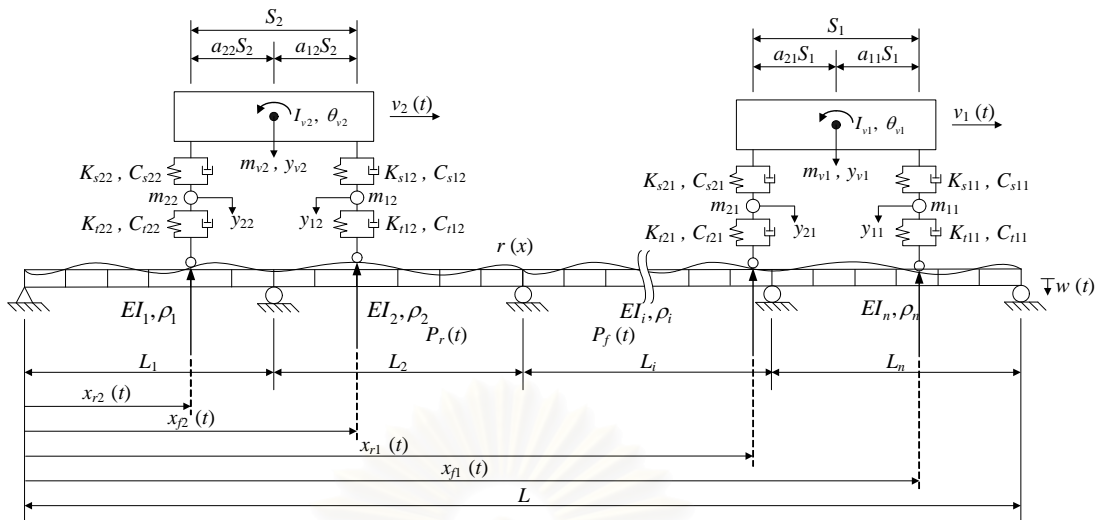


Figure 3.5 Multiple vehicles-bridge system of n -span continuous bridge

3.3 Relationship of Axle Loads and Bridge Bending Moments

The strain occurring at any measuring point at the bottom surface of the beam element in Figure 3.6 can be determined from:

$$\varepsilon_j(x_j, t) = -\gamma_j \left. \frac{\partial^2 w(x, t)}{\partial x^2} \right|_{x=x_j} \quad (3.52)$$

where γ_j is the distance between the bottom surface of the bridge and the neutral axis of the bridge section at the measuring location x_j .

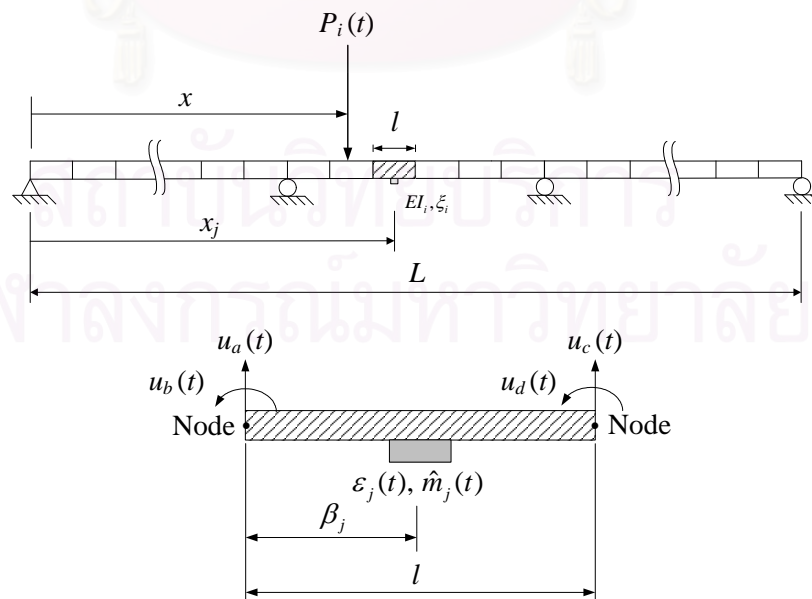


Figure 3.6 Measuring point in the beam element

Substituting $w(x,t)$ into Eq. (3.52) yields

$$\varepsilon_j(\beta_j, t) = -\left(\frac{\gamma_j}{l^3}\right) \cdot [(12\beta_j - 6l)u_a(t) + l(6\beta_j - 4l)u_b(t) - (12\beta_j - 6l)u_c(t) + l(6\beta_j - 2l)u_d(t)] \quad (3.53)$$

From the relationship between bending moment $\hat{m}_j(t)$ and strain $\varepsilon_j(t)$, Eq. (3.53) can be converted into bending moment as:

$$\hat{m}_j(t) = EI \cdot \frac{\varepsilon_j(t)}{\gamma_j} \quad (3.54)$$

Therefore, Eq. (3.54) can be rewritten in the following form:

$$\hat{m}_j(\beta_j, t) = -\left(\frac{EI}{l^3}\right) \left\{ \begin{matrix} (12\beta_j - 6l) & l(6\beta_j - 4l) & -(12\beta_j - 6l) & l(6\beta_j - 2l) \end{matrix} \right\} \begin{Bmatrix} u_a(t) \\ u_b(t) \\ u_c(t) \\ u_d(t) \end{Bmatrix} \quad (3.55)$$

where $u_a(t)$, $u_b(t)$, $u_c(t)$ and $u_d(t)$ are the nodal displacements of the corresponding beam element and β_j is the local location of the measuring point determined from the global location x_j .

3.4 Moving Load Identification

In a load identification system, the interaction between external acting loads and bridge responses is considered. The problem is to identify the external loading in time histories without investigation of other vehicle properties such as mass or suspension characteristics, etc. The input for the identification system is only the measured bridge responses (bending moments) and location of moving axles on the bridge with respect to time.

Figure 3.7 represents the system of multiple moving load-bridge interaction used in the identification system. The vehicle axle loads can be considered as a group of time-varying moving concentrated loads. The vehicle properties can be omitted in the identification system because the identified loads are the interaction forces, $\mathbf{P}_{int}(t)$ from Eq. (3.43). Hence, the dynamics of vehicle properties such as vehicle mass and suspension or tire properties are already taken into account. Therefore, system simplification by considering only the equation of motion of the bridge is

conducted in the identification system. However, this consideration can be made since the vehicle mass and the bridge mass are very different and the duration of vehicle-bridge interaction is very short. As a result, the interactive behavior between vehicles and bridge becomes less influential. Therefore, the simplification of the identification system by considering only the bridge structure and assuming the vehicle axle loads as a group of time varying concentrated loads is capable.

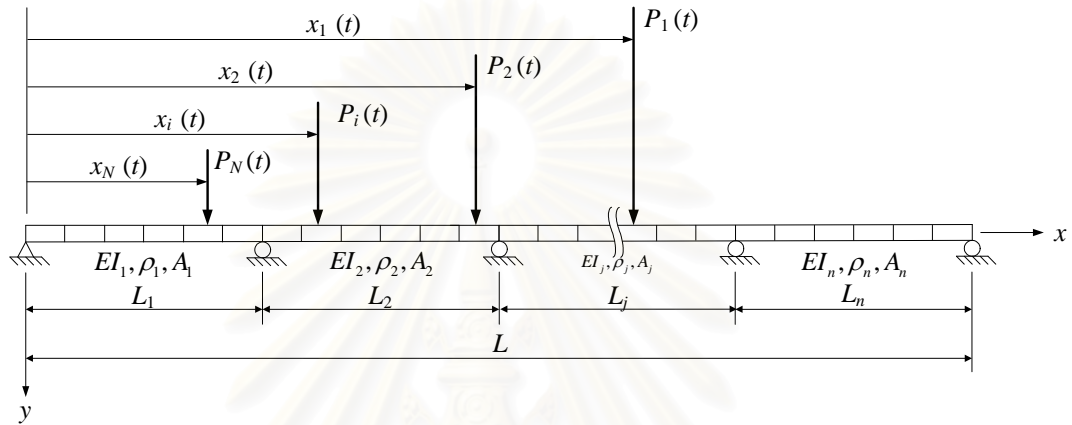


Figure 3.7 Multiple moving loads–bridge system used in axle loads identification

According to the bridge's equation of motion referred to in Eq. (3.40), the force term of the equation is then replaced by the unknown acting load vector expressed as:

$$\mathbf{M}_b \ddot{\mathbf{R}}(t) + \mathbf{C}_b \dot{\mathbf{R}}(t) + \mathbf{K}_b \mathbf{R}(t) = \mathbf{P}_b(t) \quad (3.56)$$

where $\mathbf{P}_b(t)$ is the unknown external nodal load vector which can be rewritten as

$$\mathbf{P}_b(t) = \mathbf{H}_c(x(t)) \hat{\mathbf{P}}(t) \quad (3.57)$$

in which $\hat{\mathbf{P}}(t)$ is a $N_p \times 1$ vector of the unknown applied loads.

In order to determine the bridge response from Eq. (3.56) into a step by step of the time history, the state-space formulation is utilized in the conversion of Eq. (3.56) from a second order differential equation into a set of first order differential equations as follows:

$$\dot{\mathbf{X}}(t) = \mathbf{K}^* \mathbf{X}(t) + \bar{\mathbf{P}}(t) \quad (3.58)$$

where
$$\mathbf{X}(t) = \begin{bmatrix} \mathbf{R}(t) \\ \dot{\mathbf{R}}(t) \end{bmatrix}_{2NN \times 1}, \quad \mathbf{K}^* = \begin{bmatrix} \mathbf{0} & \mathbf{I} \\ -\mathbf{M}_b^{-1}\mathbf{K}_b & -\mathbf{M}_b^{-1}\mathbf{C}_b \end{bmatrix}_{2NN \times 2NN},$$

$$\begin{aligned} \bar{\mathbf{P}}(t) &= \begin{bmatrix} \mathbf{0} \\ -\mathbf{M}_b^{-1}\mathbf{P}_b(t) \end{bmatrix}_{2NN \times 1} \\ &= \begin{bmatrix} \mathbf{0} \\ -\mathbf{M}_b^{-1}\mathbf{H}_c \end{bmatrix}_{2NN \times N_p} \cdot \hat{\mathbf{P}}(t)_{N_p \times 1} \end{aligned} \quad (3.59)$$

where \mathbf{X} represents a vector of state variables of length twice the total degree-of-freedom of the bridge ($2NN$) containing the displacements and velocities of the nodes, and N_p is the number of acting loads. These differential equations are then rewritten as discrete equations using the standard exponential matrix representation.

$$\mathbf{X}_{j+1}(t) = \mathbf{F}\mathbf{X}_j(t) + \bar{\mathbf{G}}_{j+1}(t)\bar{\mathbf{P}}_j(t), \quad (3.60)$$

$$\mathbf{F} = \mathbf{e}^{\mathbf{K}^*h}, \quad (3.61)$$

$$\bar{\mathbf{G}} = \mathbf{K}^{*-1}(\mathbf{F} - \mathbf{I}), \quad (3.62)$$

where matrix \mathbf{F} is the exponential matrix, and together with matrix $\bar{\mathbf{G}}$ represents the dynamics of the system, $j+1$ denoted the value at the $j+1^{\text{th}}$ time step of computation, the time step h represents the time difference between the variable states \mathbf{X}_j and \mathbf{X}_{j+1} in the computation, and $\bar{\mathbf{G}}$ is a matrix relating the forces to the system.

Substituting Eq. (3.59) and (3.62) into Eq. (3.60), yields:

$$\mathbf{X}_{j+1}(t) = \mathbf{F}\mathbf{X}_j(t) + \mathbf{G}_{j+1}(t)\hat{\mathbf{P}}_j(t), \quad (3.63)$$

where
$$\mathbf{G} = \bar{\mathbf{G}}_{2NN \times 2NN} \begin{bmatrix} \mathbf{0} \\ -\mathbf{M}_b^{-1}\mathbf{H}_c \end{bmatrix}_{2NN \times N_p} \quad (3.64)$$

The matrix \mathbf{F} can be obtained using exponential expansion as follows:

$$\mathbf{F} = \mathbf{e}^{\mathbf{K}^*h} = \mathbf{I} + h\mathbf{K}^* + \frac{h^2}{2!}\mathbf{K}^{*2} + \frac{h^3}{3!}\mathbf{K}^{*3} + \dots \quad (3.65)$$

where
$$\mathbf{K}^* = \mathbf{V}\mathbf{\Lambda}\mathbf{V}^{-1}. \quad (3.66)$$

Substituting Eq. (3.66) into Eq. (3.65) becomes

$$\begin{aligned}
\mathbf{F} = \mathbf{e}^{\mathbf{K}^*h} &= \mathbf{V}\mathbf{V}^{-1} + h\mathbf{V}\mathbf{\Lambda}\mathbf{V}^{-1} + \frac{h^2}{2!}\mathbf{V}\mathbf{\Lambda}\mathbf{V}^{-1}\mathbf{V}\mathbf{\Lambda}\mathbf{V}^{-1} + \frac{h^3}{3!}\mathbf{V}\mathbf{\Lambda}\mathbf{V}^{-1}\mathbf{V}\mathbf{\Lambda}\mathbf{V}^{-1}\mathbf{V}\mathbf{\Lambda}\mathbf{V}^{-1} + \dots \\
&= \mathbf{V}\mathbf{V}^{-1} + h\mathbf{V}\mathbf{\Lambda}\mathbf{V}^{-1} + \frac{h^2}{2!}\mathbf{V}\mathbf{\Lambda}^2\mathbf{V}^{-1} + \frac{h^3}{3!}\mathbf{V}\mathbf{\Lambda}^3\mathbf{V}^{-1} + \dots \\
&= \mathbf{V}\left(\mathbf{I} + h\mathbf{\Lambda} + \frac{h^2}{2!}\mathbf{\Lambda}^2 + \frac{h^3}{3!}\mathbf{\Lambda}^3 + \dots\right)\mathbf{V}^{-1} \\
&= \mathbf{V}\mathbf{e}^{\mathbf{\Lambda}h}\mathbf{V}^{-1}
\end{aligned} \tag{3.67}$$

According to Eq. (3.63), the bridge response in terms of the state variable of the next time step $j+1$ can be calculated from the state variable of the present time step j . The relationship between the identified acting load vector $\hat{\mathbf{P}}(t)$ and the bridge response \mathbf{R} can be formulated.

3.4.1 Problem Statement

The objective of this problem is to find the unknown forcing term $\hat{\mathbf{P}}(t)$. Since the input of the identification system are measured bridge responses and location of the moving loads on the structure, the goal of this problem is to find the time histories of moving force that cause the system described in Eq. (3.50) or Eq. (3.51) to best match the measurement data.

In this research, the sectional bending moment is adopted as the measurement data. Let $\mathbf{Z}(t)$ be the measured bending moment vector at k number of selected measuring points, which is expressed as:

$$\mathbf{Z}_j(t)_{k \times 1} = \{m_{1_j}(t) \quad m_{2_j}(t) \quad \dots \quad m_{k_j}(t)\}^T \tag{3.68}$$

where $m_{k_j}(t)$ is the k^{th} station of the measured bending moment of the bridge at the j^{th} time step.

While the corresponding predicted bending moment vector $\hat{\mathbf{Z}}(t)$ at the same sections are estimated by solving the equation of motion of the bridge. In practice, it is not possible to measure all the displacements and velocities, and only certain combinations of the variables \mathbf{X} are required. The measurement equation used in predicted bending moment formulation is then given as:

$$\begin{aligned}\hat{\mathbf{Z}}_j(t)_{k \times 1} &= \left\{ \hat{m}_{1_j}(t) \quad \hat{m}_{2_j}(t) \quad \cdots \quad \hat{m}_{k_j}(t) \right\}^T \\ &= \mathbf{Q}\mathbf{X}_j\end{aligned}\quad (3.69)$$

where

$\hat{m}_{k_j}(t)$ is the k^{th} station of the predicted bending moment of the bridge at the j^{th} time step

and \mathbf{Q} is a $k \times 2NN$ selection matrix used to transform the predicted measurements to state variable response vector \mathbf{X} .

It is noted that the number of measured variables k is usually much less than the number of state variables (or twice of degree-of-freedom) but greater than or equal to the number of unknown applied loads, N_p .

From the state-space formulation as of Eq. (3.63), the relationship between the state variables and applied loads can be formulated as follows:

$$\underbrace{\begin{Bmatrix} \mathbf{X}_1(t) \\ \mathbf{X}_2(t) \\ \mathbf{X}_3(t) \\ \vdots \\ \mathbf{X}_j(t) \end{Bmatrix}}_{\hat{\mathbf{X}}^*} = \underbrace{\begin{Bmatrix} \mathbf{F}\mathbf{X}_0(t) \\ \mathbf{F}^2\mathbf{X}_0(t) \\ \mathbf{F}^3\mathbf{X}_0(t) \\ \vdots \\ \mathbf{F}^j\mathbf{X}_0(t) \end{Bmatrix}}_{\hat{\mathbf{X}}_0^*} + \underbrace{\begin{bmatrix} \mathbf{G}_1 & \mathbf{0} & \mathbf{0} & \mathbf{0} & \mathbf{0} \\ \mathbf{F}\mathbf{G}_1 & \mathbf{G}_2 & \mathbf{0} & \mathbf{0} & \mathbf{0} \\ \mathbf{F}^2\mathbf{G}_1 & \mathbf{F}\mathbf{G}_2 & \mathbf{G}_3 & \cdots & \mathbf{0} \\ \vdots & \vdots & \vdots & \ddots & \mathbf{0} \\ \mathbf{F}^{j-1}\mathbf{G}_1 & \mathbf{F}^{j-2}\mathbf{G}_2 & \mathbf{F}\mathbf{G}_3 & \cdots & \mathbf{G}_j \end{bmatrix}}_{\mathbf{T}} \underbrace{\begin{Bmatrix} \hat{\mathbf{P}}_0(t) \\ \hat{\mathbf{P}}_1(t) \\ \hat{\mathbf{P}}_2(t) \\ \vdots \\ \hat{\mathbf{P}}_{j-1}(t) \end{Bmatrix}}_{\hat{\mathbf{P}}^*}. \quad (3.70)$$

In case of the system being started at rest, the initial condition term is assumed as a vector containing all zero entries and the term $\hat{\mathbf{X}}_0^*$ is then vanished. Eq. (3.70) can be rewritten as:

$$\hat{\mathbf{X}}^* = \mathbf{T}\hat{\mathbf{P}}^* \quad (3.71)$$

where

$\hat{\mathbf{X}}^*$ is a $2N \cdot NN \times 1$ state variable vector of total N time step,

\mathbf{T} is a $2N \cdot NN \times N \cdot N_p$ transformation matrix between total residual state variable vector $(\mathbf{X}^* - \mathbf{X}_0^*)$ and the total applied load vector,

$\hat{\mathbf{P}}^*$ is a $N \cdot N_p \times 1$ applied load vector of total N time step.

From Eq. (3.71), the relationship between measurements and applied loads is then represented as:

$$\underbrace{\begin{Bmatrix} \hat{\mathbf{Z}}_1(t) \\ \hat{\mathbf{Z}}_2(t) \\ \hat{\mathbf{Z}}_3(t) \\ \vdots \\ \hat{\mathbf{Z}}_j(t) \end{Bmatrix}}_{\hat{\mathbf{Z}}^*} = \underbrace{\begin{bmatrix} \mathbf{Q}\mathbf{G}_1 & \mathbf{0} & \mathbf{0} & \mathbf{0} & \mathbf{0} \\ \mathbf{Q}\mathbf{F}\mathbf{G}_1 & \mathbf{Q}\mathbf{G}_2 & \mathbf{0} & \mathbf{0} & \mathbf{0} \\ \mathbf{Q}\mathbf{F}^2\mathbf{G}_1 & \mathbf{Q}\mathbf{F}\mathbf{G}_2 & \mathbf{Q}\mathbf{G}_3 & \cdots & \mathbf{0} \\ \vdots & \vdots & \vdots & \ddots & \mathbf{0} \\ \mathbf{Q}\mathbf{F}^{j-1}\mathbf{G}_1 & \mathbf{Q}\mathbf{F}^{j-2}\mathbf{G}_2 & \mathbf{Q}\mathbf{F}\mathbf{G}_3 & \cdots & \mathbf{Q}\mathbf{G}_j \end{bmatrix}}_{\mathbf{T}^*} \underbrace{\begin{Bmatrix} \hat{\mathbf{P}}_0(t) \\ \hat{\mathbf{P}}_1(t) \\ \hat{\mathbf{P}}_2(t) \\ \vdots \\ \hat{\mathbf{P}}_{j-1}(t) \end{Bmatrix}}_{\hat{\mathbf{P}}^*} \quad (3.72)$$

which can be expressed in the simple form as:

$$\hat{\mathbf{Z}}^* = \mathbf{T}^* \hat{\mathbf{P}}^* \quad (3.73)$$

where $\hat{\mathbf{Z}}^*$ is a $k \cdot N \times 1$ measurement vector of total N time step,

\mathbf{T}^* is a $k \cdot N \times N \cdot N_p$ coefficient matrix between total residual measurement vector $\hat{\mathbf{Z}}^*$ and total applied load vector $\hat{\mathbf{P}}^*$.

Regarding Eq. (3.73), the relationship between the applied load vector $\hat{\mathbf{P}}^*$ and the measurement vector $\hat{\mathbf{Z}}^*$ is expressed as a linear relationship. Therefore, the applied load vector can be identified based on the inverse problem of Eq. (3.73).

However, practically, it is impossible to obtain an exact match of the model with measured data. This is due to the fact that all measurements have some level of noise. Hence, the solution of this problem cannot be obtained accurately by replacing $\hat{\mathbf{Z}}_j(t)$ with $\mathbf{Z}_j(t)$ and directly inverting Eq. (3.73). Therefore, the optimization method is employed to obtain the best match of the measurements by minimizing residual the error between measured and predicted responses (bending moments). The simple least-square method criterion on the error between the measured bending moments, $\mathbf{Z}(t)$, and the predicted bending moments, $\hat{\mathbf{Z}}(t)$, is given as follows:

$$\begin{aligned} E &= (\mathbf{Z}^* - \hat{\mathbf{Z}}^*)^T \mathbf{A} (\mathbf{Z}^* - \hat{\mathbf{Z}}^*) \\ &= (\mathbf{Z}^* - \mathbf{T}^* \hat{\mathbf{P}}^*)^T \mathbf{A} (\mathbf{Z}^* - \mathbf{T}^* \hat{\mathbf{P}}^*) \end{aligned} \quad (3.74)$$

where \mathbf{A} is a symmetric positive-definite weighting matrix providing the flexibility of weighting the measurements term.

3.4.2 Optimization with Tikhonov Regularization

The least square criterion stated in Eq. (3.74) can be employed but it is found to be not sufficient. This is because the problem is noise sensitivity and the obtained

solution usually exhibits large fluctuations corresponding to the level of measurement noises. In order to avoid this phenomenon, the smoothening term is added to the least-squares error. Then the moving loads can be identified through the minimization of the square error of the bending moments of the bridge, E with the regularization term. This non-linear least square problem called the ‘‘Tihonov regularization’’ method was presented by Tihonov (1963) to overcome the ill-conditioning usually found in the ill-posed problems. This conventional regularization can be expressed in time-discretization form as:

$$E = (\mathbf{Z}^* - \mathbf{T}^* \mathbf{P}^*)^T \mathbf{A} (\mathbf{Z}^* - \mathbf{T}^* \mathbf{P}^*) + \mathbf{P}^{*T} \mathbf{D} \mathbf{P}^* \quad (3.75)$$

where the additional term $\mathbf{P}^{*T} \mathbf{D} \mathbf{P}^*$ is a smoothening term known as the regularization and the method is called the Tikhonov regularization method. Matrix \mathbf{D} is a diagonal matrix with positive definite, represented as:

$$\mathbf{D} = \lambda \mathbf{I} \quad (3.76)$$

where λ is a regularization parameter.

Substituting Eq. (3.76) into Eq. (3.75), the objective function becomes

$$E = (\mathbf{Z}^* - \mathbf{T}^* \mathbf{P}^*)^T \mathbf{A} (\mathbf{Z}^* - \mathbf{T}^* \mathbf{P}^*) + \lambda \mathbf{P}^{*T} \mathbf{P}^* \quad (3.77)$$

A small value of λ causes the solution to match the data closely but produces large oscillatory deviations while a large value produces smooth forces that may not match the data well. When λ is zero, the solution becomes that for the least square problem.

Expanding Eq. (3.77), yields

$$\begin{aligned} E &= \mathbf{Z}^{*T} \mathbf{A} \mathbf{Z}^* - \mathbf{Z}^{*T} \mathbf{A} \mathbf{T}^* \mathbf{P}^* - \mathbf{P}^{*T} \mathbf{T}^{*T} \mathbf{A} \mathbf{Z}^* + \mathbf{P}^{*T} \mathbf{T}^{*T} \mathbf{A} \mathbf{T}^* \mathbf{P}^* + \lambda \mathbf{P}^{*T} \mathbf{P}^* \\ &= \mathbf{Z}^{*T} \mathbf{A} \mathbf{Z}^* - 2 \mathbf{Z}^{*T} \mathbf{A} \mathbf{T}^* \mathbf{P}^* + \mathbf{P}^{*T} \mathbf{T}^{*T} \mathbf{A} \mathbf{T}^* \mathbf{P}^* + \lambda \mathbf{P}^{*T} \mathbf{P}^* \end{aligned} \quad (3.78)$$

From Eq. (3.78), the unknown applied loads can be obtained using minimization with the derivation of the least square error with respect to the force vector as follows:

$$\begin{aligned} \frac{\partial E}{\partial \mathbf{P}^*} &= -2 \mathbf{Z}^{*T} \mathbf{A} \mathbf{T}^* + 2 \mathbf{P}^{*T} \mathbf{T}^{*T} \mathbf{A} \mathbf{T}^* + 2 \lambda \mathbf{P}^{*T} \\ 0 &= -\mathbf{Z}^{*T} \mathbf{A} \mathbf{T}^* + \mathbf{P}^{*T} (\mathbf{T}^{*T} \mathbf{A} \mathbf{T}^* + \lambda \mathbf{I}) \end{aligned} \quad (3.79)$$

Thus, the unknown applied load vector can be determined from

$$\mathbf{P}^* = (\mathbf{T}^{*T} \mathbf{A} \mathbf{T}^* + \lambda \mathbf{I})^{-1} \mathbf{T}^{*T} \mathbf{A} \mathbf{Z}^*. \quad (3.80)$$

When the weighting matrix \mathbf{A} is an identity matrix and the regularization parameter is removed, the solution becomes the pseudo-inverse solution

$$\mathbf{P}^* = \mathbf{T}^+ \mathbf{Z}^* = (\mathbf{T}^{*T} \mathbf{T}^*)^{-1} \mathbf{T}^{*T} \mathbf{Z}^* \quad (3.81)$$

3.4.3 Loads Identification Using Singular Value Decomposition

According to load identification using the least-square regularization method referred to in section 3.4.2, the solutions solved by Eq. (3.80) or Eq. (3.81) are not sufficient as the coefficient matrix \mathbf{T}^* is rank deficient, or close to rank deficient. Therefore, to overcome this ranking deficiency, and when the problem is a linear algebra, the singular value decomposition (SVD) method (Golub and Kahan, 1965) is adopted.

From the considered rank deficient matrix, when the number of measurements is equal or larger than the number of unknown applied loads ($k \geq N_p$), the coefficient matrix \mathbf{T}^* can be decomposed its singular values using singular value decomposition as follows:

$$\mathbf{T}^* = \mathbf{U} \cdot \mathbf{\Sigma} \cdot \mathbf{\Gamma}^T \quad (3.82)$$

where

\mathbf{U} is a $k \cdot N \times k \cdot N$ orthogonal matrix in which $\mathbf{U} = \{U_1, U_2, \dots, U_{k \cdot N}\}$

$\mathbf{\Sigma}$ is a $k \cdot N \times N \cdot N_p$ diagonal matrix containing the singular value of the decomposed matrix orderly arranged from the largest to the smallest value,

$\mathbf{\Gamma}$ is a $N \cdot N_p \times N \cdot N_p$ orthogonal matrix in which $\mathbf{\Gamma} = \{\Gamma_1, \Gamma_2, \dots, \Gamma_{N \cdot N_p}\}$.

Substituting Eq. (3.82) into Eq. (3.72), becomes

$$\hat{\mathbf{Z}}^* = \mathbf{U} \mathbf{\Sigma} \mathbf{\Gamma}^T \mathbf{P}^* \quad (3.83)$$

Multiplying the measured and predicted bending moment by \mathbf{U}^T becomes

$$\bar{\mathbf{Z}} = \mathbf{U}^T \mathbf{Z}^* \quad (3.84)$$

$$\bar{\mathbf{Z}}^* = \mathbf{U}^T \hat{\mathbf{Z}}^* = \mathbf{\Sigma} \mathbf{\Gamma}^T \mathbf{P}^* \quad (3.85)$$

Formulating the least square objective function of Eq. (3.84) and Eq. (3.85) yields

$$E = (\mathbf{U}^T \mathbf{Z}^* - \mathbf{\Sigma} \mathbf{\Gamma}^T \mathbf{P}^*)^T \mathbf{A} (\mathbf{U}^T \mathbf{Z}^* - \mathbf{\Sigma} \mathbf{\Gamma}^T \mathbf{P}^*) + \lambda \mathbf{P}^{*T} \mathbf{P}^* \quad (3.86)$$

Expanding Eq. (3.86), the objective function can be rewritten as:

$$\begin{aligned} E &= \mathbf{Z}^{*T} \mathbf{U} \mathbf{A} \mathbf{U}^T \mathbf{Z}^* - \mathbf{Z}^{*T} \mathbf{U} \mathbf{A} \boldsymbol{\Sigma} \boldsymbol{\Gamma}^T \mathbf{P}^* - \mathbf{P}^{*T} \boldsymbol{\Gamma} \boldsymbol{\Sigma} \mathbf{A} \mathbf{U}^T \mathbf{Z}^* + \mathbf{P}^{*T} \boldsymbol{\Gamma} \boldsymbol{\Sigma} \mathbf{A} \boldsymbol{\Sigma} \boldsymbol{\Gamma}^T \mathbf{P}^* + \lambda \mathbf{I} \mathbf{P}^{*T} \mathbf{P}^* \\ &= \mathbf{Z}^{*T} \mathbf{U} \mathbf{A} \mathbf{U}^T \mathbf{Z}^* - 2 \mathbf{Z}^{*T} \mathbf{U} \mathbf{A} \boldsymbol{\Sigma} \boldsymbol{\Gamma}^T \mathbf{P}^* + \mathbf{P}^{*T} \boldsymbol{\Gamma} \boldsymbol{\Sigma} \mathbf{A} \boldsymbol{\Sigma} \boldsymbol{\Gamma}^T \mathbf{P}^* + \lambda \mathbf{I} \mathbf{P}^{*T} \mathbf{P}^* \end{aligned} \quad (3.87)$$

Since the above equation has some terms containing singular value matrices, and if the weighting matrix \mathbf{A} is an identity matrix, the Eq. (3.87) can be rewritten in the discrete formula as follows:

$$E = \sum_{j=1}^{N \cdot N_p} \left| \sigma_j (\boldsymbol{\Gamma}_j^T \mathbf{P}^*) - (U_j^T \mathbf{Z}^*) \right|^2 + \sum_{j=N \cdot N_p + 1}^{N \cdot k} \left| (U_j^T \mathbf{Z}^*) \right|^2 + \lambda \sum_{j=1}^{N \cdot N_p} \left| \boldsymbol{\Gamma}_j^T \mathbf{P}^* \right|^2 \quad (3.88)$$

Again, the unknown applied loads can be obtained using minimization with the derivation of the least square error with respect to the force vector as follows:

$$\begin{aligned} \frac{\partial E}{\partial \mathbf{P}^*} &= 2 \sum_{j=1}^{N \cdot N_p} \left| \sigma_j (\boldsymbol{\Gamma}_j^T \mathbf{P}^*) - (U_j^T \mathbf{Z}^*) \right| \sigma_j \boldsymbol{\Gamma}_j^T + 2 \lambda \sum_{j=1}^{N \cdot N_p} \left| \boldsymbol{\Gamma}_j^T \mathbf{P}^* \right| \boldsymbol{\Gamma}_j^T \\ 0 &= \sum_{j=1}^{N \cdot N_p} \left| \sigma_j (\boldsymbol{\Gamma}_j^T \mathbf{P}^*) - (U_j^T \mathbf{Z}^*) \right| \sigma_j + \lambda \sum_{j=1}^{N \cdot N_p} \left| \boldsymbol{\Gamma}_j^T \mathbf{P}^* \right| \\ 0 &= \sum_{j=1}^{N \cdot N_p} \left| (\sigma_j^2 + \lambda) (\boldsymbol{\Gamma}_j^T \mathbf{P}^*) - \sigma_j (U_j^T \mathbf{Z}^*) \right| \end{aligned} \quad (3.89)$$

Finally, the predicted moving loads can be obtained as:

$$\mathbf{P}^* = \sum_{j=1}^{N \cdot N_p} \frac{\sigma_j}{(\sigma_j^2 + \lambda)} (U_j^T \mathbf{Z}^*) \boldsymbol{\Gamma}_j. \quad (3.90)$$

When $\lambda = 0$, \mathbf{P}^* is the least square solution and the noise effect will be amplified when $\sigma_j < U_j^T \mathbf{Z}^*$. When $\lambda > 0$, this formulation can reduce the influence of the components corresponding to those singular values σ_j^2 which are smaller than λ , so that the solution is less noise sensitive.

3.4.4 Accuracy Improvement with Updated Static Component (USC) Technique

It is found that the regularization method outlined in the previous section requires an optimal regularization parameter, λ , to identify the axle loads accurately. This optimal parameter is rather difficult to pre-assign in real applications because it depends on the configuration, speed and weight of the identified vehicle. The L-curve method (Hansen, 1992) or generalized cross-validation (Golub et al., 1979) might be employed to determine this optimal parameter, but large computing time is required.

Moreover, the obtained parameter is a sub-optimal value which does not guarantee accurate identification results. To overcome such a difficulty and to enhance identification accuracy, regularization with the updated static component (USC) technique (Pinkaw, 2006) is adopted. Since the bridge responses are composed of two components, which are the static (quasi-static) and the dynamic components, they theoretically require different values of optimal regularization parameters. Therefore, the USC technique decomposes the bridge responses into static and dynamic components. The static component is identified separately, while only the dynamic component remains in the regularization process. With iteration, the regularization method using dynamic programming is employed to identify the dynamic component. Then, the obtained identified result is used to update the associated static component until the convergent solution is achieved. The computational diagram of the proposed regularization with the updated static component technique is shown in Figure 3.6. It is noted that the static component of the time-varying quantity is simply calculated using time averaging.

To investigate the accuracy of the identified results, the identification error is defined as:

$$\text{Identification error} = \frac{\|\hat{\mathbf{P}}(t) - \mathbf{P}(t)\|}{\|\mathbf{P}(t)\|} \times 100\% \quad (3.91)$$

where $\|\cdot\|$ is the Euclidean norm of a vector. $\mathbf{P}(t)$ and $\hat{\mathbf{P}}(t)$ are the actual and the identified axle loads of the vehicle for either the front or rear axle, respectively.

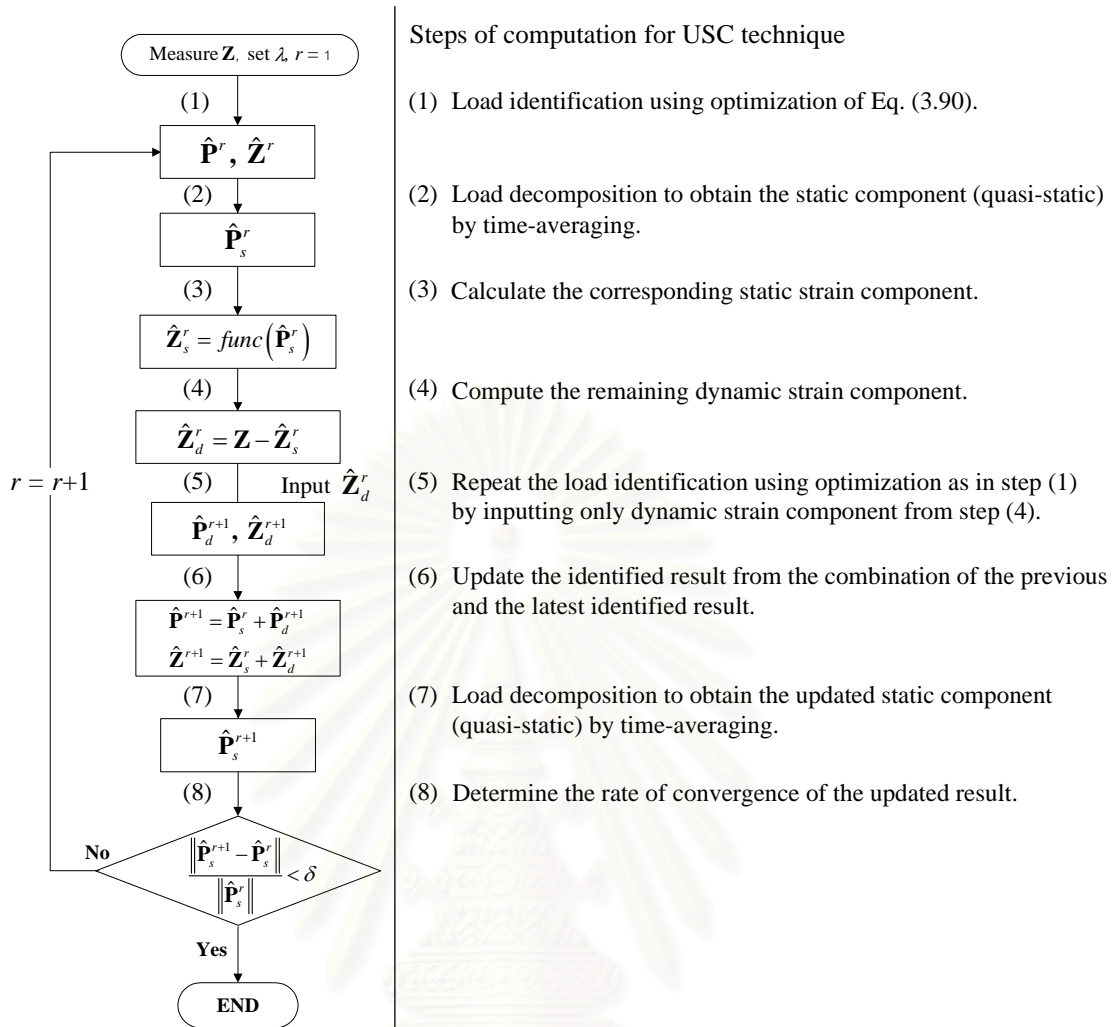


Figure 3.8 Computational procedures of load identification through regularization with the updated static component (USC) technique

Where

$\hat{\mathbf{P}}_s$ is the static load component obtained by time-averaging of identified load,

$\hat{\mathbf{Z}}_s$ is the static bending moment constructed from the static load component,

$\hat{\mathbf{Z}}_d$ is the dynamic bending moment obtained from subtracting the static bending moment from the measured bending moment,

$\hat{\mathbf{P}}_d$ is the dynamic load component obtained from the identification of the remaining dynamic bending moment, and

δ is the iterative error between the updated and previous identified load.

CHAPTER IV

NUMERICAL STUDY OF AXLE LOAD IDENTIFICATION USING COMPUTER SIMULATION

4.1 General

This chapter numerically studies moving load identification using computer simulation in order to investigate the effectiveness of the proposed method explained in Chapter III. The problems are mainly divided into two parts, namely identification of multi-axle loads moving on a single-span simply supported bridge, and identification of multi-axle loads moving on a multi-span continuous bridge. Besides the consideration of a vehicle as a moving dynamic multi-degree-of-freedom system, the simpler model of the vehicle using moving concentrated loads is also considered. The comparison of identification approaches for effectiveness and accuracy evaluation is carried out and discussed. Influences of various parameters such as number and position of response measurements, measurement noise level, sampling frequency, structural discretization, vehicle mass, moving speed, axle-spacing-to-span ratio, axle weight ratio, bridge surface roughness and regularization parameter are considered. The parametric study of the regularization parameter is also conducted. In addition, the information obtained from these studies will be used as guidance for the experimental study and future improvement of the identification approach. Based on extensive numerical examples, the identification accuracy, robustness and reliability of the proposed method can be systematically investigated.

4.2 Accuracy of Moving Load Identification

Since moving load identification has been studied and developed upon for decades, the identification methods have been adopted and modified to obtain a better solution for both accuracy and robustness. Therefore, to propose an appropriate method for this research problem, an accuracy comparison of the existing and the proposed methods is performed. Three selected identification methods including (1) conventional identification without regularization, (2) identification with optimal regularization and (3) identification with USC regularization are comparatively studied.

In this section, the bridge models used in this study are a single-span simply supported bridge with a span length of 30 m and a three-span continuous bridge with equal span lengths of 20 m. The bridge properties are listed in Table 4.1. The number of elements used in both the response simulation and load identification comes to 8 elements per bridge span.

Table 4.1 Parameters of the bridge used in the numerical study

Single-span simply supported bridge	Three-span continuous bridge
$L = 30$ m	$L = 3 @ 20$ m
$\rho A = 5000$ kg/m	$\rho A = 4000$ kg/m
$EI = 2.5 \times 10^{10}$ N-m ²	$EI = 8.0 \times 10^9$ N-m ²
$\xi = 0.02$ for all modes	$\xi = 0.02$ for all modes

To check the correctness of the identification methods, time varying concentrated loads are employed in which the effects of mass and stiffness of the acting loads are not taken into account. Hence, two time varying concentrated loads moving at a constant speed of 20 m/s are used as a vehicle's axle loads as follows:

$$\begin{aligned}
 p_1(t) &= 61.5 [1.0 + 0.1 \sin(10\pi t) + 0.05 \sin(40\pi t)] \text{ kN}, \\
 p_2(t) &= 121.0 [1.0 - 0.1 \sin(10\pi t) + 0.05 \sin(50\pi t)] \text{ kN}, \\
 S_1 &= 4.27 \text{ m}.
 \end{aligned} \tag{4.1}$$

In the case of the axle load identification of two vehicles, the load functions for the second vehicle are assumed as $p_3(t)$, $p_4(t)$ with the same axle spacing of 4.27m as follows:

$$\begin{aligned}
 p_3(t) &= 61.5 [1.0 + 0.1 \cos(10\pi t) + 0.05 \cos(40\pi t)] \text{ kN}, \\
 p_4(t) &= 121.0 [1.0 - 0.1 \cos(10\pi t) + 0.05 \cos(50\pi t)] \text{ kN}, \\
 S_2 &= 4.27 \text{ m}.
 \end{aligned} \tag{4.2}$$

The vehicles move along the bridge with the same constant speed of 20 m/s with a 15 m headway distance. For both response simulation and load identification, the sampling frequency of 100 Hz is used for all cases.

Measured bending moment responses from nine measurement stations consisting of three stations at the locations of $L/4$, $L/2$ and $3L/4$ for each bridge span are used in the identification.

4.2.1 Conventional Moving Loads Identification

The simplest identification method of the problem was an optimization, the objective function of which is formulated using least square as Eq. (3.59). The solution of this problem is called a pseudo-inverse solution as Eq. (3.75) with the absence of the regularization parameter λ . Applying singular value decomposition can eliminate the ill-condition due to the rank deficiency of the coefficient matrix. The typical figure of identified loads is shown graphically in Figure 4.1.

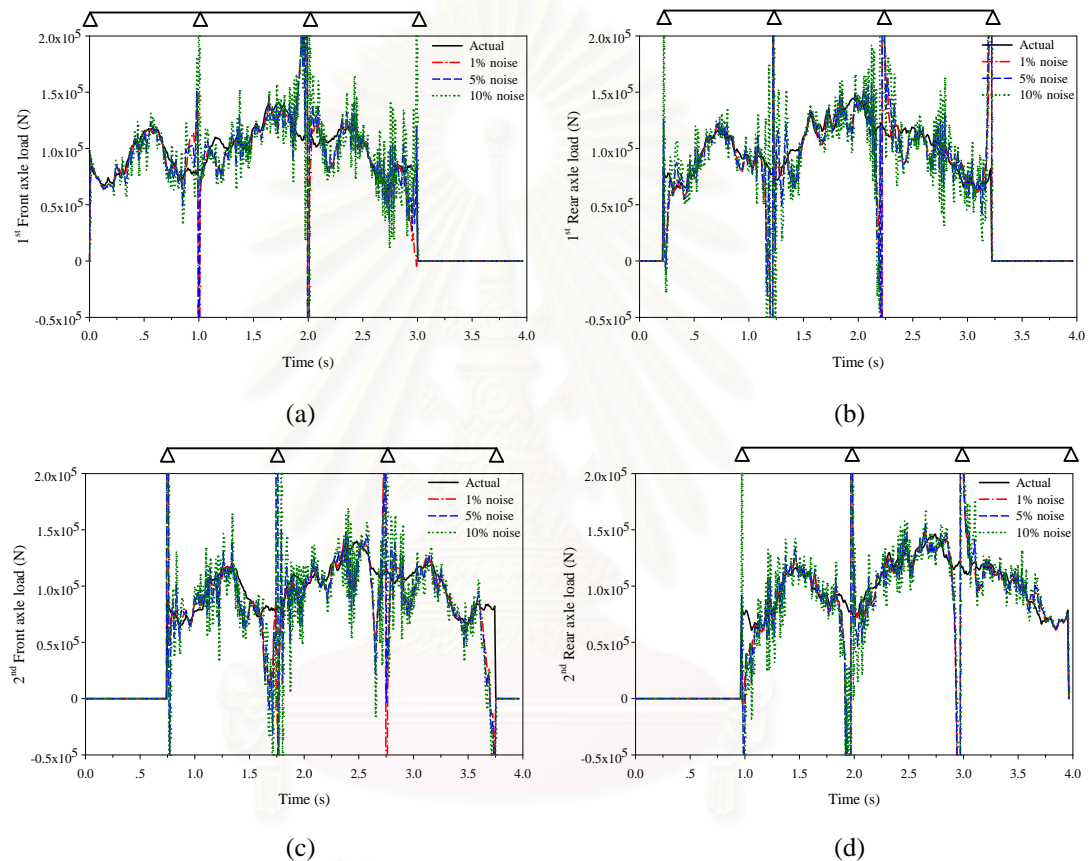


Figure 4.1 Typical identified axle loads of two vehicles' axle load identification from the conventional method: (a) front axle load of 1st vehicle, (b) rear axle load of 1st vehicle, (c) front axle load of 2nd vehicle and (d) rear axle load of 2nd vehicle

It is observed that identification using the conventional method provides an exact solution when the measurement data is not contaminated with noise, and the number of elements used in the simulation and identification systems is equivalent. However, it is impossible to avoid measurement noise in practice. The effect of measurement noise is therefore investigated as the main parameter in selection of the identification approach. According to the solution in Figure 4.1, the conventional

method is observed to be very sensitive to measurement noise. Therefore, it is concluded that this approach is not appropriate for use in practice.

4.2.2 Moving Load Identification with Optimal Regularization

As mentioned in section 4.2.1, it is found that the conventional identification method fails to identify the correct solution when the measurement noise is added particularly when the noise level is larger than 5%. In addition, it is found to be very sensitive to measurement noise. Therefore, this identification method cannot be adopted in practice to obtain accurate load time histories. To overcome this problem, the regularization method is applied in the optimization as Eq. (3.60) then the solution can be obtained from Eq. (3.75). With the presence of the regularization parameter λ the solution becomes robust to noise. The typical figure of identified loads is shown graphically in Figure 4.2.

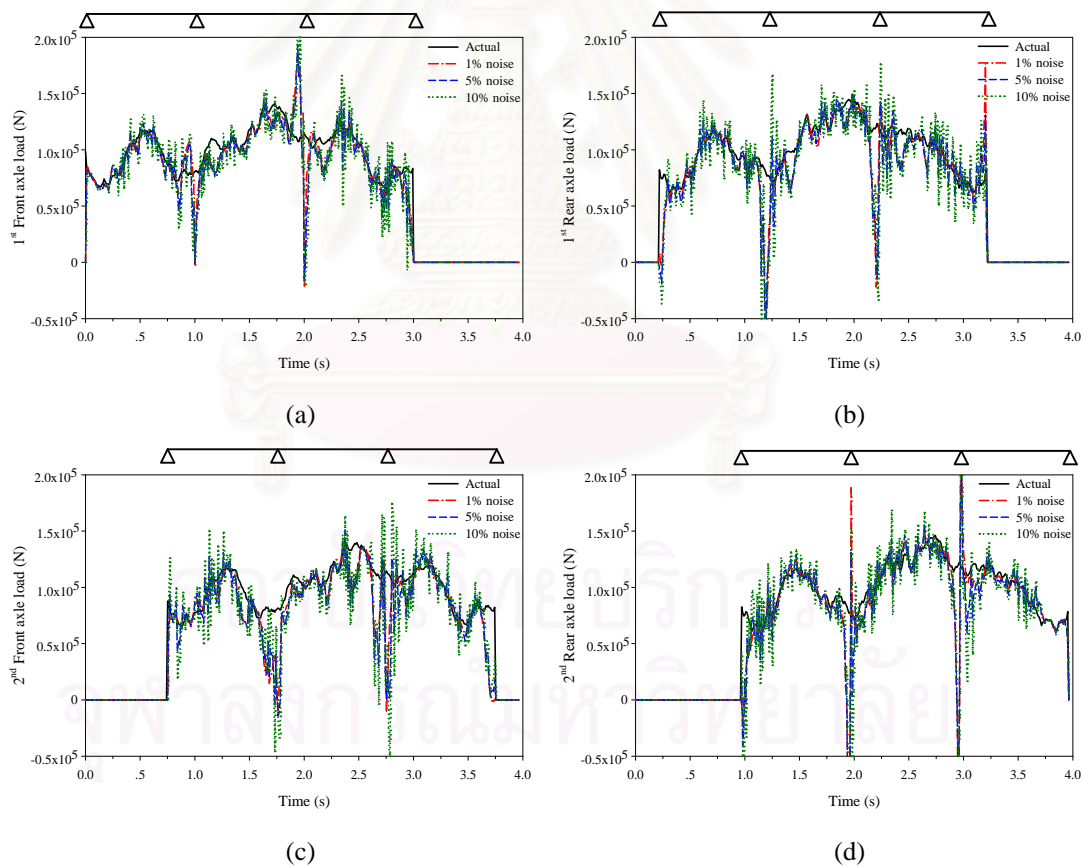


Figure 4.2 Typical identified axle loads of two vehicles' axle load identification from the optimal regularization method: (a) front axle load of 1st vehicle, (b) rear axle load of 1st vehicle, (c) front axle load of 2nd vehicle and (d) rear axle load of 2nd vehicle

Compared to the conventional identification method, the results show that the accuracy of the identified solution with noise is better and more robust to measurement noise. It is observed that using regularization, the obtained axle loads exhibit less oscillation than the conventional method without smoothing term. However, this solution of identifying axle loads at the duration when they pass the bridge supports is found to be inaccurate, particularly at the higher level of measurement noise. Moreover, determination of the optimal regularization parameter by plotting an L-curve is necessary to obtain an accurate solution.

4.2.3 Moving Load Identification with USC Regularization

According to the solution from conventional least square and least square with optimal regularization, as explained above, the problem is noise sensitivity and requires the optimal regularization parameter λ_{optimal} , which is difficult to obtain. Thus, the updated static component technique regularization is presented. The typical figure of identified loads is shown graphically in Figure 4.3. Table 4.2 and Table 4.3 show the comparison of the identification results of two moving loads and four moving loads, respectively. The results show that the identification error increases relatively in approximate proportion to the increase in the additional noise level when the number of elements used in simulation and identification is equivalent.

Table 4.2 Comparison of RPE (%) of two functional moving loads identification from various identification methods

Noise level	Moving load	RPE (%)					
		1-span simply supported bridge			3-span continuous bridge		
		Conv.	Opt. Reg.	Reg. USC	Conv.	Opt. Reg.	Reg. USC
1%	$\hat{p}_1(t)$	4.89	4.89	7.14	2.40	2.31	6.70
	$\hat{p}_2(t)$	2.06	2.06	2.46	0.92	0.89	2.90
5%	$\hat{p}_1(t)$	21.81	16.08	9.45	10.67	8.93	7.42
	$\hat{p}_2(t)$	10.28	12.06	4.54	4.63	4.80	3.55
10%	$\hat{p}_1(t)$	42.96	23.98	11.51	21.01	16.23	8.89
	$\hat{p}_2(t)$	20.56	18.74	6.01	9.25	9.70	4.63

Note: Conv. = Conventional method ($\lambda = 0$)

Opt. Reg. = Optimal regularization method ($\lambda = \lambda_{\text{optimal}}$)

Reg. USC = Regularization method with USC ($\lambda = \lambda_{\text{USC optimal}}$)

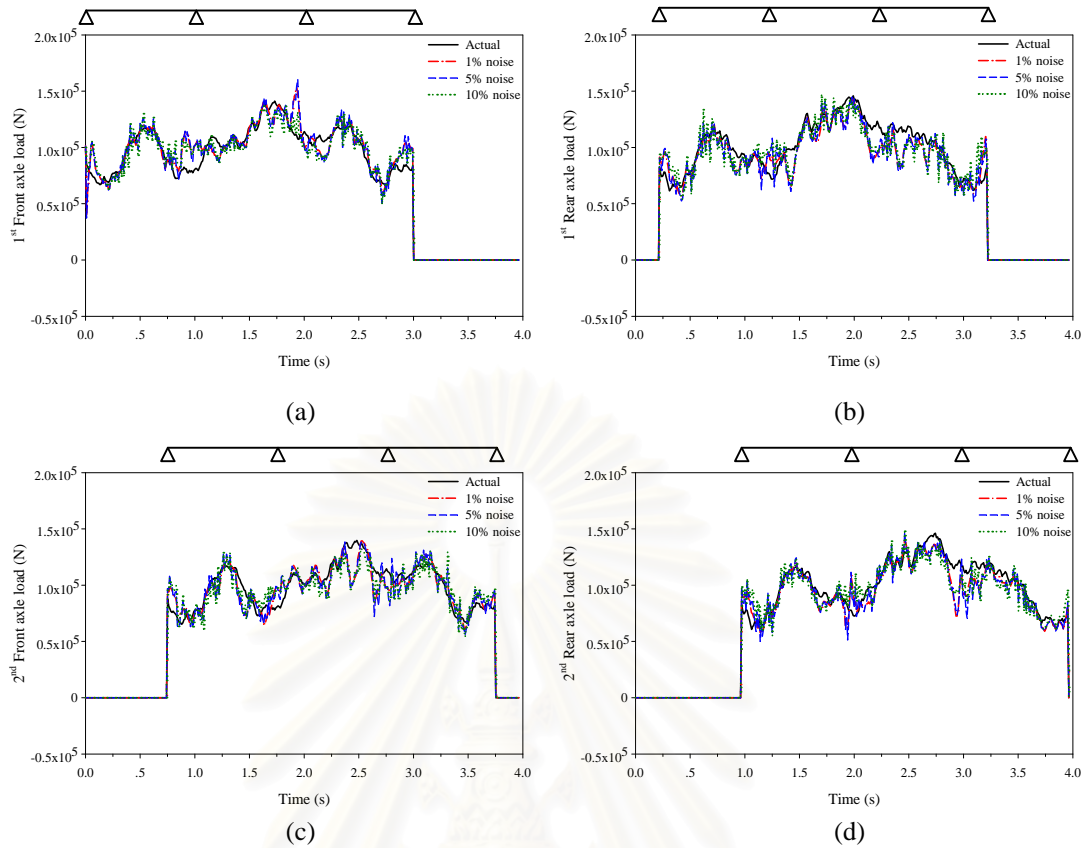


Figure 4.3 Typical identified axle loads of two vehicles' axle load identification from the regularization method with USC technique: (a) front axle load of 1st vehicle, (b) rear axle load of 1st vehicle, (c) front axle load of 2nd vehicle and (d) rear axle load of 2nd vehicle

Table 4.3 Comparison of RPE (%) of four functional moving loads identification from various identification methods

Noise level	Moving load	RPE (%)					
		1-span simply supported bridge			3-span continuous bridge		
		Conv.	Opt. Reg.	Reg. USC	Conv.	Opt. Reg.	Reg. USC
1%	$\hat{p}_1(t)$	14.34	10.37	7.32	4.44	3.90	6.50
	$\hat{p}_2(t)$	6.76	6.92	3.49	2.45	2.18	3.46
	$\hat{p}_3(t)$	13.36	11.76	4.98	4.27	4.28	6.04
	$\hat{p}_4(t)$	8.80	6.23	2.65	1.76	1.60	3.12
5%	$\hat{p}_1(t)$	69.08	20.02	8.45	22.22	13.11	7.32
	$\hat{p}_2(t)$	33.79	19.20	4.90	12.23	10.26	3.99
	$\hat{p}_3(t)$	66.81	28.40	7.59	21.36	17.76	7.56
	$\hat{p}_4(t)$	44.02	16.48	4.08	8.80	8.90	3.97
10%	$\hat{p}_1(t)$	137.51	26.65	9.44	44.44	24.98	9.01
	$\hat{p}_2(t)$	67.58	24.26	5.69	24.46	19.86	5.01
	$\hat{p}_3(t)$	133.61	36.70	10.46	42.73	27.72	9.46
	$\hat{p}_4(t)$	88.04	21.19	5.32	17.60	17.74	5.07

Note: Conv. = Conventional method ($\lambda = 0$)

Opt. Reg. = Optimal regularization method ($\lambda = \lambda_{\text{optimal}}$)

Reg. USC = Regularization method with USC ($\lambda = \lambda_{\text{USC optimal}}$)

The results show that the USC technique substantially improves the accuracy of identification. The weakness of the other methods at the time when the axle loads are approaching and leaving the bridge, and passing the internal bridge supports is obviously eliminated. The identification error still slightly increases with noise level but is not sensitive. In addition, the identified axle loads match the actual loads accurately. The results of axle load identification for a single vehicle and two vehicles are shown in Table 4.4 and Table 4.5, respectively.

Table 4.4 Comparison of RPE (%) of single-vehicle axle load identification from various identification methods

Noise level	Axle load	RPE (%)					
		1-span simply supported bridge			3-span continuous bridge		
		Conv.	Opt. Reg.	Reg. USC	Conv.	Opt. Reg.	Reg. USC
1%	Front	9.41	8.79	8.88	11.34	8.31	5.72
	Rear	16.88	9.18	6.63	28.86	10.38	6.78
5%	Front	17.91	15.23	10.46	13.91	10.64	6.86
	Rear	24.82	11.77	8.29	28.99	11.83	7.87
10%	Front	31.06	20.59	12.81	19.51	13.83	7.96
	Rear	36.38	17.42	11.77	30.46	15.28	9.39

Note: Conv. = Conventional method ($\lambda = 0$)

Opt. Reg. = Optimal regularization method ($\lambda = \lambda_{\text{optimal}}$)

Reg. USC = Regularization method with USC ($\lambda = \lambda_{\text{USC optimal}}$)

Table 4.5 Comparison of RPE (%) of two-vehicle axle load identification from various identification methods

Noise level	Axle load	RPE (%)					
		1-span simply supported bridge			3-span continuous bridge		
		Conv.	Opt. Reg.	Reg. USC	Conv.	Opt. Reg.	Reg. USC
1%	1 st Front	20.01	10.40	9.73	16.62	9.29	7.71
	1 st Rear	40.81	12.19	8.11	31.07	12.02	8.87
	2 nd Front	15.41	14.97	9.42	17.35	14.41	7.73
	2 nd Rear	27.74	9.93	7.31	43.50	12.20	7.08
5%	1 st Front	62.24	17.80	11.76	19.78	12.24	7.69
	1 st Rear	80.07	20.45	10.52	35.22	15.35	10.12
	2 nd Front	39.41	23.82	12.30	23.40	17.73	8.33
	2 nd Rear	79.68	16.89	9.51	47.45	14.60	8.09
10%	1 st Front	118.14	22.42	13.73	25.27	16.90	8.61
	1 st Rear	131.41	25.54	11.96	47.25	21.00	11.61
	2 nd Front	76.91	29.39	13.25	36.16	22.90	9.65
	2 nd Rear	146.26	21.36	10.50	55.64	20.29	9.44

Note: Conv. = Conventional method ($\lambda=0$)

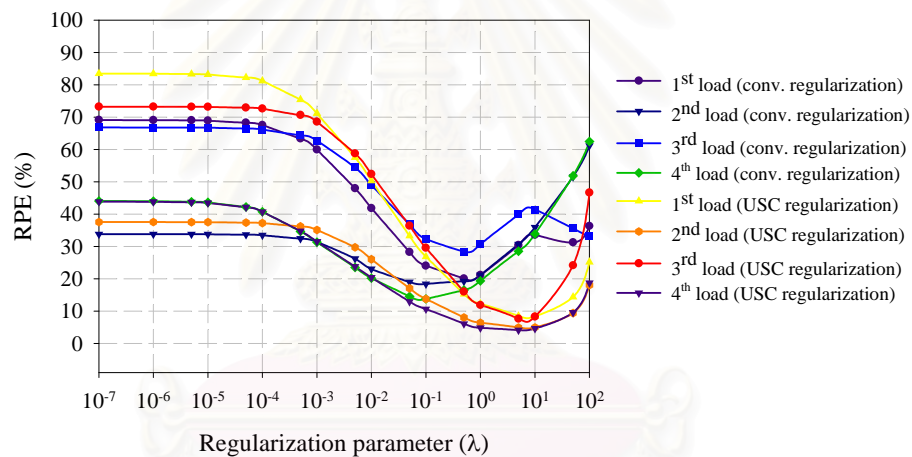
Opt. Reg. = Optimal regularization method ($\lambda = \lambda_{\text{optimal}}$)

Reg. USC = Regularization method with USC ($\lambda = \lambda_{\text{USC optimal}}$)

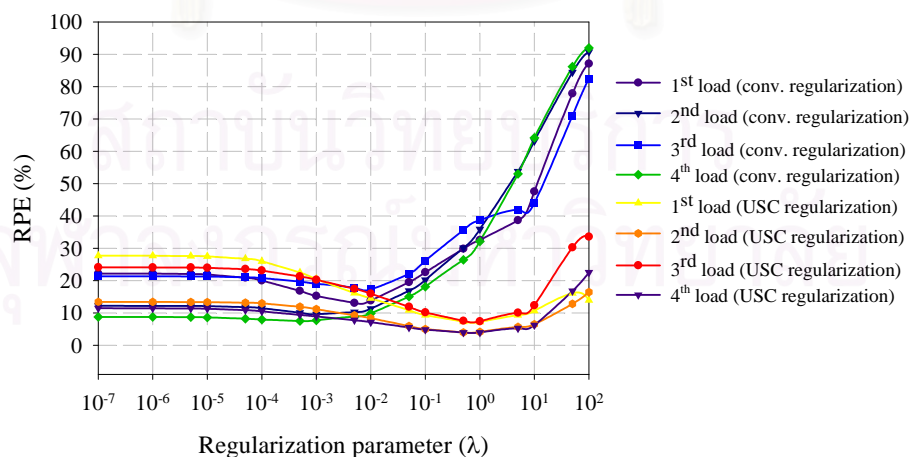
According to the solutions from Tables 4.4 and 4.5, they clearly indicate that the proposed regularization method with USC technique can identify the axle loads of

multiple vehicles accurately for both the single-span simply supported bridge and the three-span continuous bridge. The identification error in every axle is drastically decreased when the USC algorithm is applied.

However, since the comparisons presented in Tables 4.2 to 4.5 are conducted with the optimal regularization parameter for both optimal regularization and USC regularization methods, to demonstrate the effectiveness and convenience of applying the identification approaches in the practical aspect of selecting the appropriate regularization parameter, plots of the identification error at various order of regularization parameter are required. Figure 4.4 represents RPE of identified loads at various orders of regularization of four concentrated loads identification traveling on a single-span simply supported and a three-span continuous bridges at measurement noise level of 5%.



(a)



(b)

Figure 4.4 RPE of identified loads of four concentrated loads identification with various orders of regularization parameter at measurement noise level of 5%: (a) single-span simply supported bridge and (b) three-span continuous bridge

It is observed from Figure 4.4 that identification with the USC regularization method allows better solution accuracy than the conventional regularization method. Moreover, the most accurate results obtained from the USC regularization method perform at the same order of regularization parameter in the range of 0.1 to 10 approximately for both single-span and three-span bridges while the optimal parameters of the conventional regularization method perform within a different range. This is very important for the real application of the identification system because the difficulty of determining the appropriate regularization parameter directly affects the computational time. Therefore, the regularization method with USC is proposed as the identification approach for this dissertation.

4.3 The Study of Related Parameters Affecting Axle Load Identification

In this section, the parameters affecting moving load identification system is studied. The three groups of parameters consist of measurement parameters, modeling parameters and physical parameters. The effects of measurement parameters such as the number and location of sensors, measurement noise level and sampling frequency of the data acquisition system are firstly considered. Once the effects of measurement parameters are understood, the proper measurement parameters for the load identification are suggested. Then the modeling parameters and physical parameters are investigated. In this section, the assumed vehicle axle loads are simulated using a vehicle model of which the vehicle properties measured from a real truck (Mulcahy, 1983) are listed in Table 4.6. Moreover, in order to analyze the obtained numerical results in the practical aspect, the measurement noise level of 5% is taken into account for every study case.

Table 4.6 Parameter of vehicle model used in vehicle-bridge interaction

Vehicle properties			
$I_v = 1.47 \times 10^5 \text{ kgm}^2$	$m_v = 17735 \text{ kg}$	$m_1 = 1500 \text{ kg}$	$m_2 = 1000 \text{ kg}$
$k_{s1} = 2.47 \times 10^6 \text{ N/m}$	$k_{s2} = 4.23 \times 10^6 \text{ N/m}$	$k_{t1} = 3.74 \times 10^6 \text{ N/m}$	$k_{t2} = 4.60 \times 10^6 \text{ N/m}$
$c_{s1} = 3.00 \times 10^4 \text{ N/m}$	$c_{s2} = 4.00 \times 10^4 \text{ N/m}$	$c_{t1} = 3.90 \times 10^3 \text{ N/m}$	$c_{t2} = 4.30 \times 10^3 \text{ N/m}$
$S = 4.27 \text{ m}$	$a_1 = 0.519$	$a_2 = 0.481$	

4.3.1 Regularization Parameter

The study of the effect of the regularization parameter is very essential and needs to be first conducted in the parametric study. In order to overcome the difficulty of regularization parameter selection to obtain the accurate solution for various conditions of vehicle passages, the range of appropriate regularization parameters assigned in the USC algorithm is determined. Again, the number of beam elements, sampling rate and number of measurement stations similar to section 4.2 are used. Figure 4.5 shows the identification error with a different order of regularization parameters from various vehicle configurations. The optimal regularization parameter for each case and the acceptable range for parameter selection can be observed.

It can be noticed from Table 4.7 that the optimal regularization parameter is nearly the same for every case except when the vehicle mass and bridge surface roughness is different. Variation of vehicle speed, weight distribution between front and rear axles or axle spacing of the vehicle do not affect the optimal regularization parameter while the effects of vehicle mass and bridge surface roughness have a significant effect. The optimal regularization parameter tends to be larger when the vehicle mass is heavier or the bridge surface is smoother.

It is noticed that the λ_{optimal} for each case usually lies in the range between 0.01 and 1.00. Table 4.6 demonstrates the identification errors at the lower and upper bound of the regularization parameter range, and also their least errors at the λ_{optimal} . It is observed that the identification errors for every case are within 30% at the lower and upper bounds of the regularization parameter. For the moderate order of vehicle parameters in single-vehicle identification, the maximum identification error is within 12% and the optimal regularization is close to 0.10 for every case. However, the most appropriate value of regularization parameter assigned for every vehicle category and multiple vehicle passage is found to be 1.00. Therefore, the regularization parameter of 1.00 is simply adopted for every following investigation.

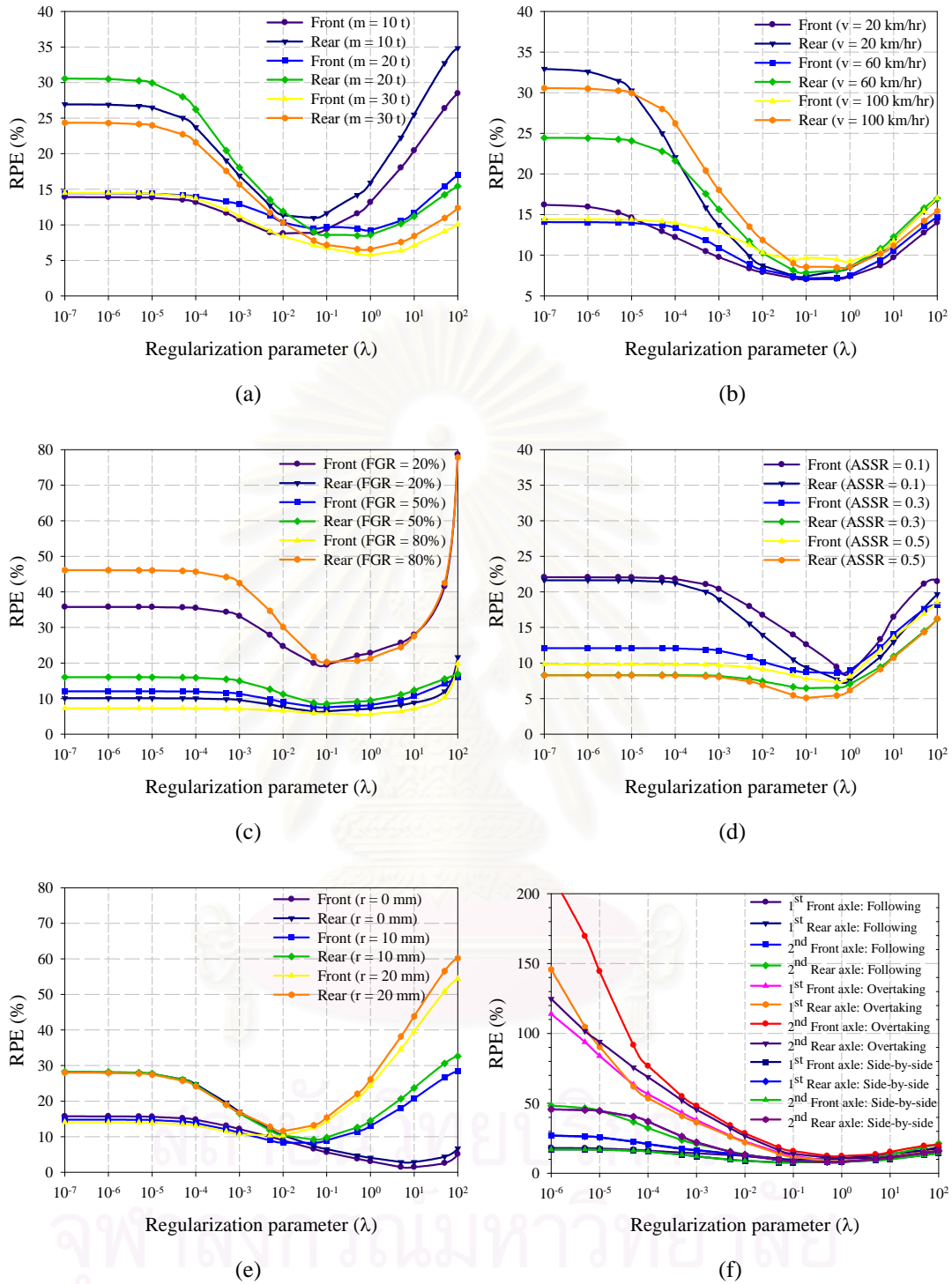


Figure 4.5 Plots of identification error of vehicle axle loads from various orders of regularization parameters: (a) vehicle mass, (b) vehicle speed, (c) FGR, (d) ASSR, (e) bridge surface roughness and (f) two-vehicle axle load identification

Table 4.7 Identification error from different influence parameters at various regularization parameters

Parameter	Axle load	RPE (%)			λ_{optimal}	
		$\lambda = 0.01$	$\lambda = 1$	λ_{optimal}		
Vehicle mass	Light: 10 t	Front axle	8.77	13.17	8.86	0.05
		Rear axle	11.36	15.92	10.97	
	Moderate: 20 t	Front axle	10.35	9.26	9.66	0.10
		Rear axle	11.88	8.60	8.57	
	Heavy: 30 t	Front axle	8.38	5.80	5.80	1.00
		Rear axle	10.31	6.58	6.58	
Vehicle speed	Slow: 20 km/hr	Front axle	7.91	7.39	7.03	0.10
		Rear axle	8.74	8.46	7.41	
	Moderate: 60 km/hr	Front axle	8.23	7.55	7.17	0.10
		Rear axle	10.28	8.59	7.87	
	Fast: 100 km/hr	Front axle	10.35	9.26	9.26	1.00
		Rear axle	11.88	8.60	8.60	
Front axle to gross weight ratio	Low: 20%	Front axle	24.72	22.79	19.48	0.10
		Rear axle	7.61	7.16	6.40	
	Moderate: 50%	Front axle	9.00	8.18	7.55	0.10
		Rear axle	11.24	9.46	8.54	
	High: 80%	Front axle	6.58	5.59	5.49	0.50
		Rear axle	30.14	21.27	20.64	
Axle spacing to span ratio	Low: 0.1	Front axle	16.75	8.64	8.64	1.00
		Rear axle	13.95	7.52	7.52	
	Moderate: 0.30	Front axle	10.18	9.00	8.57	0.50
		Rear axle	7.43	7.05	6.54	
	High: 0.50	Front axle	9.15	8.13	7.35	0.50
		Rear axle	6.89	6.17	5.44	
Magnitude of bridge surface roughness	Smooth: 0 mm	Front axle	8.98	3.05	1.44	5.00
		Rear axle	10.38	4.05	2.86	
	Moderate: 10 mm	Front axle	8.31	13.00	8.20	0.05
		Rear axle	10.36	14.51	9.21	
	High: 20 mm	Front axle	10.38	24.47	10.38	0.01
		Rear axle	11.59	26.12	11.59	
Two-vehicle axle load identification	Following	1 st Front axle	12.35	7.89	7.69	0.50
		1 st Rear axle	12.92	10.65	10.12	
		2 nd Front axle	12.56	8.80	8.33	
		2 nd Rear axle	13.53	8.65	8.09	
	Overtaking	1 st Front axle	22.73	8.57	8.57	1.00
		1 st Rear axle	22.12	9.01	9.01	
		2 nd Front axle	28.56	12.28	12.28	
		2 nd Rear axle	26.74	10.85	10.85	
	Side-by-side	1 st Front axle	8.94	8.12	7.78	0.10
		1 st Rear axle	13.18	8.16	8.59	
		2 nd Front axle	8.94	8.12	7.78	
		2 nd Rear axle	13.18	8.16	8.59	

4.3.2 Number and Location of Measurement Stations

In the response measurement, the preliminary study of the sufficient number of sensors and effective location of measurement is very important. Using insufficient information and a less dominant response signal in identification yields an inaccurate and non-robust identified solution. Conducting a sensor arrangement study does not only improve solution accuracy and efficiency of identification but also reduces the instrumental cost by using fewer sensors.

Tables 4.8 and 4.9 show sensor arrangement patterns used in the evaluation of sensor number and its location for single-vehicle and multiple-vehicle axle load identifications, respectively. The number of sensors used in identification must not be less than the number of unknown axle loads in order to analyze the problem as a determined or an overdetermined problem. Tables 4.10 and 4.11 show the identification error from a different scheme of sensor arrangement corresponding to Tables 4.8 and 4.9 at 5% measurement noise level. According to the obtained results, it is found that the identification error decreases relatively to the increasing number of sensors used in the measurement.

Table 4.8 Sensor arrangements of single-span simply supported bridge

Number of sensors	Location of sensors
3-SA	$L/4, L/2, 3L/4$
3-SB	$L/3, L/2, 2L/3$
5-SA	$L/6, L/3, L/2, 2L/3, 5L/6$
5-SB	$L/6, L/4, L/2, 3L/4, 5L/6$
7-S	$L/8, L/4, 3L/8, L/2, 5L/8, 3L/4, 7L/8$
9-S	$L/10, L/5, 3L/10, 2L/5, L/2, 3L/5, 7L/10, 4L/5, 9L/10$

Table 4.9 Sensor arrangements of three-span continuous bridge

Number of sensors	Location of sensors		
	Left span	Middle span	Right span
3-C		$L/4, L/2, 3L/4$	
5-CA	$L/2$	$L/4, L/2, 3L/4$	$L/2$
5-CB	$L/4, 3L/4$	$L/2$	$L/4, 3L/4$
7-CA	$L/4, 3L/4$	$L/4, L/2, 3L/4$	$L/4, 3L/4$
7-CB	$L/4, L/2, 3L/4$	$L/2$	$L/4, L/2, 3L/4$
7-CC	$L/2, 3L/4$	$L/4, L/2, 3L/4$	$L/4, L/2$
7-CD	$L/4, L/2$	$L/4, L/2, 3L/4$	$L/2, 3L/4$
9-C	$L/4, L/2, 3L/4$	$L/4, L/2, 3L/4$	$L/4, L/2, 3L/4$

Table 4.10 Comparison of RPE (%) of vehicle axle load identification on single-span simply supported bridge from various sensor numbers and locations

Sensor pattern	RPE (%)					
	Single vehicle's axle load identification		Two vehicles' axle load identification			
	Front axle	Rear axle	1 st Front	1 st Rear	2 nd Front	2 nd Rear
3-SA	15.21	11.79	N/A	N/A	N/A	N/A
3-SB	14.70	13.47	N/A	N/A	N/A	N/A
5-SA	10.16	7.99	11.00	9.80	11.38	8.68
5-SB	9.90	7.75	12.03	10.30	11.93	8.57
7-S	12.24	7.79	14.61	10.49	13.83	9.70
9-S	9.89	7.17	10.42	10.66	10.12	8.33

Table 4.11 Comparison of RPE (%) of vehicle axle load identification on a three-span continuous bridge from various sensor numbers and locations

Sensor pattern	RPE (%)					
	Single vehicle's axle load identification		Two vehicles' axle load identification			
	Front axle	Rear axle	Front	Rear	Front	Rear
3-C	11.67	11.42	N/A	N/A	N/A	N/A
5-CA	10.38	11.28	10.60	14.36	12.03	10.66
5-CB	7.72	8.86	8.89	12.26	10.37	9.71
7-CA	7.78	8.27	8.75	12.10	9.78	9.60
7-CB	7.01	8.36	7.68	10.53	9.13	8.65
7-CC	9.34	10.38	9.91	13.17	10.98	10.21
7-CD	7.30	7.82	8.23	10.70	8.66	8.06
9-C	6.75	7.76	7.69	10.77	8.63	8.47

For the axle load identification of a single vehicle, the identified axle loads are acceptable when using three or five sensors with the identification error within 15%. The most accurate result is obtained when nine sensors are used for both the single-span simply supported and three-span continuous bridges with RPE less than 10%. Similar to the single vehicle case, the number of sensors required in the two vehicle identification is at least 5 sensors and the best results can be achieved when using 9 sensors. It is noticed that adopting plenty of sensors – more than 5 – does not enhance solution accuracy in the case of the single-span simply supported bridge but significantly improves the accuracy for the three-span simply supported bridge. This is because the multi-span bridge system requires more sensors to accurately settle the bridge behavior in the higher vibration mode.

For the location of measurements, using 5-SB and 7CD patterns seems sufficient to identify the axle loads for the single-span simply supported bridge and the three-span continuous bridge, respectively. However, the most accurate results for both single-vehicle and multiple-vehicle axle load identifications are obtained using 9S and 9C patterns of sensor locations for the single-span simply supported bridge

and the three-span continuous bridge, respectively. Therefore, this research will use 9 sensors for all study cases for both the single-span simply supported bridge and the three-span continuous bridge.

4.3.3 Structural Discretization and Sampling Rate

Regarding the structural model, the bridge is simplified as a beam based on the finite element method. The appropriate number of elements used in the identification system must provide an accurate solution and not take too much computational time. Similarly, the sampling rate of data acquisition for signal measurement is also an important parameter as well as the structural discretization. Collecting responses at a sampling rate that is too slow cannot capture the dynamic behaviors of the bridge and loads. Moreover, the obtained solution becomes inaccurate. On the other hand, identification with a sampling rate that is too fast is unnecessary and wastes computational time. Therefore, the optimal number of beam elements used in the structural modeling and the sampling rate needed in data acquisition are firstly determined.

The relative percentage errors of the identified loads for the different number of beam elements and sampling rate are listed in Table 4.12 and the corresponding results are plotted in Figure 4.6. The solution shows that identification using 4 beam elements per bridge span results in larger identification error than those from the higher number of elements. The identification using 8 finite beam elements per span is found to be sufficient with acceptable results while using 12 or 16 elements provide more accuracy than the others but they consume much longer computational time than using 8 elements.

Table 4.12 Identification error of single-vehicle axle load identification from single-span simply supported bridge for different discretization and sampling rate

Sampling rate (Hz)	Number of elements							
	4		8		12		16	
	Front axle	Rear axle	Front axle	Rear axle	Front axle	Rear axle	Front axle	Rear axle
25	25.56	25.95	18.91	22.44	18.50	21.02	17.98	21.97
50	20.16	15.86	13.10	10.78	12.46	9.30	11.79	9.78
100	20.33	13.84	12.86	9.51	12.51	8.20	11.61	8.39
200	19.34	13.21	12.08	9.62	11.15	7.40	11.19	8.00
400	18.67	12.65	11.78	8.63	11.95	7.63	10.29	7.38

Note: All cases are identified with the same regularization parameter, λ of 1.0.

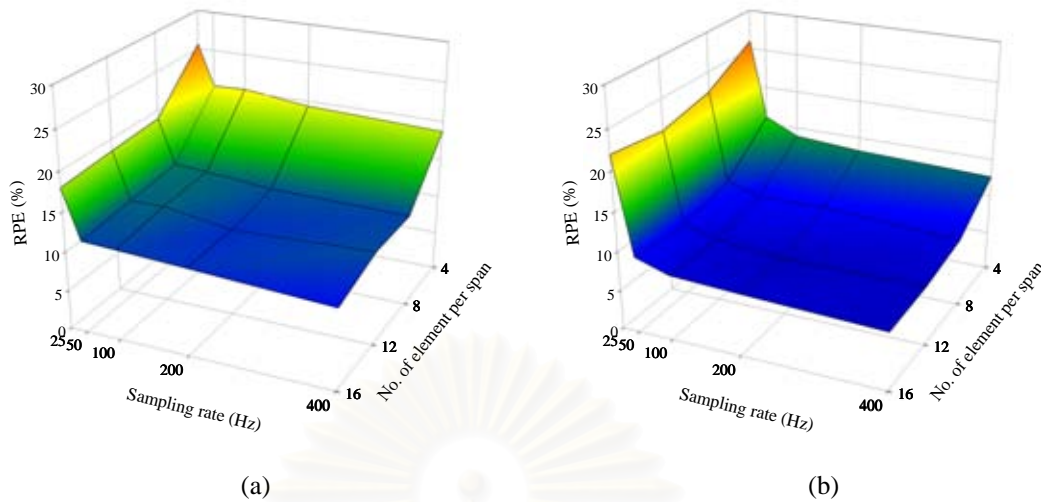


Figure 4.6 Identification error of single vehicle axle load identification from a three-span continuous bridge with various sampling rates and number of beam elements per bridge span: (a) front axle load and (b) rear axle load

In the case of the sampling rate comparison, the identification error is significantly affected by its variation since the first five fundamental frequencies of the three-span continuous bridge are 5.6, 7.1, 10.4, 22.2 and 25.3 Hz. The results from Table 4.12 show that using a sampling rate larger than 50 Hz seems sufficient and yields similar identification errors. Likewise, it is clearly observed from Figure 4.6 that the identification error is dramatically decreased and becomes steady at the sampling rate of 50 Hz. Therefore, applying a sampling rate at approximately 10 times the first mode fundamental frequency or twice the fifth mode fundamental frequency corresponding to the recommendation by Yu and Chan (2005) seems sufficient to obtain an accurate result.

Therefore, axle load identification with structural discretization of 8 beam elements per bridge span at the sampling rate of 100 Hz is used in the following investigation.

4.3.4 Vehicle Mass and Moving Speed

To study the effects of vehicle mass and moving speed on axle load identification, the identification of possible vehicle mass and moving speed as usually observed in traffic is conducted. Table 4.13 and Figure 4.7 show the identification error of a single vehicle varying in mass and moving speed from 10-30 tons and 20-

100 km/hr, respectively. The result from Figure 4.7 indicates that the vehicle with a heavier mass and traveling at a lower speed is easier to accurately identify than one with a lighter mass traveling at a higher speed. This is because the heavier vehicle induces the bending moment response with a larger signal to noise ratio, significantly affecting the identified results. An identification case with a larger signal-to-noise ratio usually provides better solution accuracy than a case with a smaller signal-to-noise ratio. Additionally, a vehicle traveling at a lower speed induces lesser dynamic behavior in the measured bridge response. Hence, the axle loads of slower vehicles can be identified more accurately than those crossing the bridge at a faster speed. It is also observed that vehicle mass affects solution accuracy more than moving speed. However, it should be noted that the proposed method can provide an identification error below 13% for all considered cases.

Table 4.13 Identification error of single-vehicle axle load identification on a three-span continuous bridge from different vehicle mass and moving speed

Moving speed (km/hr)	Vehicle mass									
	$M_s = 10$ t		$M_s = 15$ t		$M_s = 20$ t		$M_s = 25$ t		$M_s = 30$ t	
	Front	Rear	Front	Rear	Front	Rear	Front	Rear	Front	Rear
20	9.99	11.52	7.93	8.73	7.03	7.41	6.54	6.76	6.15	6.28
40	9.70	12.08	7.92	9.18	7.03	8.14	6.43	7.06	6.14	6.63
60	9.38	11.63	7.96	8.84	7.17	7.87	6.83	7.47	6.70	7.17
80	10.43	12.02	8.32	9.39	7.61	8.33	7.22	7.54	7.04	7.03
100	11.80	11.38	10.29	9.69	9.66	8.57	9.10	8.65	8.64	8.25

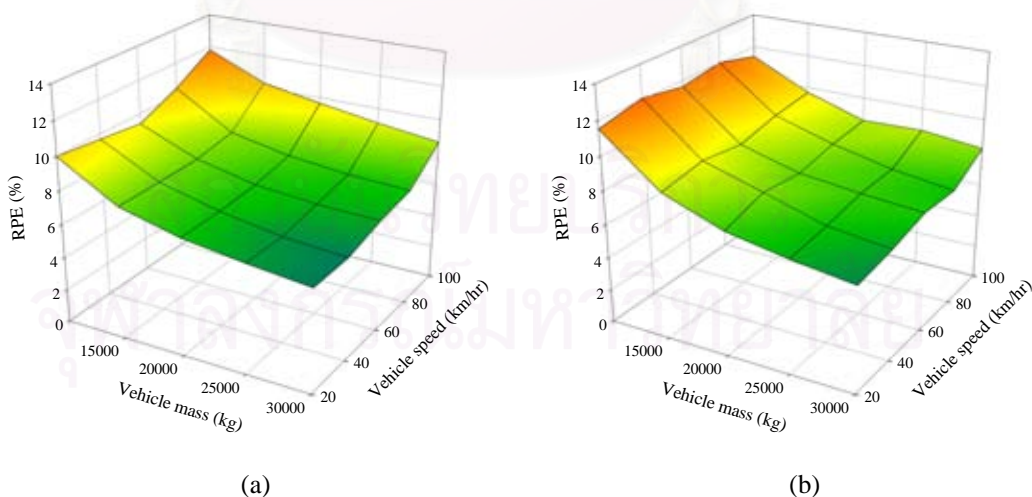


Figure 4.7 Identification error of single-vehicle axle load identification on a three-span continuous bridge with various sampling rates and number of beam elements per bridge span: (a) front axle load and (b) rear axle load

4.3.5 Bridge Surface Roughness

Bridge surface roughness is the primary parameter of the identification since it is one of the bridge properties. The effect of bridge surface roughness magnitude on the identification accuracy is investigated. The bridge surface roughness profile is simulated according to ISO-8606 specifications. Variation of maximum roughness magnitude is conducted. Table 4.14 and Figure 4.8 present the results of single-vehicle axle load identification from different roughness magnitude and moving speed. It is found that moving speed does not relate to the surface roughness and slightly affects solution accuracy in a similar manner to the results explained in section 4.3.4. In the case of bridge surface roughness, it is clearly observed that identification error is significantly influenced by the roughness magnitude. Vehicle loads moving on a bridge with smooth or small magnitude surface roughness can be identified with more accuracy than those traveling on a bridge with rough surface. Therefore, overlaying a new pavement on a bridge or selecting a bridge with smooth roughness is highly recommended in practice.

Table 4.14 Comparison of RPE (%) of single-vehicle axle load identification from different magnitude of bridge surface roughness and moving speed

Moving speed (km/hr)	Axle load	RPE (%)				
		Maximum magnitude of bridge surface roughness (mm)				
		0	5	10	15	20
20	Front	3.21	7.33	13.12	19.19	24.72
	Rear	3.26	8.38	15.21	21.92	27.42
40	Front	3.06	7.59	13.52	19.52	24.77
	Rear	3.79	9.14	16.33	22.78	27.63
60	Front	3.05	7.10	13.00	19.16	24.47
	Rear	4.05	8.01	14.51	20.93	26.11
80	Front	3.46	8.36	15.11	22.15	28.15
	Rear	4.80	9.25	16.10	23.02	28.60
100	Front	5.30	9.24	15.68	22.15	26.96
	Rear	5.42	8.24	14.21	20.48	25.80

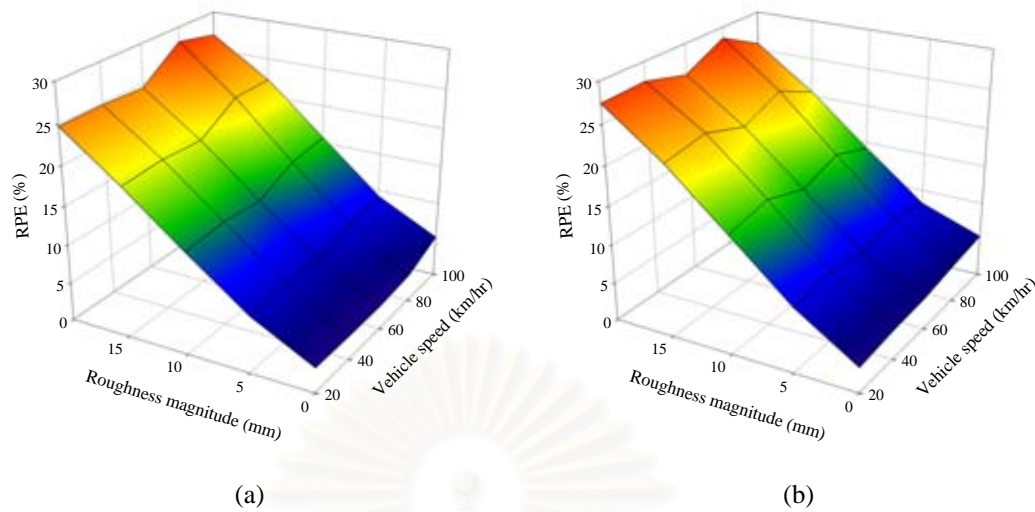


Figure 4.8 Identification error of single-vehicle axle load identification from a three-span continuous bridge with various levels of vehicle speeds and bridge surface roughness: (a) front axle load and (b) rear axle load

4.3.6 Front Axle to Gross Weight Ratio (FGR) and Axle Spacing to Span Ratio (ASSR)

In this section, effects of weight distribution between front and rear axles as well as axle spacing are considered. To study the effect of axle weight distribution, the ratio between static front axle weight and static gross weight of the vehicle is defined as the front axle to gross weight ratio (FGR). Identification accuracy due to variation of FGR from 20% to 80% is investigated. Concerning the effect of axle spacing, Yu and Chan (2004) reported that closely spaced axles are difficult to distinguish and are usually averaged in the axle load identification. Thus, the identification of vehicle axle loads with various axle spacings is investigated. The axle spacings are normalized to the bridge span length as an axle spacing to span ratio (ASSR)

In this study, the bridge span length is fixed as 20m for all three spans and the vehicle axle spacing varies from 2m to 10m. Table 4.15 and Figure 4.9 show identification error of single-vehicle axle load identification from a three-span continuous bridge for different front axle to gross weight ratios and axle spacing to span ratios.

Table 4.15 Identification error of single-vehicle axle load identification from a three-span continuous bridge for different front axle to gross weight ratios and axle spacing to span ratios

FGR (%)	Axle spacing (ASSR)									
	2 m (0.1)		4 m (0.2)		6 m (0.3)		8 m (0.4)		10 m (0.5)	
	Front axle	Rear axle	Front axle	Rear axle	Front axle	Rear axle	Front axle	Rear axle	Front axle	Rear axle
20	18.31	6.13	19.48	6.40	16.98	4.74	18.40	4.93	15.66	4.30
30	11.52	6.61	12.50	6.95	11.42	5.53	11.64	5.32	10.03	4.77
40	8.64	7.52	9.11	7.46	8.70	6.46	8.54	6.06	7.35	5.44
50	6.87	7.74	7.55	8.54	6.71	7.67	6.76	7.28	5.83	6.42
60	6.30	9.59	6.85	10.42	6.28	9.77	5.79	9.51	5.01	7.95
70	5.74	13.01	6.08	13.55	5.80	13.27	5.35	13.53	4.75	10.07
80	5.38	20.09	5.79	20.28	5.85	20.88	5.20	19.39	4.46	16.70

Note: All cases are identified with the optimal regularization parameter, $\lambda_{USC\text{ optimal}}$

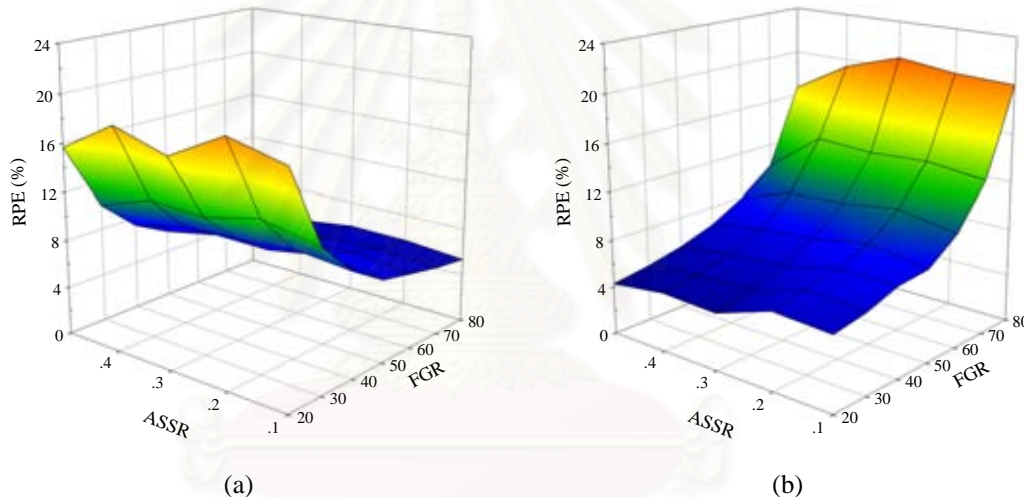


Figure 4.9 Identification error of single-vehicle axle load identification from a three-span continuous bridge for different front axle to gross weight ratios and axle spacing to span ratios: (a) front axle load and (b) rear axle load

The obtained results indicate that the FGR affects the solution accuracy more than the ASSR. An axle with a heavier weight can be identified with more accuracy than an axle with a lighter weight. This is because the identification error is calculated in terms of percentage value. From the solution with various ASSR, it is observed that axle load identification for a vehicle with closely spaced axles results in a larger RPE than identification for a vehicle with wider axle spacing. This is because the bridge response in the case of closely spaced axles is nearly indistinguishable from the

response induced by a vehicle with a tandem axle configuration. Therefore, the closely spaced axle loads become more difficult to identify accurately.

4.3.7 Number of Moving Loads and Level of Measurement Noise

In real traffic, there are many vehicles crossing the bridge at the same duration. In order to investigate the capability and effectiveness of axle load identification of a multi-axle vehicle or multiple vehicles, the effect of the number of axle loads are studied. The point load functions from section 4.2 are adopted in multi-axle vehicle load simulation. Axle loads with odd and even numbers are assumed as $p_1(t)$ and $p_2(t)$ from Eq. (4.1), respectively. Every axle load moves at the same constant speed of 30m/s and is placed between each other at an equal spacing of 4m. The measurement noise level is again considered for robustness evaluation. Table 4.16 represents the identification error of a multi-axle vehicle assumed as a group of the functional loads moving on a three-span continuous bridge with different measurement noise levels.

From Table 4.16 it is found that the proposed method is capable of identifying multi-axle loads with acceptable accuracy when the number of measurement stations is more than the number of identified axle loads. It is noticed that the maximum identification error in axle load increases relative to the additional number of axle loads. The maximum axle load error is below 25% for every study case. The RPEs from 8 axle load identification at measurement noise of 5% and 10% are only within 11% and 14%, respectively. It can be concluded that axle load identification of a multi-axle vehicle or multiple vehicles using the proposed method is effective and robust when the axle loads do not overlap each other during the travel duration.

Table 4.16 Identification error of moving load identification on a three-span continuous bridge from a different number of loads and measurement noise level

Noise level	Number of loads	RPE (%)							
		$\hat{p}_1(t)$	$\hat{p}_2(t)$	$\hat{p}_3(t)$	$\hat{p}_4(t)$	$\hat{p}_5(t)$	$\hat{p}_6(t)$	$\hat{p}_7(t)$	$\hat{p}_8(t)$
1%	1	4.34							
	2	10.94	4.75						
	3	8.77	5.31	11.53					
	4	6.72	9.20	12.91	3.97				
	5	6.28	10.73	19.11	7.95	12.60			
	6	7.02	6.82	14.35	7.44	7.68	4.86		
	7	6.26	9.77	21.44	9.08	9.41	5.23	8.73	
	8	7.32	5.63	9.04	5.48	9.41	5.62	10.64	6.10
5%	1	5.21							
	2	11.42	5.23						
	3	9.68	6.50	13.96					
	4	7.93	9.97	14.63	4.61				
	5	6.99	10.35	17.60	7.32	12.55			
	6	8.51	6.70	14.43	7.14	9.70	5.75		
	7	7.75	10.17	22.54	9.61	10.74	5.65	10.10	
	8	8.85	5.97	10.30	6.16	10.00	5.75	10.22	6.00
10%	1	4.93							
	2	12.97	6.19						
	3	11.96	7.97	16.74					
	4	10.84	11.40	17.45	6.24				
	5	9.19	10.60	18.97	7.91	14.17			
	6	11.63	7.62	17.38	8.23	14.31	7.31		
	7	11.04	11.08	24.83	10.83	13.31	6.79	13.32	
	8	11.86	7.28	13.40	7.78	12.62	7.46	11.78	6.72

4.3.8 Headway and Vehicle Speed Ratio

Regarding multiple-vehicle travel, there are many possible moving scenarios between the considered vehicles since each vehicle moves at independent speed. The multiple-vehicle movement focused on in this research is two-vehicle axle load identification. Different moving schemes between two vehicles including short headway, overtaking and side-by-side movements are studied and their effects on solution accuracy investigated. Since the relative movement between two vehicles depends on their moving speeds and headway, two indexes are defined to represent the type of vehicle travel: the vehicle speed ratio and the bridge approach time interval. The vehicle speed ratio is the ratio of the first and the second model vehicle velocities, v_1/v_2 . The bridge approach time interval, t_d , is the delay time between the arrival of the second vehicle and the first vehicle at the bridge. Table 4.17 shows the study cases representing the different movement scenarios of two-vehicle axle load identification controlled by the varying vehicle speed ratio and t_d .

Table 4.17 Movement scenarios of two-vehicle axle load identification

Case	Vehicle speed ratio (v_1/v_2)	v_1 (m/s)	v_2 (m/s)	t_d (s)	Scenarios
OVT-1	0.40	12	30	0	Overtaking at the first span
OVT-2				0.5	Overtaking at the first span
OVT-3				1.0	Overtaking at the first span
OVT-4				1.5	Overtaking at the middle span
OVT-5				2.0	Overtaking at the middle span
OVT-6	0.60	18	30	0	Overtaking at the first span
OVT-7				0.5	Overtaking at the first span
OVT-8				1.0	Overtaking at the middle span
OVT-9				1.5	Overtaking at the middle span
OVT-10				2.0	Overtaking at the last span
SBS	1.00	24	24	0	Side-by-side
FLC-1				0.5	Following with constant headway
FLC-2				1.0	Following with constant headway
FLC-3				1.5	Following with constant headway
FLC-4				2.0	Following with constant headway
FLI-1				1.67	30
FLI-2	0.5	Following with increasing headway			
FLI-3	1.0	Following with increasing headway			
FLI-4	1.5	Following with increasing headway			
FLI-5	2.0	Following with increasing headway			
FLI-6	2.50	30	12	0	Following with increasing headway
FLI-7				0.5	Following with increasing headway
FLI-8				1.0	Following with increasing headway
FLI-9				1.5	Following with increasing headway
FLI-10				2.0	Following with increasing headway

Table 4.18 and Figure 4.10 show the identification error of two-vehicle axle load identification from various bridge approach time intervals and velocity ratios. Scenarios with a velocity ratio less than 1.00 denote the movement with overtaking while others are following movements, except for the side-by-side case. Based on the obtained results, it can be observed that the identification errors are below 14% for all scenarios. However, it is noted that the minimum error is approximately 7%. Discussion on various movement scenarios is described separately in the following sections.

4.3.8.1 Short headway movement

Based on the results presented in Figure 4.10 for vehicle speed ratios between 1.0 and 2.50 corresponding to following movement with short headway, the identification is not significantly influenced by the vehicle speed ratio or the bridge approach time interval. This is particularly the case for the second vehicle which has slightly better accuracy compared to the leading vehicle as shown in Figures 4.10 (c) and (d). This is because the second vehicle travels at a slower speed for a longer

duration on the bridge. The axle loads for this vehicle scenario are identified within an RPE of 11%.

4.3.8.2 Overtaking movement

In this scenario, the following vehicle overtakes or passes the lead vehicle by traveling at a higher speed. In this situation, the problem to overcome is that of axle overlap. It is noticed from Figure 4.10 that the maximum identification error occurs in the case of a velocity ratio of 0.60 with t_d of 1.0 and 1.50, particularly for the second vehicle's axle loads. This is because the second vehicle travels at a higher speed for a shorter duration on the bridge than the first vehicle. Additionally, the RPE at a velocity ratio of 0.60 is larger than one with a velocity ratio of 0.40 because the situation in which two vehicles travel at a close moving speed means a longer duration for the overlapping of axle loads. However, the identified axle loads are all within 14% RPE of the actual dynamic loads. This indicates that the proposed method can identify axle loads accurately, even when one vehicle is overtaking another while on the bridge.

Table 4.18 Identification error of two-vehicle axle loads identification from various bridge approach time intervals and velocity ratios

Velocity ratio (v_1/v_2)	Axle load	RPE (%)				
		Bridge approach time interval, t_d (s)				
		0	0.5	1.0	1.5	2.0
0.40	1 st Front	7.57	7.84	8.02	7.56	7.83
	1 st Rear	8.85	9.07	8.86	9.44	9.22
	2 nd Front	9.64	9.91	10.92	10.20	10.63
	2 nd Rear	9.88	10.27	10.30	11.58	9.30
0.60	1 st Front	8.61	8.68	8.76	8.03	7.62
	1 st Rear	8.47	10.00	9.47	9.63	8.64
	2 nd Front	9.59	11.68	13.08	10.23	8.54
	2 nd Rear	10.54	10.94	10.93	9.85	9.10
1.00	1 st Front	8.37	8.97	9.05	8.90	8.47
	1 st Rear	8.19	10.78	9.78	8.53	9.00
	2 nd Front	8.37	9.92	9.31	8.83	8.59
	2 nd Rear	8.19	10.05	8.70	8.86	9.09
1.67	1 st Front	9.41	9.05	9.58	8.89	9.04
	1 st Rear	10.56	10.14	9.59	9.23	9.11
	2 nd Front	8.65	7.93	7.42	7.81	7.56
	2 nd Rear	8.65	8.15	7.92	8.04	8.38
2.50	1 st Front	9.14	9.23	8.82	8.91	9.30
	1 st Rear	10.20	9.38	8.99	9.23	9.25
	2 nd Front	7.40	7.49	6.99	7.49	7.21
	2 nd Rear	8.69	8.62	8.68	8.93	8.63

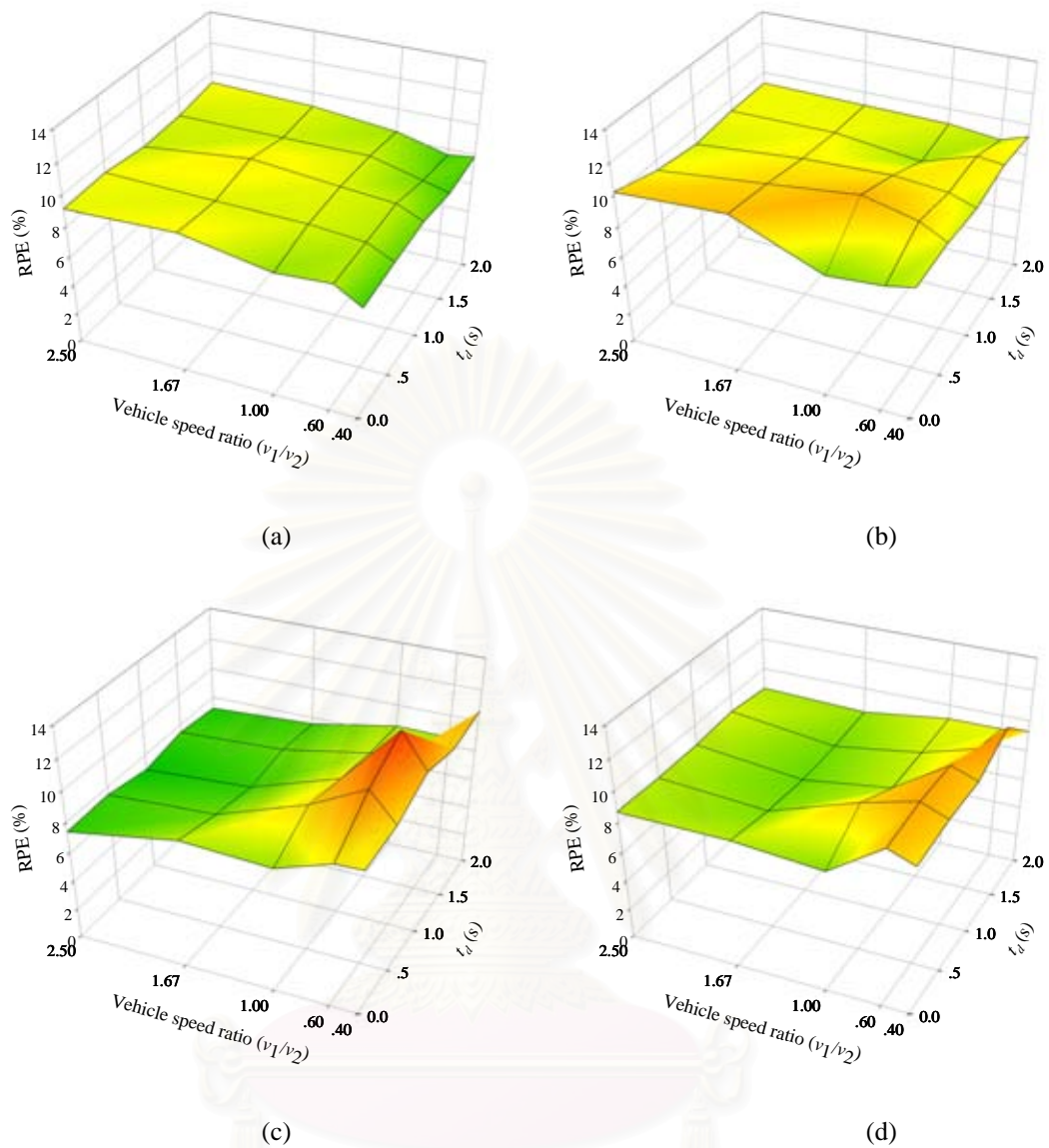


Figure 4.10 Identification error of two-vehicle axle load identification from a three-span continuous bridge with various vehicle speed ratios and bridge approach time intervals: (a) front axle load of 1st vehicle, (b) rear axle load of 1st vehicle, (c) front axle load of 2nd vehicle and (d) rear axle load of 2nd vehicle

4.3.8.3 Side-by-side movement

For a third two-vehicle axle load identification scenario, both vehicles are assumed to be moving side-by-side (SBS) at the same speed and location along the entire length of the bridge. Although the combined vehicle load can be identified as a single 2-axle vehicle, the independent axle loads of each vehicle are required. Therefore, the method identifies this scenario as a 2-vehicle 4-axle configuration.

Results from Table 4.18 indicate that identification errors for dynamic axle loads in a SBS scenario are below 9% for all axle loads.

However, it is noticed that the identified axle loads and RPE of the first and the second vehicles are equivalent. This is because both vehicles have the same properties and the system is simplified as a one-dimensional problem from modeling the bridge as beam elements. Therefore, there is a limitation on identification of side-by-side movement between two vehicles when their physical properties are not equivalent. However, the presence of multiple vehicles with the same properties and moving at the same location along the entire bridge length is rarely observed in actual traffic.

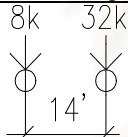
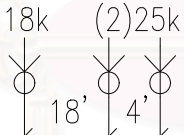
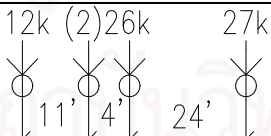
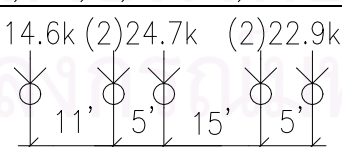
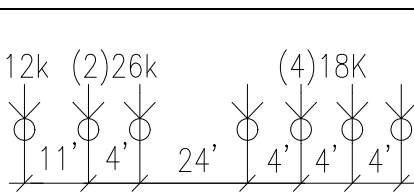
Based on the identification results and discussion of three possible vehicle travel scenarios, it can be concluded that the proposed USC method is generally applicable in practice for normally occurring traffic conditions because the method can accurately identify multiple axle loads if the axle loads do not overlap during the entire bridge crossing.

4.3.9 Vehicle Type and Axle Load Configuration

In order to investigate the capability and efficiency of the proposed method for real application, identification of the axle load of a vehicle with various truck configurations is conducted. The truck categories employed in this section are selected from the highest fatigue damage potential vehicles presented by Laman and Ashbaugh (2007). Five truck categories with different numbers of axles from 2 axles to 7 axles including H-20, PA-EX9, PA-EX2, SHV-3S2 and PA-EX6 vehicles were selected. H-20 is the half truck of HS-20 used in highway design specified by AASHTO. PA-EX is a Pennsylvania exclusion vehicle and SHV is a hauling vehicle. The time histories of axle loads are again assumed using the load function as Eq. (4.1) with different amplitude value corresponding to the axle weight for each vehicle type. The trucks travel along the three-span continuous bridge at a constant speed of 20 m/s. The axle spacings, weight distribution and corresponding RPE of axle loads are presented in Table 4.19. To verify the approach effectiveness, plots of identification error versus regularization parameter of each truck, λ , are again represented in Figure 4.11.

Based on the graphs from Figure 4.11, it can be clearly observed that the optimal regularization parameter is about 1.0 for every vehicle category. This result is similar to the study described in section 4.3.1 and proves that using λ of 1.00 is effective for every vehicle type and movement characteristic. According to the identification results listed in Table 4.19, it is found that the proposed method is capable of identifying vehicle axle loads accurately with the identification error within 13% for the first axle and less than 9% for others. The results also indicate that the closely spaced axle loads such as the second and third axles of the PA-EX9 vehicle, the last four axles of the PA-EX6 vehicle are distinguishable in the identification without losing their accuracy. Axle loads which have heavier weight are identified with the better results than those with lighter weight. Axles that are more widely spaced compared to other axles are identified more accurately than ones closely spaced, i.e. the RPEs of the last axle of the H-20 and PA-EX2 vehicles are only 3.06% and 4.25%, respectively.

Table 4.19 Identification error of vehicle axle load from different vehicle category

Vehicle Type	Axle Weight Distribution	RPE (%)	
H-20		1 st Axle	12.57
		2 nd Axle	3.06
PA-EX9		1 st Axle	6.14
		2 nd Axle	6.71
		3 rd Axle	6.80
PA-EX2		1 st Axle	12.34
		2 nd Axle	8.28
		3 rd Axle	7.01
		4 th Axle	4.25
SHV-3S2		1 st Axle	9.71
		2 nd Axle	7.64
		3 rd Axle	7.81
		4 th Axle	7.53
		5 th Axle	7.46
PA-EX6		1 st Axle	12.83
		2 nd Axle	7.95
		3 rd Axle	7.11
		4 th Axle	7.84
		5 th Axle	7.66
		6 th Axle	8.12
		7 th Axle	8.80

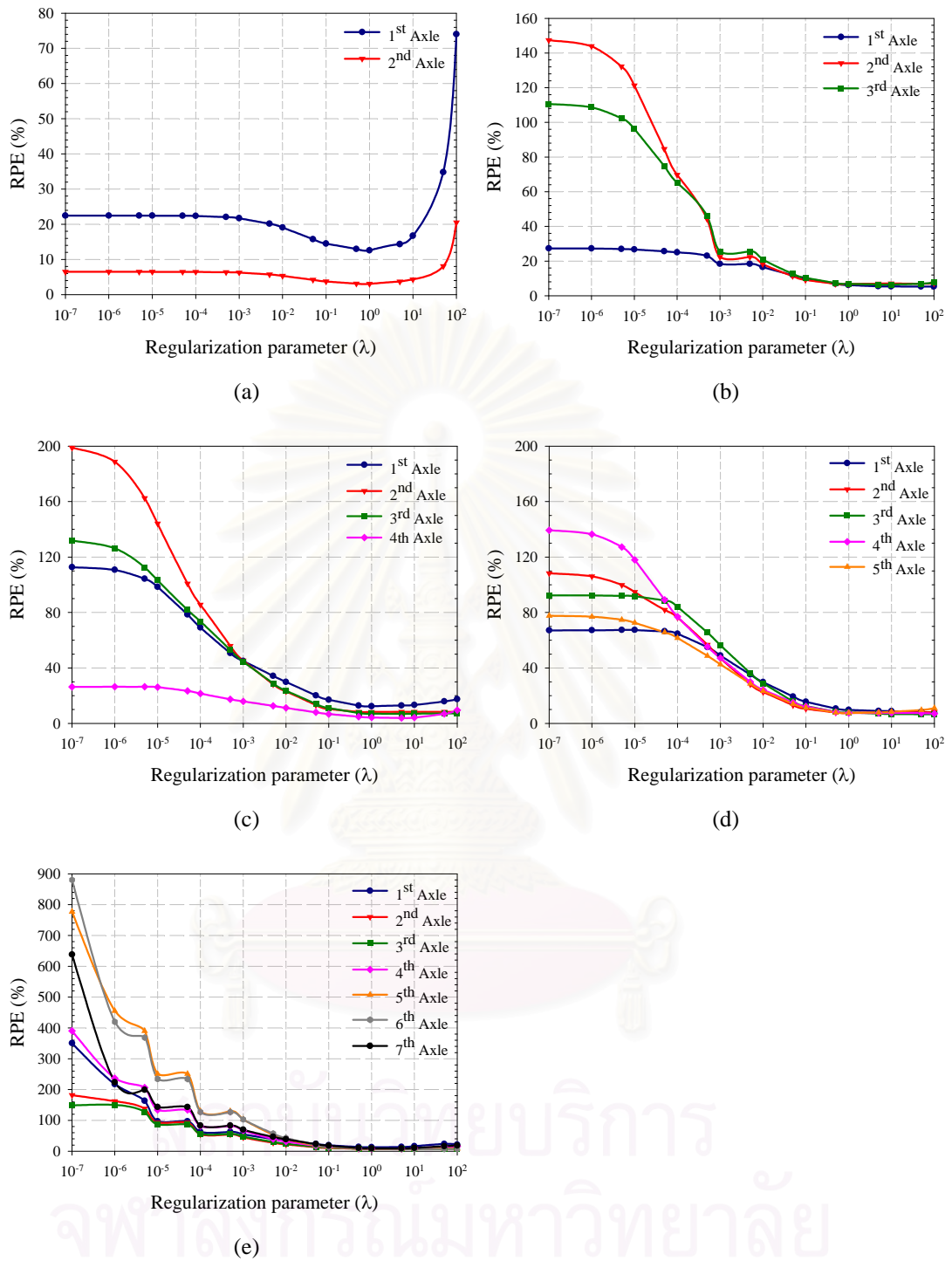


Figure 4.11 Plots of identification error of different vehicle categories from various orders of regularization parameter: (a) H-20, (b) PA-EX9, (c) PA-EX2, (d) SHV-3S2 and (e) PA-EX6

4.4 Summary

According to the numerical study, the investigation on the effectiveness and accuracy of the proposed regularization with USC method based on the parametric study is presented. Comparison of the existing identification methods including the conventional least-square, the optimal regularization and the proposed regularization with USC methods is conducted. It is found that the proposed method performs with the most accuracy and robustness compared to other approaches. Identification with accurate results and robustness on high measurement noise level can be achieved. Ill-conditioning usually found at the duration when axle loads crossing the internal supports of multi-span bridges is overcome when the USC technique is applied. Moreover, difficulty in regularization parameter selection is also eliminated since the parameter can be assigned with a wide range without disruption of solution accuracy.

The number and location of sensors used in the measurement of nine sensors with three sensors for each bridge span is the most sufficient for both two and four loads identification. The sampling rate recommended for the use in the data acquisition system is at least ten times the first fundamental frequency or twice the five mode fundamental frequency of the bridge. The most efficient number of finite beam elements employed in structural modeling is 8 elements per bridge span. A vehicle with heavier mass and moving at a slower speed can be identified with higher accuracy than that with lighter mass and moving at a faster speed. However, vehicle mass is more influential to the solution accuracy than moving speed. Axle spacing and weight distribution between axles significantly influence solution accuracy. A lightweight vehicle with closely spaced axles is more difficult to identify accurately than a heavyweight vehicle with widely spaced axles. Using a bridge with smooth or very low surface roughness is highly recommended since the identification error is very sensitive and increases relatively to the higher level of roughness magnitude.

In addition, the proposed method is also capable of accurately identifying the axle loads of multi-axle and multiple vehicles in any travel scenario. The axle loads of a vehicle traveling on the bridge at a slower speed can be identified more accurately than those moving at a faster speed. Finally, based on the identification results of various truck categories, it is concluded that the proposed method is effective and robust for any vehicle configuration and possible travel situation.

CHAPTER V

EXPERIMENTAL STUDY OF AXLE LOAD IDENTIFICATION USING SCALED MODEL

5.1 General

According to the numerical study conducted in Chapter IV, the experimental study using a scaled model in the laboratory or full-scale testing with an existing bridge is necessary in order to investigate the effectiveness and identification accuracy of the proposed USC method. However, it is difficult to control the system in conducting a full-scale test with a real bridge and vehicles. Moreover, actual load monitoring using instrumented vehicles is very expensive. Laboratory testing using a scaled model is therefore more convenient than the full-scale experiment since the vehicle travel can be controlled and the involved parameters can be measured precisely. In this chapter, the experimental design, experimental set-up, system calibration, methodology of testing and experimental results are described and discussed.

5.2 Experimental Design

The design procedure of this experiment consists of a scaled bridge model design and a scaled vehicle model design. The scaled bridge is firstly designed based on vibration characteristics. The fundamental frequency of the bridges is used as the target parameter to be considered. Then the vehicle model is designed to conform to the order of actual bridge responses as occurring in actual practice. The scaled dimensions of both the bridge and vehicle can be determined from their physical characteristics such as the axle spacing to span ratio and duration of travel with respect to the actual situation.

5.2.1 Design of Bridge Model

Based on the computer simulation, the desired actual bridge model is analyzed and compared to the scaled bridge model. Using the natural frequencies as the main parameter, the relevant dimension of the bridge is then obtained by adjusting the scaled bridge model's dimension until the fundamental vibration modes agree with the target bridge. The target bridge is firstly defined by again using an empirical

function between the first modal natural frequency and span length of the bridge presented by Chaallal and Shahawy (1998) as follows:

$$f_0 = 82L^{-0.9} \quad (5.1)$$

where f_0 is the first natural frequency of the bridge, and L is bridge span length. Using this relationship, the sectional dimension of the target bridge is then adjusted to determine a mass and stiffness of the bridge that satisfies the fundamental frequency obtained from Eq. (5.1). Figure 5.1 demonstrates the relationship between bridge fundamental frequency and its span length from 883 existing bridges in Europe presented by Chaallal and Shahawy.

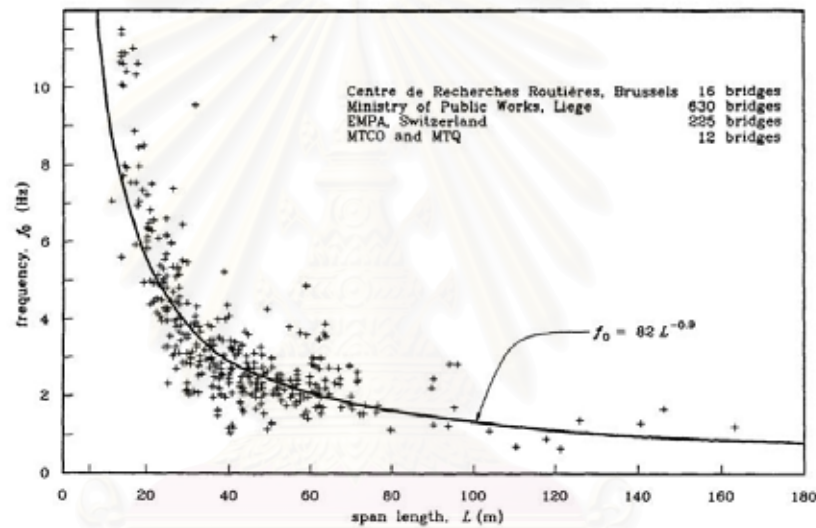


Figure 5.1 Plot of relationship between natural frequencies against span length observed from 898 highway bridges in Europe

The actual bridge simulated as a scaled bridge model is a reinforced concrete deck slab bridge. The bridge model is made from steel plate and its fundamental frequency should be equivalent to the real bridge. Moreover, the order of strain responses measured from the passage of the vehicle between the real and scaled bridges should be similar. With these requirements, the dimensions of the scaled bridge model are determined. The bridge is scaled down 10 times in length. Table 5.1 shows the dimensions and properties of the real reinforced concrete bridge and the scaled steel bridge model. The acting load for the scaled bridge model is 1/1000 times the full-scale system. Figure 5.2 shows the comparison of typical bending moment

signals from the real RC deck slab bridge and the scaled steel bridge loaded with point load functions.

Table 5.1 Parameters of real and scaled bridge models

Real RC bridge	Scaled steel bridge
$L = 20:20:20$ m	$L = 2.0:2.0:2.0$ m
$EI = 9.458 \times 10^9$ N-m ²	$b = 0.5$ m, $h^* = 0.010$ m
$\rho A = 4320$ kg/m	$EI = 8,596$ N-m ²
$\gamma = 1.24$ m	$\rho = 7850$ kg/m ³ (steel)
First ten fundamental frequencies 5.81, 7.45, 10.87, 23.24, 26.48, 32.50, 52.33, 57.16, 65.89 and 93.28	First ten fundamental frequencies 5.81, 7.45, 10.87, 23.24, 26.48, 32.50, 52.33, 57.16, 65.89 and 93.28

* Thickness of the scaled model is designed according to size available in the market.

** The fundamental frequencies are theoretically calculated from physical properties.

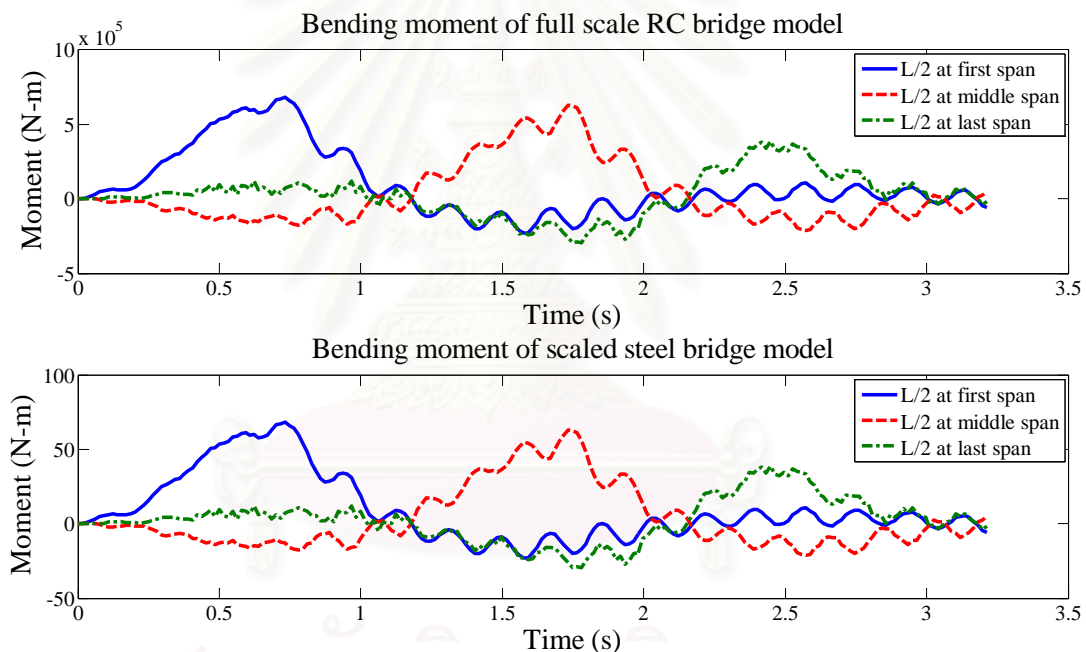


Figure 5.2 Comparison of typical bending moment signals from full-scale RC deck slab bridge model and scaled steel bridge model

5.2.2 Design of Vehicle Model

The vehicles considered in this experimental study are two-axle vehicles. Based on the full-scale system, the real vehicle is assumed as a heavy truck with gross weight of 210 kN. According to bridge's parameters listed in Table 5.1, the designed bridge model is approximately scaled down 10 times in length compared to the desired bridge. The vehicle model with regard to its axle spacing is then scaled down

at the same proportions, i.e. 10 times. The gross weight is designed to be convenient in testing approximately scaled down 1000 times from the real truck as 210 N. From these proportions, with respect to the parameters in Table 5.1, the bridge responses from both the target and designed bridges are closely matched. Two 2-axle vehicle models with non-articulated frames, spring suspension and rubber tires are fabricated. The axle spacing to span ratio (ASSR) of the existing 2-axle trucks normally ranges from 0.15 to 0.40, therefore, an ASSR equal to 0.16 (axle spacing of 32cm) is selected for the model vehicles in order to study the identification of closely spaced axles.

5.3 Experimental Set-Up

The experimental set-up of a vehicle-bridge system model fabricated in the laboratory is diagrammatically shown in Figure 5.3. The bridge model is a continuous bridge with three spans and is extended at both ends with the leading and trailing spans. The leading span is used for the vehicle to increase its speed before approaching the bridge. The trailing span is used to stop the moving vehicle after leaving the bridge. Model vehicle travel is controlled by aluminum guide rails attached to the scaled bridge roadway surface. Three guide rails are attached at the quarter points to allow three different vehicle travel paths. The vehicles are pulled along the bridge with strings, and truck speed is controlled by DC motors. Vehicle speed does not need to be constant because the identification procedure only requires the axle positions while traveling on the bridge. Practically, the axle position can be determined by installing sufficient photoelectric sensors, infrared sensors, tape switches, or other devices.

Bending moments are determined based on the measured strain at nine different sections: $L/4$, $L/2$ and $3L/4$ in each of the three spans according to the 9-C sensor pattern explained in section 4.3.2 of Chapter IV. Five strain gauges are mounted at $L/2$ and three gauges are mounted at $L/4$ and $3L/4$. Precision tension/compression load cells are installed on each model vehicle axle in order to measure vehicle-bridge interaction forces. Two photoelectric sensors are positioned at each end of the model bridge to monitor the travel duration of the model vehicles. In addition, each model vehicle is equipped with white/black optical detection sensors to record the positions that model vehicles have passed as a function of time. By counting pulses from reading the black and white strips, the vehicle position as well as corresponding speeds can be determined. Data acquisition is completed with a 48-

channel data logger set at a sampling rate of 1024 Hz for all 41 connected sensors including: 33 strain gauges, 4 load cells, 2 optical sensors and 2 photoelectric sensors. Figure 5.4 shows photographs of the instruments used in the experiment.

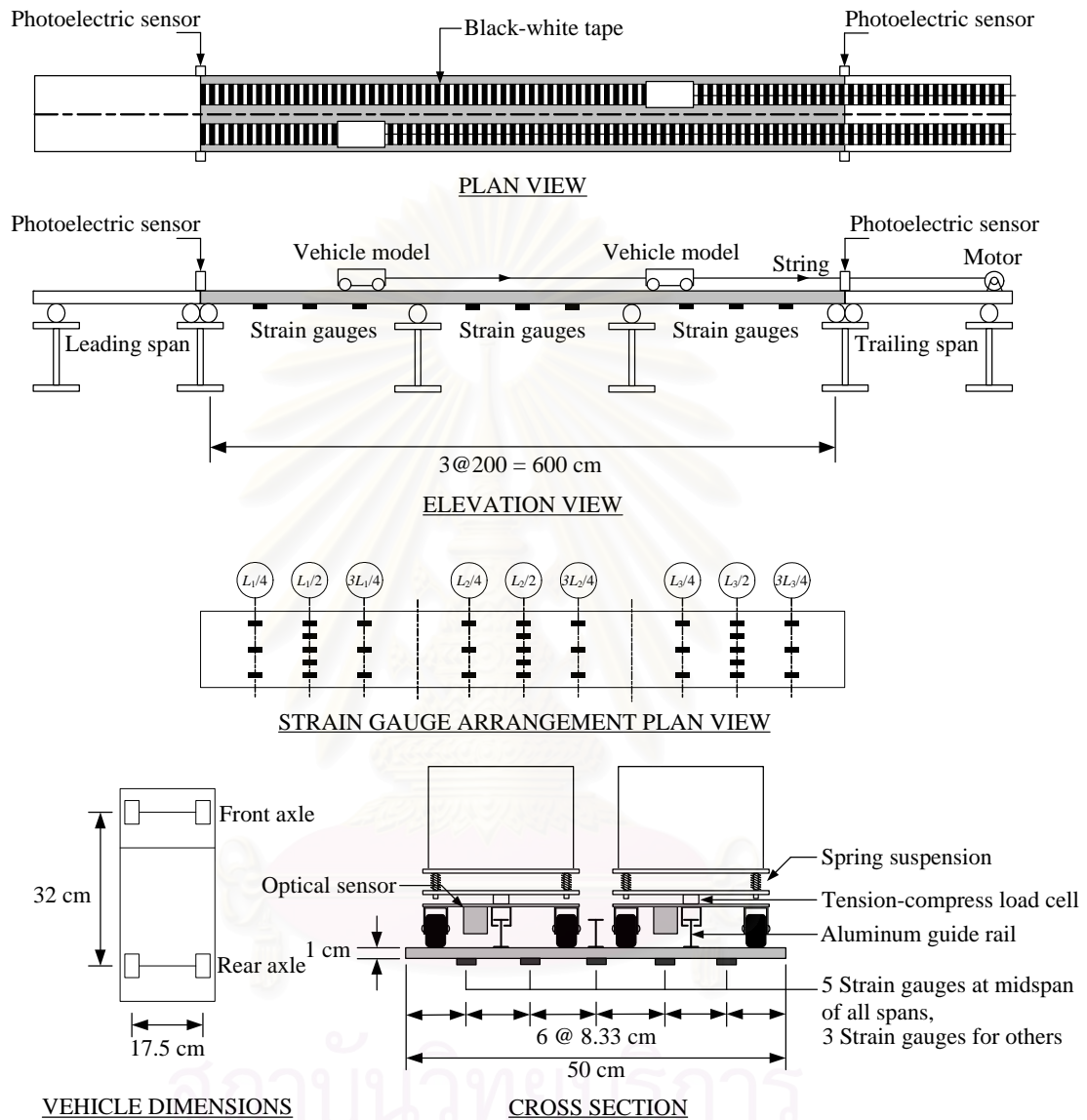


Figure 5.3 Experimental set-up

Every strain gauge, load cell, optical and photoelectric sensor is connected through the completion bridge boxes which simultaneously convert the measured analog signals to digital signals and submit them to the data logger. The optical sensor used in vehicle location detection has 2 infrared sensors. One is used for signal emission while the other is a signal receiver. Based on the light reflected and absorbed by the equally spaced and alternating black and white tape, the optical sensor records

data with constant values of 0 and 1.0 when it reads the black and white stripes respectively as shown in Figure 5.5. Similarly, with the same principle of light reflection, the photoelectric sensor has an emitter and a receiver used to detect any objects that move between them. The 24 V DC motors are used in dragging the vehicle models. With the variable rotational speed controller, the moving speeds of the vehicles can be adjusted to simulate different vehicle travel situations. The tension/compression load cells used in actual axle load observation have their capacity of $\pm 100\text{kg}$ with a precision of $\pm 0.2\%$ error.

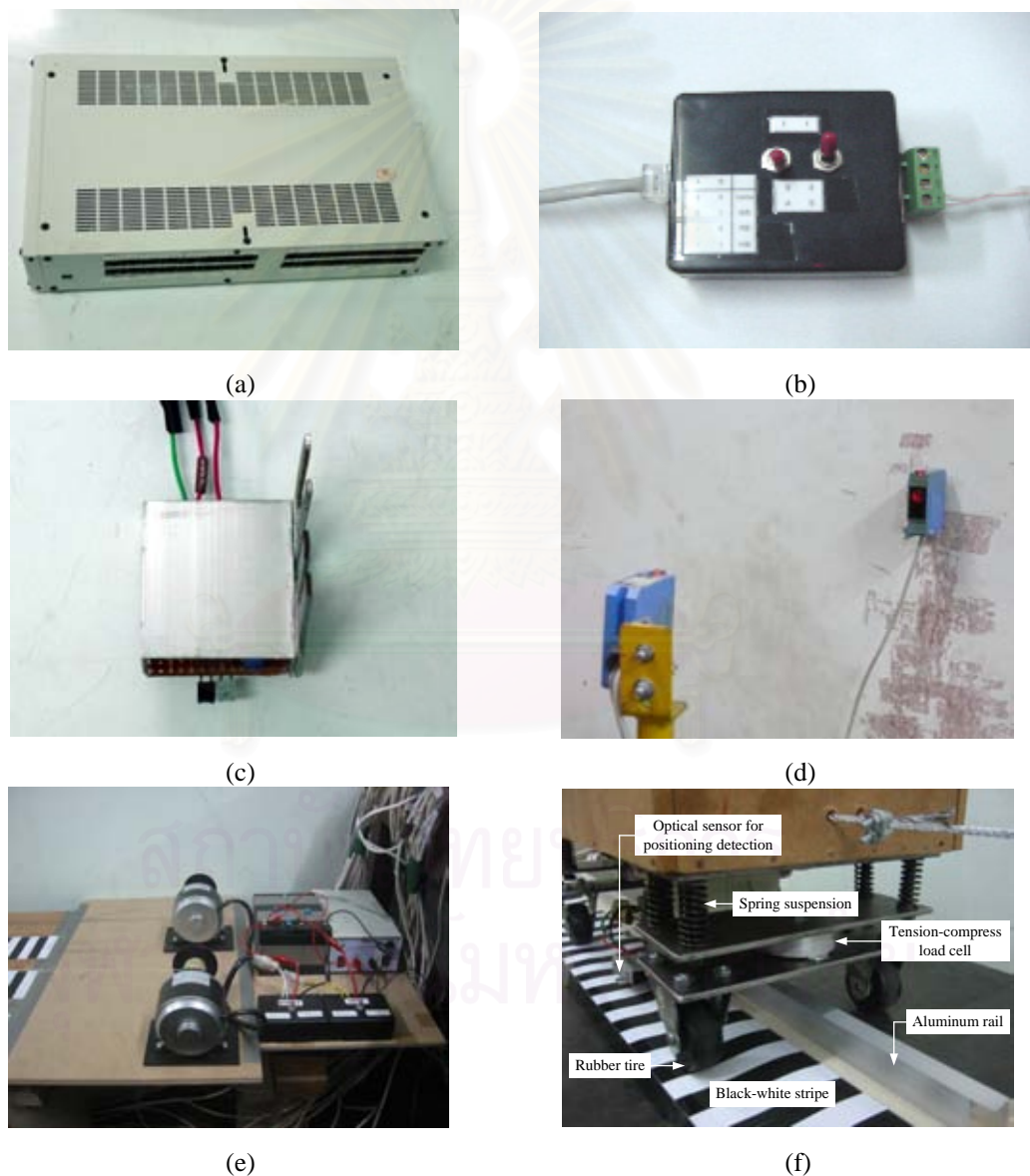


Figure 5.4 Photographs of instruments used in the experiment: (a) 48-channel data logger, (b) completion bridge box, (c) optical sensor, (d) photoelectric sensor, (e) DC motor and (f) details of vehicle suspension and sensors installation

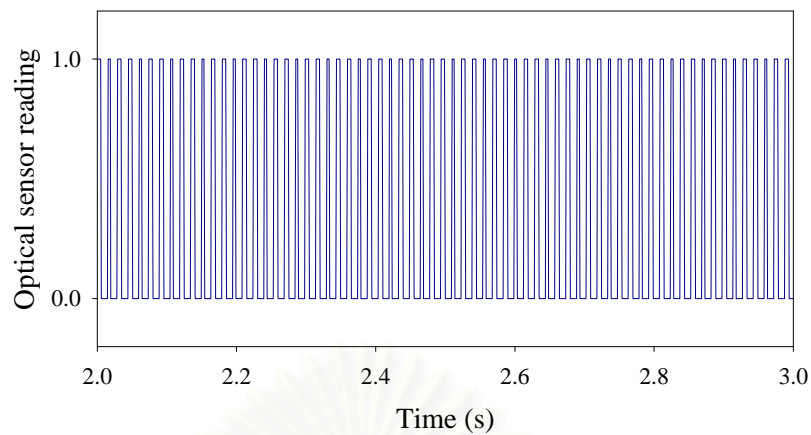


Figure 5.5 Typical measured signal of the optical sensor reading used for a vehicle's position measurement

5.4 Single Vehicle Axle Load Identification

Experimental verification of the USC regularization method on single vehicle axle load identification is firstly considered. Effects of vehicle mass and moving speed on identification accuracy are investigated. The effect of the transverse direction of vehicle travel is also observed in order to investigate the efficiency of model simplification from using a beam model. Two configurations of vehicle model including two-axle and four-axle vehicles are identified and discussed.

5.4.1 Two-Axle Vehicle

In this section, consideration of the effect of vehicle mass and moving speed, the effect of the transverse direction of vehicle travel and the effect of bridge surface roughness on identification accuracy are experimentally studied. A vehicle model with axle spacing of 32 cm with gross vehicle mass (GVM) varying from 10 kg to 30 kg is employed.

5.4.1.1 Effect of Vehicle Mass and Moving Speed

A model vehicle is pulled along the bridge in the longitudinal centerline of the deck with speed and vehicle mass varying from 0.2 m/s to 1.8 m/s and 10 kg to 30 kg, respectively. Figure 5.6 presents the RPE of the obtained front and rear axle loads identified by the regularization method with USC and λ is equal to 0.1 for all cases.

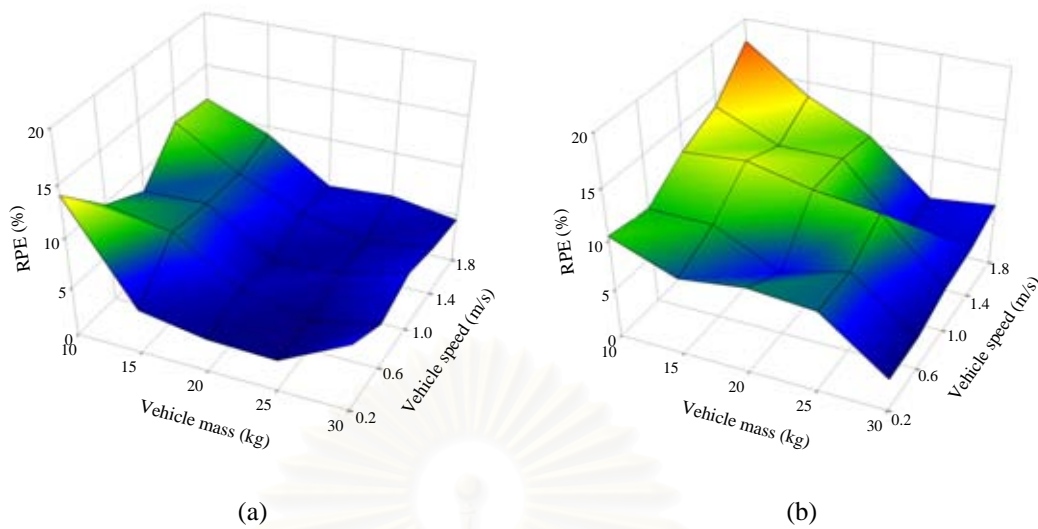
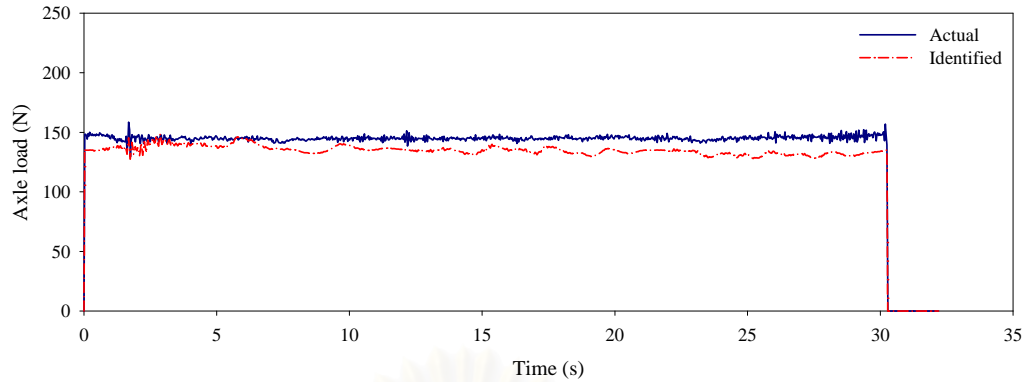
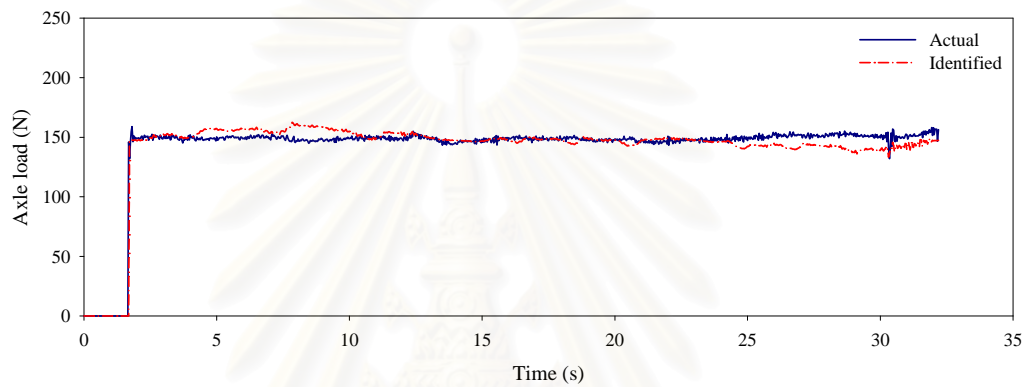


Figure 5.6 RPE of identified dynamic axle load of single vehicle load identification: (a) front axle load and (b) rear axle load

Figures 5.7 and 5.8 show the identified axle load time histories of heavyweight and lightweight two-axle vehicles traveling at slow and fast speeds, respectively. The obtained results indicate that identification of a heavy vehicle traveling at a slow speed results in a lower RPE than identification of light vehicle traveling at a fast speed. This is because vehicles at lower speeds induce less dynamic interaction with the bridge. In addition, heavy vehicles normally induce a larger signal to noise ratio than vehicles with low mass. Therefore, a collected response with smaller dynamic interaction and a larger signal to noise ratio usually provides a more accurate identification than one with larger dynamic interaction and smaller signal to noise ratio. Moreover, it is also observed that vehicle mass has a greater influence on identification accuracy than moving speed. These results agree quite well with those found in the numerical study using computer simulation (section 4.3.4). The maximum RPEs of front and rear axle loads are both below 20%. Furthermore, the RPEs for identification of the 30 kg model vehicle are below 10% for every speed level for both front and rear axle loads.



(a)



(b)

Figure 5.7 Time histories of identified axle load of a two-axle vehicle with 30 kg GVM traveling at slow speed: (a) front axle load and (b) rear axle load

5.4.1.2 Effect of Transverse Direction of Vehicle Travel

To study the effect of transverse vehicle position, experiments with a model vehicle crossing the bridge in three transverse positions are conducted. The three transverse vehicle travel positions are 1) on the bridge centerline; 2) 12.5 cm from the left edge of the bridge; and 3) 12.5 cm from the right edge of the bridge as shown in Figure 5.9. A model vehicle with gross vehicle mass (GVM) varying from 10 kg to 30 kg in increments of 5 kg is adopted. Model vehicle speed is maintained at a constant speed of 0.6 m/s for all cases. Figure 5.10 presents the RPE of the identified single-vehicle axle load traveling along the bridge at three transverse positions. The results indicate that the USC technique accurately identifies axle loads for any transverse position. However, it is observed that the RPEs of all three travel positions except the rear axle load in the case of right lane travel are below 10%. The maximum difference in RPE of the left and right lane travels is within 4.5% compared to the center lane

travel. Moreover, the effect of vehicle mass yields the same tendency as previously discussed in the above section. Therefore, using average sectional bending moments converted from strain gauges equally distributed in each section as the input responses is sufficient and effective.

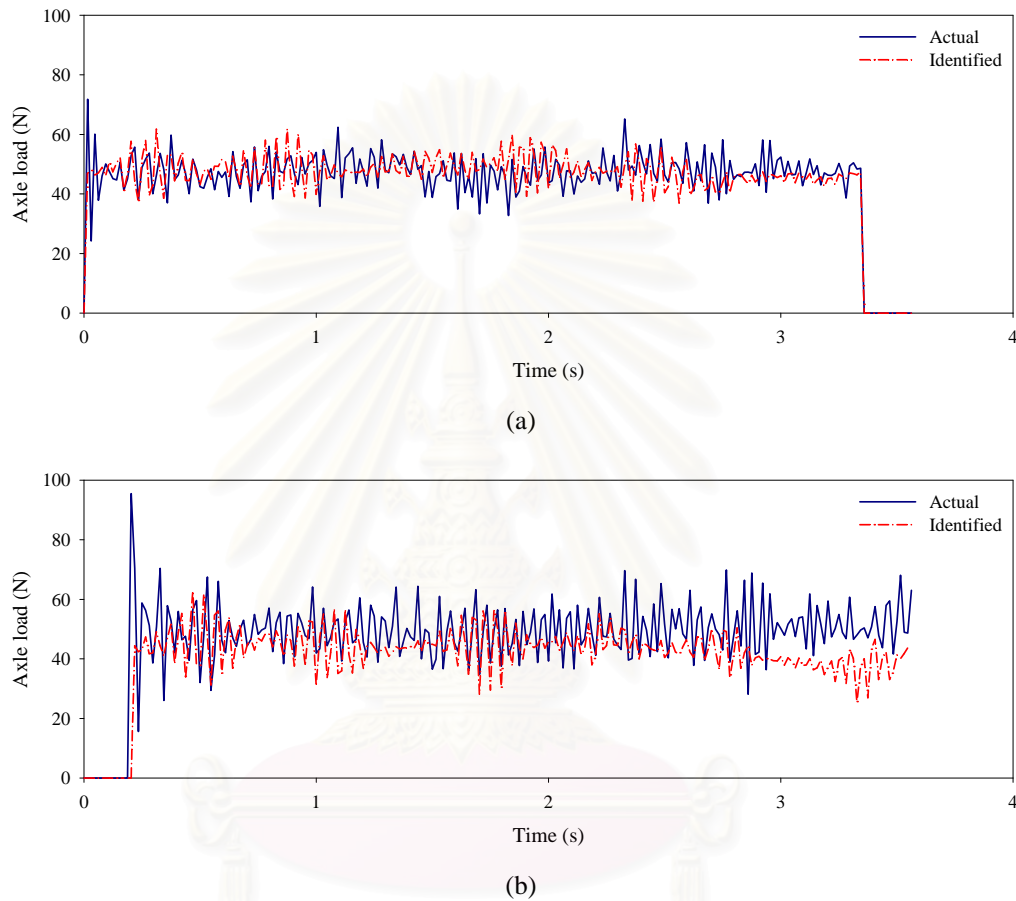
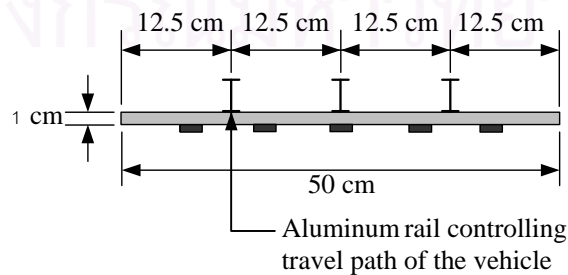


Figure 5.8 Time histories of identified axle load of a two-axle vehicle with 10 kg GVM traveling at fast speed: (a) front axle load and (b) rear axle load



BRIDGE CROSS SECTION

Figure 5.9 Travel paths of vehicles controlled by aluminum guide rails

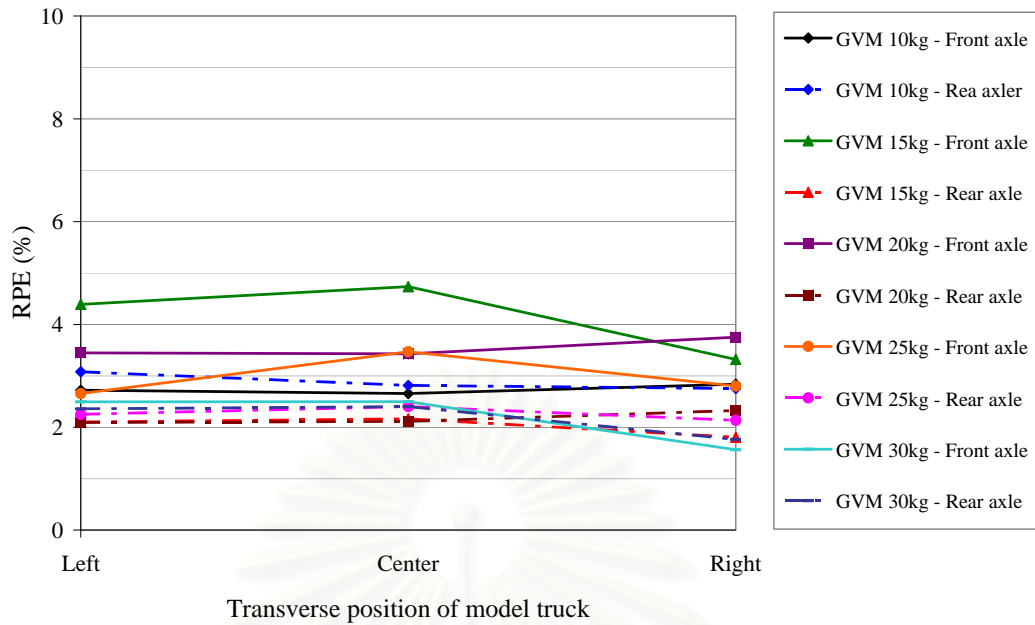


Figure 5.10 RPE of identified dynamic axle loads of single model vehicle traveling on different transverse positions of the bridge

5.4.1.3 Effect of Road Surface Roughness

According to the results from the numerical study on the effect of bridge surface roughness discussed in section 4.3.5, it is obviously found that the surface roughness of the roadway significantly affects identification accuracy. This section presents the experimental study on the effect of bridge surface roughness in order to verify and evaluate the effectiveness of the proposed method beyond the numerical study. The main purpose of this experimental investigation is to study the capability of the proposed approach from identifying pulsing axle loads induced by an irregular roadway profile. To do so, the obstructive objects are placed on the pavement in order to induce impact upon the axle loads. The obstructive object assumed to simulate irregular roughness is a piece of acrylic plate with a thickness and width of 2 mm and 15 mm, respectively. The acrylic plate is transparent which is convenient for installation on the black-white tape and it is also lightweight so it does not affect the mass of bridge. Figure 5.11 shows the photograph of the acrylic plate used as bridge surface roughness.

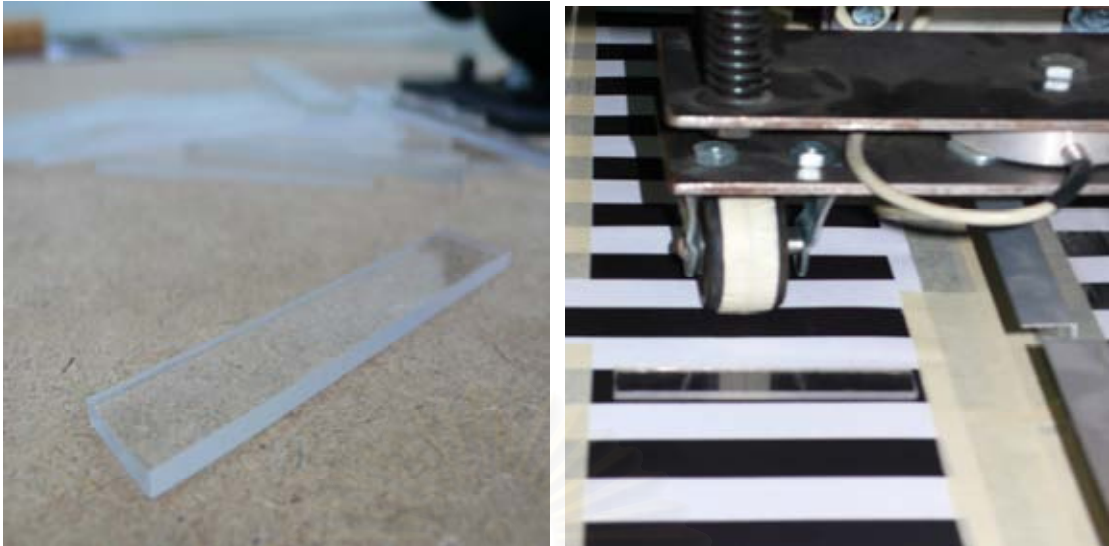


Figure 5.11 Acrylic plate used as an obstructive object to vehicle travel for the study on the effect of bridge surface roughness

To study the efficiency on pulse load identification, a different roughness pattern is conducted by varying the spacing of the obstructive objects as shown in Table 5.2. The acrylic plates are placed at three different spacing intervals from large spacing (200 cm) to close spacing (50 cm). It is observed from sections 4.3.2 and 5.4.1.1 that the effect of moving speed slightly affects solution accuracy but vehicle mass induces a greater effect. Therefore, the effect of vehicle mass is considered as well as the roughness pattern. A two-axle vehicle model with GVM varying from 10 kg to 30 kg is moved at the centerline of the bridge at a constant speed of 0.60 m/s. Figures 5.12 and 5.13 represent the bending moment responses and the corresponding actual axle-load time histories of a two-axle vehicle moving on different roughness patterns, respectively. It is observed from both figures that the additional roughness object induces a dynamic impact to the bridge and the dynamic component of the axle load increases up to almost 70%, especially in the case of roughness pattern III which is placed with close spacing of 50 cm.

Table 5.2 Arrangement of obstructive objects used in surface roughness study

Roughness pattern	No. of obstructive objects	Location of acrylic plate placement
I	3	$L_1/2, L_2/2, L_3/2$
II	5	$L_1/2, L_2/2, L_3/2$ and at internal bridge supports (2m & 4m)
III	11	$L_1/4, L_1/2, 3L_1/4, L_2/4, L_2/2, 3L_2/4, L_2/4, L_3/2, 3L_3/4,$ and at internal bridge supports (2m & 4m)

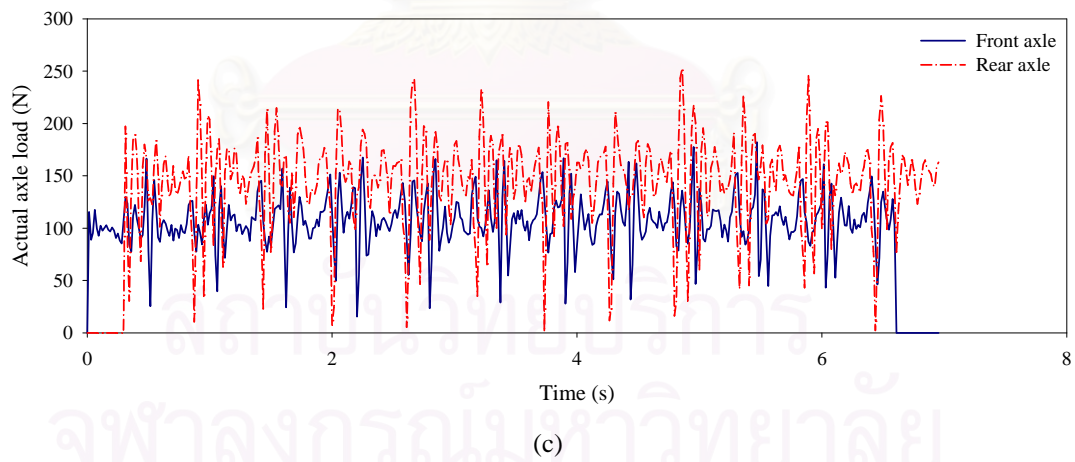
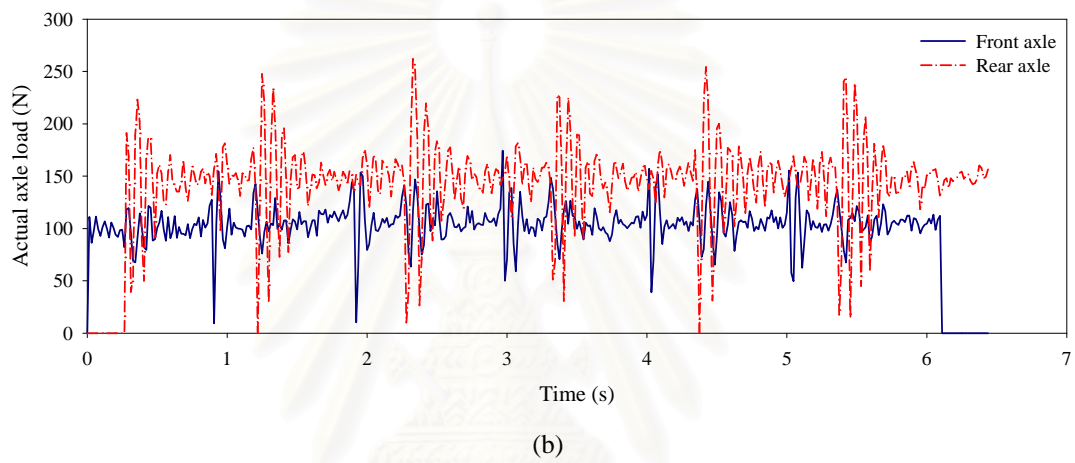
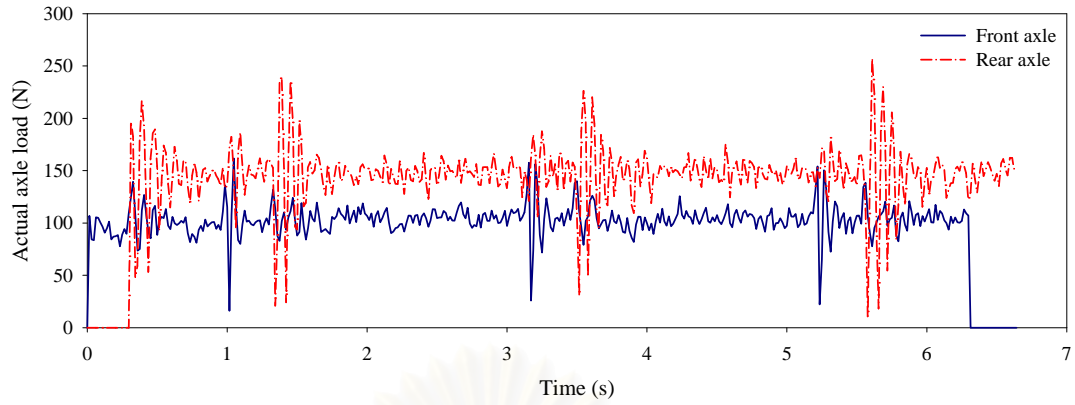


Figure 5.12 Time histories of actual axle loads of a two-axle vehicle, 25 kg GVM traveling on different roughness patterns: (a) roughness pattern I (b) roughness pattern II and (c) roughness pattern III

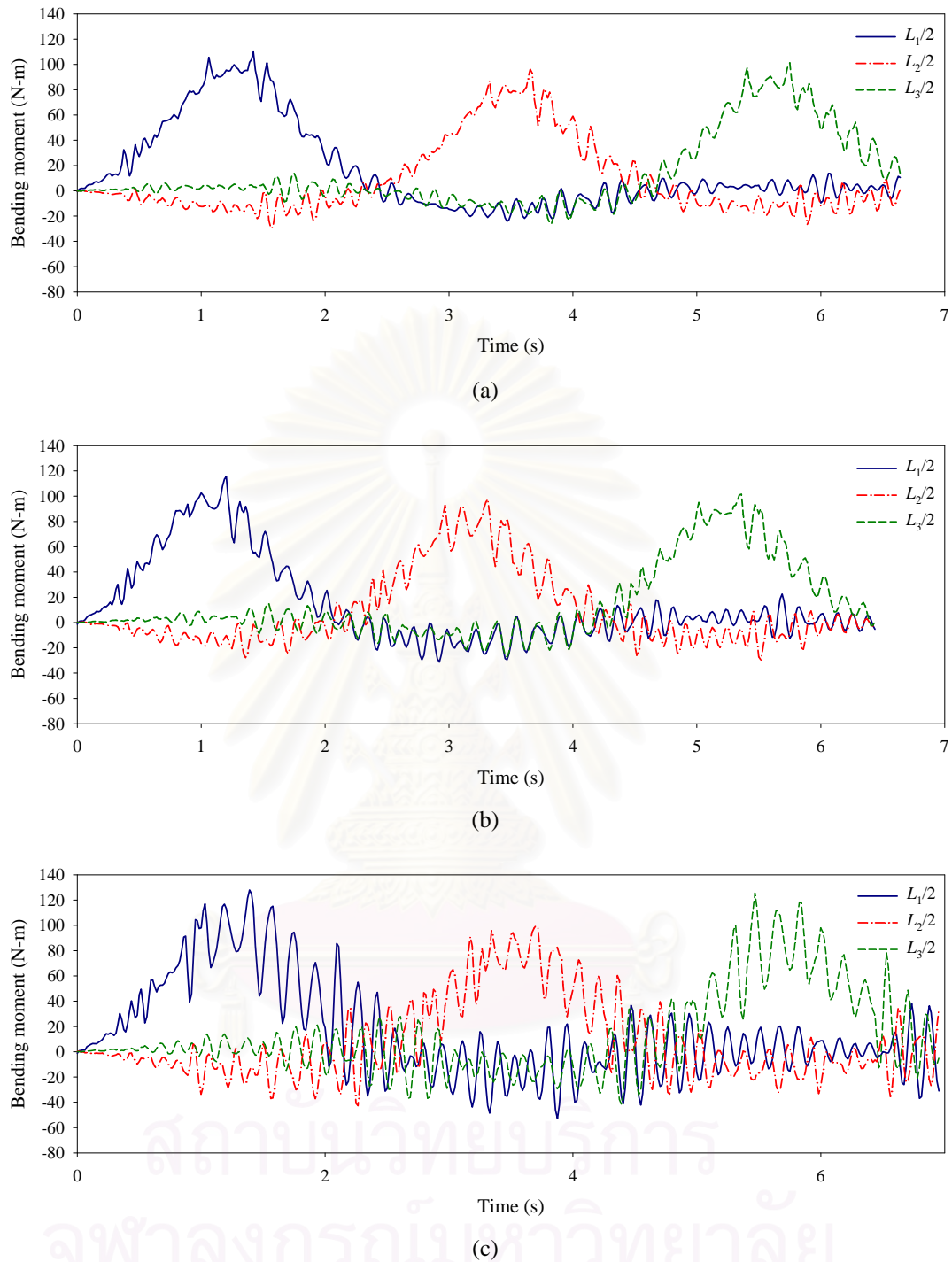


Figure 5.13 Time histories of bending moment responses of a two-axle vehicle, 25 kg GVM traveling on different roughness patterns: (a) roughness pattern I (b) roughness pattern II and (c) roughness pattern III

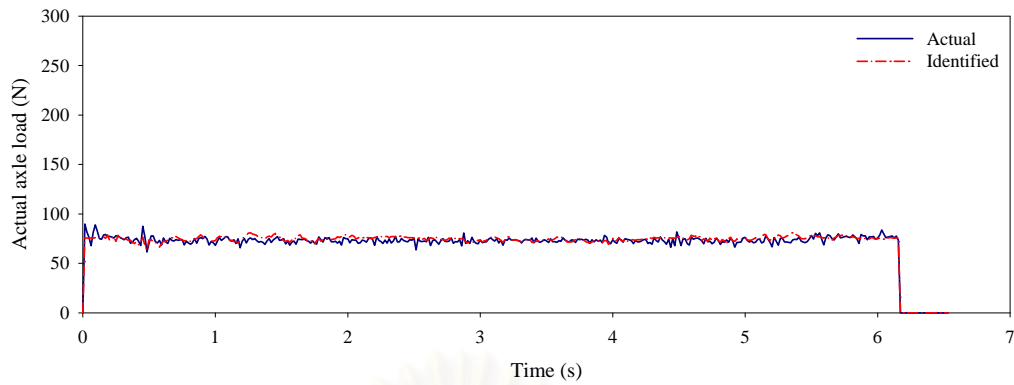
To evaluate the effectiveness of the proposed identification method, the RPE and correlation coefficient of identified axle loads are discussed. Table 5.3 lists the RPE of the identified axle loads of a two-axle vehicle traveling on the bridge with

various roughness patterns. The RPE of the axle loads from Table 5.3 results in the same behavior as found in the numerical study (section 4.3.5). Axle loads occurring from the pattern III surface roughness are more difficult to identify accurately than others induced by roughness patterns I and II. It is also found that a vehicle with lower mass is more likely to provide larger identification error than a heavier vehicle due to the effect of the signal to noise ratio. The surface roughness directly affects solution accuracy more than the effect of vehicle mass. Therefore, selecting a smooth bridge surface or smoothening the roadway surface by overlaying a new pavement before using the identification system is recommended. However, since the target vehicles whose axle loads are to be identified are heavyweight vehicles, the identification accuracy for heavy vehicles is acceptable within the RPE of 15%.

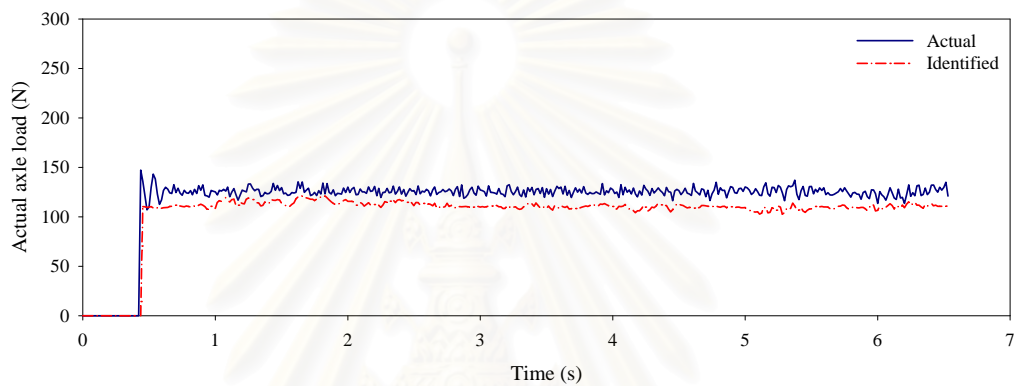
Table 5.3 RPE (%) of identified axle loads of a two-axle vehicle traveling on the bridge with various roughness patterns

GVM (kg)	RPE (%)							
	Smooth surface		Roughness pattern I		Roughness Pattern II		Roughness Pattern III	
	Front axle	Rear axle	Front axle	Rear axle	Front axle	Rear axle	Front axle	Rear axle
10	7.93	12.31	11.96	19.21	26.68	44.30	54.16	82.43
15	8.20	12.82	11.70	13.27	18.29	24.92	21.03	32.62
20	3.79	11.43	12.56	10.19	15.82	19.89	20.26	20.03
25	4.26	10.63	9.20	11.16	11.45	15.02	15.51	18.78
30	6.02	4.66	7.34	8.07	9.08	9.52	11.83	12.78

Figures 5.14 to 5.16 show the time histories of the identified axle loads of a two-axle vehicle, 20 kg GVM traveling on smooth surface, roughness patterns I and II, respectively. It is noticed from Figure 5.15 that the proposed USC method can accurately identify the axle load on rough bridge surface for both the static and dynamic components. However, in the case of roughness pattern II (see Figure 5.16) it is found that the time histories of identified axle load around the internal bridge supports cannot be accurately identified. This is because in the roughness patterns II and III, there are obstructive objects placed at the internal bridge supports. The bridge response at the duration when the vehicle axles are located on the supports is very small since the axle loads are directly transferred to the support.



(a)



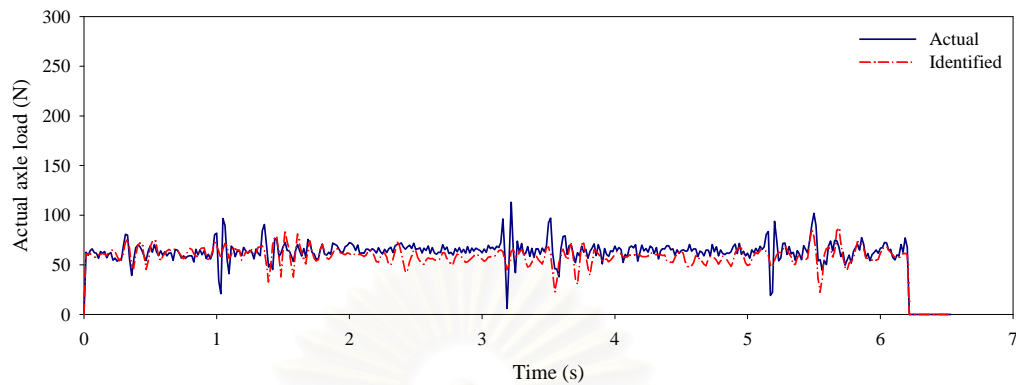
(b)

Figure 5.14 Time histories of identified axle load of a two-axle vehicle, 20 kg GVM traveling on smooth surface: (a) front axle (b) rear axle

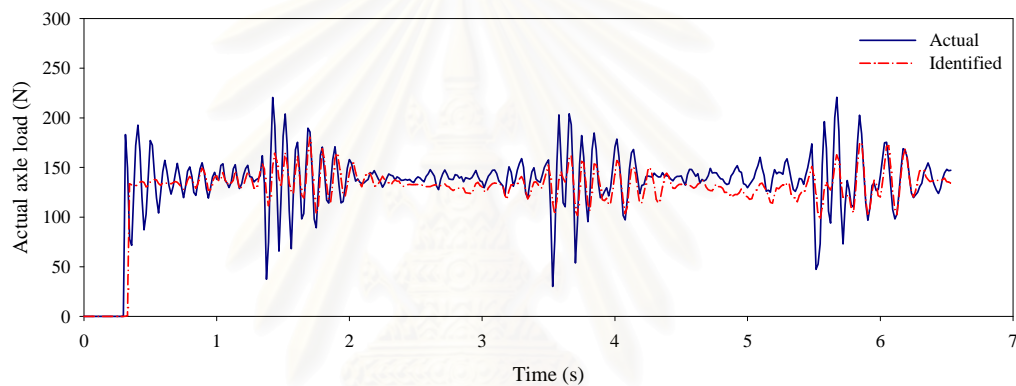
5.4.2 Four-Axle Vehicles

Past research on axle load identification has considered only the case of a two-axle vehicle with the exception of the study by Yu and Chan (2004) focusing on a three-axle vehicle. In this section, the axle load identification of a multi-axle vehicle employing a four-axle vehicle is experimentally studied in order to extend and verify the effectiveness of the proposed method before conducting the axle load identification study of multiple vehicles. The vehicle is fabricated by assembling two 2-axle vehicles together with free-connection without spacing between the rear bumper of the first vehicle and the front bumper of the second. Figure 5.17 shows the dimensions and axle spacings of the four-axle vehicle. The gross vehicle mass (GVM) ratio of the load configuration of the vehicle varies between the first and the second vehicle (GVM_1/GVM_2) from 0.60 to 1.67. The vehicle model travels along the bridge

at the bridge centerline with a moving speed varying from 0.2 m/s to 1.8 m/s at an increment of 0.4 m/s.



(a)



(b)

Figure 5.15 Time histories of the identified axle load of a two-axle vehicle, 20 kg GVM traveling on roughness pattern I: (a) front axle (b) rear axle

The experimental scenarios and results of four-axle vehicle load identification are represented in Table 5.4. Figure 5.18 represents the RPE of the identified axle load of four-axle vehicle. The results from Figure 5.18 are obtained from identification with λ of 0.1 for all cases. It is observed that a vehicle part with heavier mass (larger M_s) can have its axle loads identified more accurately than another part with lighter mass (lower M_s), i.e. in the case of a GVM ratio equal to 0.80, the RPEs of the 1st and 2nd axle loads (lighter part) are higher than the RPEs of the 3rd and 4th axle loads (heavier part). Moreover, moving speed slightly affects the solution accuracy but not systematically. It is also observed that the maximum RPE is at 75% approximately for the 3rd axle load at a GVM ratio of 1.67. This is because in this case the 3rd axle load is the front axle load of the vehicle part with a GVM of 15kg which

is very light compared to another with a GVM of 25kg. Besides, the axle spacing between the 2nd and 3rd axles is very close at only 11cm (approximately one-third of the axle spacing between the 1st and 2nd axles or the 3rd and 4th axles). Based on the effect of ASSR, the closely spaced axle is identified with higher identification error than those with wider axle spacings.

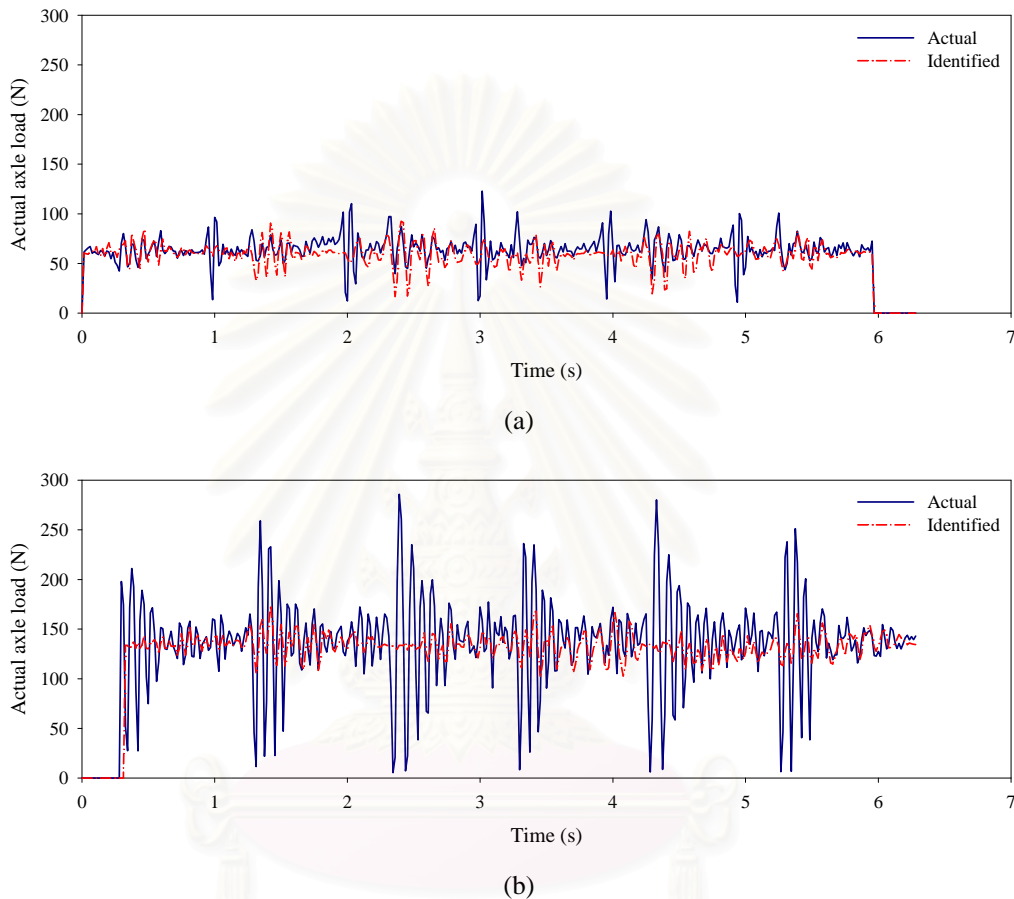


Figure 5.16 Time histories of identified axle load of a two-axle vehicle, 20 kg GVM traveling on roughness pattern II: (a) front axle (b) rear axle

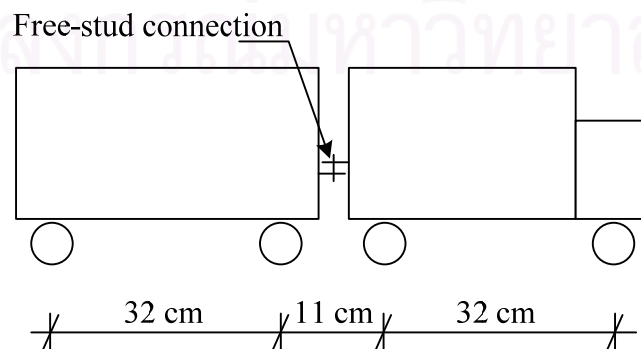


Figure 5.17 Axle spacings and trailer connection of four-axle vehicle model

Table 5.4 Experimental scenarios and results of four-axle vehicle load identification

GVM Ratio (M_{s1}/M_{s2})	M_{s1} (kg)	M_{s2} (kg)	v (m/s)	RPE (%)			
				1 st Axle	2 nd Axle	3 rd Axle	4 th Axle
0.60	15	25	0.2	33.12	7.91	5.47	3.67
	15	25	0.6	29.27	8.09	5.88	5.25
	15	25	1.0	28.26	6.42	6.73	7.45
	15	25	1.4	27.26	7.80	6.41	8.28
	15	25	1.8	23.18	6.63	5.84	9.19
0.80	20	25	0.2	53.86	9.34	12.38	7.15
	20	25	0.6	43.37	15.82	10.74	7.13
	20	25	1.0	37.67	12.94	9.95	6.94
	20	25	1.4	29.64	13.79	10.18	6.89
	20	25	1.8	28.25	11.66	13.01	8.83
1.00	20	20	0.2	48.28	23.51	32.64	5.21
	20	20	0.6	41.44	23.12	31.37	12.14
	20	20	1.0	45.51	26.03	29.32	11.76
	20	20	1.4	37.05	27.08	34.36	12.09
	20	20	1.8	39.56	25.47	30.66	11.82
1.25	25	20	0.2	4.93	25.04	38.05	8.90
	25	20	0.6	11.49	27.60	33.62	10.64
	25	20	1.0	11.75	25.40	34.31	9.40
	25	20	1.4	8.86	30.28	72.51	17.02
	25	20	1.8	11.39	27.26	33.84	8.44
1.67	25	15	0.2	5.58	29.21	67.36	2.48
	25	15	0.6	6.05	32.65	71.27	16.38
	25	15	1.0	7.50	31.39	72.44	15.98
	25	15	1.4	8.86	30.28	72.51	17.02
	25	15	1.8	11.45	29.43	74.81	15.61

However, in order to explain this behavior thoroughly, all scenarios are re-identified with their optimal regularization parameter. Table 5.5 and Figure 5.19 show the obtained results. It is clearly noticed from Table 5.5 that moving speed significantly affects the optimal regularization parameter and the obtained accuracy. A vehicle traveling at a higher speed requires a higher order of regularization parameters since it induces higher dynamic impact to the bridge than a vehicle traveling at a slower speed. In addition, it is clearly observed that identification with optimal λ effectively reduces the RPE for all scenarios with a maximum error of approximately 17%. Therefore, it is noted that the range of appropriate regularization parameters of a multi-axle vehicle depends on weight distribution, axle spacings and moving speed. The range of the appropriate regularization parameters of this multi-axle vehicle study lies from 0.0005 to 0.01. In this case, the most appropriate λ of this 4-axle vehicle that can be used for all scenarios is 0.001.

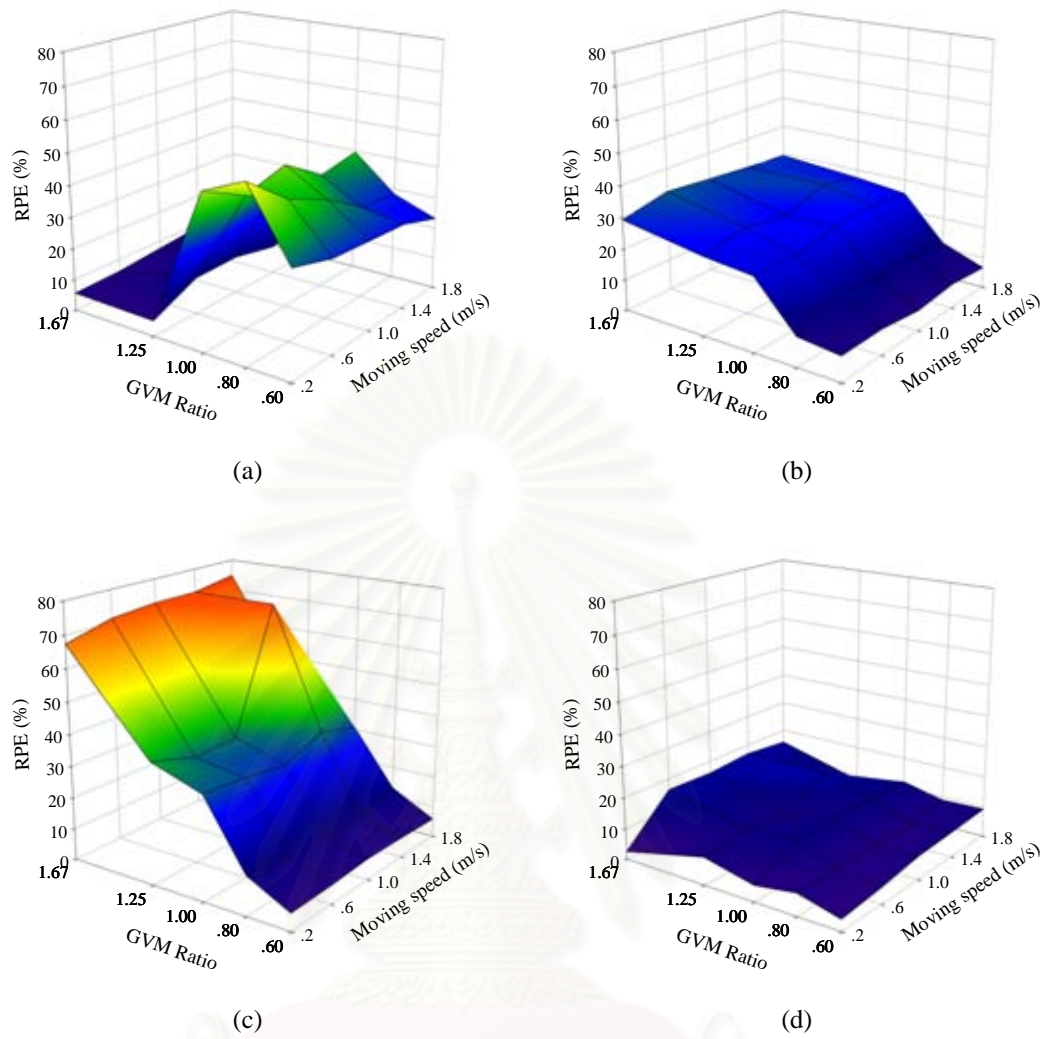


Figure 5.18 RPE of identified axle load of four-axle vehicle with different GVM ratios and moving speed: (a) 1st Axle load, (b) 2nd Axle load, (c) 3rd Axle load, and (d) 4th Axle load

สถาบันวิทยบริการ
จุฬาลงกรณ์มหาวิทยาลัย

Table 5.5 Experimental scenarios and results of four-axle vehicle load identification (identified with optimal λ)

GVM Ratio (M_{s1}/M_{s2})	M_{s1} (kg)	M_{s2} (kg)	v (m/s)	RPE (%)				Optimal λ
				1 st Axle	2 nd Axle	3 rd Axle	4 th Axle	
0.60	15	25	0.2	5.72	3.05	2.85	2.77	0.0001
	15	25	0.6	7.06	3.37	2.74	2.75	0.0005
	15	25	1.0	9.33	8.33	4.30	4.59	0.001
	15	25	1.4	12.29	6.54	4.16	6.08	0.005
	15	25	1.8	13.35	9.41	4.67	7.92	0.01
0.80	20	25	0.2	7.75	4.26	7.05	3.98	0.00001
	20	25	0.6	9.38	5.07	8.51	4.02	0.0001
	20	25	1.0	10.37	4.68	8.94	6.16	0.001
	20	25	1.4	12.70	4.80	10.72	7.92	0.001
	20	25	1.8	14.89	3.95	14.85	14.09	0.01
1.00	20	20	0.2	6.99	4.34	8.78	3.34	0.00001
	20	20	0.6	7.50	5.44	13.23	4.25	0.00005
	20	20	1.0	11.17	6.09	16.56	6.88	0.0001
	20	20	1.4	11.69	4.44	13.54	7.55	0.0005
	20	20	1.8	13.89	5.60	10.64	9.51	0.001
1.25	25	20	0.2	3.56	3.20	7.19	3.61	0.00001
	25	20	0.6	4.88	5.24	11.73	3.87	0.0001
	25	20	1.0	6.96	5.42	14.98	6.83	0.0001
	25	20	1.4	7.82	5.19	15.38	7.83	0.0005
	25	20	1.8	8.74	6.45	10.40	9.21	0.0005
1.67	25	15	0.2	2.94	2.70	7.08	3.49	0.00001
	25	15	0.6	3.90	3.85	13.89	4.44	0.00005
	25	15	1.0	5.26	4.20	15.83	6.33	0.0005
	25	15	1.4	6.52	4.37	12.88	7.39	0.0005
	25	15	1.8	6.99	6.31	10.86	9.51	0.001

Figure 5.20 shows the RPE of identified axle loads computed with λ of 0.001. The identified axle load results in acceptable accuracy with maximum RPE of 30% for the 3rd axle load. However, since the weight distribution of vehicle axles are unknown in a real situation, gathering information on the appropriate range of regularization parameter for each vehicle category is suggested before using an identification method in practice.

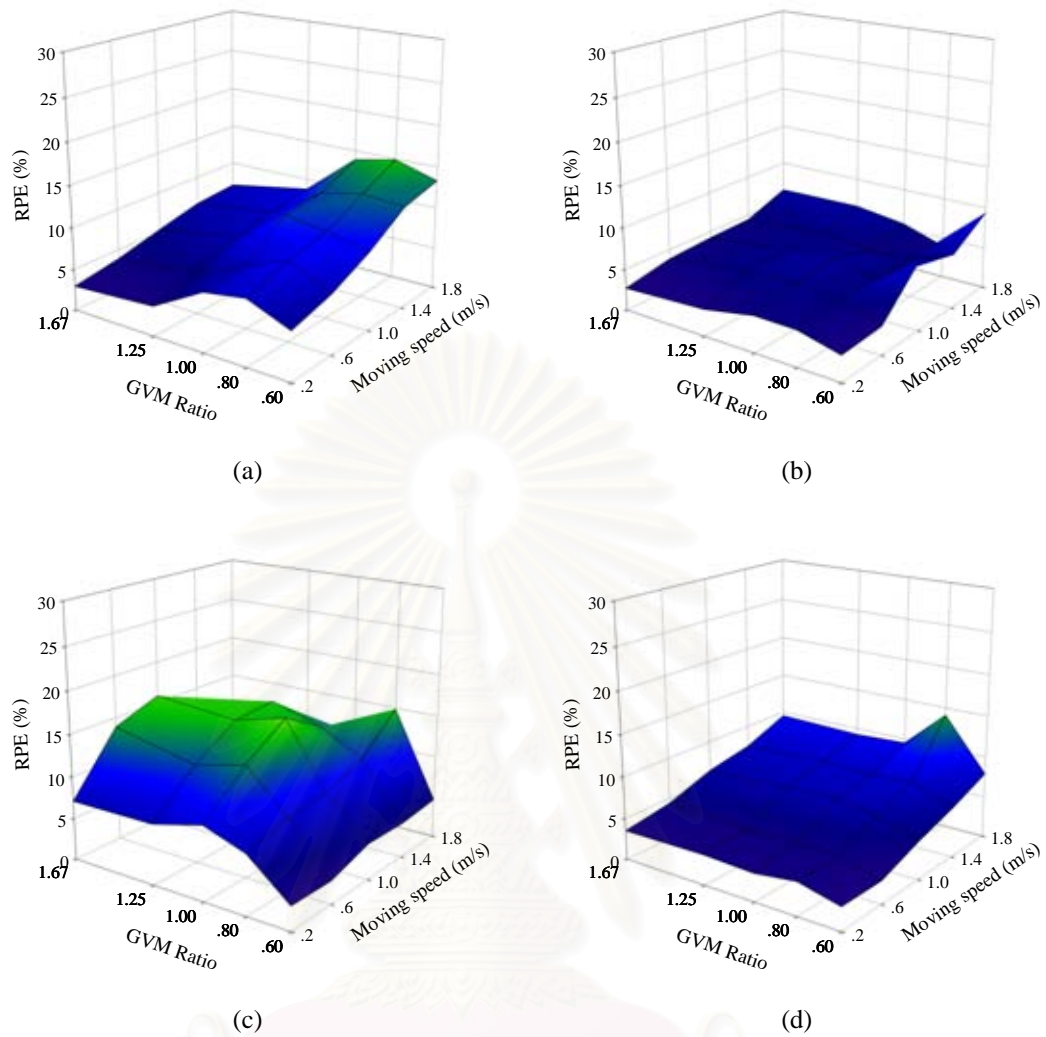


Figure 5.19 RPE of identified axle load of four-axle vehicle with different GVM ratio and moving speed (identified with optimal λ): (a) 1st Axle load, (b) 2nd Axle load, (c) 3rd Axle load and (d) 4th Axle load

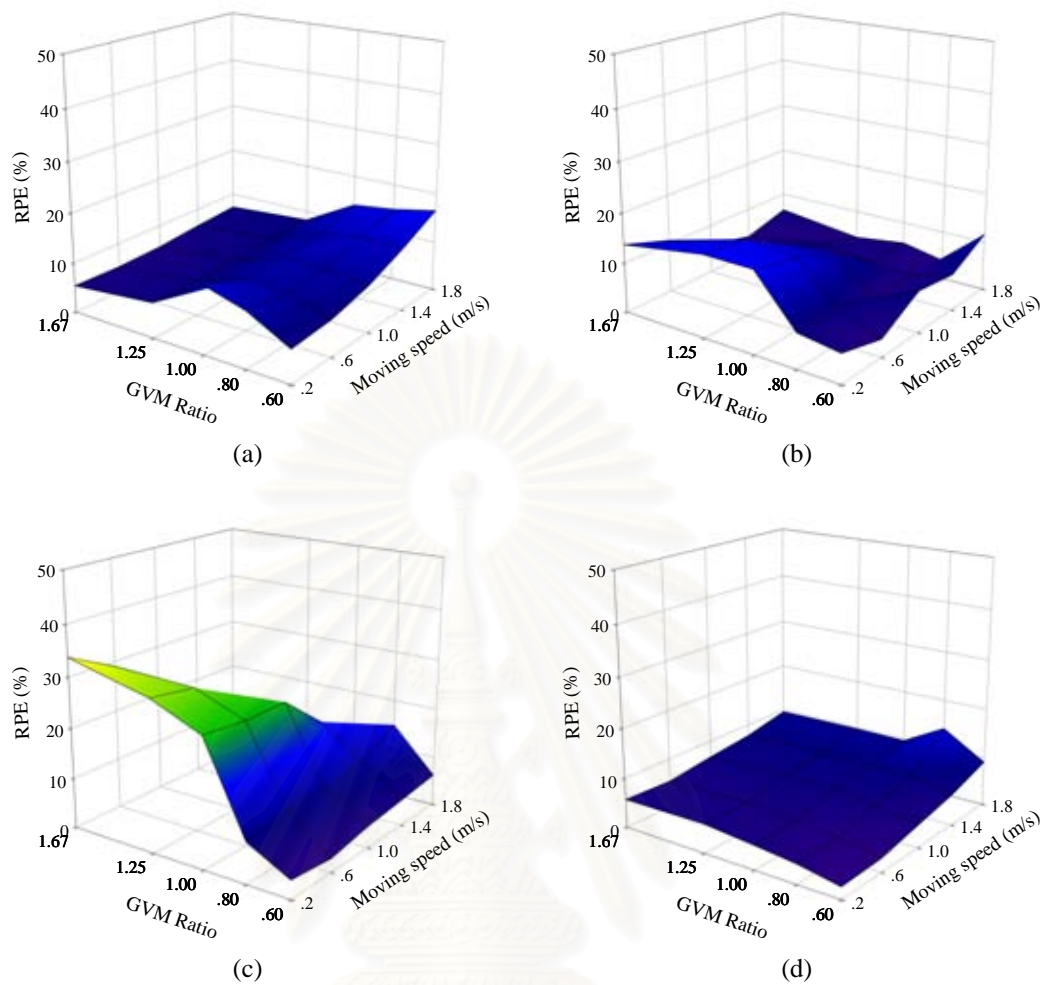


Figure 5.20 RPE of identified axle load of four-axle vehicle with different GVM ratios and moving speed (identified with λ of 0.001): (a) 1st Axle load, (b) 2nd Axle load, (c) 3rd Axle load and (d) 4th Axle load

5.5 Multiple-Vehicle Axle Load Identification

Multiple-vehicle axle load identification is studied by conducting several experiments under several conditions involving two model vehicles. Two 25 kg GVM model vehicles are adopted for the experiments. The typical measured bending moments and their corresponding measured axle loads of two model vehicles are shown in Figure 5.21. Table 5.6 presents all the experiment scenarios of vehicle travel to simulate all realistic possibilities. The first and the second vehicles travel in the left and the right traffic lanes, respectively. To control the vehicle travel, two indices are defined: vehicle speed ratio and bridge approach time interval. The vehicle speed ratio is the ratio of the first and the second model vehicle velocities, v_1/v_2 . The

bridge approach time interval, t_d , is the delay time between the arrival of the second vehicle and the first vehicle at the bridge. The regularization parameter λ is set to 0.1 as well as in the case of single vehicle axle load identification.

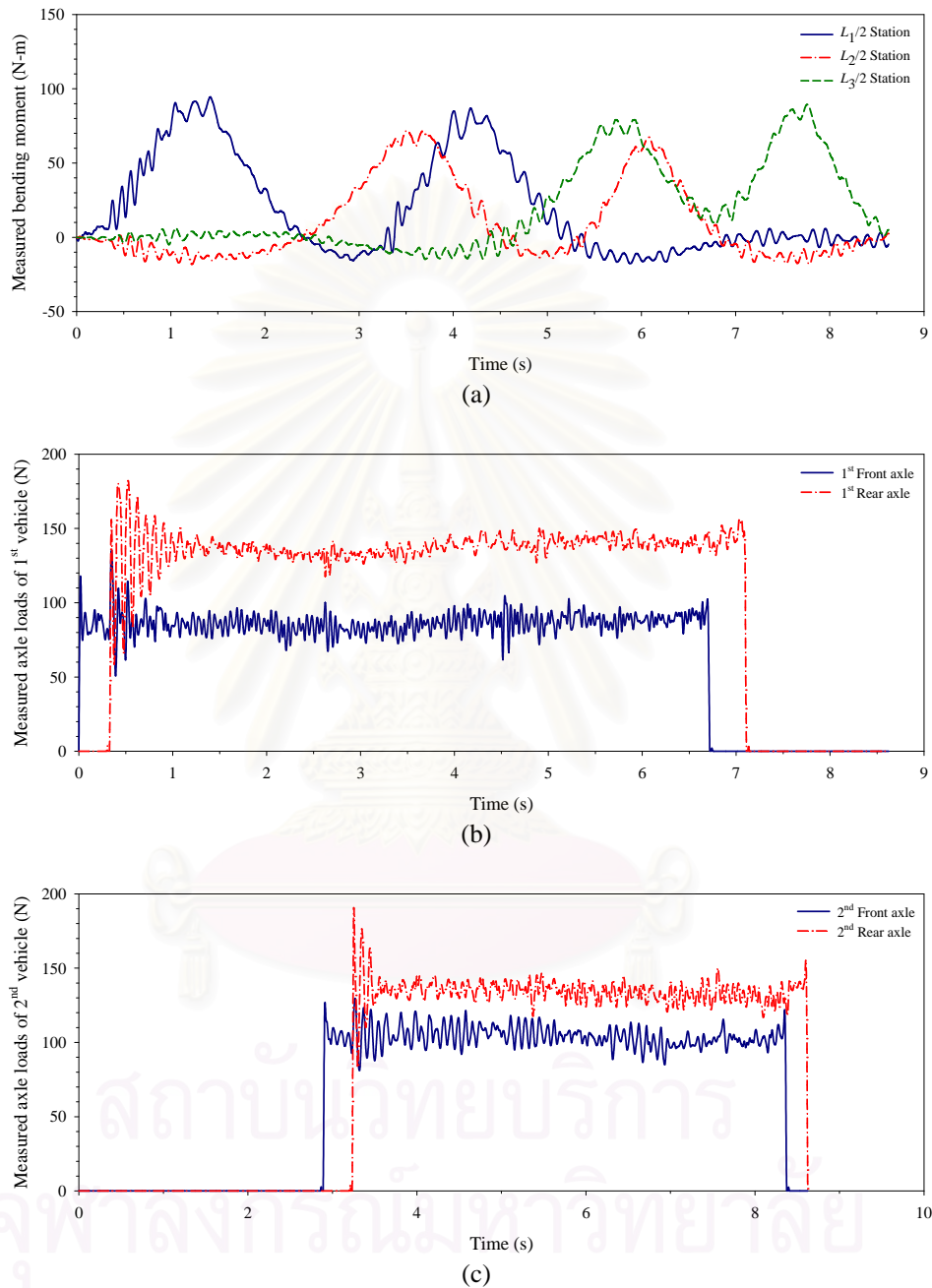


Figure 5.21 Typical measured bending moments and the corresponding measured axle loads of two-vehicle axle load identification: (a) measured time histories of bridge bending moments, (b) measured time histories of front and rear axle loads of 1st model vehicle and (c) measured time histories of front and rear axle loads of 2nd model vehicle

Table 5.6 Experimental scenarios of two-vehicle axle load identification

Case	Vehicle speed ratio (v_1/v_2)	v_1 (m/s)	v_2 (m/s)	t_d (s)	Scenarios
OVT-1	0.43	0.6	1.4	0	Overtaking
OVT-2				1	Overtaking
OVT-3				2	Overtaking
OVT-4				3	Overtaking
OVT-5				4	Overtaking
OVT-6	0.71	1.0	1.4	0	Overtaking
OVT-7				1	Overtaking
FLD-1				2	Following with decreasing headway
FLD-2				3	Following with decreasing headway
FLD-3				4	Following with decreasing headway
SBS	1.00	1.0	1.0	0	Side-by-side
FLC-1				1	Following with constant headway
FLC-2				2	Following with constant headway
FLC-3				3	Following with constant headway
FLC-4				4	Following with constant headway
FLI-1	1.40	1.4	1.0	0	Following with increasing headway
FLI-2				1	Following with increasing headway
FLI-3				2	Following with increasing headway
FLI-4				3	Following with increasing headway
FLI-5				4	Following with increasing headway
FLI-6	2.33	1.4	0.6	0	Following with increasing headway
FLI-7				1	Following with increasing headway
FLI-8				2	Following with increasing headway
FLI-9				3	Following with increasing headway
FLI-10				4	Following with increasing headway

Figure 5.22 presents the RPE of all two-vehicle axle load scenarios as a function of vehicle speed ratio and t_d . All experimental schemes provide solutions within 15% for a vehicle. For the first vehicle, the RPEs of both the front and the rear axle loads significantly increase with respect to the increase of the vehicle speed ratio. The RPEs of the second vehicle are all below 10% and tend to increase slightly at vehicle speed ratios below 1.00. To determine the correctness of the proposed method, the correlation coefficients of identified axle loads are presented in Table 5.7. Three categories of two vehicle travel are discussed as follows.

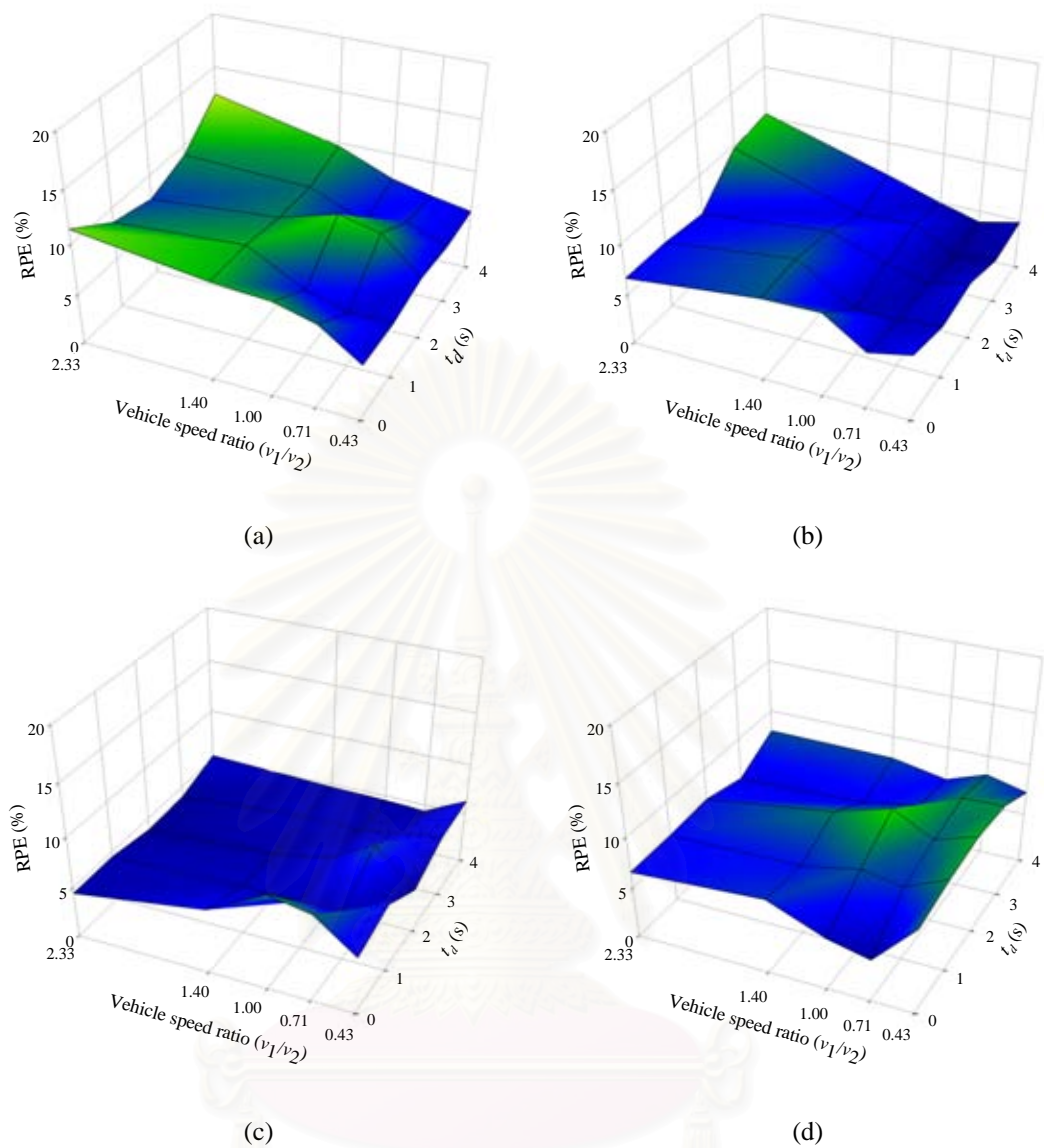


Figure 5.22 The RPE of identified dynamic axle load of two-vehicle axle load identification: (a) front axle load of 1st vehicle, (b) rear axle load of 1st vehicle, (c) front axle load of 2nd vehicle and (d) rear axle load of 2nd vehicle

Table 5.7 Correlation coefficients of identified vehicle axle loads from different two-vehicle axle load identification scenarios

Case	1 st Front axle	1 st Rear axle	2 nd Front axle	2 nd Rear axle
OVT-1	0.9758	0.9453	0.9939	0.9919
OVT-2	0.9522	0.9585	0.9921	0.9906
OVT-3	0.9495	0.9494	0.9929	0.9915
OVT-4	0.9592	0.9381	0.9927	0.9912
OVT-5	0.9642	0.9472	0.9949	0.9918
OVT-6	0.9151	0.9169	0.9809	0.9833
OVT-7	0.9551	0.9218	0.9915	0.9875
FLD-1	0.9783	0.9778	0.9911	0.9857
FLD-2	0.9869	0.9820	0.9868	0.9856
FLD-3	0.9880	0.9871	0.9923	0.9902
SBS	0.9157	0.8896	0.9441	0.9219
FLC-1	0.9855	0.9756	0.9868	0.9881
FLC-2	0.9874	0.9727	0.9887	0.9877
FLC-3	0.9857	0.9811	0.9906	0.9889
FLC-4	0.9885	0.9881	0.9914	0.9905
FLI-1	0.9900	0.9859	0.9882	0.9868
FLI-2	0.9911	0.9848	0.9874	0.9917
FLI-3	0.9907	0.9888	0.9889	0.9872
FLI-4	0.9887	0.9845	0.9893	0.9894
FLI-5	0.9908	0.9836	0.9908	0.9905
FLI-6	0.9922	0.9877	0.9817	0.9828
FLI-7	0.9926	0.9884	0.9874	0.9841
FLI-8	0.9933	0.9893	0.9924	0.9884
FLI-9	0.9903	0.9831	0.9928	0.9927
FLI-10	0.9865	0.9807	0.9910	0.9916

5.5.1 Short Headway Movement

Figure 5.23 presents the typical results of two-vehicle axle load identification with short headway. Figure 5.24 demonstrates the zoom of typical identified axle load time histories from the same case shown in Figure 5.23. The axles of both vehicles travel on the bridge without overlapping and are identified individually in the time history. Based on the results presented in Figure 5.22 for vehicle speed ratios between 1.0 and 2.33 corresponding to short headway, the identification is not significantly influenced by the vehicle speed ratio or the bridge approach time interval. This is particularly the case for the second, slower vehicle which spends a longer duration on the bridge. The axle loads for this vehicle scenario are identified within an RPE of 13%. From the axle load time history resulting from two vehicles with short headway (Figure 5.22), it is observed that the actual and identified axle load time histories compare well for the four axle loads according to a correlation of 0.981 shown in Table 5.7. This also indicates that the time histories exhibit no significant fluctuation in accuracy over time or disruption in identification when the vehicles cross over bridge supports. In addition, the axle loads are consistently identified through the

entire bridge crossing for each axle without the distortion that might be expected as a result of the residual bridge vibration caused by the lead vehicle.

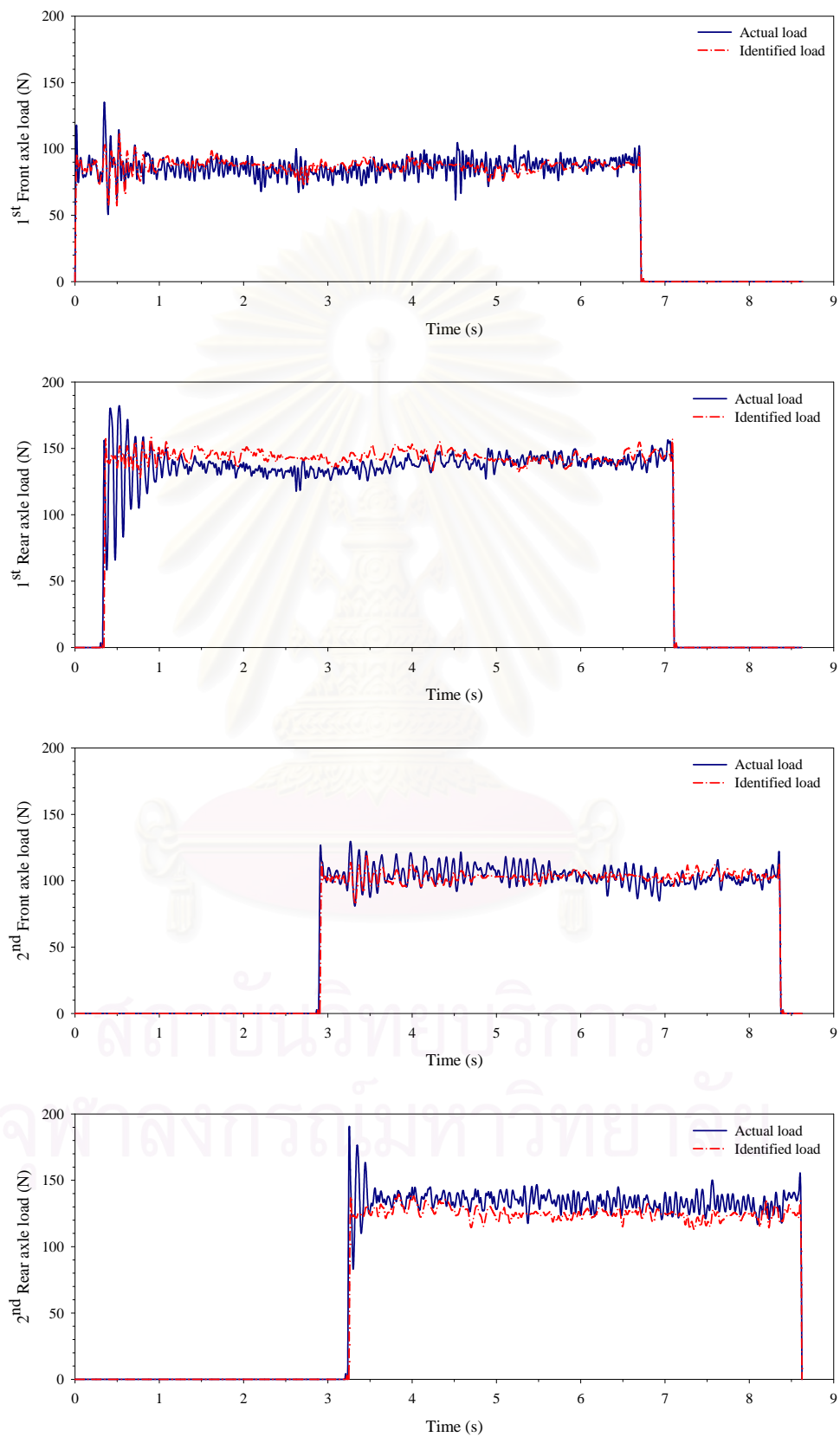


Figure 5.23 Identified axle loads of two vehicles with short headway (FLC-3)

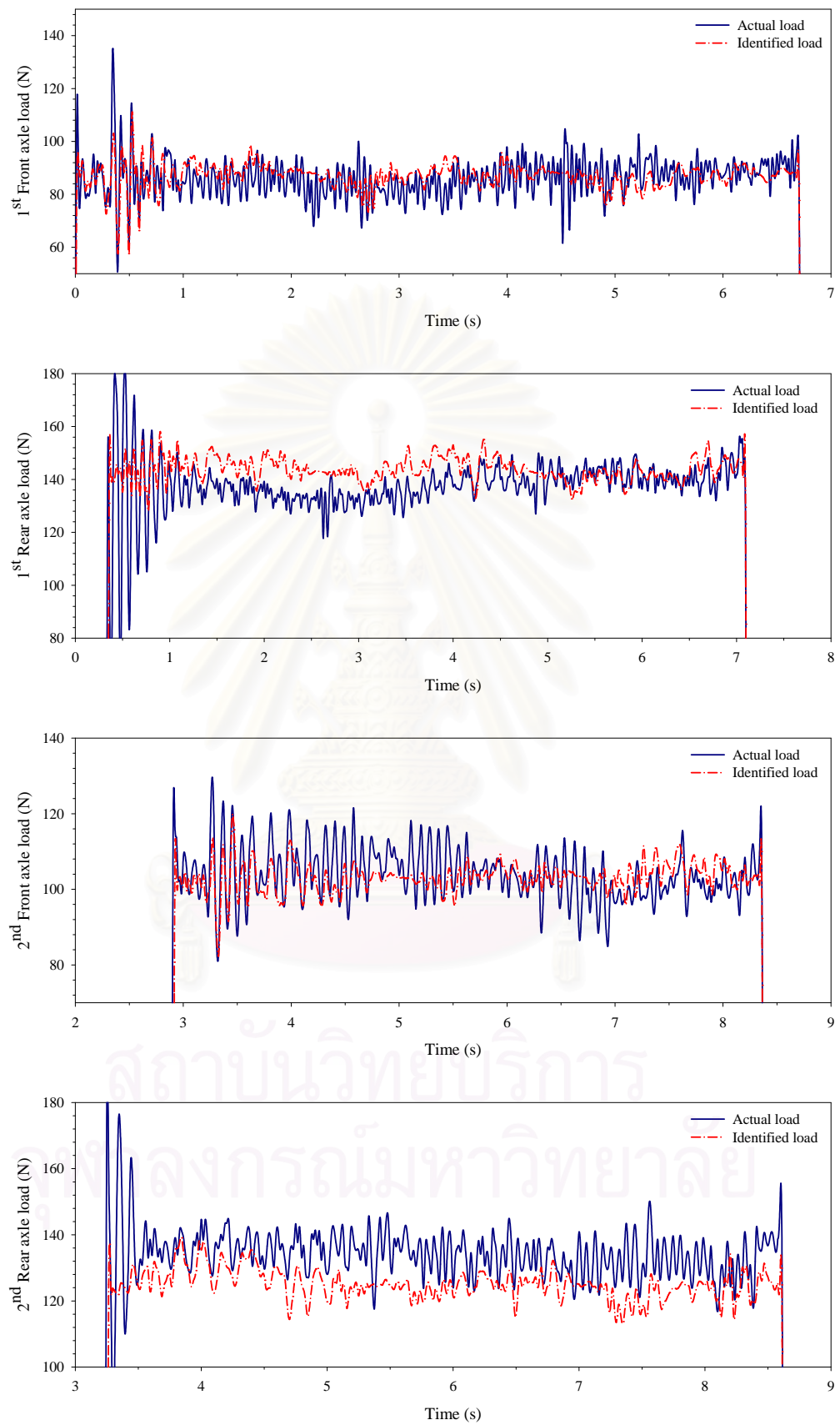


Figure 5.24 Zoom of typical identified axle loads of two vehicles (FLC-3)

5.5.2 Overtaking Movement

Figure 5.25 presents the results of two-vehicle axle load identification in an overtaking travel situation. In this scenario, the following vehicle overtakes or passes the lead vehicle by traveling at a higher rate of speed. In this situation, the problem to overcome is that of axle overlap. It can be observed from Figure 5.22 for a vehicle speed ratio below 1.0 that the identified axle loads are all within 10% RPE of the actual dynamic loads. This indicates that the proposed method can identify axle loads accurately, even when one vehicle is overtaking another while on the bridge. Separation of the identified axle loads during overtaking and passing the bridge support is achieved because the axle loads are identified independently and controlled by static influence lines from the USC algorithm.

5.5.3 Side-by-Side Movement

Figure 5.26 presents the results of a two-vehicle axle load identification scenario where both vehicles move side-by-side (SBS) at the same speed and location along the entire length of the bridge. Both vehicles travel at the same speed of 1.0 m/s. Although the combined vehicle load can be identified as a single 2-axle vehicle, the independent axle loads of each vehicle are required. Therefore, the method identifies this scenario as a 2 vehicle, 4-axle configuration. Figure 5.22, in the case of a vehicle speed ratio of 1.0 and bridge approach time interval, $t_d = 0$ is exactly this scenario. Figure 5.22 indicates that identification errors for dynamic axle loads in a SBS scenario are below 10% for all axle loads. The identified axle loads for both vehicles exhibit the same time-history shape with a small difference in the median force. The median of identified axle loads of the first vehicle are smaller than the second vehicle as 3.4 N and 2.0 N for the front and the rear axle loads, respectively. This is because the GVM of the first vehicle is slightly smaller than the second vehicle as 9.8 N. The axle positions for both vehicles are the same for the duration of the bridge crossing. Therefore, the four axle loads are similar to the two axle loads scenario separated into four axle loads as average values for the same axle position. Hence, the system simplification from assuming the bridge as the beam structure is not appropriate for multiple-vehicle axle load identification of side-by-side movement. However, the multiple presence of vehicles with the same number of axles and axle spacing are rarely observed in actual traffic. The scenario of two identically configured vehicles traveling at the same speed SBS is even rarer.

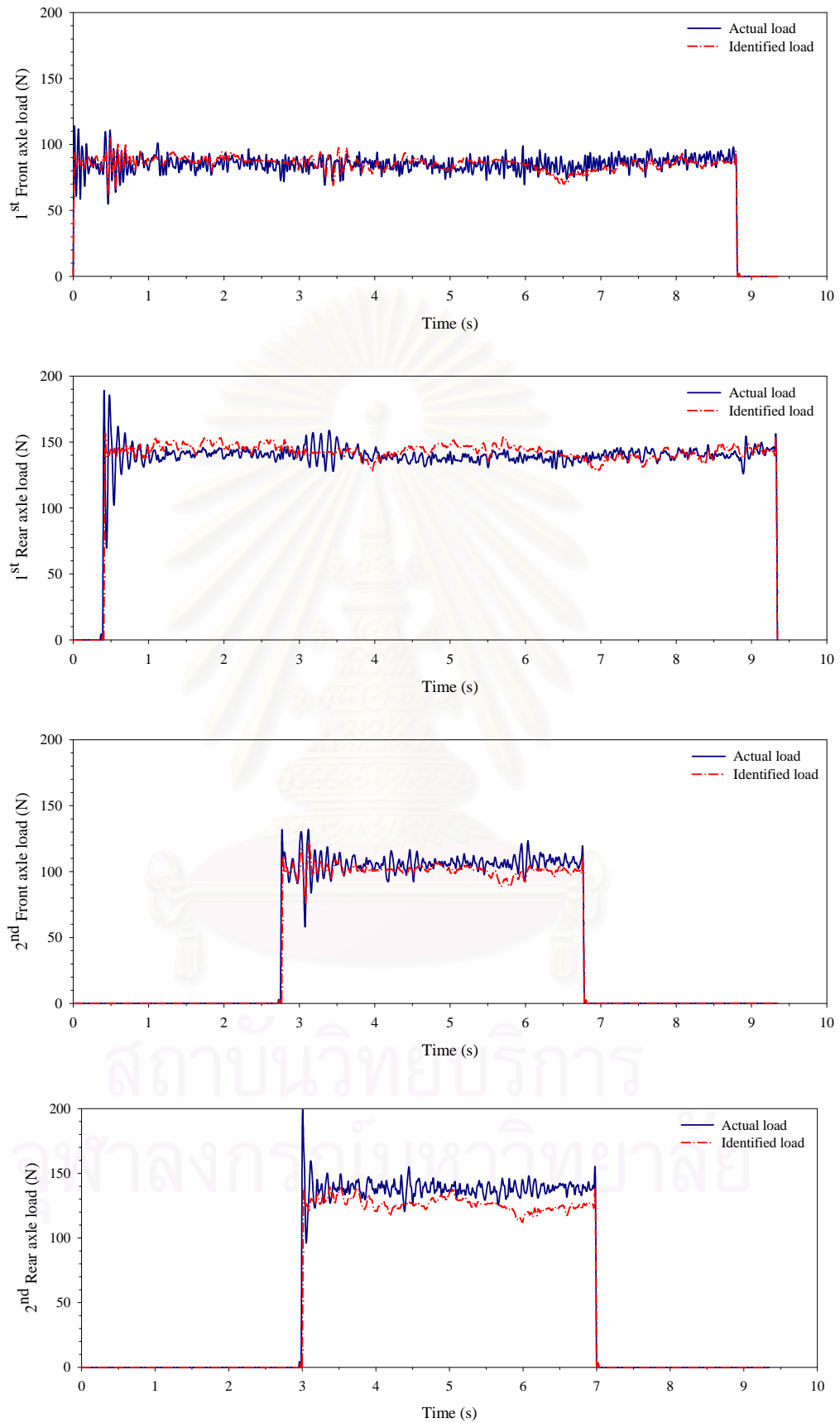


Figure 5.25 Identified axle loads of two vehicles with overtaking movement (OVT-4)

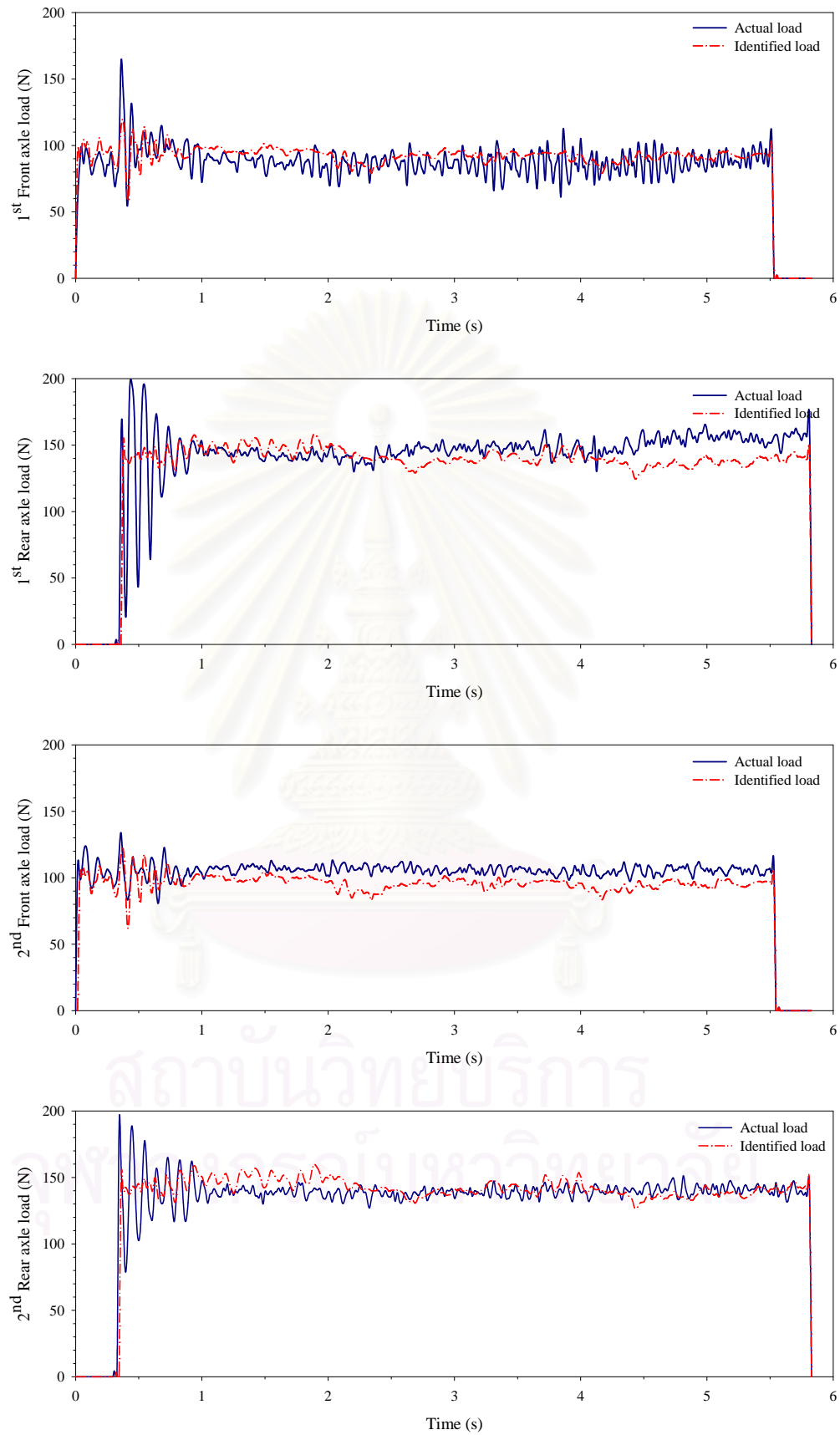


Figure 5.26 Identified axle loads of two vehicles with side-by-side travel (SBS)

Therefore, the proposed USC method is generally applicable in practice for normally occurring traffic conditions because the method can identify multiple axle loads accurately if the axle loads do not overlap during the entire bridge crossing.

According to the objective function in the optimization, the identified axle loads are a group of acting forces that induce the bridge to have the best match between the reconstructed and the measured bending moments. Therefore, if there is an overestimated axle load, other axle loads would tend to be underestimated in order to keep minimizing the objective function, i.e. the results shown in Figure 5.23 and Figure 5.25. This characteristic is also found from other researchers using a similar objective function (Law et al., 2007).

Figure 5.27 presents the percentage error of the estimated static gross vehicle weight in the case of two vehicles. The estimated static axle loads are represented by the median forces of dynamic load time histories in the duration that the axle loads travel on the bridge span. It is observed that the static gross weights of both vehicles are below 8%. It is also noticed that the error of the first vehicle gross weight is less than 5% in the cases when the vehicle speed ratio is 1.00 and below. For the second vehicle gross weight, the error of is less than 5% when the vehicle speed ratio is above 1.00. This result shows that a vehicle traveling on the bridge at a lower speed can have its static weight identified more precisely than one traveling at a higher speed. This is because the slower vehicle travels on the bridge with longer time histories and induces lesser dynamic interaction than the faster vehicle.

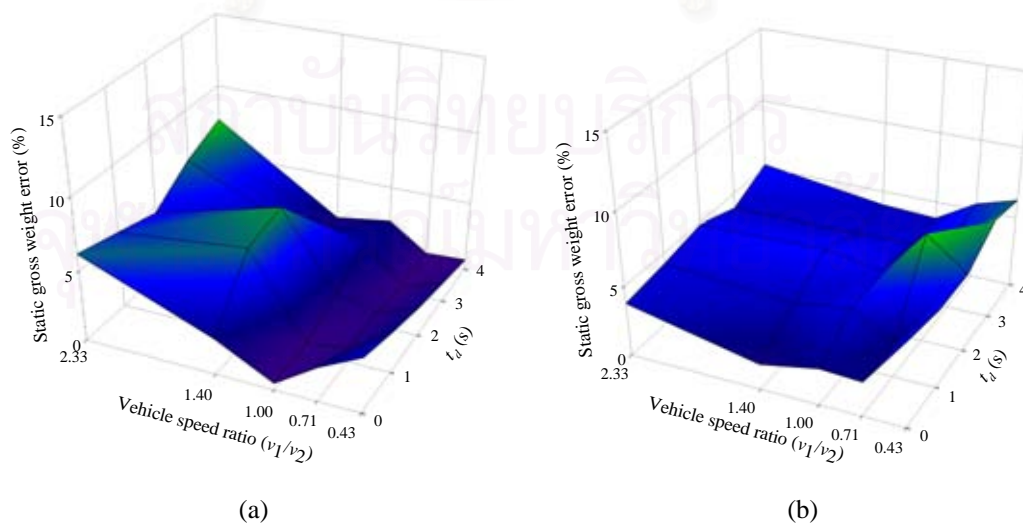


Figure 5.27 Percentage error of static vehicle gross weight from two-vehicle axle load identification: (a) 1st vehicle gross weight and (b) 2nd vehicle gross weight

In order to determine the accuracy of the proposed USC method, a comparison between measured bending moments and bending moments reconstructed from the identified loads is performed in order to verify the correctness of bending moment optimization. Table 5.8 presents the correlation between measured and reconstructed bending moments for three typical experimental cases. It is observed that the identified axle loads induce a near identical match of bridge bending moments with a correlation greater than 0.99 for every nine measuring stations. These coefficients imply that the proposed approach is correct, very effective and can be applied in problems related to multiple-moving load identification, particularly in multiple-vehicle axle load identification. However, it should be noted that in order to obtain a more accurate solution in practice, it is highly recommended that noise filtering be applied in data acquisition. This is because the signal to noise ratio becomes smaller for a higher iteration number according to the USC algorithm.

Table 5.8 Correlation coefficients of reconstructed bending moments from different two-vehicle axle load identification scenarios

Measuring station	Correlation coefficients of bending moments at measuring stations				
	OVT-4	FLD-2	SBS	FLC-3	FLI-4
$L_1/4$	0.9982	0.9979	0.9987	0.9978	0.9963
$L_1/2$	0.9990	0.9982	0.9990	0.9988	0.9987
$3L_1/4$	0.9963	0.9966	0.9984	0.9935	0.9952
$L_2/4$	0.9988	0.9946	0.9982	0.9962	0.9969
$L_2/2$	0.9997	0.9990	0.9994	0.9990	0.9989
$3L_2/4$	0.9983	0.9961	0.9977	0.9931	0.9974
$L_3/4$	0.9946	0.9967	0.9987	0.9928	0.9966
$L_3/2$	0.9995	0.9989	0.9997	0.9989	0.9993
$3L_3/4$	0.9991	0.9984	0.9994	0.9988	0.9990

5.6 Summary

An experimental study is conducted to investigate the effectiveness of the USC identification method. The actual dynamic axle loads of vehicles are directly measured and used in accuracy evaluation. The bridge model is made from steel plate and its fundamental frequency is designed to be similar to a real bridge.

According to the experimental results, the single-vehicle axle load identification indicates that the solution accuracy depends on vehicle mass, moving speed and bridge surface roughness. A heavy vehicle traveling at slow speed will result in more accurately identified axle loads than a lighter vehicle moving at faster speed. Moreover, the effect of vehicle transverse positioning is eliminated by using average sectional bending moments converted from strain gauges uniformly

distributed in each bridge section. Vehicle axle loads traveling on a smooth bridge surface are more accurately identified than those moving on a rough surface. However, identification of large impact axle load induced by roadway roughness is more likely to yield large identification error especially for a lightweight vehicle. Overlaying a new pavement on a rough surface bridge or selecting a smooth surface bridge is recommended for system application. Additionally, although the static component of axle load is identified accurately through the time history, the dynamic component at the duration when the axle loads are located at the internal bridge support cannot be identified since the bridge response is very small.

In the case of a multi-axle vehicle, the identification accuracy mainly depends on axle spacing and weight ratio. A vehicle axle with lower weight and closer axle spacing is identified with lower solution accuracy than one with higher weight and wider axle spacing. Besides, investigation into an appropriate range of regularization parameters for each vehicle category should be carried out before applying the identification system in order to gain the most accurate result.

For identification in the case of the multiple presence of axle loads, various scenarios of two vehicles traveling with either short headway, overtaking, or SBS are studied to determine the accuracy and effectiveness of the proposed method. The presentation of identified axle loads reveals that the proposed USC method returns accurate identification of dynamic axle load time histories under 10% RPE from 22 of 25 study cases. The USC method identifies axle loads for all tested scenarios without distortion due to overlapping because the axle loads are independently identified, corresponding to the static influence lines of the USC algorithm.

In addition, the identified axle loads can be accurately identified at any location along the bridge including when the vehicles pass bridge supports. This is a significant improvement in obtaining loads without a significant fluctuation in accuracy over time or disruption in identification when the vehicles cross over bridge supports, as has troubled previous studies on load identification from continuous bridge responses.

The identified dynamic axle loads are determined within an RPE of 10% with a few cases determined up to 13%. Moreover, correlation between identified axle loads and reconstructed bending moments demonstrate that the approach is very effective – within less than 1% error. For the static gross weight estimation, the USC method provides solution within 8% error for both the two vehicles. Finally, it is

conclusively expected that the proposed method is applicable to a practical system designed to accurately identify multiple-vehicle axle load time histories, and that it can also be applied in the practice of the static gross weight determination of the weigh-in-motion system.



สถาบันวิทยบริการ
จุฬาลงกรณ์มหาวิทยาลัย

CHAPTER VI

AXLE LOAD IDENTIFICATION WITH INCOMPLETE MEASUREMENT INFORMATION

6.1 General

In this chapter, the capability of the proposed identification method on axle load identification with incomplete measurement information is investigated in order to determine the limitations of the identification approach and to gather any useful information for recommendations toward real application. This is because in the real application, it might not be possible to measure every enquired signal due to a lack of workability in instrument installation, limitations in the instruments used in the data acquisition system, etc. An effectiveness evaluation based on the experimental results identified with incomplete information is given. Discussion on the limitations of the identification approach is also provided.

6.2 Axle Load Identification with Incomplete Velocity Information

Regarding the algorithm of the identification method, the time history of the axle load positioning while the vehicles are moving on the bridge is one required input. Based on the bridge behavior and its identification system in the time-domain, vehicles can travel along the bridge independently at any speed and with any acceleration characteristics since the system only requires the proper locations of the axle loads. In practice, the correct axle load positioning can be obtained by using several photoelectric sensors or employing image processing technology. However, employing such technology is expensive and requires very large memory storage and computing. On the other hand, using lots of photoelectric sensors is also expensive and requires a multi-channel data acquisition system. In addition, the moving speed of vehicles traveling in the real situation is usually almost constant since the considered time duration when the vehicles pass the bridge is very short. Therefore, this study conducts axle load identification when the vehicles are assumed as moving at constant speed for which the measuring system needs only two photoelectric sensors located at the beginning and the end supports of the bridge. The percentage error of vehicle position time history is calculated from Eq. (6.1) as follows:

$$\text{position error} = \frac{\|\mathbf{x}_i - \hat{\mathbf{x}}_i\|}{\|\mathbf{x}_i\|} \times 100\% \quad (6.1)$$

where \mathbf{x}_i and $\hat{\mathbf{x}}$ are actual and simplified position vectors of the i^{th} vehicle, respectively.

In the experiment explained in Chapter V it is difficult to control the moving speed of vehicles so as to be exactly constant throughout the duration of vehicle travel. Therefore, the axle load is re-identified with the simplified vehicle position based on constant speed assumption in order to determine the sensitivity of the vehicle position error. Figure 6.1 shows the plots of actual and constant speed assumption time histories of the vehicle axle position. The corresponding time histories of actual and simplified bending moments are shown in Figure 6.2.

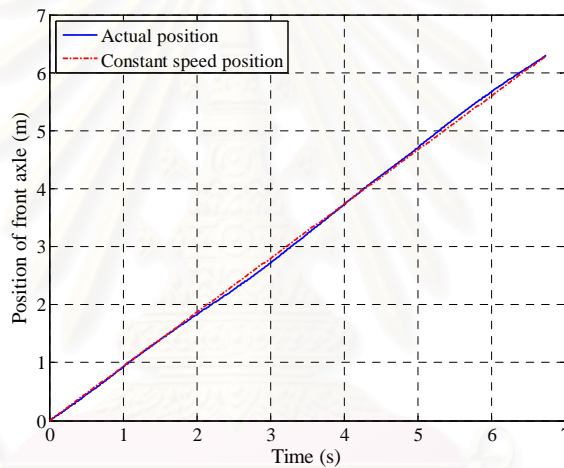


Figure 6.1 Actual and constant speed assumption time histories of vehicle axle position of a 2-axle vehicle, 25 kg GVM, traveling at a velocity of 1.0 m/s

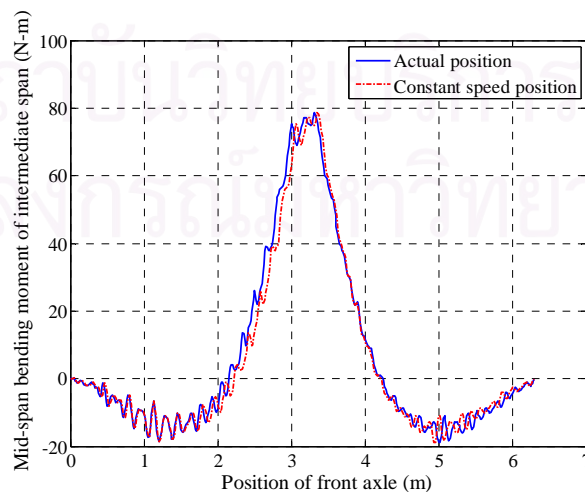
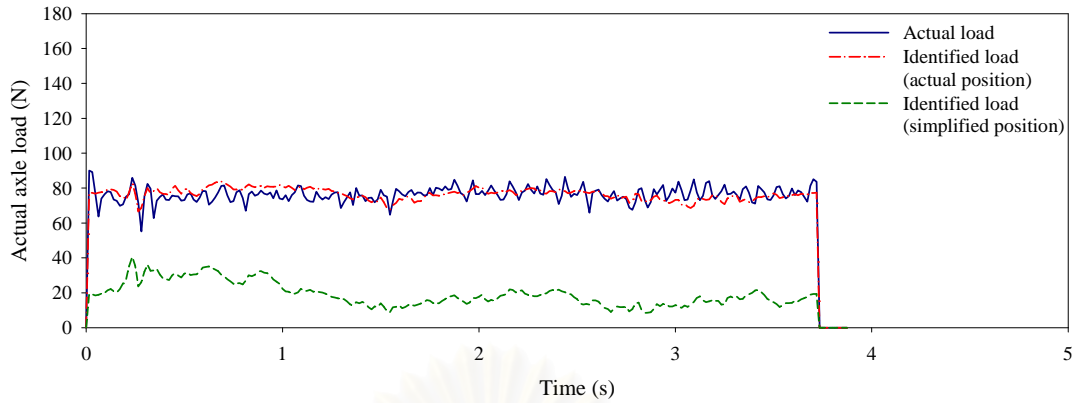


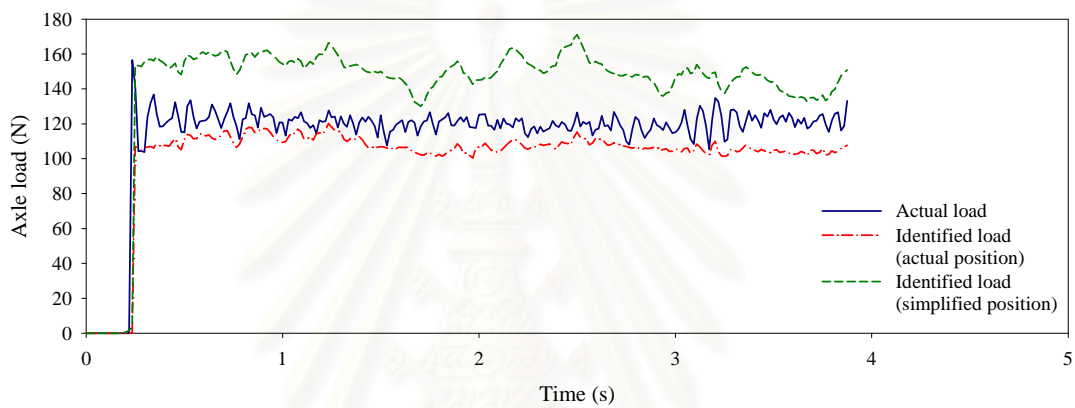
Figure 6.2 Actual and constant speed assumption time histories of the bending moment of a 2-axle vehicle, 25 kg GVM, traveling at a velocity of 1.0 m/s

The relative percentage error of vehicle axle loads identified with constant speed simplification is shown in section I of Appendix C. It is observed from the results of identification with constant speed assumption for both single-vehicle and multiple-vehicle cases that the identification error is very sensitive to the axle load position. A small difference in axle position can result in a large solution error compared to a solution obtained from identification with actual position. It is also noticed that the RPE of identified axle loads can increase up to 100% from identification with the error in vehicle position only 5%. This is because the axle position directly affects the relevant bending moment. Hence, the bending moment used in the identification for each time step is not to be consistent with the actual axle position.

Figures 6.3 and 6.4 present examples of identified axle load time histories due to small and large differences in vehicle position, respectively. With comparison to the actual axle load and identified axle loads with actual vehicle position, the obtained axle load from identification based on simplified vehicle position results in a very large difference in both the static and dynamic components throughout the time histories of the vehicle travel. This is because the physical characteristic of the relationship between the acting load and bridge bending moment controlled by the vehicle position is incorrect. The obtained axle loads are loads that only satisfy the objective function with least residual error. Therefore, the solution from identification with simplified vehicle position becomes inaccurate. This property can be noticed especially in Figure 6.4 where the identified front axle load is minus while the rear axle load is an overestimation with a large difference. Moreover, the effects of vehicle mass and moving speed on the identification seem to vanish when the position error is presented since the effect of the position error is much more influential. Further results and discussion on multiple vehicle identification by assuming vehicle travel as constant speeds are given in section I of Appendix C.



(a)



(b)

Figure 6.3 Time histories of identified axle loads of a two-axle vehicle moving on a three-span continuous bridge with 3.08% position error ($GVM = 20 \text{ kg}$, $v = 1.8 \text{ m/s}$); (a) front axle load (b) rear axle load

Additionally, the effects of vehicle speed ratio and bridge approach time interval on identification accuracy cannot be correctly discussed when the vehicle position error is observed. Therefore, it is concluded that the effect of vehicle position error directly affects identification accuracy. Assuming vehicle position time history with constant speed travel is acceptable only in a case of the position error being less than 2%. Applying many axle position detectors is recommended in practice in order to obtain the best identification accuracy.

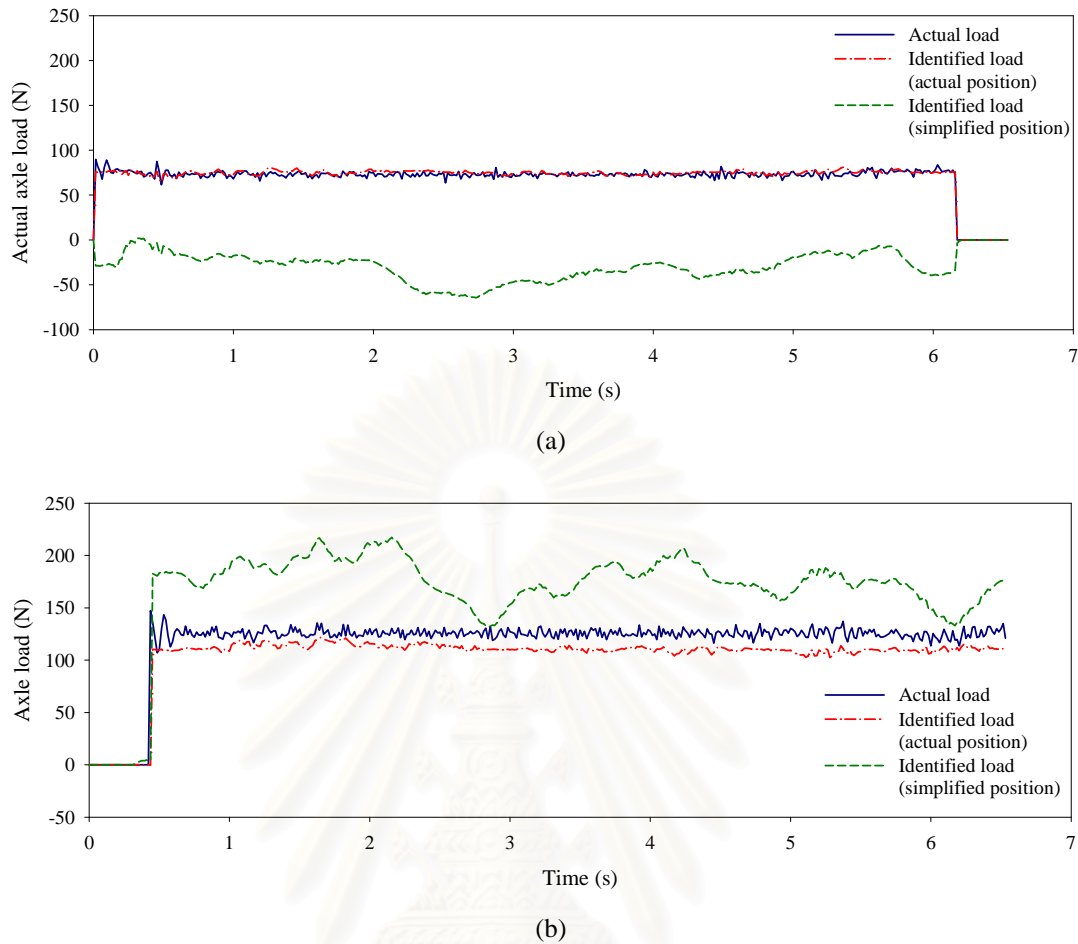


Figure 6.4 Time histories of identified axle loads of a two-axle vehicle moving on a three-span continuous bridge with 8.48% position error ($GVM = 20 \text{ kg}$, $v = 1.0 \text{ m/s}$); (a) front axle load (b) rear axle load

6.3 Axle Load Identification with Incomplete Bending Moment Information

According to the numerical study on the number of sensors used in identification, the experimental investigation presented in Chapter V is identified with 9 sections of bending moment. Based on the results from simulation in section 4.3.2, it is noted that the identification system is applicable when the number of measurement stations is not less than the number of unknown axle loads. However, difficulty in sensor installation due to the lack of workability in approaching the specified location or limitations of the instrument capacity might be encountered in practice. Hence, in this section, the identification of axle loads with incomplete sensor stations is carried out and discussed in order to evaluate the efficiency and to investigate the robustness of the proposed method when applied in a real situation.

The sensors are removed from 1 up to 5 stations. The measurement station arrangement with various patterns of sensor removal and the corresponding identification results are shown in section II of the Appendix C.

Figure 6.5 represents the RPE of the identified axle loads of both vehicles re-identified with incomplete measured bending moment station. The plot from Figure 6.5 indicates that the maximum RPE slightly increases with respect to the number of removed measurement stations. However, the maximum percentage error and correlation coefficient of all axle loads are below 14% and 10% respectively. Removing a sensor used in identification does not seriously affect solution accuracy. The best identification accuracy for all vehicle axle loads from sensor removal of 1 to 5 stations is below 6%, except in the case of 1 station removal which provides the lowest error within 8%.

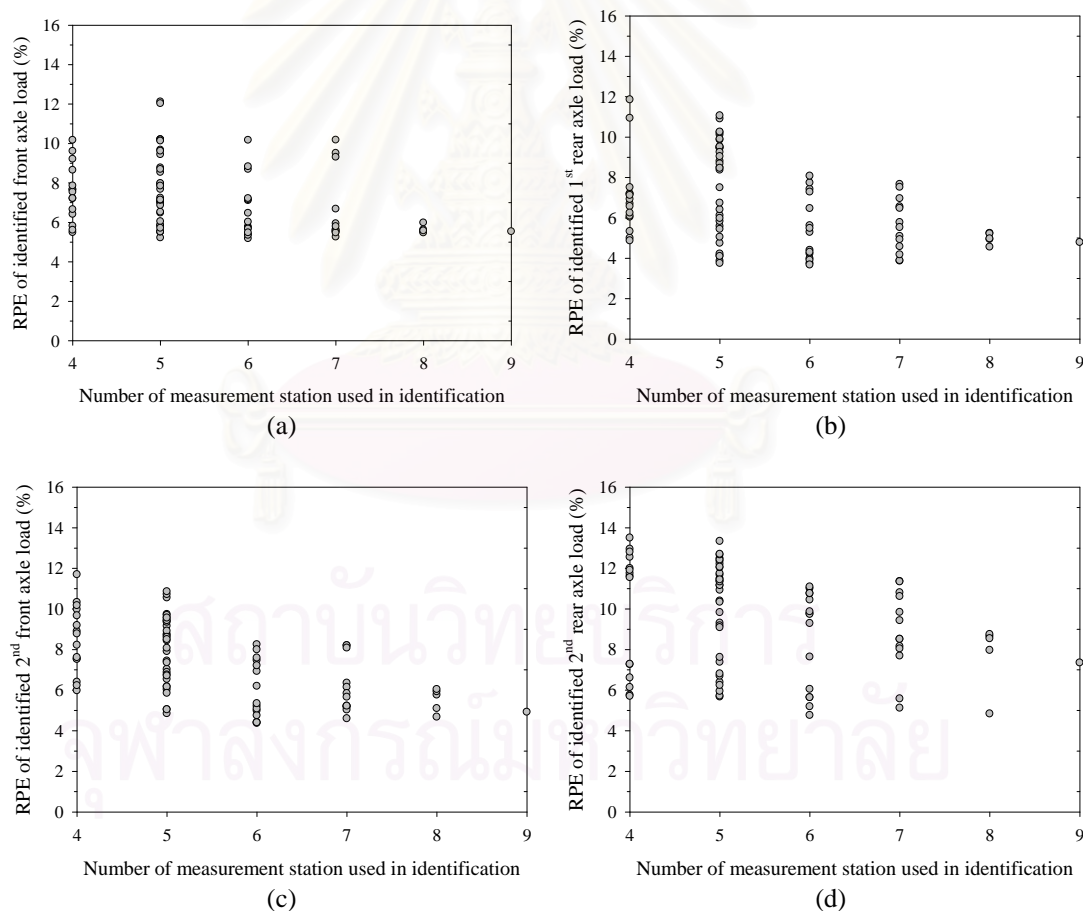


Figure 6.5 RPE (%) of identified axle loads of two vehicles traveling with overtaking movement (OVT-7) re-identified with incomplete measured bending moment station; (a) 1st front axle load (b) 1st rear axle load (c) 2nd front axle load and (d) 2nd rear axle load

Additionally, from the plots of obtained results shown in Figure 6.5 as well as the RPE of identified axle loads listed in Table C.4 in Appendix C, it is noted that there are some cases where the RPE of identified axle loads are below 6% for every vehicle axle. There are seven cases of sensor patterns including 8R-D, 7R-C, 6R-J, 6R-N, 5R-G, 5R-Y and 4R-A which provide a very accurate solution even though some measurement stations are removed. Table 6.1 summarizes the sensor patterns of these considered cases. From these patterns, it is noticed that the identification requires at least two measurement stations from the intermediate span in which the sensor at mid-span is critical and at least one sensor at $L/4$ of the first and the last bridge spans is required (4R-A pattern).

Table 6.1 Sensor patterns of vehicle axle load identification with removed measurement stations providing identification error within 6%

No. of removed sensor	Sensor pattern	Measurement station (● = used, ○ = not used)								
		$L_1/4$	$L_1/2$	$3L_1/4$	$L_2/4$	$L_2/2$	$3L_2/4$	$L_3/4$	$L_3/2$	$3L_3/4$
1	8R-D	●	●	●	○	●	●	●	●	●
2	7R-C	○	●	●	○	●	●	●	●	●
3	6R-J	●	○	●	○	●	●	●	○	●
3	6R-N	●	●	○	○	●	●	○	●	●
4	5R-G	○	○	●	○	●	●	○	●	●
4	5R-Y	●	○	○	○	●	●	○	●	●
5	4R-A	○	○	●	○	●	●	○	○	●

Figure 6.6 demonstrates the comparison of identified axle load time histories from identification with different sensor numbers removed. The most accurate results for each sensor removal case including 8R-B, 6R-J and 4R-A from station removal of 1, 3 and 5 respectively, are compared. The identified axle loads provide a very good match particularly in the static component. It is also observed that the identified axle loads exhibit the lowest correlation coefficient of only 0.9225. Therefore, it can be concluded that identification with sensor removal is still capable without disturbing solution accuracy when the number of measurement stations is not less than the number of identified axle loads.

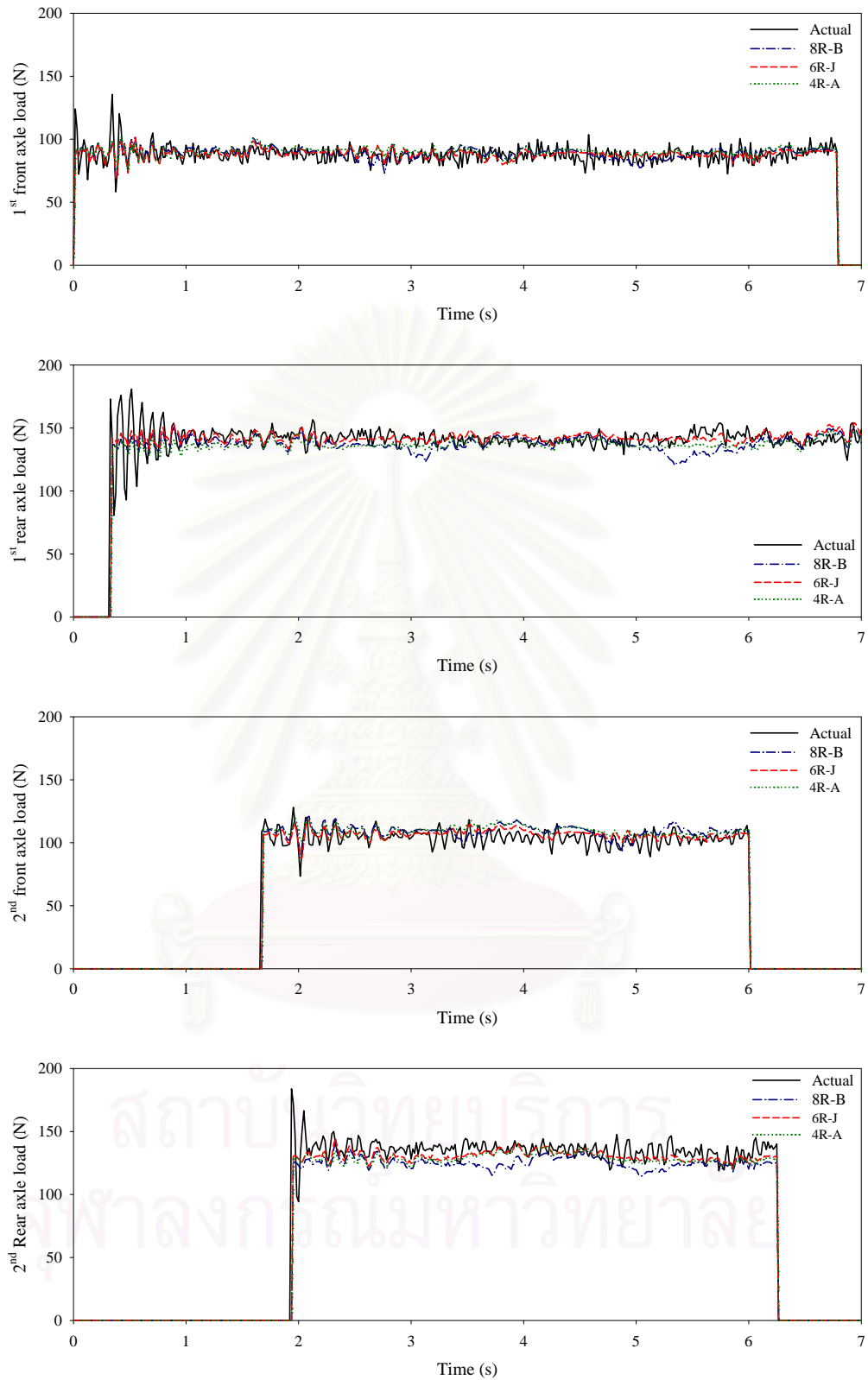


Figure 6.6 Time histories of identified axle loads calculated with various numbers of measurement stations

6.4 Axle Load Identification with Bridge Responses of Target Span

According to the identification process mentioned in Chapters IV and V, the identified axle loads are calculated from bridge responses at the time history of the vehicle crossing the entire length of the continuous bridge. Identification using measurement information from all bridge spans is beneficial concerning the aspect of the overall dynamic behavior of the vehicle axle load which cannot be considered on a short span bridge. However, it is also observed that axle load time histories identified on a multi-span bridge system exhibit accuracy weakness at the internal bridge supports due to the support condition in the transformation matrix introducing zero entries at the bridge support. The proposed USC method enhances solution accuracy at the bridge support especially the static component of the identified loads which is significantly improved. In addition, identification from longer time history information requires longer computational time since the size of the transformation matrix is large. The multiple presence of vehicles is more likely to be observed leading to worse solution accuracy. Moreover, it might not be necessary to implement and employ measurement data in the identification for all bridge spans since only a critical span is of interest.

Alternatively, in order to reduce the computational time and to identify the vehicle axle loads on a particular bridge span, identification with reduced measurement signal from the bridge span in question is studied. Therefore, in this section the identification of vehicle axle load of a multi-span bridge with the target span is considered and its effectiveness on solution accuracy is also discussed. Measurement signals used in identification are cut off from the regular signal recorded on the entire continuous bridge by considering only the duration that the first vehicle axle approaches the first support of the particular span and the last vehicle axle leaves the other support of the target span. However, it is noted that identification with structural simplification by considering the target span as a single-span bridge is not practicable because there is the continuity from the adjacent bridge spans. Hence, the axle load traveling on other spans can induce bridge response of the target span leading to incorrect bridge response reconstruction.

Axle load identification on a particular span is mainly divided into two categories. One is identification with a determined or overdetermined problem while the other is an underdetermined problem depending on the number of measurement stations used in the identification. The determined problem is a problem in which the

number of unknown parameters equals the number of equations. If it is a case in which the numbers of identified axle loads and measurement stations are equivalent and the number of signal stations employed in the measurement is higher than the number of vehicle axle loads, the problem becomes overdetermined. If the number of axle loads exceeds the number of measurement stations, the identification is an underdetermined problem.

Regarding the results from the numerical and experimental studies mentioned in Chapters IV and V for the identification of a single-vehicle identification, the identification with middle span will be overdetermined (2 unknowns; 3 measurement stations) and will be underdetermined in the case multiple-vehicle identification (4 unknowns; 3 measurement stations). To investigate the effectiveness of the axle load identification using target span, the measurement data from the experiment in Chapter V is adopted. Tables 6.2 and 6.3 present the identified results of overdetermined and underdetermined study cases of selected scenarios from the experiment in Chapter V re-identified with bending moments from the middle bridge span, respectively. The overdetermined cases are selected from single-vehicle identification while the underdetermined cases are sorted from multiple-vehicle identification in the case of the multiple presence of vehicles in the middle span being observed. For the considered study cases listed in Table 6.3, the first vehicle is the vehicle that first approaches the first bridge span, then the other vehicle is noted as the second vehicle similar to the definition made and described in Chapter V.

Table 6.2 RPE of identified axle load and correlation coefficients of bending moments in the case of an overdetermined problem from the experiment identified with target span

GVM (kg)	Moving speed (m/s)	RPE (%)		Correlation coefficient of bending moments		
		Front axle	Rear axle	L/4	L/2	3L/4
10	0.2	14.27	15.95	0.9920	0.9993	0.9964
10	1.0	8.93	11.02	0.9842	0.9987	0.9888
10	1.8	13.33	18.40	0.9688	0.9961	0.9758
20	0.2	2.70	14.32	0.9974	0.9993	0.9955
20	1.0	4.01	15.40	0.9980	0.9986	0.9968
20	1.8	4.20	13.04	0.9965	0.9992	0.9966
30	0.2	6.18	1.63	0.9985	0.9995	0.9975
30	1.0	8.94	7.37	0.9980	0.9993	0.9976
30	1.8	4.40	4.01	0.9976	0.9982	0.9969

Table 6.3 RPE of identified axle load and correlation coefficients of bending moments in the case of an underdetermined problem from the experiment identified with target span

Study case	RPE (%)				Correlation coefficient of bending moments		
	1 st front axle	1 st rear axle	2 nd front axle	2 nd rear axle	L/4	L/2	3L/4
OVT-3	5.58	5.59	5.11	12.67	0.9992	0.9993	0.9978
OVT-4	6.06	5.98	9.06	11.42	0.9988	0.9998	0.9991
OVT-5	12.96	4.67	5.60	9.74	0.9984	0.9996	0.9987
OVT-6	48.62	7.30	28.62	15.82	0.9981	0.9993	0.9988
OVT-7	12.79	4.74	8.14	13.39	0.9976	0.9994	0.9984
SBS	8.44	6.90	12.35	2.72	0.9979	0.9992	0.9977
FLI-1	8.71	8.17	5.67	5.44	0.9956	0.9981	0.9953

The results from Table 6.3 indicate that identification using only the bridge response from a particular bridge span is capable. Vehicle mass, as well as identification with bridge response from all spans, has the same tendency to affect solution accuracy while moving speed has no obvious effect. The RPE of identified axle loads are all below 16% and the most accurate scenario allows identification error of only 4.40%. The correlation coefficient of the reconstructed bending moment demonstrates that the algorithm of the proposed identification method is correct with the correlation coefficient error of 4% in the case of 10kg GVM and below 2% for others.

The results observed from Table 6.7 indicate that identification using bending moments from target span allows an identification error of axle loads within 15%, except for the OVT-6 scenario. Moreover, the correlation coefficients listed in Table 6.7 imply that the identification method is correct. In the case of the OVT-6 scenario, the RPE is up to 49% because it is difficult to distinguish the overlapping axle loads of two vehicles in the analysis of bending moment considered at the particular duration compared to other cases (see Figure 6.7). Moreover, identification with a lower number of measurement stations also decreases the information used in an optimization. Examples of the time histories of identified axle loads of two-vehicle travel in the cases of overtaking and following scenarios are presented in section III of Appendix C.

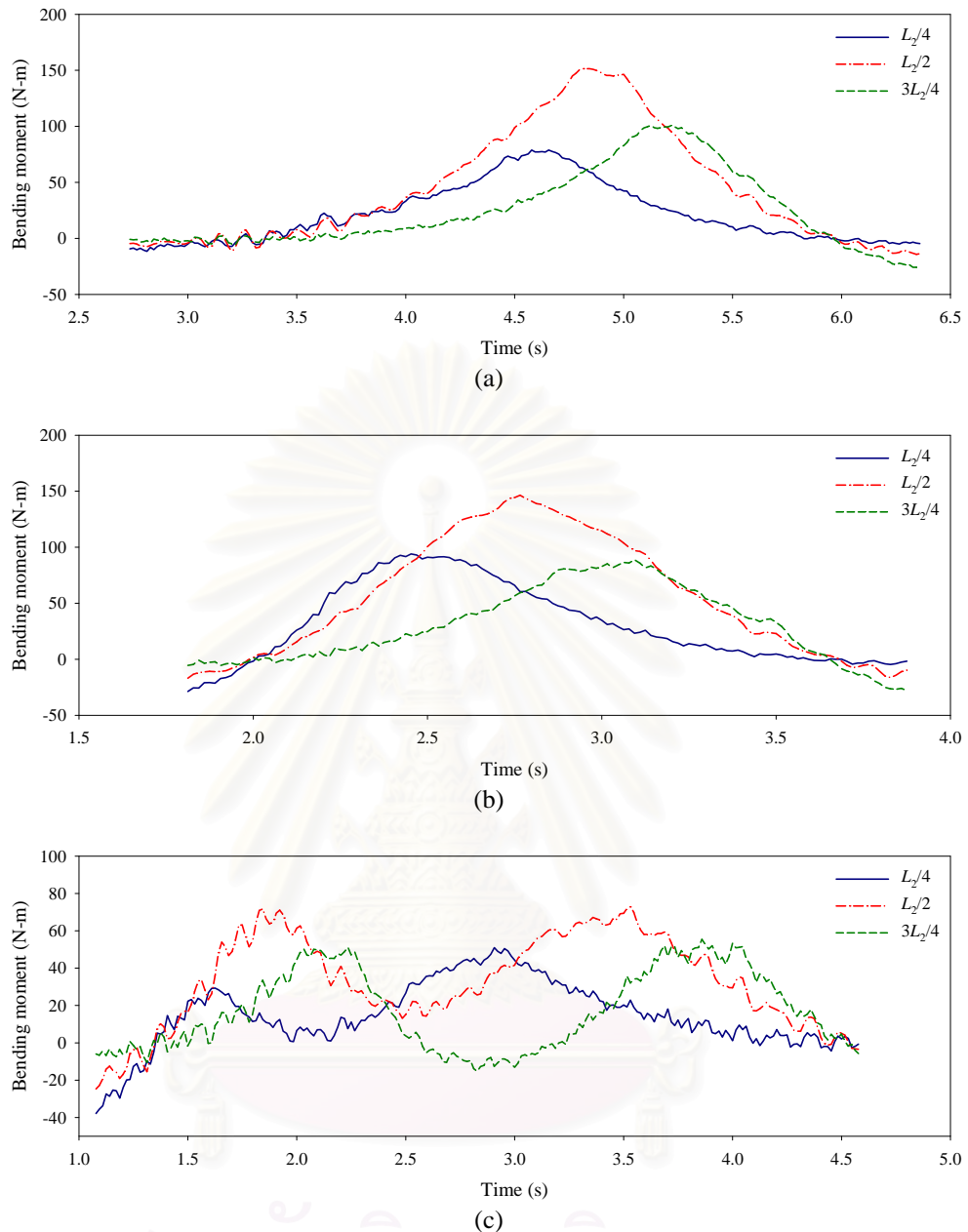


Figure 6.7 Time histories of shortening measured bending moments of middle span used in axle load identification: (a) OVT-4 scenario (b) OVT-6 scenario and (c) FLI-1 scenario

Therefore, it can be concluded that identification of vehicle axle load with bridge response from target span and the shortening time history of vehicle travel by considering only the duration that a vehicle crosses the particular span is capable and effective for static axle load estimation. In addition, since the duration in an optimization is reduced as well as there being a fewer number of measurement

stations, the axle load of an axle traveling with longer overlapping duration is more difficult to identify accurately than those traveling with less overlapping in overtaking or side-by-side movements.

6.5 Summary

Axle load identification with incomplete measurement information is conducted in order to investigate efficiency and robustness as well as the limitations of the proposed identification method. The measurement information considered in this study consists of three parameters including vehicle positioning, number of measurement stations and number of bridge spans used in identification.

For the study of incomplete vehicle velocity information, the normal axle position of traveling vehicles can be observed using many photoelectric sensors or by employing image processing technology. Using less vehicle axle detectors may provide a large error in axle position. However, most vehicles traveling in a real situation usually move at constant speed because the recorded duration is very short. Therefore, an evaluation of solution accuracy from identification with the vehicle position assumed to be traveling at constant speed is carried out. The obtained results indicate the axle position is very sensitive to the accuracy of identified axle loads. A small error in vehicle position can initiate a large error in load time histories. This is because the axle load acting on the bridge and the relevant bending moment response is incorrect. Hence, assuming vehicle speed as constant in the identification is not appropriate. Accurately measuring the axle position throughout the duration of vehicle travel is highly recommended.

Secondly, the study of incomplete bending moment information is conducted. In practice, there is the possibility that some instruments used to measure bridge response cannot be installed due to difficulty in approaching the particular location or local structural damage. Axle load identification with a reduced number of measurement stations is studied. Various schemes of sensor removal from 1 to 5 stations from the existing 9 sections of bending moment are identified. The results indicate that maximum RPE increases relative to the number of removed measurement stations with the maximum percentage error and correlation coefficient of all axle loads below 14% and 10% respectively. The identified axle loads provide very good matches particularly in the static component. Therefore, it is concluded that identification with sensor removal is effective without disturbing solution accuracy

when the number of identified axle loads is not higher than the number of measurement stations.

Finally, axle load identification by considering only a particular span is conducted. This is because it might not be necessary to instrument all bridge spans in order to determine the axle loads acting on a particular span. Moreover, the computational time can be reduced from the corresponding duration by considering only the time gap in which the vehicle crosses the target span. The identified axle loads exhibit acceptable accuracy within RPE of 16%, particularly for the static component of axle load. However, the method fails to accurately identify the dynamic component. This is because the duration in an optimization is reduced as well as there being less measurement stations. It is also observed that the axle load of an axle traveling with longer overlapping duration is more difficult to identify accurately than those traveling independently or with overlapping movement, due to the overlapping between each other.



CHAPTER VII

CONCLUSIONS AND RECOMMENDATIONS

7.1 Conclusions

Based on the numerical and experimental studies as in chapters IV and V, the effectiveness and accuracy of proposed identification method using regularization via the SVD method adopting the USC technique was investigated. The proposed method has been proven to be more robust against measurement noise and also to provide better identification accuracy than the existing identification approaches. The problem of ill-conditioning usually found when axle loads cross the internal supports of multi-span bridges is completely overcome using the USC technique. Moreover, difficulty in regularization parameter selection is also eliminated since the parameter can be assigned with a wide range without disruption to solution accuracy. In addition, the proposed method is capable of accurately identifying the axle loads of multi-axle and multiple vehicles with any travel scenarios. The effect of incomplete measurement information on identification accuracy is also found to be not significant providing the total number of measurement stations is greater in number than the unknown axle loads. The following detailed conclusions for each aspect can be drawn.

7.1.1 Axle Load Identification from Bridge Bending Moment

Conclusive remarks concerning axle load identification with the proposed USC regularization method from the parametric study conducted with numerical and experimental investigations are given as follows:

1. A vehicle with a heavier mass and moving at a slower speed can be identified with greater accuracy than a vehicle with lighter mass and moving at a faster speed.
2. Closely spaced and lightweight vehicle axles are more difficult to identify accurately than those with wider spacing and heavier in weight.
3. The effect of vehicle transverse positioning is eliminated by using average sectional bending moments converted from strain gauges uniformly distributed in each bridge section.

4. A vehicle traveling on a smooth bridge surface is more accurately identified than one moving on a rough surface. However, identification of a large impact axle load induced by roadway roughness tends to yield large identification error, especially for a lightweight axle.
5. Although the static component of an axle load is identified accurately throughout the time history, the dynamic component at the duration when the axle loads are present around the internal bridge supports cannot be identified since the bridge response is very small.
6. In the case of the multi-axle vehicle, identification accuracy mainly depends on axle spacing and weight ratio. A vehicle axle with a lower weight and closer spacing is identified with lower solution accuracy than one with a heavier weight and wider spacing.
7. The maximum identification errors from the experimental results for a 2-axle vehicle and two 2-axle vehicles are 18% and 13%, respectively. However, in the case of the axle load identification of a 4-axle vehicle, the maximum error is 35% at λ of 0.001 and up to 75% at λ of 0.1.
8. The proposed identification method can accurately identify all possible scenarios without distortion resulting from the vehicle axles overlapping with each other because the axle loads are independently identified, corresponding to the static component of the USC algorithm.
9. Because the problem is simplified to the two-dimensional axle load identification of multiple vehicles traveling for a long duration of overlapping or moving side-by-side there tends to be large identification error.
10. For the static gross weight estimation, the USC method provides solution within 8% error for both the two vehicles for all considered cases.

7.1.2 Axle Load Identification with Incomplete Measurement Information

Axle load identification with incomplete measurement information is conducted in order to investigate efficiency and robustness as well as the limitations of the proposed identification method. The measurement information considered in this study consists of three parameters including vehicle positioning, number of

measurement stations and number of bridge spans. The conclusions for this study are provided as follows:

1. The accuracy of identified axle loads is very sensitive to axle position. Small error in vehicle position can initiate large error in load time histories. This is because the axle load acting on the bridge and the relevant bending moment response is incorrect. Hence, assuming vehicle speed as constant in the identification might not be appropriate.
2. Based on identification with reduced measurement stations, it is found that identification with some sensor removal is still effective without disturbing solution accuracy when the number of identified axle loads is not higher than the number of measurement stations. The RPE of vehicle axle loads slightly increases with the number of removed measurement stations. However, the maximum percentage error and correlation coefficient of all axle loads are still below 14% and 10% respectively. In addition, the estimation of the identified axle is observed as being very good particularly for the static component.
3. In the case of axle load identification using the response from a target span with reduced response time history, the identified axle loads exhibit acceptable accuracy within an RPE of 16%, particularly for the static component of axle load. However, the method fails to accurately identify the dynamic component. This is because the duration in an optimization is reduced as well as there being a fewer number of measurement stations. It is also observed that it is more difficult to accurately identify the axle load of an axle traveling with a longer overlapping duration than those traveling independently or moving with a short overlapping duration between each other.

7.2 Recommendations

Recommendations of the study on the practical application of the axle load identification system and suggestions for further study are given in the following sections.

7.2.1 Recommendations toward Real Application

Regarding the effectiveness and robustness investigation of the proposed identification method, in order to achieve the greatest benefits of the identification system, the limitations and recommendations for application are provided as follows:

1. Concerning the number and location of sensors used in the measurement, nine sensors with three sensors for each bridge span proves to be the most efficient at identifying multiple axle loads.
2. The sampling rate recommended for use in the data acquisition system is at least 10 times the first fundamental frequency or 2 times the five mode fundamental frequency of the bridge.
3. Although the proposed method is robust to the level of measurement noise, applying noise filtering in data acquisition seems necessary.
4. The effective number of finite beam elements employed in structural modeling is 8 elements per bridge span.
5. Using a bridge with smooth or very low surface roughness or overlaying a new pavement on an existing bridge in operation is highly recommended.
6. Investigation on an appropriate range of regularization parameters for each vehicle category should be carried out before applying the identification system in order to obtain the most accurate result.
7. Accurate measurement of axle position throughout the duration of vehicle travel has to be provided.
8. Identification with less number of measurement stations or identification using information only from a target span is capable but the accuracy of the identified axle load, especially for the dynamic component, will deteriorate.

7.2.2 Recommendations for Further Study

Regarding the results and limitations of the current study, the following are recommendations for further study:

1. Study on a greater number of vehicles and more different bridge types and number of spans should be considered.

2. The tolerance of identification accuracy to the error of vehicle position measurement should be improved in order to obtain a more robust solution in practice.
3. An improved approach reducing the computational time consumed by the identification system should be studied and developed.
4. Identification with an underdetermined system should be developed in order to reduce computational time and instrument costs.



สถาบันวิทยบริการ
จุฬาลงกรณ์มหาวิทยาลัย

REFERENCES

- Akarawittayapoom, T. (2003). Accuracy improvement of a moving truck identification by iteration method. Master's Thesis, Department of Civil Engineering Graduate School Chulalongkorn University (in Thai).
- Asnachinda, P. (2004). Moving truck weight identification by a scale-down model. Master's Thesis, Department of Civil Engineering Graduate School Chulalongkorn University (in Thai).
- Asnachinda, P., Pinkaew, T. and Laman, J.A. (2007). Multiple vehicle axle load identification from dynamic bridge response: An experimental study. Proceeding of Experimental Vibration Analysis for Civil Engineering Structures 2007. 227-236.
- Asnachinda, P., Pinkaew, T. and Laman, J.A. (2008). Multiple vehicle axle load identification from continuous bridge bending moment response. Engineering Structures, doi:10.1016/j.engstruct.2008.02.018
- Bellman, R. (1967). Introduction to the mathematical theory of control processes. New York : Academic Press.
- Sedchaicharn, B. (1998). Dynamic interaction between 10-wheel truck and steel multi-girder overpass bridge. Master's Thesis, Department of Civil Engineering Graduate School Asian Institute of Technology.
- Cebon, D. (1993) Interaction between heavy vehicles and roads. L. Ray Buckendale Lecture, SP-951, SAE Trans 930001, Cambridge University.
- Chaallal, O. and Shahawy, M. (1998). Experimental evaluation of dynamic amplification for evaluation of bridges performance. Technical report No.ETS.DRSR.98.11 Department of Construction Engineering, University of Quebec.
- Chamchuenwong A. (1998). Weigh-In-Motion analysis and fatigue assessment of a steel overpass bridge under normal traffic condition in Bangkok. Master's Thesis, Department of Civil Engineering Graduate School Asian Institute of Technology.
- Chan T.H.T. and Ashebo D.B. (2006). Moving axle load from multi-span continuous bridge: laboratory study. Journal of Vibration and Acoustics, 128: 521-526.

- Chan T.H.T. and Ashebo D.B. (2006). Theoretical study of moving force identification on continuous bridges. Journal of Sound and Vibration, 295(3-5): 870-883.
- Chan, T.H.T., Law, S.S. and Yung, T.H. (2000). Moving force identification using an existing prestressed concrete bridge. Engineering Structures, 22: 1261-1270.
- Chan, T.H.T., Law, S.S., Yung, T.H. and Yuan, X.R. (1999). An interpretive method for moving force identification. Journal of Sound and Vibration, 219(3): 503-524.
- Chopra A.K. (2001). Dynamics of structures : Theory and applications to earthquake engineering. 2nd ed. New Jersey : Prentice-Hall.
- Dempsey, A.T., O'Brien, E.J. and O'Connor, J.M. (1995). A bridge weigh-in-motion system for the determination of gross vehicle weights. In Post Proceedings of First European Conference on Weigh-In-Motion of Road Vehicles, eds. B. Jacob et al., ETH, Zurich: 239-249.
- European Commission 4th Framework Programme Transport (2001). Weighing-in-motion of Axles and Vehicles for Europe (WAVE) – Bridge WIM systems (B-WIM). University College Dublin.
- Foongsook, P. (2005). Study of moving truck weight identification by field. Master's Thesis, Department of Civil Engineering Graduate School Chulalongkorn University (in Thai).
- Fryba, L. (1973). Vibration of solids and structure under moving loads, Noordhoff International Publ., Prague.
- Golub, G.H., Heath, M. and Wahaba, G. (1979). Generalized cross validation as a method for choosing a good ridge parameter. Technometrics, 21: 215-223.
- Golub, H.H. and Kahan, W. (1965). Calculating the singular value and pseudo-inverse of a matrix. Journal of Society for Industrial and Applied Mathematics: Series B, Numerical Analysis, 2(2):205-224.
- Green, M.F., Cebon, D. (1997). Dynamic interaction between heavy vehicles and highway bridges. Computers and Structures, 62(2): 253-264.
- Hanselman, D. and Littlefield, B. (1996). Mastering MATLAB : a comprehensive tutorial and reference. New Jersey : Prentice-Hall.
- Hansen, P.C. (1992). The use of L curve in the regularization of discrete ill-posed problems. SIAM Journal of Science and Computing, 14: 1487-1503.
- Hart, G.C. (1999). Structural Dynamics for Structural Engineers. New York : John Wiley & Sons.

- Henchi, K., Fafard, M., Talbot, M., Dhatt, G. (1998). An efficient algorithm for dynamic analysis of bridges under moving vehicles using a coupled modal and physical components approach. Journal of Sound and Vibration, 212(4): 663-683.
- Henchi, K., Fafard, Dhatt, G. and Talbot, M. (1997). Dynamic behaviour of multi-span beams under moving loads. Journal of Sound and Vibration, 199(1): 33-50.
- Laman, J.A. and Ashbaugh, J.R. (2007). Highway network bridge fatigue damage potential of special truck configurations. Transportation Research Record, 1969(2000): 81-92.
- Laurita, J., Sellner, G. and DuPlessis, D. (1994). Weigh-In-Motion technology improves highway truck weight regulation. Public Works: 41-42.
- Law, S.S., Bu, J.Q., Zhu, X.Q. and Chan S.L. (2004). Vehicle axle loads identification using finite element method. Journal of Engineering Structures. 26(8): 1143-1153.
- Law, S.S, Bu, J.Q., Zhu, X.Q. and Chan S.L. (2007). Moving load identification on a simply supported orthotropic plate. International Journal of Mechanical Sciences. 49(11): 1262-1275.
- Law, S.S., Chan, T.H.T., and Zeng, Q.H. (1999). Moving force identification a frequency and time domains analysis. Journal of Dynamics Systems, Measurement, and Control. 121: 394-401.
- Law, S.S., Chan, T.H.T. and Zeng, Q.H. (1997). Moving force identification: A time domain method. Journal of Sound and Vibration. 201(1): 1-22.
- Law, S.S., Chan, T.H.T., and Zeng, Q.H. (2001). Regularization in moving force identification. Journal of Engineering Mechanics ASCE. 127(2): 136-148.
- Law, S.S., and Fang, Y.L. (2001). Moving force identification: Optimal state estimation approach. Journal of Sound and Vibration. 239(2): 233-254.
- Lin, Y.H. and Trethewey, M.W. (1990). Finite element analysis of elastic beams subjected to moving dynamic loads. Journal of Sound and Vibration, 136(2): 323-342.
- Marchesiello, S., Fasana, A., Garibaldi, L. and Piombo, B.A.D. (1999). Dynamics of multi-span continuous straight bridges subject to multi-degrees of freedom moving vehicle excitation. Journal of Sound and Vibration. 224(3): 541-561.
- Memory, T.J., Thambiratnam, D. P. and Brameld, G. H. (1995). Free vibration analysis of bridges. Engineering Structures. 17(10): 705-713.
- McCall, B. and W. Vodrazka. (1997). Jr. States' successful practices weigh-in-motion handbook. FHWA.

- Miao, T.J. and Chan, T.H.T. (2002). Bridge live load models from WIM data. Engineering Structures. 24: 1071-1084.
- Moses, F. (1979). Weigh-In-Motion system using instrumented bridges. Transportation Engineering Journal ASCE. 105:233-249.
- Mulcahy, N.S. (1983). Bridge response with tractor-trailer vehicle loading. Earthquake Engineering and Structural Dynamics, 11:649-665.
- Nowak, A.S. (1993). Live load model for highway bridges. Structural Safety. 13: 53-66.
- Nowak, A.S. and Hong, Y.K. (1991). Bridge live-load models. Journal of Structural Engineering ASCE. 117(9): 2757-2767.
- Nowak, A.S., Nassif, H. and DeFrain, L. (1993). Effect of truck loads on bridges. Journal of Transportation Engineering ASCE. 119: 853-867.
- Peters, R.J. (1986). CULWAY – an unmanned and undetectable highway speed vehicle weighing system. In Proc 13 th AARB Conference, Australian Road Research Board, 13(6).
- Pinkaew, T. (2006). Identification of vehicle axle loads from bridge responses using updated static component technique. Engineering Structures. 28(11): 1599-1608.
- Pinkaew, T. and Asnachinda, P. (2007). Experimental study on the identification of dynamic axle loads of moving vehicles from the bending moments of bridges. Engineering Structures, 29(9): 2282-2293.
- Rieker, J.R., Lin, Y.H., Trethewey, M.W. (1996). Discretization consideration in moving load finite element beam models. Finite Element Analysis Des, 21: 129-144.
- Standard Specification for Highway Weigh-in-Motion (WIM) Systems with User Requirements and Test Method. (2002). American Society fir Testing and Materials. ASTM E1318-02.
- Thater, G., Chang, P., Schelling, D.R. and Fu, C.C. (1998). Estimation of bridge static response and vehicle weights by frequency response analysis. Canada Journal of Civil Engineering. 25: 631-639.
- Tikhonov, A.N. (1963). Solution of incorrectly formulated problems and the regularization method. Soviet Math Dokl. 4:1035-1038. (English translation of Dokl Akad Nauk SSSR. (1963), 151:501-504.)

- Yang, Y., Chang, C.H., Yau, J.D. (1999). An element for analyzing vehicle bridge systems considering vehicle's pitching effect. International Journal for Numerical Methods in Engineering, 46: 1031-1047.
- Yang, Y. and Lin, B.H. (1995). Vehicle-bridge interaction analysis by dynamic condensation method. Journal of Structural Engineering, 121(11): 1636-1643.
- Yang, Y. and Wu, Y. (2001). A versatile element for analyzing vehicle-bridge interaction response. Engineering Structures, 23: 452-469.
- Yu, L. and Chan, T.H.T. (2004). Identification of multi-axle vehicle loads on bridges. Journal of Vibration and Acoustics. 126: 17-26.
- Yu, L. and Chan, T.H.T. (2002). Moving force identification from bending moment response of bridge. Journal of Structural Engineering and Mechanics. 14(2): 151-170.
- Znidaric, A., Znidaric, J. and Tercej, S. (1991). Determination of the true traffic load in the process of safety assessment of existing bridges. In Proceedings of the 12 th Congress of Structural Engineering of Slovenia: 241-246 (in Slovenian).
- Zhu, X.Q., Law, S.S. and Bu, J.Q. (2006). A state space formulation for moving loads identification. Journal of Vibration and Acoustics. 128: 509-520.
- Zhu, X.Q. and Law, S.S. (2003). Dynamic axle and wheel loads identification: laboratory studies. Journal of Sound and Vibration. 268: 855-879.
- Zhu, X.Q. and Law, S.S. (2003). Identification of moving interaction forces with incomplete velocity information. Mechanical Systems and Signal Processing. 17(6): 1349-1366.
- Zhu, X.Q. and Law, S.S. (2000). Identification of vehicle axle loads from bridge dynamic responses. Journal of Sound and Vibration. 236(4): 705-724.
- Zhu, X.Q. and Law, S.S. (1999). Moving forces identification on a multi-span continuous bridge. Journal of Sound and Vibration. 228(2): 377-396.
- Zhu, X.Q. and Law, S.S. (2005). Moving load identification on multi-span continuous bridge with elastic bearings. Mechanical System and Signal Processing, 20(7): 1759-1782.
- Zhu, X.Q. and Law, S.S. (2002). Moving loads identification through regularization. Journal of Engineering Mechanics ASCE. 128(5): 989-1000.

Zhu, X.Q. and Law, S.S. (2001). Orthogonal function in moving loads identification on multi-span bridge. Journal of Sound and Vibration. 245(2): 329-345.



สถาบันวิทยบริการ
จุฬาลงกรณ์มหาวิทยาลัย



APPENDICES

สถาบันวิทยบริการ
จุฬาลงกรณ์มหาวิทยาลัย

APPENDIX A

MODEL CALIBRATION

From the fabricated bridge and vehicle models, since there might be some incorrectness in the physical properties due to materials and instruments, the model calibration is very necessary in order to obtain the most accuracy and effectiveness of the solution. This is because using incorrect data in identification certainly leads to incorrect solution. The calibration is the procedure employed to determine the proper parameters of the material (i.e. elastic modulus E , moment of inertia I , support continuity), to determine the vibration characteristics (fundamental frequency, damping ratio ξ), and to correct the signal measurement recorded by the instruments. The model calibration in this experiment consists of calibrations of vehicle model and bridge model.

I. Calibration of Model Vehicle

Calibration of vehicle model is firstly carried out because the bridge model is loaded by the vehicle model. Calibration of bridge model is therefore required the corrected vehicle model. Vehicle model calibration is an instrument calibration on tension/compression load cells used as actual axle load detectors. Based on the recorded signal using 48-channel data logger collecting digital signal from load cells, the digital signal is converted from analog signal induced by axle load detector. The obtained data is then raw data with incorrect value and unit. Relationship between the reading signal and the actual axle load is needed to be investigated. The load cell calibration is conducted by recording the signal measurement while incremental weighing the load cell with the recognized masses. Figure A.1 to Figure A.4 show the recorded calibration signals with the corresponding signal/load conversion of the tension/compression load cell of front and rear axles of both model vehicles. It is obviously noticed that the relationship between the acting load and measured signal is linear when applying and removing the weighted masses.

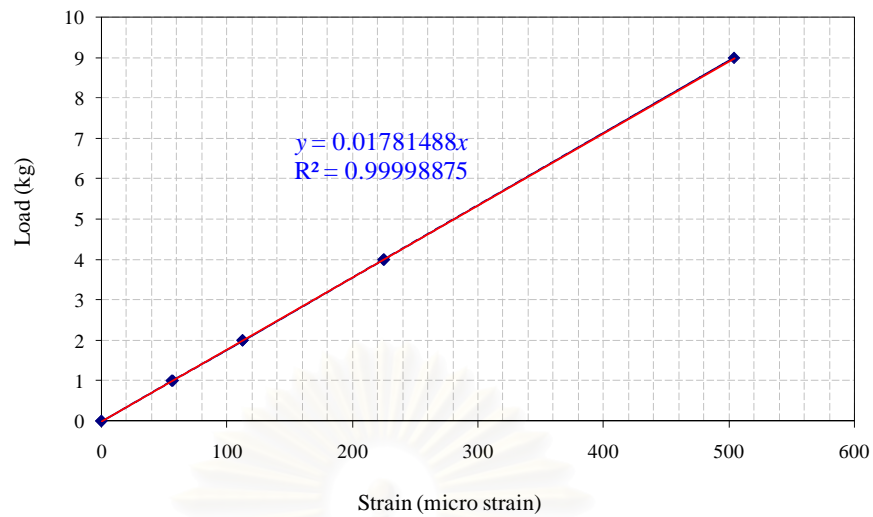


Figure A.1 Calibration chart of a tension/compression load cell used for actual load detection of front axle of 1st vehicle

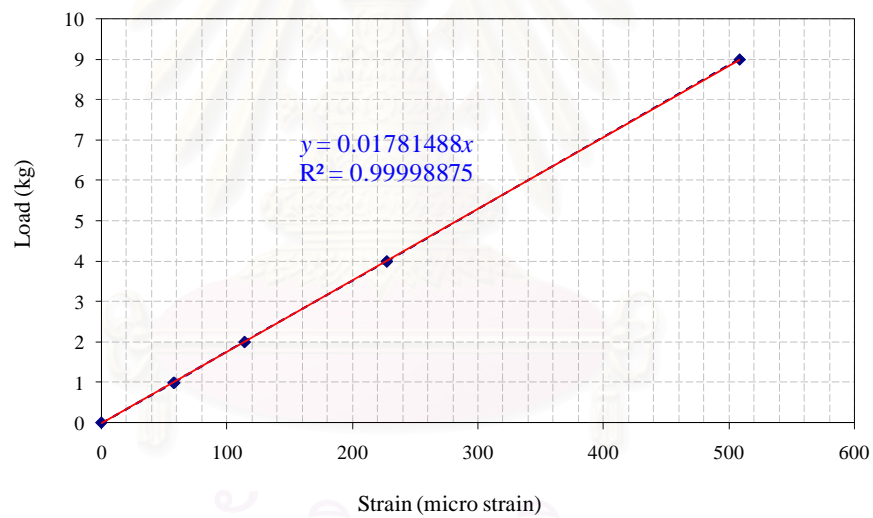


Figure A.2 Calibration chart of a tension/compression load cell used for actual load detection of rear axle of 1st vehicle

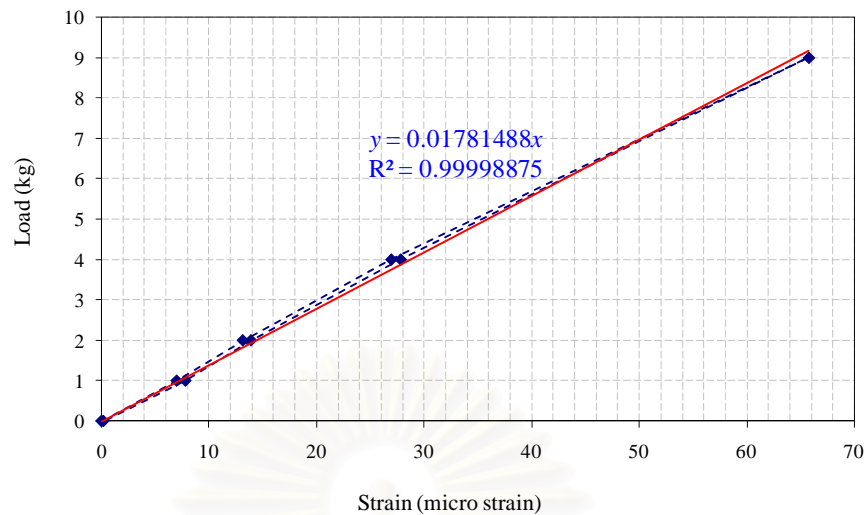


Figure A.3 Calibration chart of a tension/compression load cell used for actual load detection of front axle of 2nd vehicle

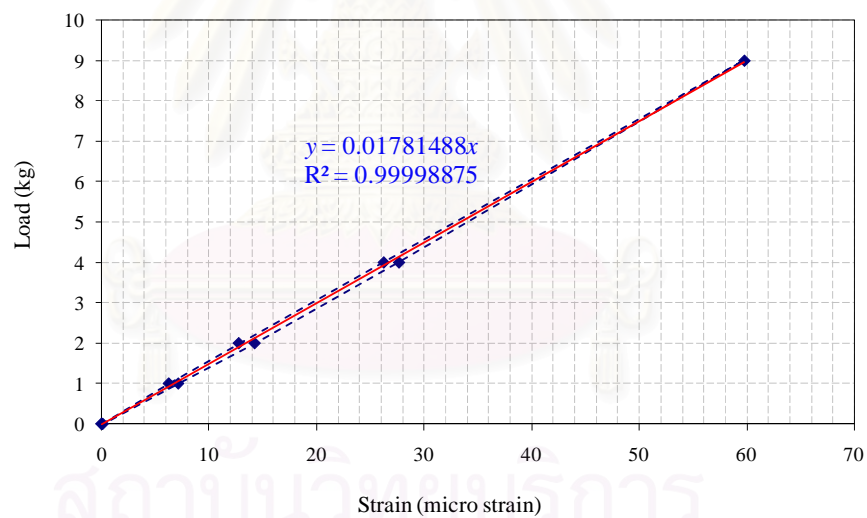


Figure A.4 Calibration chart of a tension/compression load cell used for actual load detection of rear axle of 2nd vehicle

II. Calibration of Model Bridge

Calibration of bridge model consists of determination flexural stiffness, EI which is a multiplication of elastic modulus and moment of inertia, determination of rotational spring stiffness coefficients and determination of vibration properties including fundamental frequency and damping ratio. Determination bridge

fundamental frequency and damping ratio needed to be carried out in the dynamic system which is the parameters from static system including the flexural stiffness must be firstly achieved.

For the bridge model fabrication, since the bridge model is made from three steel plates (one per span) connected each other with bolts, the analytical model must be modified due to the continuity at the internal supports has been changed. Figure A.2 shows the analytical bridge model of continuity modification used in experimental bridge calibration and identification. The bridge is modeled with assembled 24 finite element beam elements with support continuity modification using hinge and rotational spring as a connecting joint.

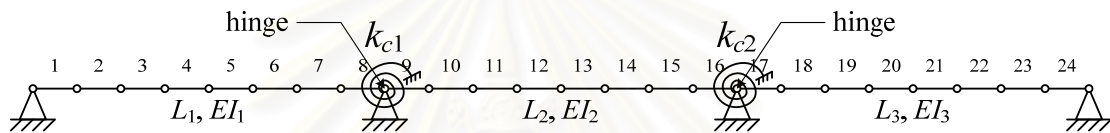


Figure A.5 Analytical bridge model of continuity modification used in experimental bridge calibration and identification

Based on finite element method, the stiffness matrix of the bridge model has been also modified. The rotational springs at the first and second internal bridge supports are denoted their stiffness by k_{c1} and k_{c2} , respectively. The stiffness matrices of the rotational springs are expressed as follows:

$$\mathbf{K}_{c1} = \begin{bmatrix} k_{c1} & -k_{c1} \\ -k_{c1} & k_{c1} \end{bmatrix}_{2 \times 2}; \mathbf{K}_{c2} = \begin{bmatrix} k_{c2} & -k_{c2} \\ -k_{c2} & k_{c2} \end{bmatrix}_{2 \times 2}. \quad (\text{A.1})$$

The global stiffness matrix of the bridge model, \mathbf{K}_b is then represented in Eq. (A.2).

$$\mathbf{K}_b = \begin{bmatrix} \left[\begin{array}{c} \mathbf{K}_1 \\ \begin{bmatrix} k_{c1} & -k_{c1} \\ -k_{c1} & k_{c1} \end{bmatrix} \\ \mathbf{K}_2 \\ \begin{bmatrix} k_{c2} & -k_{c2} \\ -k_{c2} & k_{c2} \end{bmatrix} \\ \mathbf{K}_3 \end{array} \right] \end{bmatrix}_{48 \times 48} \quad (\text{A.2})$$

where \mathbf{K}_1 , \mathbf{K}_2 and \mathbf{K}_3 are respectively sub-stiffness matrices of the first, middle and last bridge spans which each stiffness is assembled from 8 local finite beam stiffness matrices. The stiffness matrices of the rotational springs are assembled at the last and the first degree of the freedoms of the adjacent bridge span stiffness matrices as shown in Eq. (A.2).

Bridge flexural stiffness coefficients and rotational spring stiffness are determined based on testing in static condition or least dynamic condition by measuring the bending moments induced by recognized axle loads vehicle moving at the crawl speed. The measured bending moment is corrected with constant coefficient as follow:

$$\mathbf{Z}_{calibrated} = \boldsymbol{\alpha} \mathbf{Z}_{measured} \quad (\text{A.3})$$

where $\mathbf{Z}_{calibrated}$ is the calibrated bending moment matrix with the size of $k \times NN$,

$\mathbf{Z}_{measured}$ is the measured bending moment matrix with the size of $k \times NN$,

$\boldsymbol{\alpha}$ is the correction coefficient matrix containing coefficients used in flexural stiffness correction and the matrix is diagonal with the size of $k \times k$ (9×9).

Based on an optimization, the coefficient matrix can be determined by minimizing the residual error between the analytical and measured bending moments.

A relevant least squares objective function is expressed as

$$\Delta(\alpha, k_c) = \sum_{j=1}^k \left[\sum_{i=1}^{NN} \left(\mathbf{Z}_{analytical}^i - \boldsymbol{\alpha} \mathbf{Z}_{measured}^i \right)^2 \right]_j \quad (\text{A.4})$$

where $\mathbf{Z}_{analytical}$ is the analytical bending moment matrix with the size of $k \times NN$ constructed from theoretical bridge model. The analytical bending moment is calculated with bridge stiffness modified with the addition of rotational spring stiffness. It is noted that the sectional bending moments used in identification are adopted from average value of bending moments converted from strains measured from strain gauges installed at the same section.

The objective function in Eq. (A.4) is optimized using computer program, MATLAB with “fminunc” command utilizing Quasi-Newton algorithm. However, regarding to the correction coefficient matrix, optimization with 11 parameters (9 coefficients for flexural stiffness, α_{1-9} ; 2 variables for rotational spring stiffness, k_{c1} and k_{c2}) may lead the calibrated parameters to be improper and requires very long

computational time. Consequently, calculation with reduced parameters from 11 into 5 parameters is preferable. By assuming flexural stiffness of each section in the same bridge span to be equivalent, the rotational stiffness coefficients are reduced into three parameters, $\alpha_{1-3} = \alpha_a$, $\alpha_{4-6} = \alpha_b$ and $\alpha_{7-9} = \alpha_c$. The optimized flexural stiffness coefficients and rotational stiffness variables of the bridge model are listed in Table A.1. Figure A.3 shows the typical signal of the measured and analytical bending moments of the calibrated bridge model.

Table A.1 Calibrated coefficients and variables of the experimental bridge model

Flexural stiffness coefficients	Rotational spring stiffness variables
$\alpha_a = 1.238$	$k_{c1} = 23,207 \text{ N-m/rad}$
$\alpha_b = 1.155$	$k_{c2} = 19,404 \text{ N-m/rad}$
$\alpha_c = 1.111$	

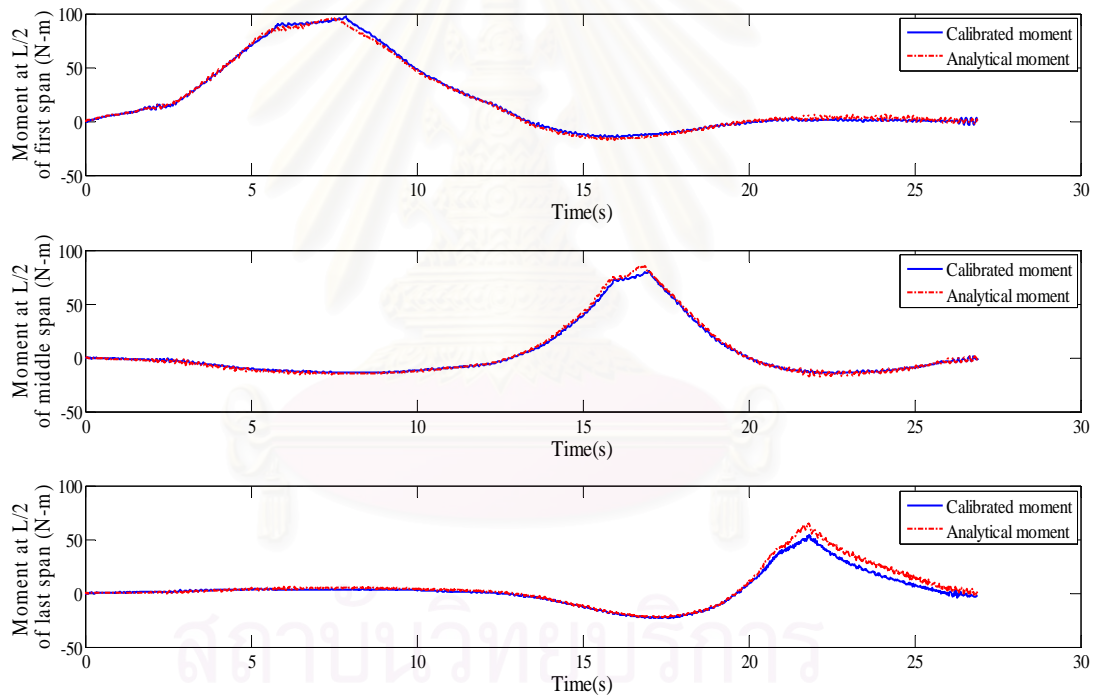


Figure A.6 Typical signals of the measured and analytical bending moments of the calibrated bridge model

Subsequently, the vibration properties of the bridge model including damping ratio and fundamental frequency are investigated. Both properties can be determined from free vibration testing by applying initial displacement. Figure A.4 shows the free vibration strain response at mid-span of the intermediate span. Employing Fast Fourier Transform (FFT) to transform the response into frequency domain, the

fundamental frequency of the bridge is obtained. The damping ratio of the bridge can be calculated from rate of response decay by Eq. (A.5). It is observed from Figure A.5 that the fundamental frequency of the bridge model equals to 6.32 Hz which is close to the fundamental frequency of the designed bridge (see Table 5.1) and the calculated damping ratio ξ equals to 0.018 or 1.8%.

$$\ln\left(\frac{x_n}{x_{n+1}}\right) = 2\pi\xi \quad (\text{A.5})$$

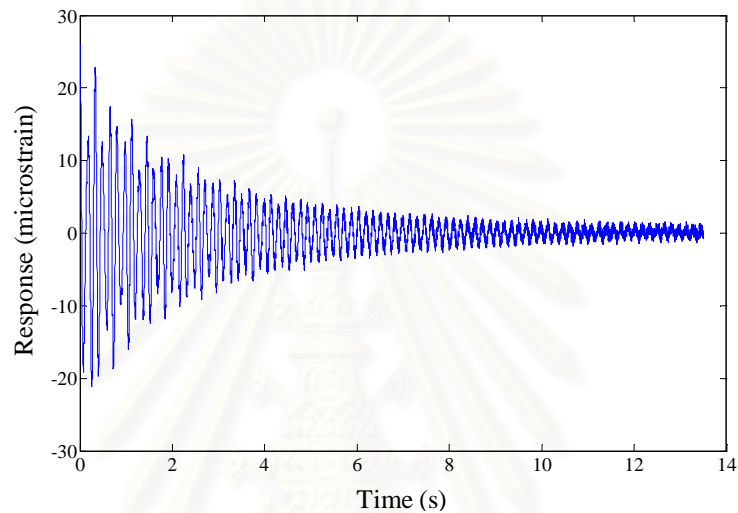


Figure A.7 Free vibration strain response at mid-span of the intermediate span of bridge model

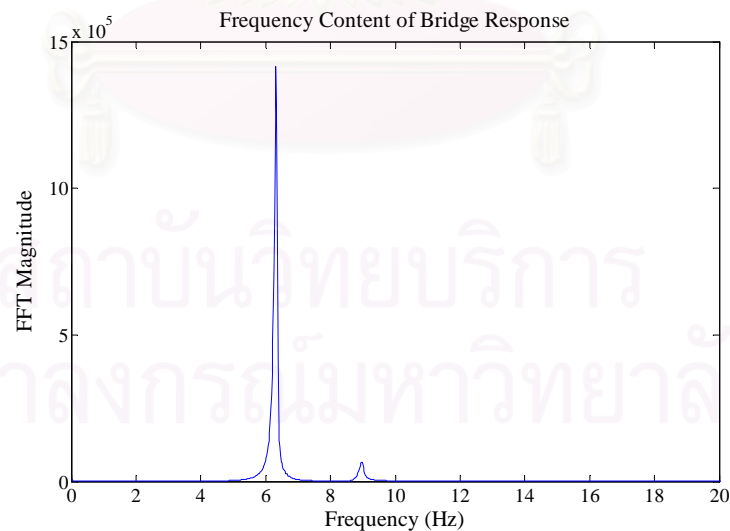


Figure A.8 Frequency domain of Fast Fourier Transform (FFT) magnitude from free vibration test of bridge model

APPENDIX B

DATA ACQUISITION AND NOISE FILTERING

Regarding to the actual axle load observed by load cells as shown in Figure B.1, the FFT is applied to the time history axle load to estimate frequency of the vibration force. It is noticed from Figure B.2 that the vehicle axle load excites with the frequency below 15 Hz approximately. The bending moment signal is contaminated by measurement noise with amplitude of 2 micro-strains at dominant frequency of 50 Hz which is the frequency of electrical current approximately. Therefore, the measurement noises with frequency of 50Hz and above are filtered out. The noise filtering approach based on data smoothening method called moving average (“smooth” command in MATLAB) is employed. Moving average method is one of the low-pass filters with filter coefficients equal to the reciprocal of the average data span. The filtered signal at each step is calculated by an average value of data span around the considered step point. The frequency of data span ratio between the initial sampling rate and number of average data span should not less than the frequency of excitation. In the study, an average span at 21 data points with approximate frequency of 48 Hz (1042/21 Hz) which is lower than noise frequency of 50 Hz and higher than excitation frequency of axle loads (15 Hz) and is used.

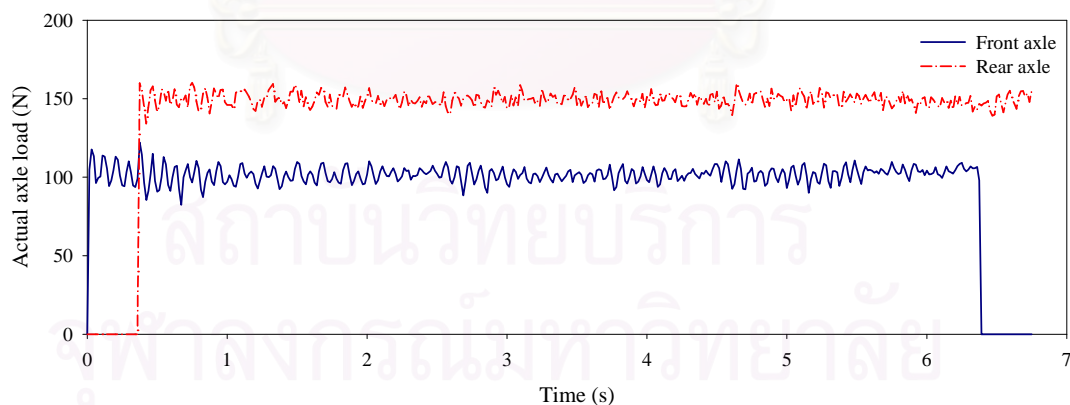


Figure B.1 Typical time histories of actual vehicle axle loads observed by tension/compression load cells

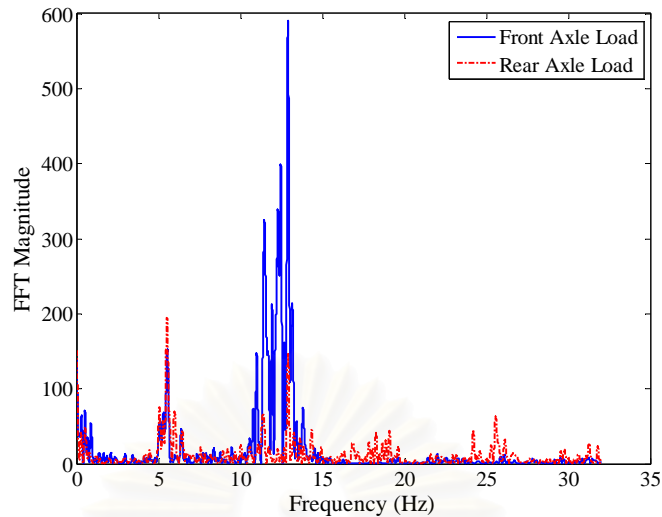


Figure B.2 Frequency domain of Fast Fourier Transform (FFT) magnitude of measured vehicle axle load

According to the data acquisition from 48-channel data logger recording at sampling rate of 1024 Hz, identification with this sampling rate seems to be unnecessary and wasteful. Accurate solution can be achieved with lower sampling rate as discussed in section 4.3.3 in Chapter IV. Since the fundamental frequency of the bridge is 5.4 Hz, identification at sampling rate of 64 Hz which is higher than 10 times of the fundamental frequency is preferable. This is because it is a divisible number with 1/16 times of the initial sampling frequency which is convenient in data reduction. Therefore, the pre-identification signals are processed from the initial recorded signal filtered measurement noise by moving average method with average span of 17 points and then re-sampled at the sampling rate of 64 Hz in order to reduce the unnecessary data. Figure B.3 shows comparison of the initial and processed measured bending moments and corresponding measured axle loads.

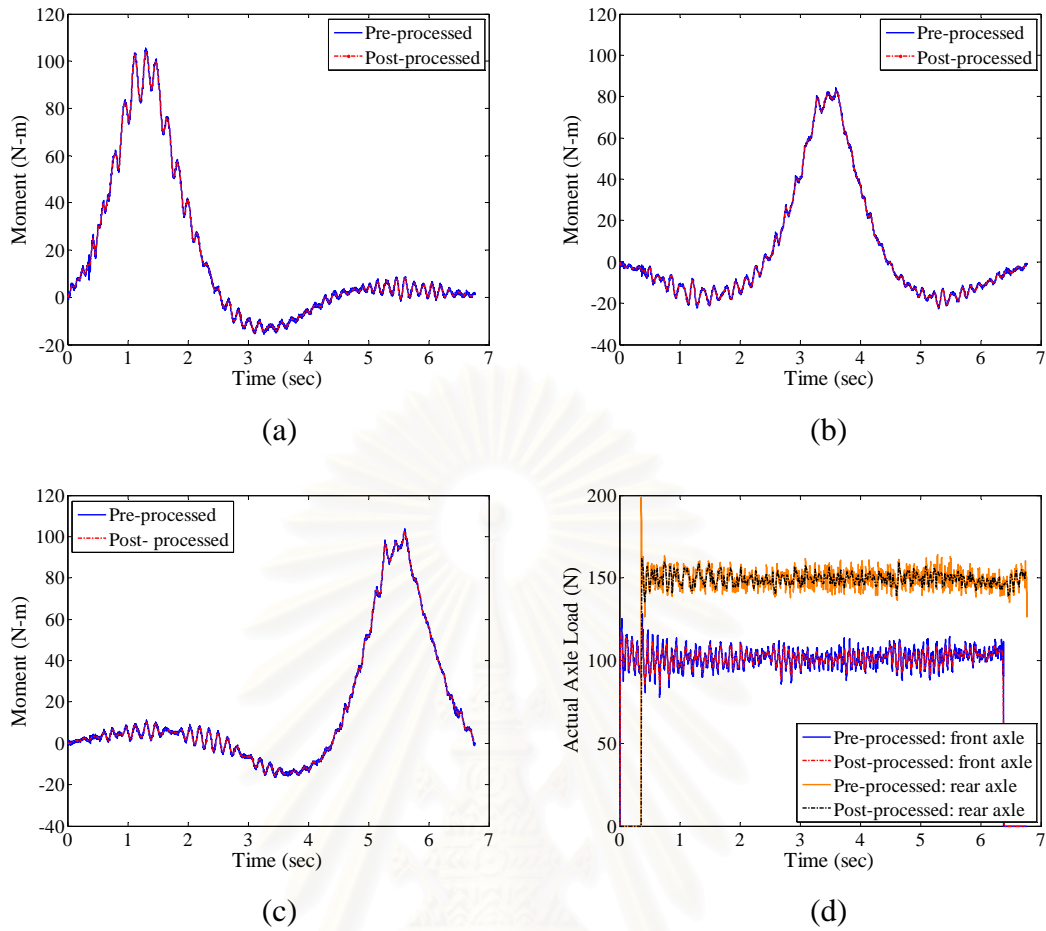


Figure B.3 Typical pre-processed and post-processed bending moments and corresponding measured axle loads: (a) bending moment at section $L_1/2$, (b) bending moment at section $L_2/2$, (c) bending moment at section $L_3/2$, and (d) front and rear axle loads

สถาบันวิทยบริการ
จุฬาลงกรณ์มหาวิทยาลัย

APPENDIX C

AXLE LOAD IDENTIFICATION WITH INCOMPLETE MEASUREMENT INFORMATION

I. Axle Loads Identification with Incomplete Velocity Information

The RPE of identified axle loads of single and multiple vehicles from identification by assuming their position time histories from constant speed of travels is listed in Tables C.1 and C.2, respectively. In case of multiple vehicle identification, it is observed that simplification of vehicle position with constant speed provides large solution accuracy particularly in the case of vehicle position error is above 5%. This is because the overall length of continuous bridge is a long distance compared to the axle spacing which requires longer duration of travel than single span bridges. Therefore, vehicle travel with non-uniform speed for all duration is usually observed.

Table C.1 RPE (%) of 2-axle vehicle re-identified its axle load with simplified vehicle position by assuming moving speed of vehicle travel to be constant

GVM (kg)	v (m/s)	Position error (%)	Actual position		Simplified position	
			Front axle	Rear axle	Front axle	Rear axle
10	0.2	9.26	14.02	10.44	127.38	54.53
10	0.6	5.53	9.84	9.75	100.65	51.95
10	1.0	1.61	7.93	12.31	32.54	9.18
10	1.4	0.78	11.94	13.98	12.60	20.14
10	1.8	2.04	11.53	17.87	20.20	17.84
15	0.2	2.78	4.49	7.92	34.13	28.85
15	0.6	4.69	8.72	9.76	103.11	21.78
15	1.0	5.95	8.20	12.82	123.90	26.21
15	1.4	3.93	8.07	11.36	90.28	29.36
15	1.8	1.89	9.16	13.55	48.38	7.31
20	0.2	5.00	3.36	8.78	99.76	31.42
20	0.6	6.98	4.48	6.54	130.50	46.35
20	1.0	8.48	3.79	11.43	141.36	41.19
20	1.4	1.50	5.43	11.44	21.56	4.29
20	1.8	3.08	5.07	10.75	74.96	24.62
25	0.2	16.00	3.17	8.27	187.62	55.75
25	0.6	2.89	3.08	8.37	52.88	15.20
25	1.0	1.29	4.26	10.63	10.82	13.20
25	1.4	1.65	3.96	5.15	9.86	8.23
25	1.8	2.67	5.49	5.58	55.16	30.93
30	0.2	7.63	6.81	3.33	102.06	65.35
30	0.6	6.23	4.66	3.43	100.04	75.55
30	1.0	3.11	6.02	4.66	9.94	21.36
30	1.4	0.79	5.00	5.11	5.31	11.88
30	1.8	2.36	4.44	6.35	50.02	26.02

Table C.2 RPE (%) of multiple vehicles identification re-identified its axle load with simplified vehicle position by assuming moving speed of vehicle travel to be constant

Case	Position error (%)		Actual position				Simplified position			
	First vehicle	Second vehicle	First front	First rear	Second front	Second rear	First front	First rear	Second front	Second rear
OVT-1	1.28	3.00	5.59	6.56	5.66	8.41	17.32	6.37	45.68	52.24
OVT-2	3.39	1.75	5.49	5.23	6.74	9.20	45.00	23.22	29.68	36.49
OVT-3	3.75	1.66	6.17	5.74	4.30	9.63	66.57	34.80	8.00	17.66
OVT-4	2.42	3.44	5.70	4.29	5.99	9.14	48.10	31.96	30.21	43.59
OVT-5	1.81	2.48	5.91	4.80	6.30	7.20	11.52	8.59	15.65	25.88
OVT-6	1.69	7.35	8.35	5.640	8.63	4.21	184.38	22.41	69.06	15.30
OVT-7	1.50	2.58	5.54	4.79	4.92	7.35	25.77	24.34	20.17	18.99
FLD-1	1.08	0.89	9.58	4.50	7.79	8.30	23.36	13.87	4.60	16.21
FLD-2	0.97	1.09	7.28	3.74	5.56	9.00	16.51	11.62	13.37	20.33
FLD-3	1.07	2.06	6.62	3.91	4.37	8.14	23.83	14.57	27.93	35.35
SBS	3.30	2.96	9.42	8.34	9.42	5.14	72.91	27.04	65.20	47.13
FLC-1	1.01	10.98	6.66	4.79	4.81	8.05	20.96	16.54	151.95	72.28
FLC-2	0.89	1.71	10.48	5.57	5.52	10.35	13.72	7.90	20.43	6.71
FLC-3	1.11	6.10	6.31	6.13	4.72	7.35	19.03	8.94	101.24	56.34
FLC-4	1.00	3.06	7.50	4.95	4.56	6.76	16.25	7.51	63.11	35.82
FLI-1	3.37	3.09	9.76	8.18	6.42	7.43	60.17	32.51	52.38	51.23
FLI-2	0.51	1.24	9.61	8.28	4.86	6.93	13.27	5.92	15.25	20.05
FLI-3	0.86	1.25	8.84	7.49	4.44	8.76	23.37	6.15	15.83	23.65
FLI-4	0.66	1.53	8.56	5.78	4.92	6.34	10.67	8.54	24.94	28.27
FLI-5	0.85	2.02	9.66	6.67	4.70	7.77	13.57	9.92	34.59	36.79
FLI-6	1.90	2.65	11.41	6.68	4.47	6.61	37.73	30.11	14.11	10.14
FLI-7	1.08	4.11	8.65	6.65	4.51	6.70	12.87	5.79	74.77	72.33
FLI-8	0.85	0.95	7.63	6.15	3.82	6.95	13.31	13.20	10.30	18.94
FLI-9	1.18	3.01	9.02	9.69	3.93	5.91	19.62	21.20	43.17	20.64
FLI-10	0.68	3.81	12.33	10.35	5.26	7.91	10.56	16.14	65.96	66.33

Results from Table C.2 indicate that position error of single vehicle does not affect only the solution accuracy of its axle loads but also the solution accuracy of the axle loads of another vehicle (i.e. in the case of OVT-7). Although most of the position errors of both vehicles in the multiple vehicles experiment are below 3%, the identified axle loads exhibit in large value of more than 30% for all cases. Figure C.1 to Figure C.3 represent the time histories of identified axle loads of three example scenarios of shot headway, overtaking and side-by-side movements, respectively. In the case of FLC-3, it is found that the identified axle loads of the first vehicle results in an acceptable accuracy with very close order of static component while the dynamic component is quite similar to the axle loads identified with actual vehicle position. This is because the first vehicle nearly travels with uniform speed. However, the method fails to correctly identify axle loads of the second vehicle since the second vehicle travels with non-uniform speed with the position error of 6.1%. The results from Figures C.2 and C.3 indicate that if there is an overestimate axle load, other axle loads will be underestimated in order to keep minimizing the objective.

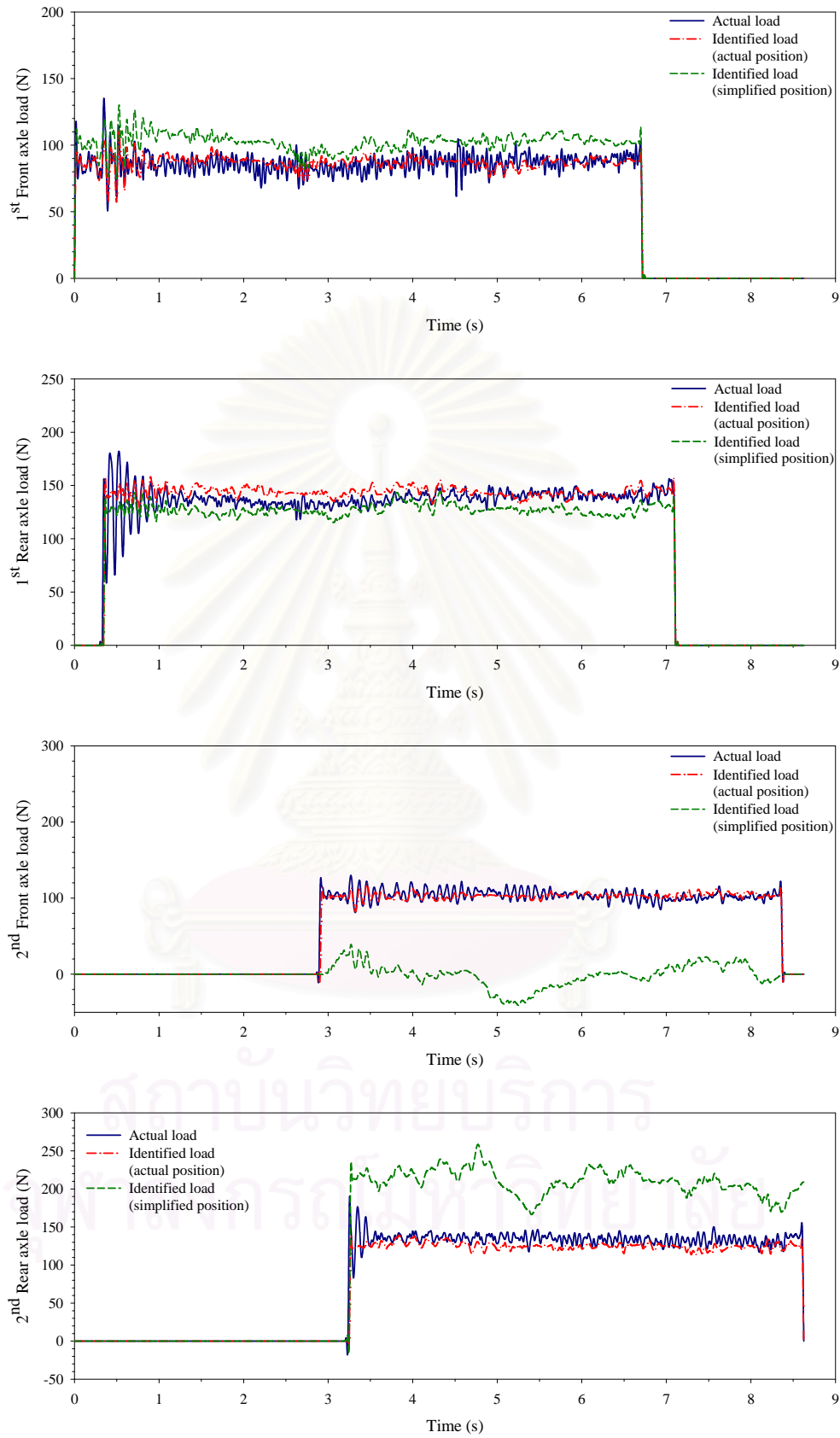


Figure C.1 Time histories of identified axle loads of multiple vehicles with short headway scenario (FLC-3) re-identified with constant speed position

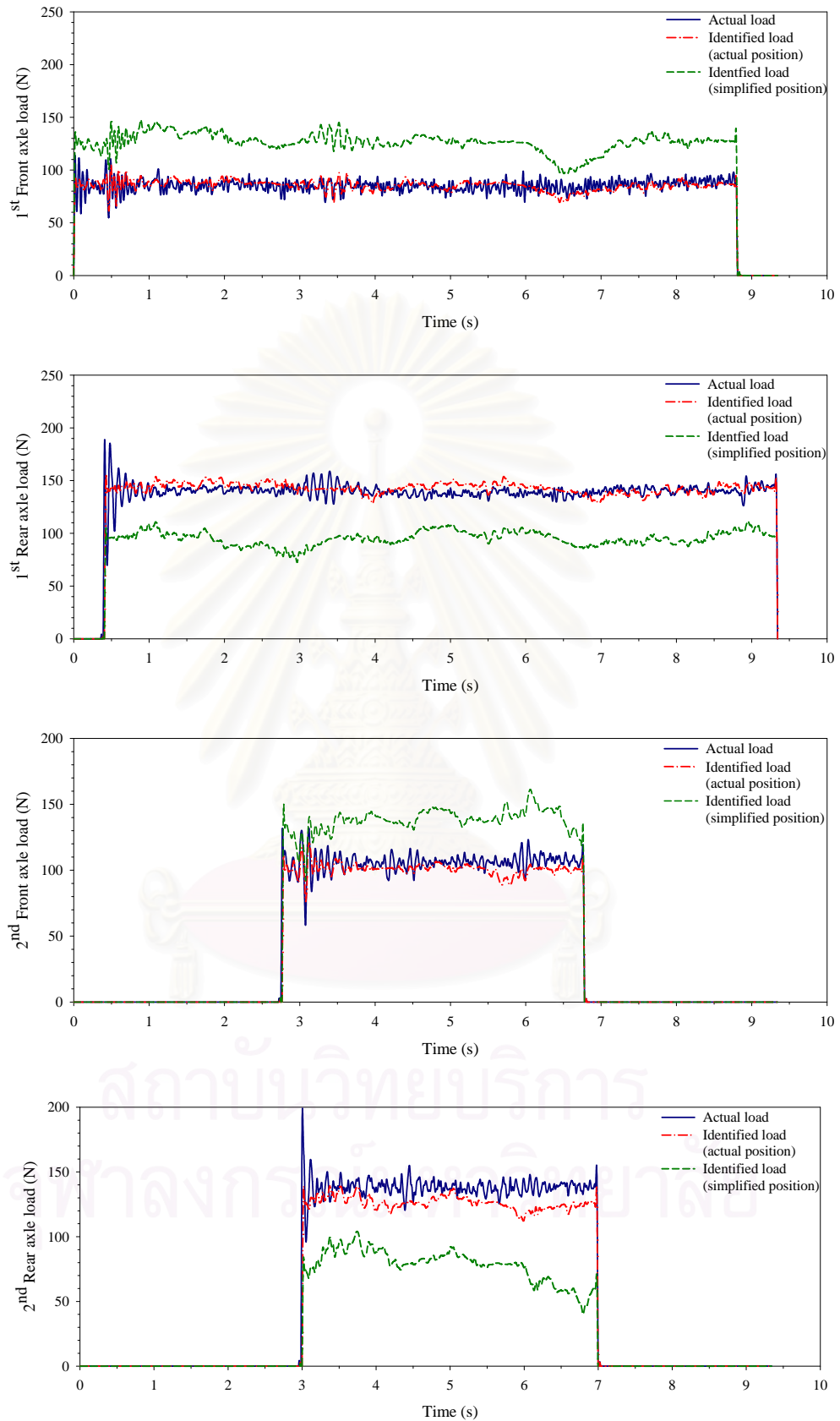


Figure C.2 Time histories of identified axle loads of multiple vehicles with overtaking scenario (OVT-4) re-identified with constant speed position

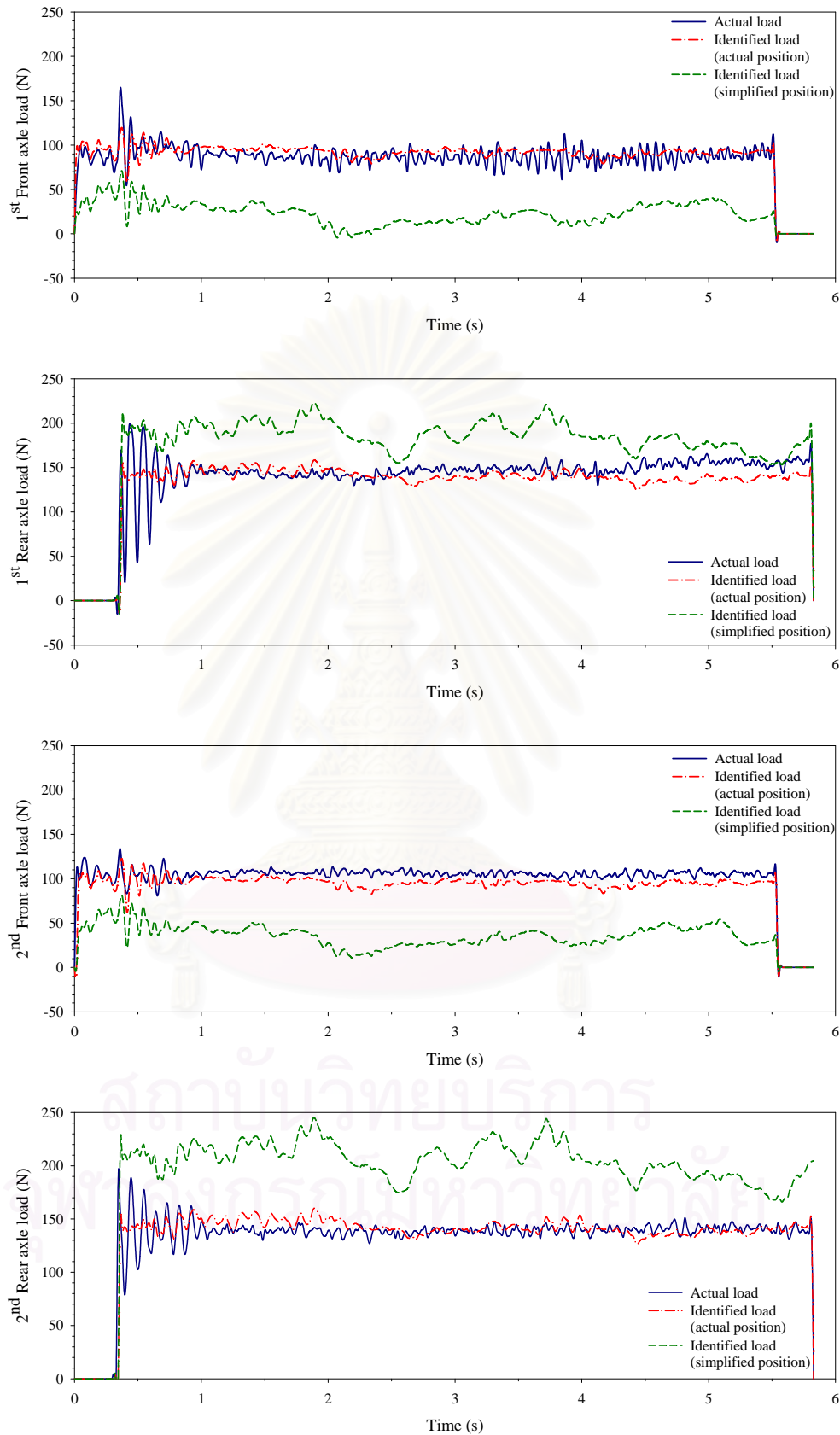


Figure C.3 Time histories of identified axle loads of multiple vehicles with side-by-side scenario (SBS) re-identified with constant speed position

II. Axle Loads Identification with Incomplete Bending Moment Information

The experimental data from Chapter V is considered and used for identification with fewer numbers of sectional bending moments. In case of the number of total removed measurement station is less than 4 stations; number of station that can be removed for each span must not exceed 1 station. In case of the number of overall sensor removal is more than 3 sections; the measurement station can be taken off up to 2 stations for each bridge span except the intermediate span that allows only 1 station removal. This is because the vibration behavior of the bridge is dominated with the first fundamental frequency of the intermediate span. Remaining the most intermediate span information is preferable. The repetitive formation of sensor arrangement with symmetrical pattern is also reduced. The overall sensor patterns with removed measurement stations from 1 to 5 stations for re-identification of axle loads are listed in Table C.3. As the overall 81 cases from different sensor patterns, the total sensor arrangement is consisted of 5, 13, 15, 33 and 15 cases for 1-5 sensor removal respectively. The selected experimental case is an overtaking travel (OVT-7) which the second vehicle follows the first vehicle with fast speed at the bridge approach time interval, t_d of 2 seconds and it overtakes the first vehicle in the last bridge span. Table C.4 represents the RPE and correlation coefficient of identified axle load of the corresponding sensor removal cases listed in Table C.3.



Table C.3 Sensor pattern of vehicle axle load identification with removed measurement stations

No. of removed sensor	Sensor pattern	Measurement station (● = used , ○ = not used)								
		$L_1/4$	$L_1/2$	$3L_1/4$	$L_2/4$	$L_2/2$	$3L_2/4$	$L_3/4$	$L_3/2$	$3L_3/4$
0	9R	●	●	●	●	●	●	●	●	●
1	8R-A	○	●	●	●	●	●	●	●	●
1	8R-B	●	○	●	●	●	●	●	●	●
1	8R-C	●	●	○	●	●	●	●	●	●
1	8R-D	●	●	●	○	●	●	●	●	●
1	8R-E	●	●	●	●	○	●	●	●	●
2	7R-A	●	○	●	○	●	●	●	●	●
2	7R-B	●	●	○	●	○	●	●	●	●
2	7R-C	○	●	●	○	●	●	●	●	●
2	7R-D	●	○	●	●	○	●	●	●	●
2	7R-E	●	●	○	●	●	○	●	●	●
2	7R-F	○	●	●	●	○	●	●	●	●
2	7R-G	●	○	●	●	●	○	●	●	●
2	7R-H	●	●	○	●	●	●	○	●	●
2	7R-I	○	●	●	●	●	○	●	●	●
2	7R-J	●	○	●	●	●	●	○	●	●
2	7R-K	○	●	●	●	●	●	○	●	●
2	7R-L	●	○	●	●	●	●	●	○	●
2	7R-M	○	●	●	●	●	●	●	○	●
3	6R-A	○	●	●	○	●	●	○	●	●
3	6R-B	○	●	●	○	●	●	●	○	●
3	6R-C	○	●	●	○	●	●	●	●	○
3	6R-D	○	●	●	●	○	●	○	●	●
3	6R-E	○	●	●	●	○	●	●	○	●
3	6R-F	○	●	●	●	○	●	●	●	○
3	6R-G	○	●	●	●	●	○	○	●	●
3	6R-H	○	●	●	●	●	○	●	○	●
3	6R-I	●	○	●	○	●	●	○	●	●
3	6R-J	●	○	●	○	●	●	●	○	●
3	6R-K	●	○	●	●	○	●	○	●	●
3	6R-L	●	○	●	●	○	●	●	○	●
3	6R-M	●	○	●	●	●	○	○	●	●
3	6R-N	●	●	○	○	●	●	○	●	●
3	6R-O	●	●	○	●	○	●	○	●	●

Table C.3 (continued): Sensor pattern of vehicle axle load identification with removed measurement stations

No. of removed sensor	Sensor pattern	Measurement station (● = used , ○ = not used)								
		$L_1/4$	$L_1/2$	$3L_1/4$	$L_2/4$	$L_2/2$	$3L_2/4$	$L_3/4$	$L_3/2$	$3L_3/4$
4	5R-A	○	○	●	●	●	●	○	○	●
4	5R-B	○	○	●	●	●	●	○	●	○
4	5R-C	○	○	●	●	●	●	●	○	○
4	5R-D	○	●	○	●	●	●	○	○	●
4	5R-E	○	●	○	●	●	●	○	●	○
4	5R-F	●	○	○	●	●	●	○	○	●
4	5R-G	○	○	●	○	●	●	○	●	●
4	5R-H	○	○	●	○	●	●	●	○	●
4	5R-I	○	○	●	○	●	●	●	●	○
4	5R-J	○	○	●	●	○	●	○	●	●
4	5R-K	○	○	●	●	○	●	●	○	●
4	5R-L	○	○	●	●	○	●	●	●	○
4	5R-M	○	○	●	●	●	○	○	●	●
4	5R-N	○	○	●	●	●	○	●	○	●
4	5R-O	○	○	●	●	●	○	●	●	○
4	5R-P	○	●	○	○	●	●	○	●	●
4	5R-Q	○	●	○	○	●	●	●	○	●
4	5R-R	○	●	○	○	●	●	●	●	○
4	5R-S	○	●	○	●	○	●	○	●	●
4	5R-T	○	●	○	●	○	●	●	○	●
4	5R-U	○	●	○	●	○	●	●	●	○
4	5R-V	○	●	○	●	●	○	○	●	●
4	5R-W	○	●	○	●	●	○	●	○	●
4	5R-X	○	●	○	●	●	○	●	○	○
4	5R-Y	●	○	○	○	●	●	○	●	●
4	5R-Z	●	○	○	○	●	●	●	○	●
4	5R-AA	●	○	○	○	●	●	●	●	○
4	5R-BB	●	○	○	●	○	●	○	●	●
4	5R-CC	●	○	○	●	○	●	●	○	●
4	5R-DD	●	○	○	●	○	●	●	●	○
4	5R-EE	●	○	○	●	●	○	○	●	●
4	5R-FF	●	○	○	●	●	○	●	○	●
4	5R-GG	●	○	○	●	●	○	●	●	○
5	4R-A	○	○	●	○	●	●	○	○	●
5	4R-B	○	○	●	○	●	●	○	●	○
5	4R-C	○	○	●	○	●	●	●	○	○
5	4R-D	○	○	●	●	○	●	○	○	●
5	4R-E	○	○	●	○	○	●	○	●	○
5	4R-F	○	○	●	●	○	●	●	○	○
5	4R-G	○	○	●	●	●	○	○	○	●
5	4R-H	○	○	●	●	●	○	○	●	○
5	4R-I	○	●	○	○	○	●	○	○	●
5	4R-J	○	●	○	○	●	●	○	●	○
5	4R-K	○	●	○	●	○	●	○	○	●
5	4R-L	○	●	○	●	○	●	○	●	○
5	4R-M	○	●	○	●	●	○	○	○	●
5	4R-N	●	○	○	○	○	●	○	○	●
5	4R-O	●	○	○	●	○	●	○	○	●

Table C.4 RPE (%) and correlation coefficients of identified axle loads from identification with sensor removal

No. of removed sensor	Sensor pattern	RPE (%)				Correlation coefficients			
		1 st front axle	1 st rear axle	2 nd front axle	2 nd rear axle	1 st front axle	1 st rear axle	2 nd front axle	2 nd rear axle
0	9R	5.54	4.79	4.92	7.35	0.9551	0.9218	0.9915	0.9875
1	8R-A	5.63	4.94	5.77	8.65	0.9537	0.9214	0.9915	0.9874
1	8R-B	5.53	5.24	5.93	7.97	0.9565	0.9225	0.9914	0.9876
1	8R-C	5.98	5.22	6.04	8.75	0.9533	0.9216	0.9914	0.9874
1	8R-D	5.47	4.56	4.68	4.84	0.9549	0.9224	0.9914	0.9875
1	8R-E	5.58	4.97	5.10	8.54	0.9557	0.9228	0.9917	0.9876
2	7R-A	5.54	5.09	5.22	5.12	0.9567	0.9229	0.9914	0.9877
2	7R-B	6.68	6.55	6.35	10.81	0.9525	0.9215	0.9916	0.9873
2	7R-C	5.50	4.58	5.21	5.58	0.9538	0.9223	0.9913	0.9873
2	7R-D	5.64	5.78	6.15	9.43	0.9567	0.9230	0.9916	0.9877
2	7R-E	10.18	7.66	8.20	11.36	0.9495	0.9175	0.9911	0.9872
2	7R-F	5.56	4.93	5.84	9.84	0.9542	0.9228	0.9917	0.9875
2	7R-G	9.51	7.52	8.20	10.62	0.9523	0.9180	0.9910	0.9873
2	7R-H	5.60	3.87	5.15	8.51	0.9546	0.9293	0.9915	0.9878
2	7R-I	9.31	6.96	8.08	11.34	0.9497	0.9165	0.9911	0.9871
2	7R-J	5.26	3.89	5.03	7.69	0.9578	0.9302	0.9915	0.9880
2	7R-K	5.47	4.18	4.60	8.16	0.9552	0.9297	0.9916	0.9878
2	7R-L	5.94	6.48	5.66	8.04	0.9555	0.9208	0.9912	0.9874
2	7R-M	5.79	5.53	5.22	8.51	0.9525	0.9198	0.9914	0.9872
3	6R-A	5.38	4.22	4.37	5.19	0.9561	0.9310	0.9915	0.9879
3	6R-B	5.78	5.29	4.99	5.64	0.9523	0.9200	0.9911	0.9871
3	6R-C	7.11	6.47	7.47	6.05	0.9516	0.9213	0.9911	0.9869
3	6R-D	5.71	3.98	4.75	9.77	0.9541	0.9305	0.9918	0.9878
3	6R-E	5.67	5.62	5.22	9.74	0.9536	0.9213	0.9917	0.9874
3	6R-F	7.16	7.42	8.25	10.45	0.9514	0.9221	0.9916	0.9872
3	6R-G	7.22	4.40	6.93	11.01	0.9540	0.9270	0.9915	0.9878
3	6R-H	8.69	7.74	7.21	11.09	0.9471	0.9137	0.9908	0.9869
3	6R-I	10.17	7.28	7.59	7.64	0.9547	0.9185	0.9911	0.9874
3	6R-J	5.18	3.75	4.41	4.76	0.9587	0.9314	0.9916	0.9882
3	6R-K	5.35	3.91	5.08	9.29	0.9562	0.9304	0.9916	0.9880
3	6R-L	6.47	8.07	6.20	9.87	0.9560	0.9211	0.9915	0.9875
3	6R-M	8.83	5.48	8.00	10.76	0.9561	0.9272	0.9913	0.9879
3	6R-N	5.48	3.67	4.40	5.64	0.9561	0.9309	0.9917	0.9882
3	6R-O	6.02	4.30	5.34	10.77	0.9520	0.9287	0.9915	0.9874

Table C.4 (continued): RPE and correlation coefficients of identified axle loads from identification with sensor removal

No. of removed sensor	Sensor pattern	RPE (%)				Correlation coefficients			
		1 st front axle	1 st rear axle	2 nd front axle	2 nd rear axle	1 st front axle	1 st rear axle	2 nd front axle	2 nd rear axle
4	5R-A	5.52	4.75	7.03	9.31	0.9571	0.9285	0.9915	0.9879
4	5R-B	6.48	5.59	9.56	9.18	0.9540	0.9285	0.9914	0.9876
4	5R-C	5.83	9.86	8.76	9.83	0.9514	0.9217	0.9909	0.9870
4	5R-D	7.00	5.05	7.44	10.40	0.9524	0.9276	0.9915	0.9876
4	5R-E	8.54	6.12	9.74	10.34	0.9492	0.9273	0.9914	0.9874
4	5R-F	7.03	5.83	7.91	9.09	0.9553	0.9281	0.9912	0.9877
4	5R-G	5.22	3.87	5.04	5.67	0.9575	0.9305	0.9915	0.9880
4	5R-H	6.53	8.37	6.03	6.39	0.9545	0.9187	0.9908	0.9870
4	5R-I	7.88	9.46	8.68	6.70	0.9526	0.9207	0.9910	0.9868
4	5R-J	5.51	4.12	6.54	11.38	0.9542	0.9294	0.9916	0.9879
4	5R-K	5.86	8.49	6.88	11.16	0.9545	0.9208	0.9914	0.9874
4	5R-L	6.86	9.45	9.69	11.49	0.9515	0.9224	0.9913	0.9872
4	5R-M	7.96	5.44	9.16	12.36	0.9553	0.9263	0.9913	0.9879
4	5R-N	7.98	8.81	8.07	11.68	0.9489	0.9151	0.9906	0.9871
4	5R-O	9.67	9.52	10.55	11.75	0.9488	0.9188	0.9908	0.9871
4	5R-P	5.52	3.75	4.85	6.81	0.9542	0.9307	0.9917	0.9880
4	5R-Q	7.68	7.50	6.17	7.38	0.9509	0.9193	0.9913	0.9872
4	5R-R	9.44	8.68	8.91	7.62	0.9488	0.9207	0.9913	0.9870
4	5R-S	6.05	4.22	6.16	12.49	0.9496	0.9286	0.9915	0.9874
4	5R-T	7.24	8.46	6.76	12.22	0.9501	0.9202	0.9915	0.9871
4	5R-U	8.77	9.52	9.41	12.42	0.9469	0.9214	0.9914	0.9869
4	5R-V	10.20	5.98	9.35	13.34	0.9516	0.9256	0.9913	0.9876
4	5R-W	10.20	9.25	8.44	12.67	0.9458	0.9146	0.9907	0.9869
4	5R-X	12.12	10.12	10.72	12.70	0.9451	0.9180	0.9909	0.9869
4	5R-Y	5.71	4.10	5.04	5.72	0.9568	0.9301	0.9916	0.9883
4	5R-Z	7.85	9.04	5.85	5.95	0.9537	0.9194	0.9912	0.9876
4	5R-AA	9.62	10.22	8.61	6.24	0.9511	0.9210	0.9913	0.9874
4	5R-BB	7.12	6.41	7.36	12.04	0.9506	0.9253	0.9910	0.9872
4	5R-CC	7.14	9.90	6.71	10.93	0.9523	0.9197	0.9911	0.9872
4	5R-DD	8.69	10.91	9.43	11.16	0.9486	0.9208	0.9910	0.9869
4	5R-EE	10.19	6.74	9.56	12.07	0.9542	0.9260	0.9910	0.9877
4	5R-FF	10.13	10.26	8.50	11.34	0.9490	0.9159	0.9905	0.9871
4	5R-GG	12.03	11.06	10.86	11.44	0.9478	0.9193	0.9907	0.9870
5	4R-A	5.82	5.00	5.98	5.76	0.9583	0.9292	0.9914	0.9879
5	4R-B	7.65	6.70	8.90	6.14	0.9553	0.9289	0.9914	0.9876
5	4R-C	6.41	11.85	8.22	6.61	0.9517	0.9206	0.9905	0.9866
5	4R-D	5.49	5.33	7.54	11.62	0.9556	0.9287	0.9917	0.9879
5	4R-E	6.66	6.92	10.33	11.76	0.9518	0.9283	0.9915	0.9877
5	4R-F	5.61	10.94	9.19	12.00	0.9529	0.9239	0.9912	0.9874
5	4R-G	7.67	6.57	9.98	12.55	0.9554	0.9253	0.9912	0.9878
5	4R-H	9.61	7.20	11.70	11.91	0.9535	0.9269	0.9913	0.9878
5	4R-I	7.54	4.87	6.40	7.27	0.9543	0.9293	0.9917	0.9879
5	4R-J	9.21	6.04	8.78	7.28	0.9515	0.9290	0.9917	0.9877
5	4R-K	7.21	6.10	7.52	12.95	0.9502	0.9273	0.9916	0.9874
5	4R-L	8.65	7.18	9.67	12.81	0.9466	0.9272	0.9915	0.9872
5	4R-M	10.17	7.12	10.17	13.50	0.9516	0.9249	0.9913	0.9876
5	4R-N	7.86	6.25	6.23	5.70	0.9567	0.9290	0.9916	0.9883
5	4R-O	7.22	7.51	7.61	11.55	0.9515	0.9258	0.9911	0.9873

III. Axle Loads Identification with Bridge Responses of Target Span

Figure C.4 and Figure C.5 represent time histories of identified axle load in a case of 30 kg GVM, 2-axle vehicle moving with velocity of 0.2 m/s and 1.8 m/s, respectively. It is observed that the identified axle loads from Figure C.4 match the actual axle loads very well. However, in the case of a faster speed scenario, although the RPE of the identified axle loads are below 5%, plots of identified load time histories shown in Figure C.5 indicate that the obtained solution lose information on dynamic component and only static component that very well matches the actual loads. This is because the problem loses the information on bridge initial condition from cutting duration of the time histories and identifying with fewer measurement stations.

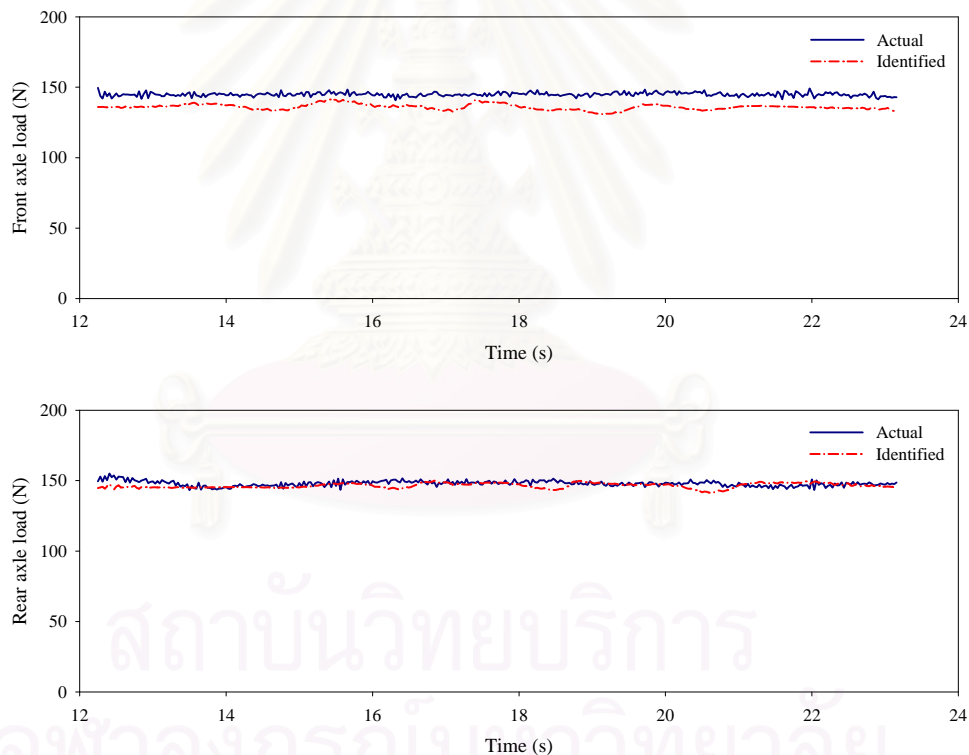


Figure C.4 Time histories of identified axle loads of 30 kg GVM, 2-axle vehicle moving with velocity of 0.2 m/s identified its axle load with response from the target bridge span

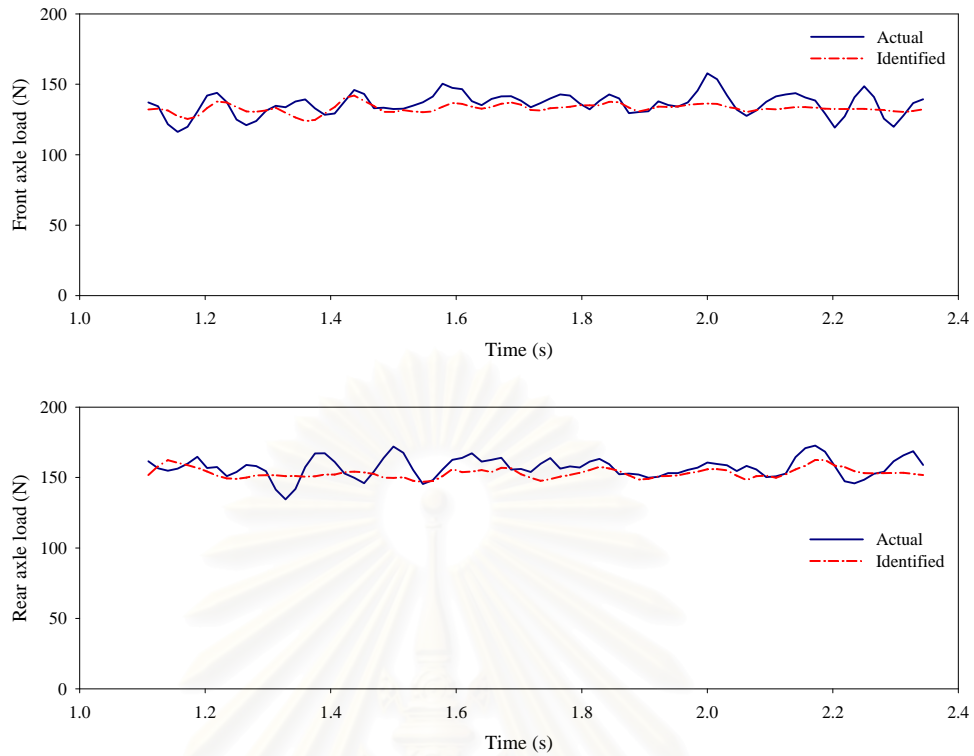


Figure C.5 Time histories of identified axle loads of 30 kg GVM, 2-axle vehicle moving with velocity of 1.8 m/s identified its axle load with response from the target bridge span

Example of time histories of identified axle loads of two vehicle travel in the case of overtaking (OVT-6) and following (FLI-1) scenarios are represented in Figure C.6 and Figure C.7, respectively. Similarly to the single vehicle identification which is an over-determined problem, results from both figures exhibit acceptable accuracy, particularly in static component of axle load.

สถาบันวิทยบริการ
จุฬาลงกรณ์มหาวิทยาลัย

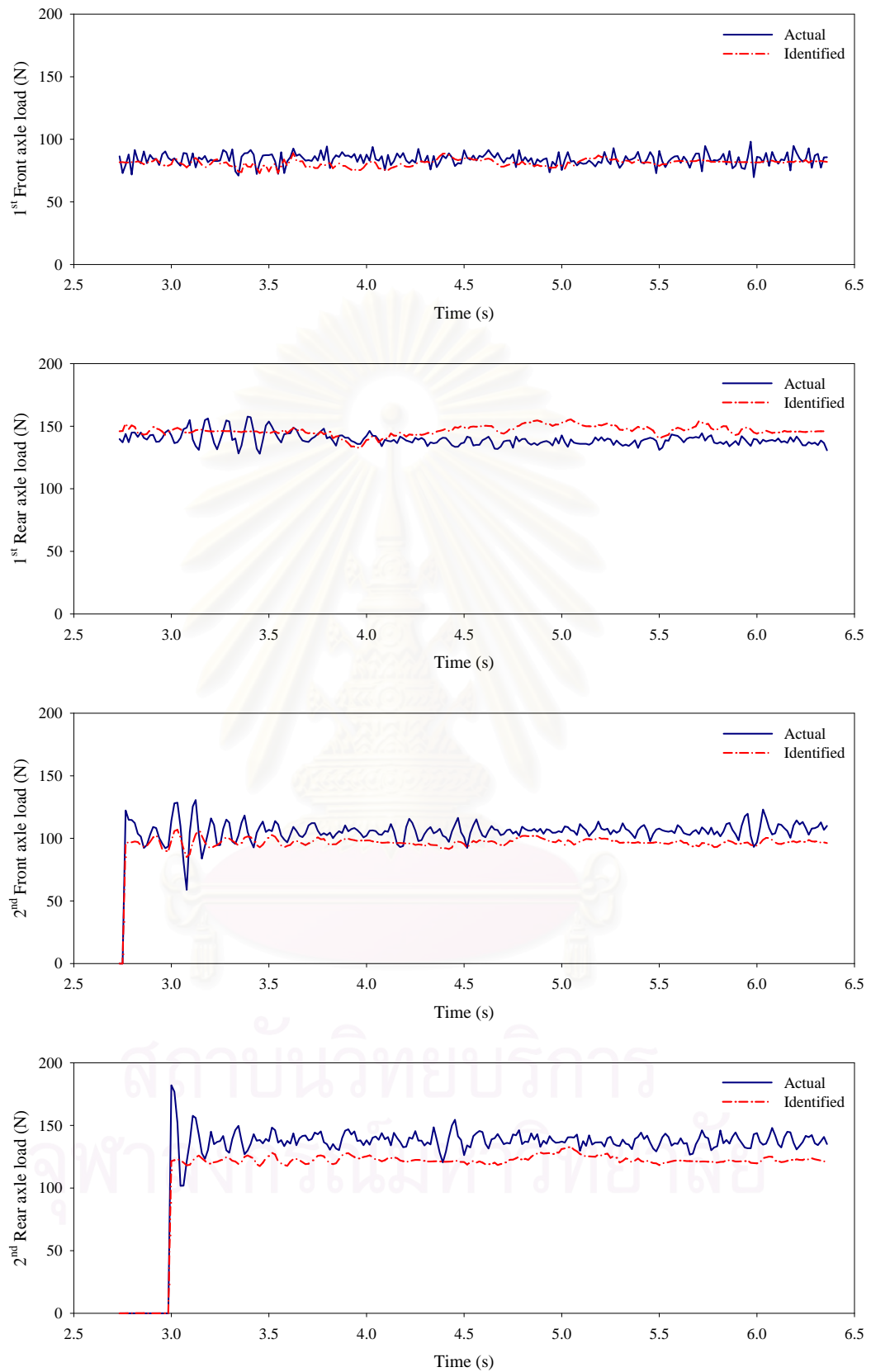


Figure C.6 Time histories of identified axle loads of OVT-4 scenario identified its axle load with response from the target bridge span

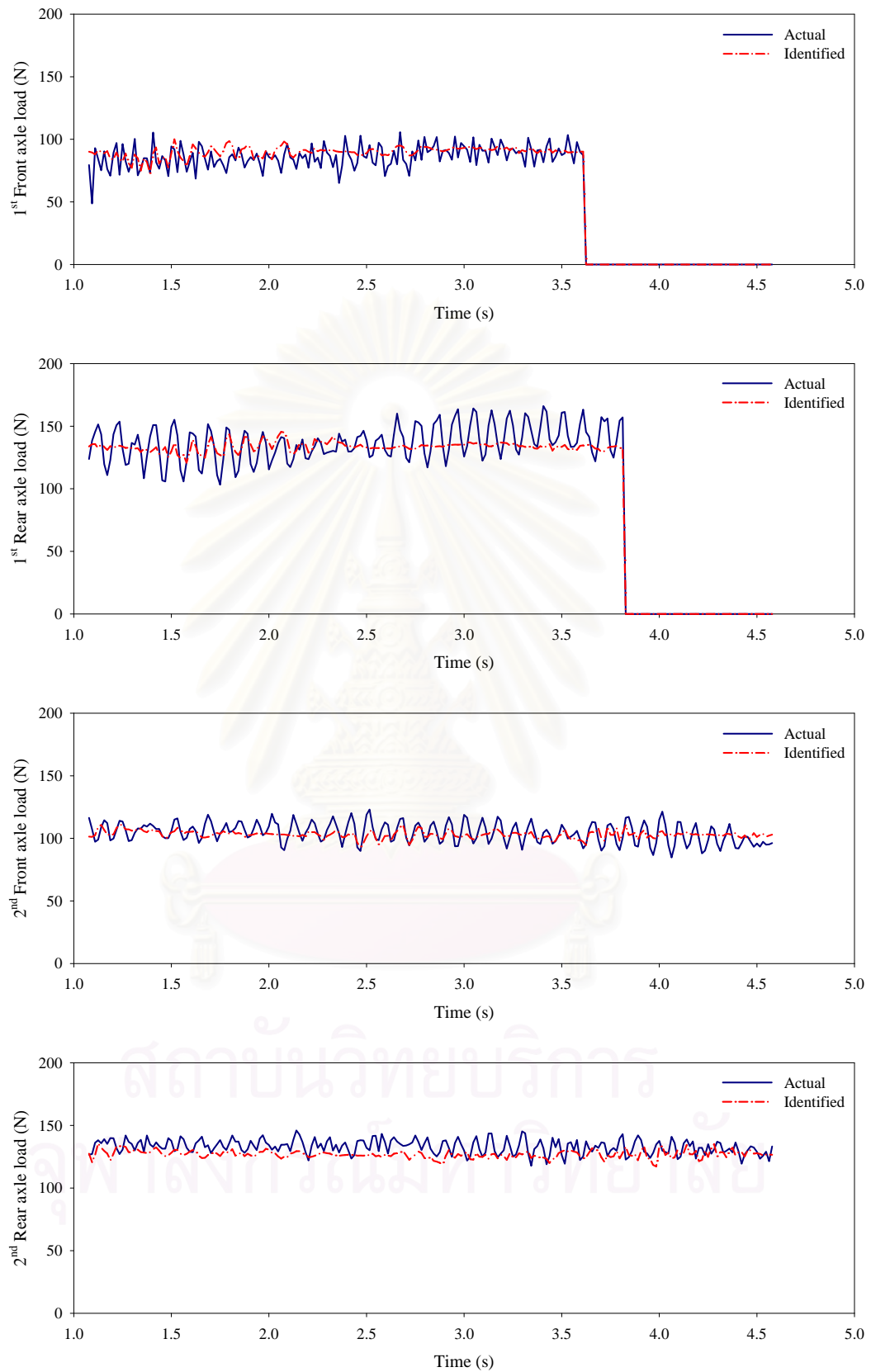


Figure C.7 Time histories of identified axle loads of FLI-1 scenario identified its axle load with response from the target bridge span

VITA

PATTARAPONG ASNACHINDA

I was born in Chiang Mai, on July 12th, 1980. I graduated the elementary and secondary level at Montfort College in Chiang Mai. Then I finished the bachelor's degree of civil engineering at Chiang Mai University in 2002. After that, I moved to Bangkok to continue my graduate level study at Chulalongkorn University and graduated the master's degree of civil engineering in structural engineering in 2004. In the second semester of academic year 2004, I began the study in Ph.D. program of civil engineering in the structural engineering division working with Associate Professor Tospol Pinkaew, my research supervisor. In 2005, I received the scholarship from commission on higher education, ministry of education for financial support. During the study in 2007, I spent my time for 8 months in United States at the Pennsylvania State University to do research with Associate Professor Jeffrey A. Laman who is a specialist in the field of my study. Finally, I will be a lecturer at Burapha University at Chonburi after my graduation on the commitment of my scholarship.

สถาบันวิทยบริการ
จุฬาลงกรณ์มหาวิทยาลัย